

博士論文

**Controlled Solid State Molecular
Assembly Up To Macroscopic Order**

(固相における分子集合体形成)

陳 振

November 2016

The present thesis records the research work independently completed by the author under the guidance of Professor Takuzo Aida at the University of Tokyo, which is used to apply for the PhD degree. The subject content of this thesis is “controlled solid state molecular assembly up to macroscopic order”, including four chapters. The front three chapters mainly focused on the controlled polymeric assembly up to 2D homeotropic order in solid state. And, the fourth chapter independently discussed the supramolecular assembly capable of self-replication up to 1D crystalline fibers in solid state.

Chapter 1 generally reviewed the recent progresses to control the macroscopic order in solid-state of materials, including the orientation of polymer chains and crystallization of small molecules. Firstly, the orientation of polymer chains is highlighted in this chapter from the horizontal to vertical orientation, which is widely applied for developing high-performance polymer-based devices. Then, the particular molecular designs on monomers enabled to form the macroscopic order in crystals through topochemical reactions or polymerizations are discussed.

Chapter 2 mainly discussed the assembling mechanism to form a 2D rectangular or hexagonal geometry in solid state of newly designed bottlebrush polymers carrying three polarized mesogenic units in individual side chains. The key to this anomalous assembling was a recognition that individual cylindrical polymers can be designed to possess oppositely oriented local dipoles that emanate from the terminus in their ellipsoidal cross section. The interaction of these local dipoles possibly forces neighboring cylinders to tightly connect bilaterally, affording an assembly with a 2D rectangular geometry instead of a hexagonal geometry.

Chapter 3 extracted necessary structural parameters for cylindrical bottlebrush polymers to develop a 2D homeotropic order upon hot-pressing in Teflon sheets through the systematic study, including the intrinsically strong preference for the self-assembly into a 2D rectangular lattice, and a large total π -plane surface area of the mesogenic units. With a physical assistance of the surface grooves on Teflon sheets that sandwich polymer samples, homeotropic ordering is likely nucleated and gradually propagates upon hot-pressing toward the interior of the film. Consequently, the 2D rectangular lattice is constructed such that its *b*-axis (side chains) aligns along the surface grooves, while its *c*-axis (polymer backbone) aligns homeotropically on a Teflon sheet.

Chapter 4 presented a self-replicating supramolecular polymerization in solid state enabled to accurately control the autocatalytic cyclotetramerization of 4,5-dithiophthalonitrile derivatives (PNC) to assemble the crystalline fibers of metal-free phthalocyanines (Pc) featuring a high yield (> 80%) and selectivity. The key process during polymerization is that isotropic PNC pasted on the template columnar nucleus consisting of Pc molecules through a hydrogen-bonding interaction of the amide groups, and spontaneously cyclized to form a new Pc in a molecular distance. In one step, PNC polymerize to afford a crystalline fiber assembled by highly pure Pc, which may provide a new idea for synthetic methodologies and design of self-synthesizing materials.

Zhen CHEN

2016. 11

CONTENTS

1

CHAPTER 1

Solid-state Molecular Assembly Up To Macroscopic Order

- 01 *General Information*
- 03 *Macroscopic Order Formed by Orientation of Polymers*
- 13 *Macroscopic Order Formed by Topochemical Reactions in Solid State*
- 18 *Summary*

21

CHAPTER 2

Solid-state Assembly Of Bottlebrush Polymers To 2D lattices

- 21 *Introduction*
- 24 *Results and Discussion*
- 35 *Conclusion*
- 37 *Supporting Information*

61

CHAPTER 3

Controlling Bottlebrush Polymers Assembly To 2D Homeotropic Order

- 61 *Introduction*
- 64 *Results and Discussion*
- 79 *Conclusion*
- 80 *Supporting Information*

107

CHAPTER 4

Soild-state Self-replication Of Phthalocyanines Driven By Supramolecular Polymerization

- 107 *Introduction*
 - 109 *Results and Discussion*
 - 119 *Conclusion*
 - 120 *Supporting Information*
- 

Chapter

1

Solid-state Molecular Assembly Up To Macroscopic Order

The performances of advance materials are highly dependent on the physical properties of constituent molecules. However, in order to fully exploit the potential utilities of such materials, the ability to control their macroscopic order and molecular packing is equally important.

1.1. General Information

We cannot image this colorful world without organic materials. For example, polymers are widely used in plastic, fiber, rubber, package, coating, adhesive, and composites, which required polymers to exhibit highly specific performances. These performances including high mechanical strength, toughness, electrical conductivity, and piezoelectrical response and so on, mainly stem from the soild-state structures of polymers. Primary structures of polymer at molecular level, in terms of the sequence of monomers, stereoregularity, and molecular weight, can be more easily manipulated by synthetic strategies (1–6). On the other hand, secondary structures in soild state, induced by self-assembly (7–14), crystallization (15–20), and orientation (21–25), is harder to be controlled but it can afford ordered polymeric materials with more sophisticated performances.

Comparing to the self-assembly and crystallization, ordered structures of polymers in soild state can be more easily obtained by external orientation. For example, polymer composed of a rigid backbone grafted by flexible side chains can exhibit liquid-crystalline behavior (21–25). The flow-induced alignment of molecular chains

- [1] N. Badi, J-F. Lutz. *Chem. Soc. Rev.* **38**, 3383 (2009).
- [2] J. Niu, R. Hili, D. R. Liu. *Nature Chem.* **5**, 282 (2013).
- [3] K. Satoh, M. Kamigaito. *Chem. Rev.* **109**, 5120 (2009).
- [4] G. W. Coates. *Chem. Rev.* **100**, 1223 (2000).
- [5] S. Aoshima, S. Kananoka. *Chem. Rev.* **109**, 5254 (2009).
- [6] J. -S. Wang, K. Matyjaszewski. *J. Am. Chem. Soc.* **117**, 5614 (1995).
- [7] H. -C. Kim, S. -M. Park, W. D. Hinsberg. *Chem. Rev.* **110**, 146 (2010).
- [8] F. S. Bates, G. H. Fredrickson. *Phys. Today* **52**, 32 (1999).
- [9] F. S. Bates, G. H. Fredrickson. *Annu. Rev. Phys. Chem.* **41**, 525 (1990).
- [10] C. M. Bates *et al.* *Science* **338**, 775 (2012).
- [11] T. L. Morkved *et al.* *Science* **273**, 931 (1996).
- [12] S. Park *et al.* *Science* **323**, 1030 (2009).

- [13] J. K. W. Yang *et al.* *Nature Nanotech.* **5**, 256 (2010).
 [14] A. Tavakkoli K *et al.* *Science* **336**, 1294 (2012).
 [15] L. Mandelkern. *Chem. Rev.* **55**, 903 (1955).
 [16] V. D. Gupta. *Chem. Rev.* **62**, 665 (1962).
 [17] E. Bare, A. Hiltner, H. D. Keith. *Science* **235**, 1015 (1987).
 [18] J. -J. Xu *et al.* *Nature Mater.* **8**, 348 (2009).
 [19] P. J. Lemstra. *Science* **323**, 725 (2009).
 [20] H. -P. Wang *et al.* *Science* **323**, 757 (2009).
 [21] L. Kloppenburg *et al.* *Macromolecules* **32**, 4460 (1999).
 [22] C. Ghobril *et al.* *ACS Macro. Lett.* **3**, 359 (2014).
 [23] K. Okoshi *et al.* *Macromolecules* **35**, 4556 (2002).
 [24] R. Ishige *et al.* *Macromolecules* **41**, 7566 (2008).
 [25] D. K. Cinader, W. R. Burghardt. *Macromolecules* **31**, 9099 (1998).

during drawing processing imparts a high degree of orientation in ordered solid-state structure of polymers (23–25). Fibers own their outstanding mechanical strength to such unidirectional orientation. More importantly, orientation of polymer chains by external force is not only available for more polymeric candidates but also can realize a large-area molecular order of polymer materials, which is essential for developing high-performance polymer-based devices.

As the cases of materials based on small molecules, their ability of crystallizing to control the ordered structures in solid state is more essential than the molecular design for developing high-performance organic device, for example the organic field effect transistors (OFETs) and perovskite-based solar cells. This chapter will mainly focus on the orientation of polymer chains and some interesting crystallization of small molecules to discuss the solid-state molecular assembly up to macroscopic order, reviewing the big progresses in this two field and illustrate the relationship between the structure and properties.

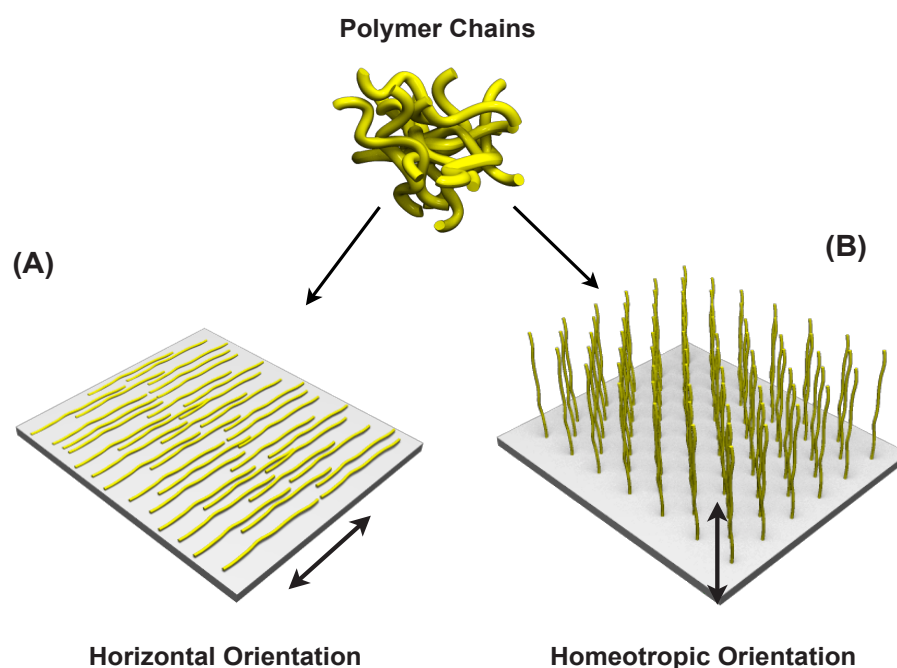


Figure 1 | Schematic illustrations of two different configurations of polymer chains on a substrate. (A) Horizontal orientation of polymer chains lying down on the substrate. **(B)** Homeotropic orientation of polymer chains vertically standing on the substrate.

1.2. Macroscopic Order Formed by Orientation of Polymers

1.2.1. Horizontal Orientation of Polymers

In general, there are two types of oriented configuration of polymers on the substrates, horizontal orientation (Figure. 1A) and vertical (homeotropic) orientation (Figure. 1B). Considering its large aspect ratio, linear polymer chain tends to lie down and be more preferably oriented horizontally on substrates. Except for extrusion and drawing process, other successful strategies include mechanical rubbing (26–28), external field (29), modified or patterned surface (30,31), photoalignment (32,33), and nanoinprinting (34), which also can realize one-dimensional (1D) orientation of polymer chains. Such 1D order of polymer material allows for manufacturing of anisotropic functional thin films with an ultrahigh structural precision.

Due to a 1D anisotropic orientation, photoluminescence (PL) or electroluminescence (EL) polymers exhibit a highly polarized light-emission, which is potentially applied for polarized organic light-emitting diodes (OLEDs), solid-state laser and 3D imaging (35,36). Lüssem et al. synthesized a segmented polymer consisting of arylenevinylene conjugated segments linked by flexible alkane chains with ester groups (Figure. 2A) (27). The rubbing polymer was aligned into a 1D anisotropic monodomain with highly polarized PL (anisotropy, $r = (I_{\parallel} - I_{\perp}) / (I_{\parallel} + I_{\perp}) = 0.61$) and EL ($r = 0.64$). Grell et al. reported a fully conjugated polymer, polyfluorene bearing branched alkane chains (Figure. 2B), was shown to align on a rubbed film with a higher anisotropy ($r = 0.82$) of EL (28). Recently, Stasio et al. fabricated highly oriented film by tensile drawing of polydiphenylene vinylene (PDV.Li, Figure. 2C) in polyvinyl alcohol matrix, which emitted the highest polarized PL with anisotropy (r) of

- [26] H. Sirringhaus, R. J. Wilson, R. H. Friend. *Appl. Phys. Lett.* **77**, 406 (2000).
 [27] G. Lüssem et al. *Adv. Mater.* **7**, 923 (1995).
 [28] M. Grell et al. *Adv. Mater.* **11**, 671 (1999).
 [29] M. V. Kakade et al. *J. Am. Chem. Soc.* **129**, 2777 (2007).
 [30] D. E. Johnston et al. *ACS Nano* **8**, 243 (2014).
 [31] C. Luo, A. et al. *Nano Lett.* **14**, 2746 (2014).
 [32] K. Sakamoto, T. Yasuda, K. Miki, M. Chikamatsu, R. Azumi. *J. Appl. Phys.* **109**, 013702 (2011).
 [33] D. Sainova et al. *Adv. Funct. Mater.* **12**, 1616 (2002).
 [34] Z. -J. Zheng et al. *Nano Lett.* **7**, 987 (2007).
 [35] M. Grell, D. D. C. Bradley. *Adv. Mater.* **11**, 895 (1995).
 [36] L. Akcelrud. *Prog. Polym. Sci.* **28**, 875 (2003).
 [37] F. D. Stasio et al. *Adv. Mater.* **23**, 1855 (2011).

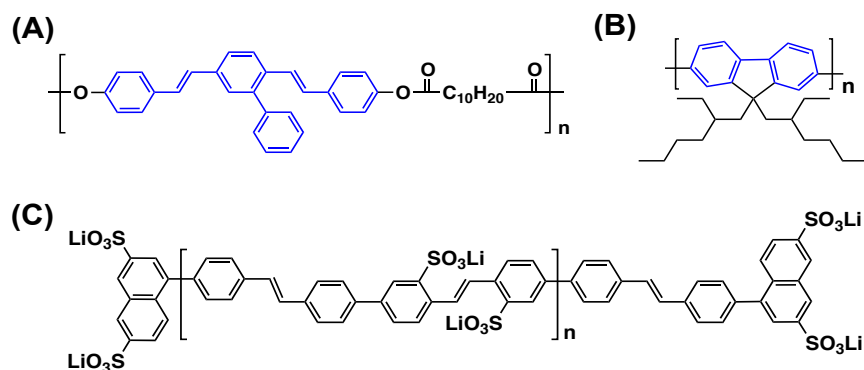


Figure 2 | Molecular formulae of luminescence polymers exhibiting highly polarized light-emission. (A) Segmented polymer containing arylenevinylene groups (blue segment) ester-linked by flexible alkane chains.²⁷ Long spacer allows for easier molecular rearrangement and 1D alignment. (B) Polyfluorene bearing branched alkane chains.²⁸ Branched side chains will offer a lower effective diameter and hence larger aspect ratio than linear chains. (C) Polydiphenylene vinylene functionalized by sulfonic Li⁺ ions to ensure water solubility.³⁷

0.91 to date (37).

Oriented conjugated polymers with anisotropic conductivity are significantly fascinating for organic field-effect transistors (OFETs) and organic photovoltaics (OPVs). Taking the conformation of aromatic rings in polymer chains into account, two kinds of orientation are present, face-on and edge-on orientations, which represent that π -plane of polymer chains align parallel or normal to the substrate or interface, respectively (Figure. 3A). It is well known that the edge-on orientation of poly(3-alkylthiophene) (P3AT) is more suitable for OFETs than the face-on orientation (38–40). Sirringhauus et al. well controlled the orientation of lamella structure of poly(3-hexylthiophene) (P3HT), and found that the charge mobility as high as 0.1 cm²/(Vs) was observed for the edge-on orientation and mobility anisotropy for in- and out-of-plane π - π stacking was more than a factor of 100 (Figure. 3B) (40). However, the charge mobility of face-on orientation was merely 2 × 10⁻⁴ cm²/(Vs), possibly resulting from the 2D interchain character of the polaronic charge carriers. On the other hand, an important feature for OPVs is to make charge transport perpendicular to the interfaces of donor and acceptor, suggesting the face-on orientation is better suited to OPVs (41–43). Tumbleston et al. demonstrated that face-on and edge-on orientation formed by the polymer relative to donor/acceptor heterointerfaces was a critical parameter for device performance (Figure. 3C) (43). The cells with a preferential face-on orientation was shown to a higher photo-conversion efficiency (PCE) as two times as the PCE of edge-on orientation.

[38] B. S. Ong, Y. Wu, P. Liu, S. Gardner. *J. Am. Chem. Soc.* **126**, 3378 (2004).

[39] J. Zaumseil, H. Sirringhauus. *Chem. Rev.* **107**, 1296 (2007).

[40] H. Sirringhauus et al. *Nature* **401**, 685 (1999).

[41] G. -J. Zhao, Y. -J. He, Y. -F. Li. *Adv. Mater.* **22**, 4355 (2010).

[42] B. C. Thompson, J. M. J. Frechet. *Angew. Chem. Int. Ed.* **47**, 58 (2008).

[43] J. R. Tumbleston et al. *Nature Photon.* **8**, 385 (2014).

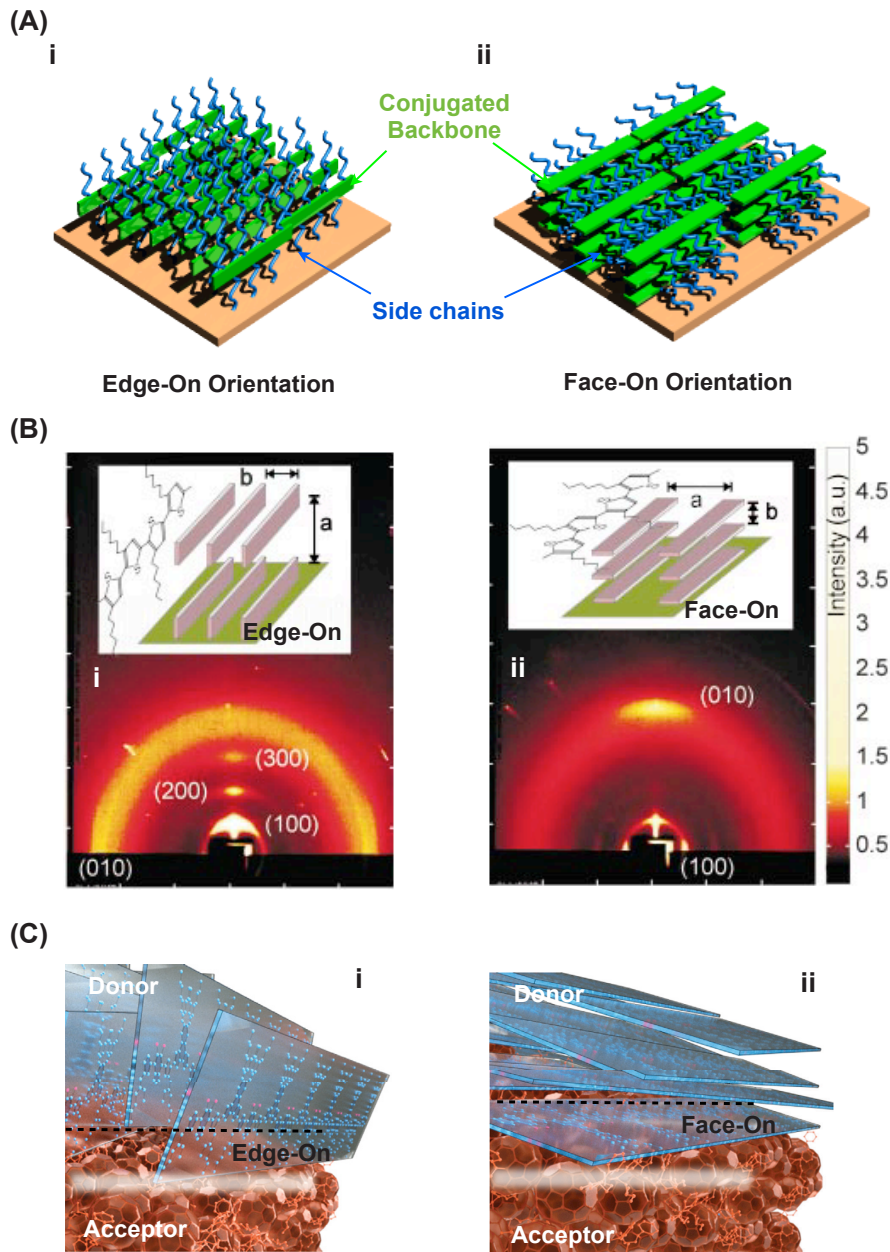


Figure 3 | Edge-on and face-on orientation of conjugated polymers used for OFETs and OPVs. (A) Schematic illustrations of two different molecular arrangements of polymer chains on a substrate: edge-on (i, π -plane is vertical to the substrate) and face-on (ii, π -plane is parallel to the substrate) orientation. (B) Wide-angle X-ray scattering images of P3HT with edge-on (i) and face-on (ii) orientation on a FET substrate.⁴⁰ The ordered domains adopting edge-on configuration are oriented with the (100)-axis normal to the film and (010)-axis in the plane of film. In contrast, face-on crystallites are preferentially oriented with the (100)-axis in the plane and (010)-axis normal to the film. (C) Schematic illustrations of donor/acceptor interfaces adopting edge-on and face-on orientation.⁴³ Near to donor/acceptor heterojunctions of OPV, donor polymer is oriented in edge-on (i) and face-on (ii) configurations with respect to fullerene domain interfaces.

1.2.2. Homeotropic Orientation of Polymers

Comparing to the horizontal orientation, it is much more difficult to make polymer chains vertically stand up and orient on the substrate, because of the inherent flexibility and entanglement of polymer chains. A bigger challenge is how to overcome the gravitational effect. Until now, few examples can achieve the vertical orientation of polymers, including nanopores (44,45), nanoimprinting (46), solvent-vapor treatment (47), surface-grafting polymerization (48–50), and surface separation of fluorine (51,52). Therefore, it is a fundamental but important question in polymer science to control the vertical orientation of polymers for developing functional polymeric materials.

One of the effective techniques to precisely control the packing of polymer chains is nano-confined crystallization of semicrystalline polymers by templates or imprinting. By using block copolymer nanotemplates, Lee et al. fabricated ultrahigh density arrays of conducting polypyrrole (PPy) nanorods, in which PPy backbones are highly oriented vertically to the substrate (Figure. 4A) (44). Owing to such high degree of chain orientation, the nanorods were shown to have a higher conductivity than thin films. Aryal et al. reported the utilization of nanoimprint lithography to fabricate ordered nanostructures of P3HT and control chain vertical alignment within the P3HT nanostructures (Figure. 4B) (46). The driving force for this alignment stems from the nanoconfinement *via* π - π and hydrophobic interaction between polymer chains and mold surfaces during nanoimprinting.

Through synthetic strategies, polymer chains enable to high-densely grow on a modified substrate surface randomly distributed with

[44] J. I. Lee *et al.* *Nano Lett.* **8**, 2315 (2008).

[45] K. -H. Lo *et al.* *Adv. Funct. Mater.* **21**, 2729 (2011).

[46] M. Aryal, K. Trivedi, W. -C. Hu. *ACS Nano* **3**, 3085 (2009).

[47] G. -H. Lu, L. -G. Li, X. -N. Yang. *Adv. Mater.* **19**, 3594 (2007).

[48] Y. -M. Chen. *Macromolecules* **45**, 2619 (2012).

[49] J. E. Poelma, B. P. Fors, G. F. Meyers, J. W. Kramer, C. J. Hawker. *Angew. Chem. Int. Ed.* **52**, 6844 (2013).

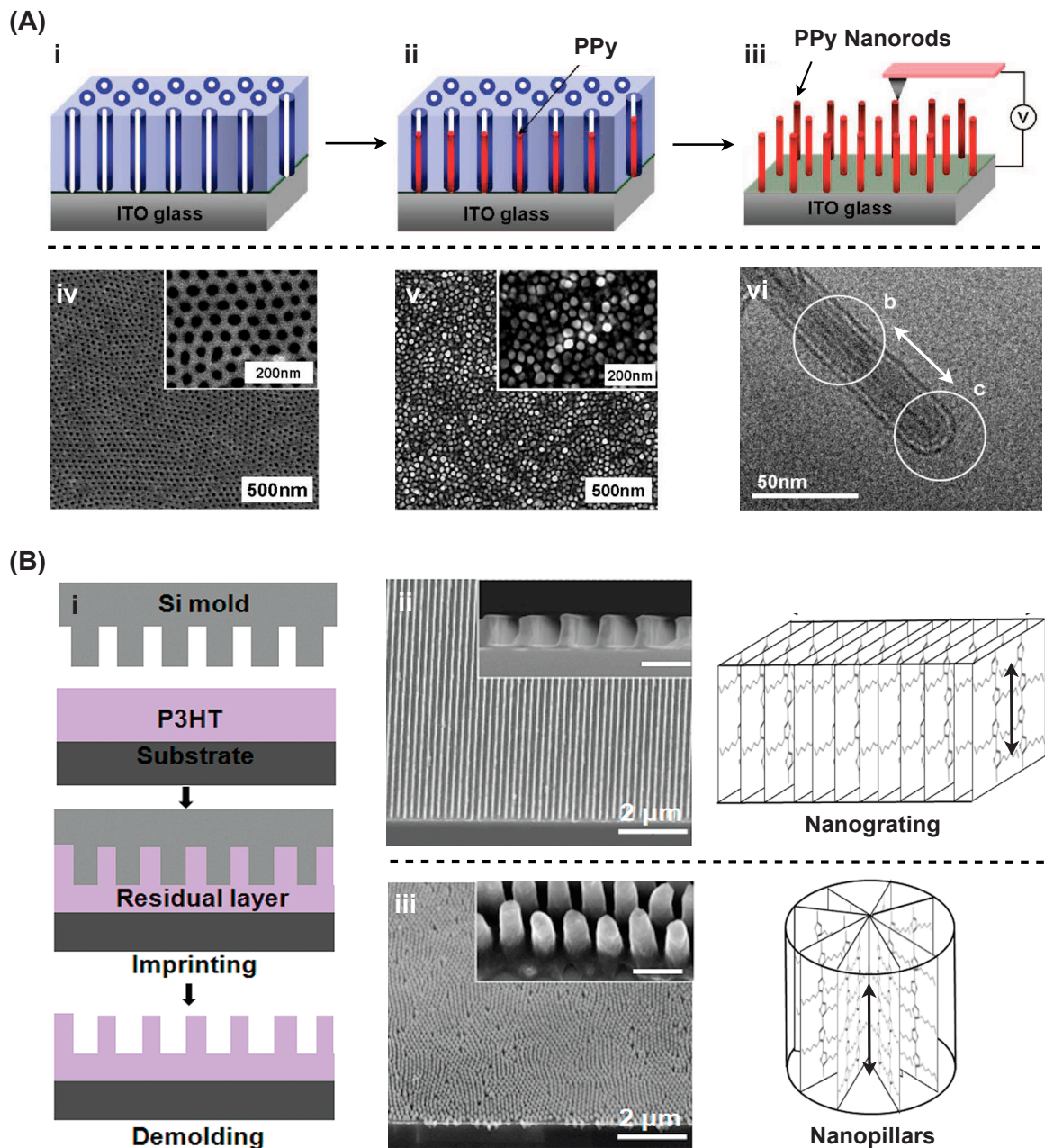


Figure 4 | Vertical orientation of semicrystalline polymers by nanoconfined crystallization. (A) Nanotemplating strategy⁴⁴: As shown in schematic illustrations (i – iii), PPy is confined in a nanoporous template [SEM image (iv)], and after removing the template PPy nanorods are obtained [SEM (v) and TEM (vi) image]. (B) Nanoimprinting strategy⁴⁶: Followed with schematic illustration (i), nanogratings [SEM image (ii)] and nanopillars [SEM image (iii)] consisted of P3HT are fabricated, in which polymer backbones are vertical oriented to the substrate. Arrow denotes the oriented direction of backbone.

initiator groups by surface-grafting polymerization (Figure. 5) (48,49). Ideally, these “polymer hairs” are vertically growing on the substrates, but actually, they mutually entangle and twine, due to the flexible

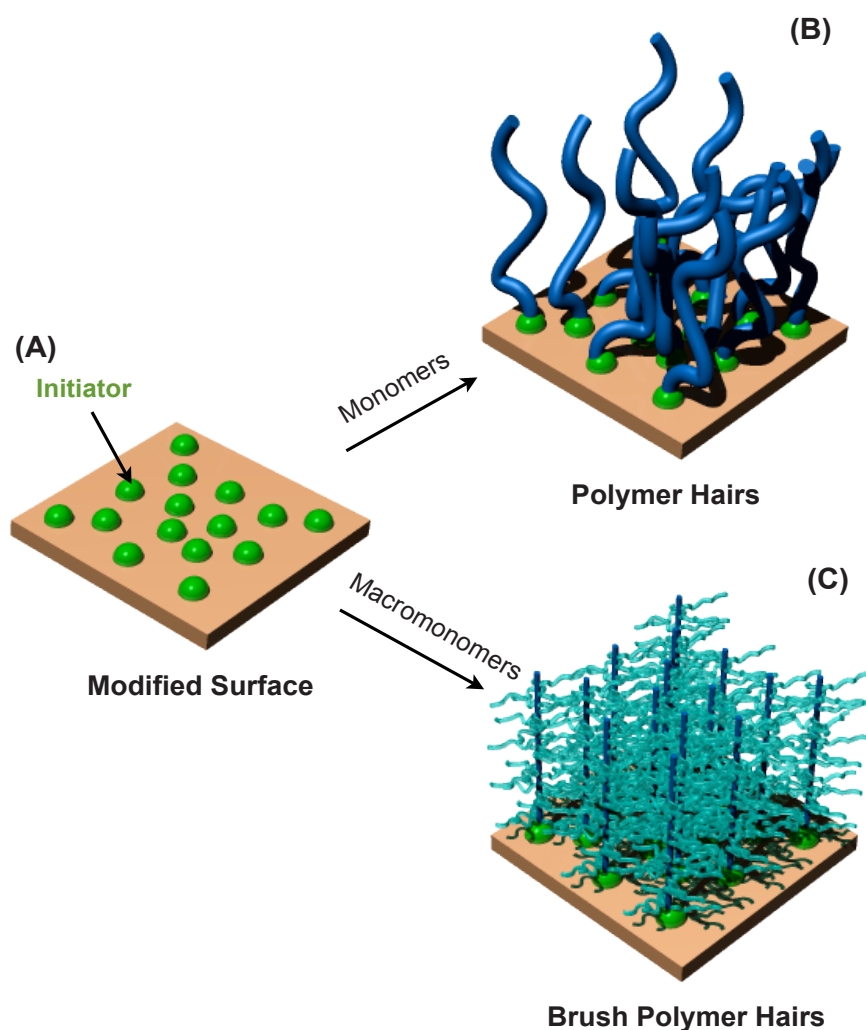


Figure 5 | Schematic illustrations of surface-grafting polymerization. A modified surface randomly distributed with initiator groups (A) can induce the polymerization of small monomers or macromonomers. Then, polymer hairs (B) or brush polymer hairs (C) grow up on the surface. Design of brush-type can make polymer backbones extend to some extent.

conformations of polymer chains. “*Bush polymer hairs*” is one of solutions to enhance the rigidity of polymer backbones and afford a more vertical configuration (Figure. 5C) (50).

[50] H. -J. Jeon, C. P. Grigoropoulos, K. E. Healy. *et al. J. Am. Chem. Soc.* **133**, 6138 (2011).

[51] J. -S. Ma, K. Hashimoto, T. Koganezawa, K. Tajima. *J. Am. Chem. Soc.* **135**, 9644 (2013).

[52] G. -R. Sun *et al. J. Am. Chem. Soc.* **135**, 4203 (2013).

[53] M. P. Krafft, J. G. Riess. *Chem. Rev.* **109**, 1714 (2009).

Some particular molecular designs enable polymer chains spontaneously stand up on the substrates, for instance, fluorine-containing polymers. As we all know, fluorine is one of especial elements in nature, because it hates others but only loves itself. Just because of it, surface segregation will occur when fluorine-containing molecule is mixed with other components but only enriched in the surfaces (53). Tajima *et al.* (51) discovered a new end-on orientation of P3BT-F₁₇ capped with fluoroalkyl end chains, in which conjugated

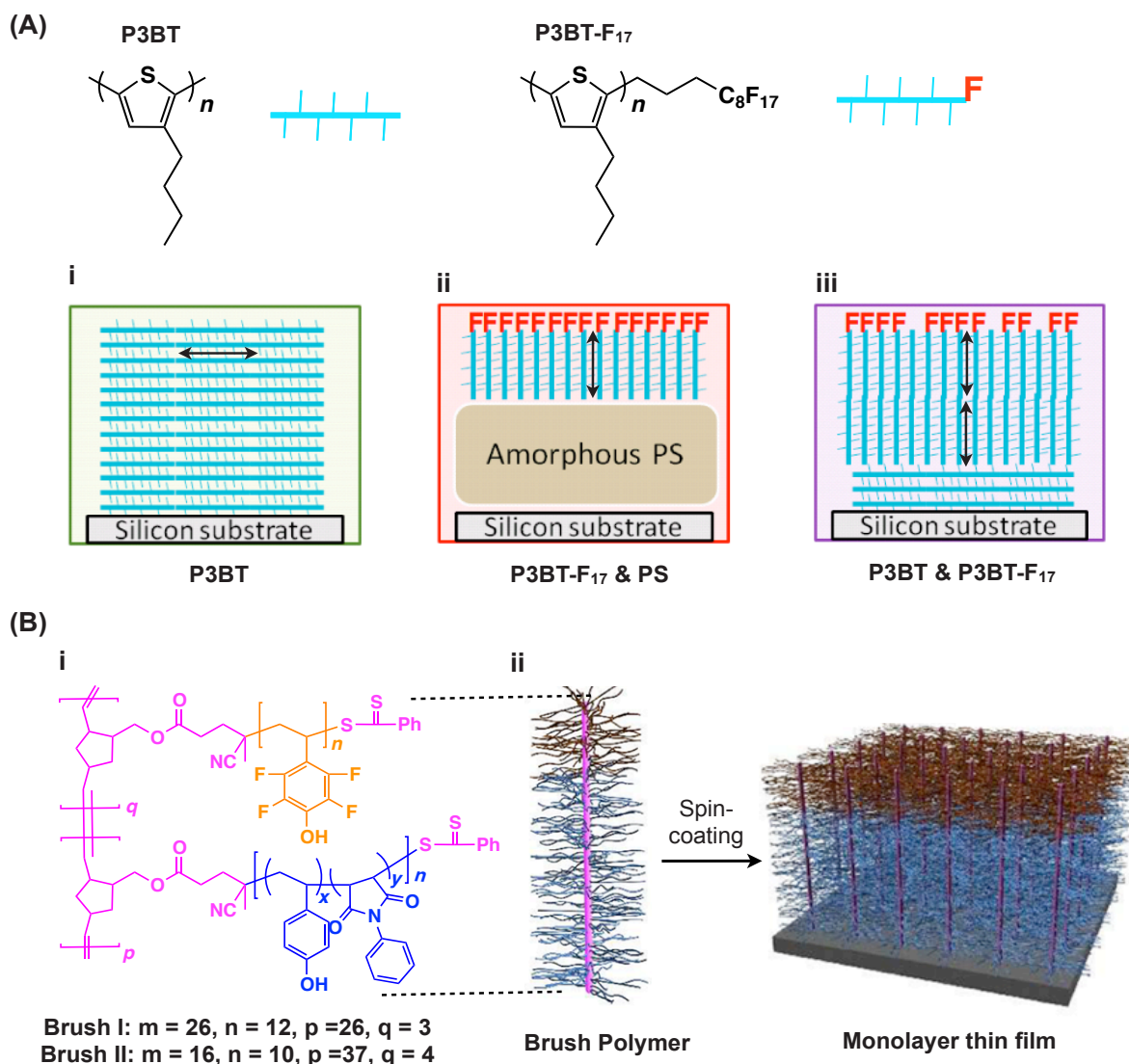


Figure 6 | Vertical orientation of polymers by surface segregation of fluorine. (A) Molecular formulae of P3BT and P3BT-F₁₇ and schematic illustrations (i – iii) of their orientation.⁵¹ Comparing to horizontal orientation of P3BT (i), P3BT-F₁₇ prefers to vertically align in surface (ii) and can assist the vertical orientation of P3BT (iii). (B) Molecular formulae (i) of brush block copolymer and schematic illustrations (ii) of its vertical orientation in monolayer thin film.⁵²

backbones are parallel packing with each other via π - π stacking but vertical to the substrates, resulting from surface segregation of fluorine in end chains (Figure. 6A). Such end-on orientation resulted in a more than 30-fold enhancement of the hole-mobility. Wooley et al. (52) synthesized a diblock copolymer brush, one of blocks containing fluorine, and found that upon simple spin-coating, brush polymer was spontaneously vertically stand up to form a monolayer, in which fluorine block is separated and enriched in the thin film surface (Figure. 6B).

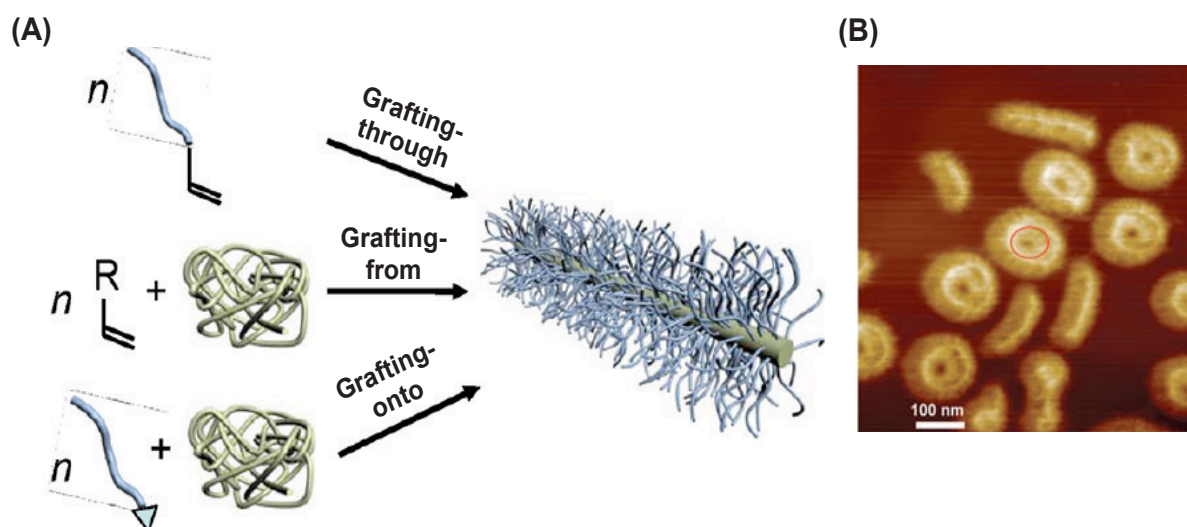


Figure 7 | Synthetic strategies and morphologies of brush polymers. (A) Schematic illustration of three main synthetic strategies: grafting through (polymerization of macromonomers), grafting onto (polymerization of polymeric side chains from backbone), and grafting from (pasting polymeric side chains to backbone).⁵⁴ (B) AFM images of bottlebrush polymers and its ring structure, prepared by spin coating of a dilute solution.⁵⁶

To design polymers as a cylindrical shape is one of rational strategies to realize the homeotropic orientation of polymer chains. Linear polymer densely grafted with polymeric side chains adopts a cylindrical shape, which is termed by bottlebrush polymer. In order to obtain a bottlebrush polymer, three main synthetic strategies are employed, that are, “grafting through”, “grafting onto”, and “grafting from” (Figure. 7A) (54). From a view of conformation, the flexible polymer backbones become more extended and stiffer, resulting from the size-exclusion repulsive effect originating from the steric overcrowding of polymeric side chains, (Figure. 7B) (54–56). At the same time, long polymeric side chains hinder overlapping and entanglement with neighboring polymer molecules, providing a possibility to build up an ordered structures from single macromolecules.

Interestingly, another bottlebrush polymers carrying dendritic side groups instead of linear side chains preform homeotropic orientation in bulk, probably resulting from huger steric hindrance effect (Figure. 8) (55–57). Percec *et al.* (57) first reported a hexagonal columnar phase structure formed by brush polymers pendent with dendritic side groups. Subsequently, they further explored this polymers can be aligned homeotropically on the certain surface (58,59).

In 2010, our group accidentally found that upon hot-pressed by

[54] S. S. Sheiko, B. S. Sumerlin, K. Matyjaszewski. *Prog. Polym. Sci.* **33**, 759 (2008).

[55] P. Dziezok, S. S. Sheiko, K. Fischer, M. Schmidt, M. Möller. *Angew. Chem. Int. Ed.* **36**, 2812 (1997).

[56] S. S. Sheiko *et al.* *Nature* **440**, 191 (2006).

[57] V. Percec *et al.* *Nature* **391**, 161 (1998).

[58] V. Percec *et al.* *J. Am. Chem. Soc.* **127**, 15257 (2005).

[59] V. Percec *et al.* *J. Am. Chem. Soc.* **130**, 7503 (2008).

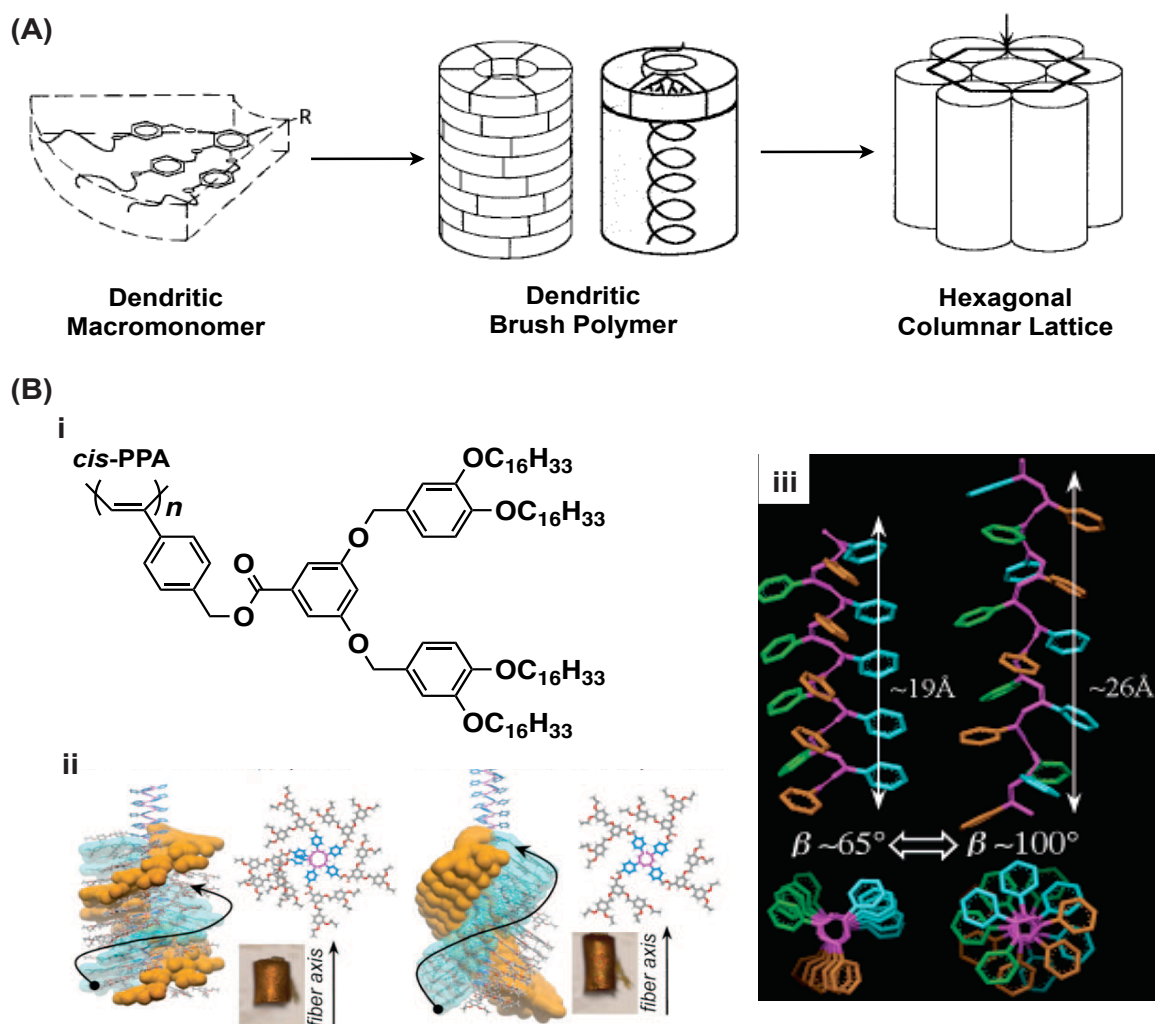


Figure 8 | Self-assembly of brush polymers bearing dendritic side groups in bulk. (A) Schematic illustration of dendritic brush polymer and its hexagonal columnar lattice.⁵⁷ (B) (i) Molecular formulae of dendritic brush polymer with a *cis*-PPA as backbone.^{58,59} (ii) Schematic illustration of thermoreversible extension and contraction in a macroscopic scale.⁵⁹ This reversible behavior results from *cis*-to-*trans* conformational isomerization of *cis*-PPA (iii).⁵⁸

stretched Teflon sheet, a resulting thin film composed of a bottlebrush polymer carrying three azobenzene units in its side chains exhibits a bending motion when azobenzene units are photoisomerized (Figure. 9A and 9B) (60). Of a big surprise is in-depth structural analysis of the film revealed that the constituent polymer molecules are anisotropically oriented in such a way that their backbones align homeotropically to the film plane, while their side chains align horizontally (Figure. 9C). This unique structural ordering is quite intriguing and may give a clue to answer how to orient polymers homeotropically.

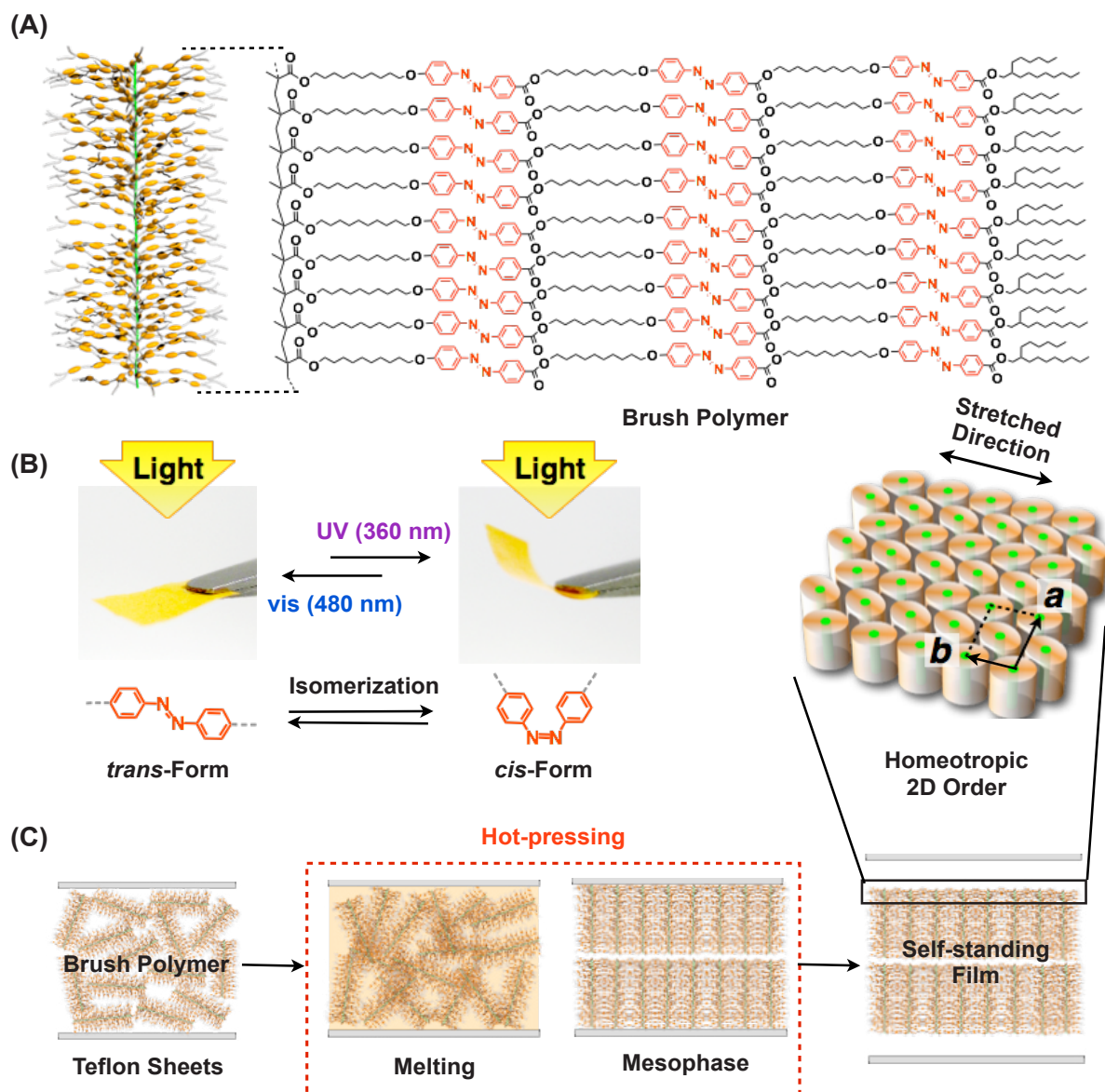


Figure 9 | Homeotropic 2D order of a polymer brush by hot-pressed processing.⁶⁰ (A) Molecular and schematic structure of polymer brush carrying azobenzene-containing mesogenic side chains. (B) Photographs of a hot-pressed film before (left) and after (right) exposure to UV light (360 nm). The bent film recovered the initial flat shape upon irradiation of vis light (480 nm). (C) Schematic illustrations of the procedure for hot-pressing by using two stretched Teflon sheets and the molecular arrangement in a hot-pressed film.

1.3. Macroscopic Order Formed by Topochemical reactions in solid state

Crystal or single crystal is one of most common molecular assemblies in solid state up to a macroscopic order. However, the macroscopic order in crystals is usually dissociated accompanied by the thermal-induced melting or dissolving of the constituent molecules. The topochemical reaction in solid state has provided a promising solution to cross-link and immobilize a stable macroscopic order in crystals (61, 62). In crystals, molecules are periodical arranged in the lattices in which the confinement and preorganization of the solid state forces a chemical reaction to proceed effectively, or even quantitatively triggered by heating or light-radiating (63). These chemical reactions in solid state are so-called topochemical reactions.

In 1960s, Schmidt and co-workers firstly reported that the [2+2] cycloaddition of olefins yielded the cyclobutanes in crystals induced by photoreactions (64). For a classic example, cinnamic acid crystallizes in two polymorphic forms, and packs in the unidirectional stacks in which the distance between the adjacent molecules is less than 0.42 nm, which is the length of overlapping double bonds (Figure. 10A) (65, 66). Therefore, the cinnamic acids react photochemically in crystals to produce the cyclobutanes with the same stereo-chemistry (XX). Then, Wegner et al. discovered that the polymerization of 1,4-diacetylene could occur in the solid state *via* a topochemical reaction (67). If the 1,4-diacetylene monomers are preorganized at a distance consistent with the repeat distance in the final polymer, the thermal or photo-energy can induce the polymerization. The molecular distance could be well controlled in some crystalline diacetylenes (Figure. 10B) (68, 69). Recently, Dou et al. demonstrates a visible-triggered topochemical quantitative polymerization of a conjugated dye molecule to afford a large-polymer single crystal

[61] M. Hasegawa. *Chem. Rev.* **83**, 507 (1983).

[62] K. Biradha, R. Santa. *Chem. Soc. Rev.* **42**, 950 (2013).

[63] V. Ramamuthy, J. Sivaguru. *Chem. Rev.* **116**, 9914 (2016).

[64] G. M. J. Schmidt. *Pure Appl. Chem.* **12**, 647 (1971).

[65] M. D. Cohen, G. M. J. Schmidt. *J. Chem. Soc.* **1964**, 1996.

[66] M. D. Cohen, G. M. J. Schmidt, F. I. Sonntag. *J. Chem. Soc.* **1964**, 2000.

[67] G. Wegner. *Z. Naturforsch.* **24B**, 824 (1969).

[68] R. H. Baughman. *J. Polym. Sci., Polym. Phys. Ed.* **12**, 1511 (1974).

[69] J. W. Lauher, F. W. Fowler, N. S. Goroff. *Acc. Chem. Res.* **41**, 1215 (2008).

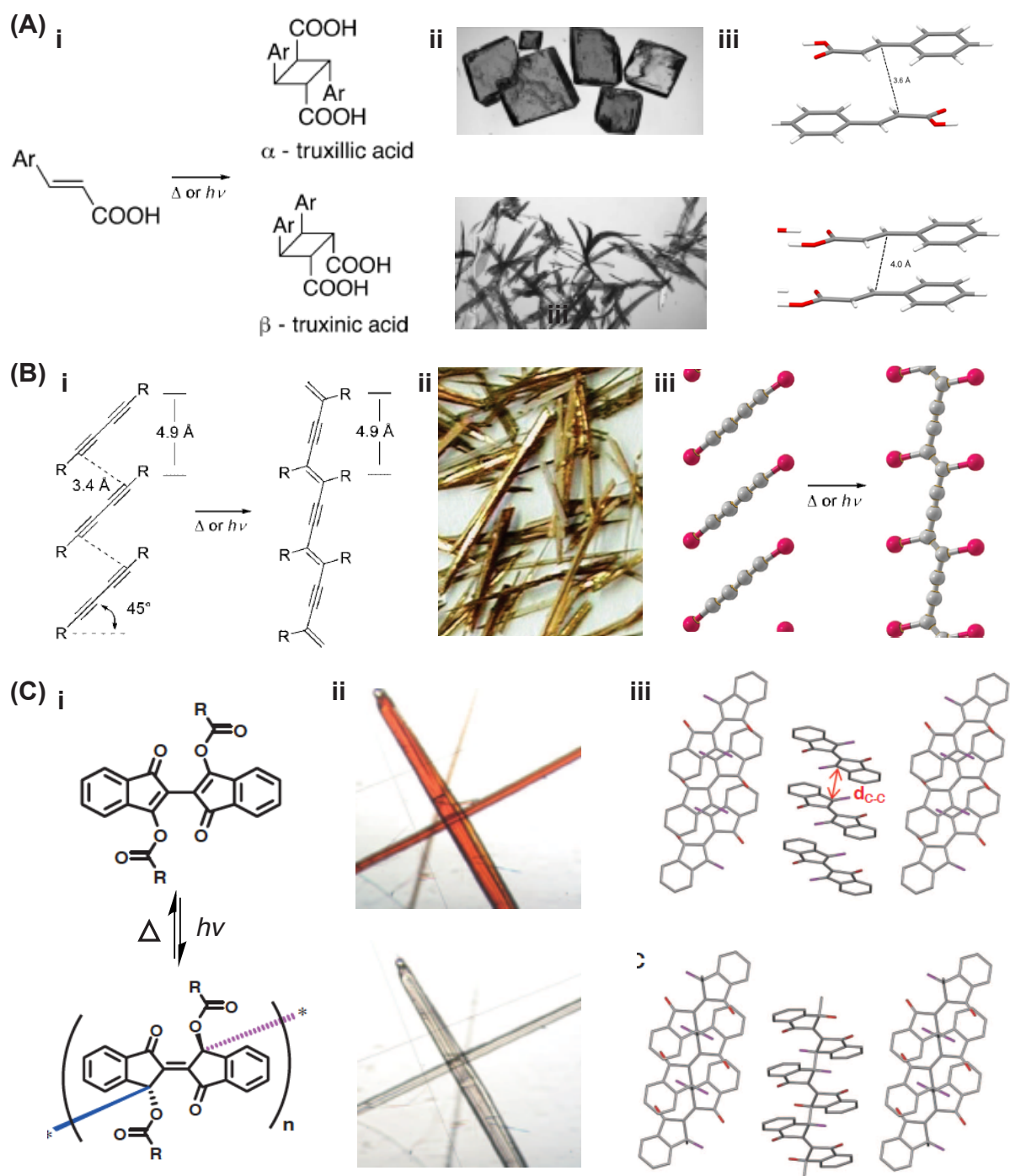


Figure 10 | Topochemical reactions in crystals to yield one-dimensional polymers. (A) The [2+2] cycloaddition of cinnamic acids (i) and molecular packing (iii) in two crystalline structures, α (up, ii) and β (lower, ii). (B) The topochemical polymerization of 1,4-diacetylene (i) and molecular packing (iii) in single crystals (ii). (C) The visible-triggered topochemical polymerization of a conjugated dye molecule (i) and molecular packing (iii) in single crystals (ii).

(Figure. 10C) (70). In addition, the resulting polymer decomposed to the dye monomers upon thermolysis, indicating a reversible process of polymerization and depolymerization.

Except for the one-dimensional (1D) polymerization, two-dimensional (2D) polymers can also be synthesized by topochemical cross-linked reactions in some specific molecular designs and crystalline lattices (71). At certain angle, the macroscopic order in crystals can be exclusively immobilized in the cases of two-dimensional polymers. Ozaki et al. showed that upon UV-irradiation, alkyne-containing linear monomers simultaneously topochemically polymerized to form a 2D polymer consisting of linear polyacetylene and polydiacetylene chains, which can be clearly observed by STM (Figure. 11A) (72). This example is also the first true covalently linked 2D polymer. Then, Kissel et al. rationally synthesized a macroscopically ordered, 2D polymer composed by cup-shaped monomers (73). These particularly designed photoreactive monomers packed into a layered structure parallel to the hexagonal crystal face, in which [4 + 2]-cycloaddition of an alkyne and the 9,10-anthracene position of an adjacent monomer was feasible to occur induced by photopolymerization. After exfoliation in solutions, individual 2D polymers were isolated as large-area, monolayered molecular sheets (Figure. 11B).

Recently, Kory et al. designed a rotor-shaped anthracene monomer and found its non-centrosymmetric single crystal could be converted into a chiral 2D polymer through a photochemical dimerization by [4 + 4]-cycloaddition of anthracene, which also enabled to reverse back to the monomers upon thermolysis (Figure. 11C) (74). The highlighting of this work is the synthesis of resulting 2D polymers on the gram scale. Nearly at the same time, Kissel et al. prepared the lamellar structured single crystal of a fan-shaped monomer, in which the monomers adopted a quasi-hexagonal packing motif with a face-to-face stacking in the individual layers (75). As a result, the distance between anthracene faces was suitable for a photo-induced polymerization of monomers by the [4 + 4] cycloaddition, affording a nanoporous 2D polymer (Figure. 11D).

Without topochemical reactions, in general, the macroscopic order formed by crystallization is unstable. However, a space-filling design is one of the possible strategies to assemble a large-area molecular film. Seiki et al. showed that a 2D nested hexagonal crystallization of a triptycene enabled to develop an organic thin film with an exceptional completely oriented 2D (hexagonal triptycene array) + 1D (layer stacking) structure, which can be used in various high-performance organic materials and devices (Figure. 12) (76).

[70] L.-T. Dou *et al.* *Science* **343**, 272 (2014).

[71] J. W. Colson, W. R. Dichtel. *Nature Chem.* **5**, 453 (2013).

[72] H. Ozaki *et al.* *J. Chem. Phys.* **103**, 1226 (1995).

[73] P. Kissel *et al.* *Nature Chem.* **4**, 287 (2012).

[74] M. J. Kory *et al.* *Nature Chem.* **6**, 779 (2014).

[75] P. Kissel *et al.* *Nature Chem.* **6**, 774 (2014).

[76] N. Seiki *et al.* *Science* **348**, 1122 (2015).

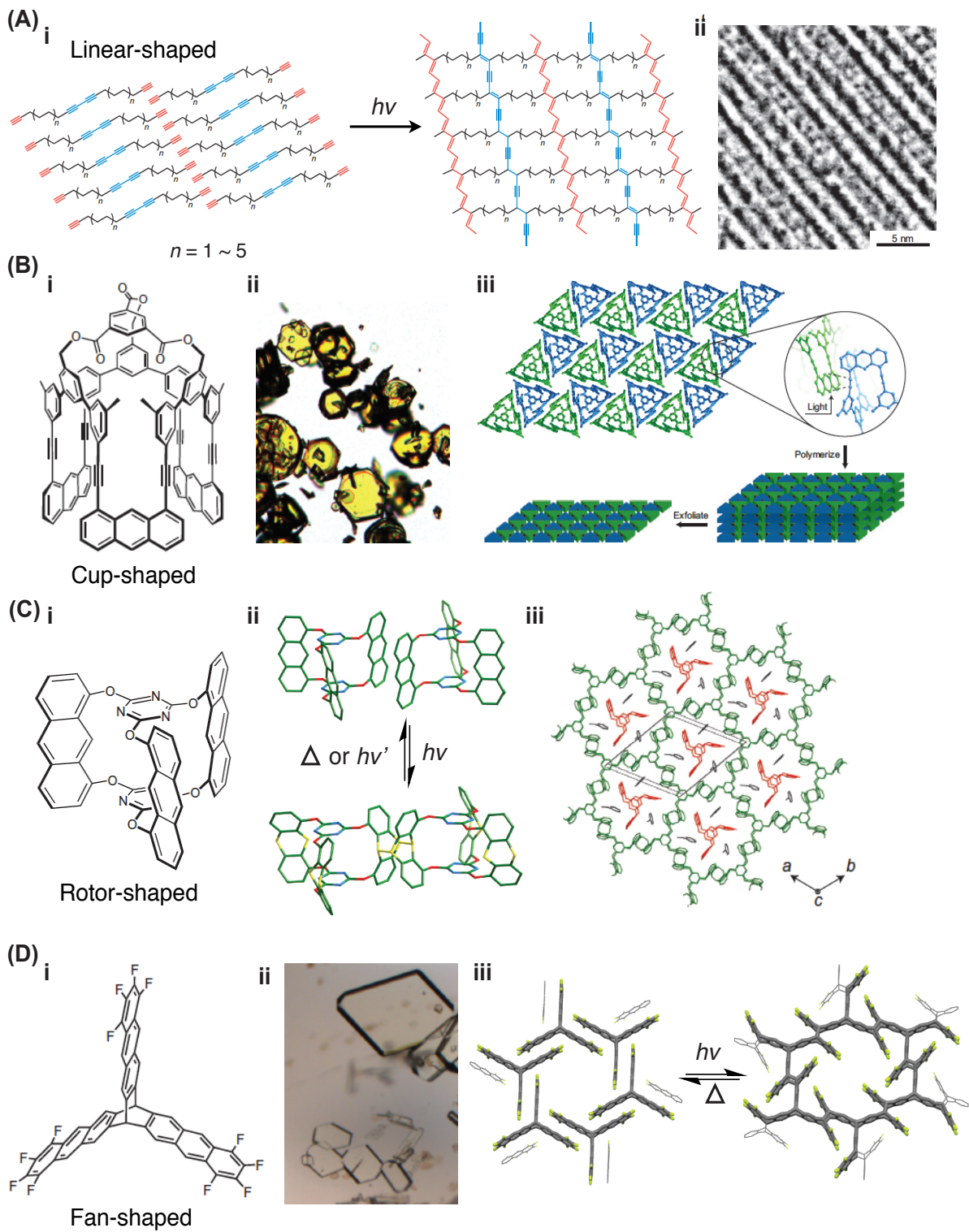


Figure 11 | Topochemical polymerizations in crystals to yield two-dimensional polymers. (A) Photochemically topochemical polymerization of linear-shaped monomers to form a 2D polymer consisting of linear polyacetylene and polydiacetylene chains (i), observed by STM (ii). (B) Photochemically topochemical polymerization of cup-shaped monomers in single crystal (i and ii) to form a 2D polymer through the [4 + 2]-cycloaddition of an alkyne and the 9,10-anthracene position (iii). (C) Reversible topochemical polymerization of rotor-shaped monomers in single crystal (i and ii) to form a 2D polymer on gram scales through the [4 + 4]-cycloaddition of anthracene (iii). (D) Reversible topochemical polymerization of fan-shaped monomers in single crystal (i and ii) to form a nanoporous 2D polymer through the [4 + 4]-cycloaddition of anthracene (iii).

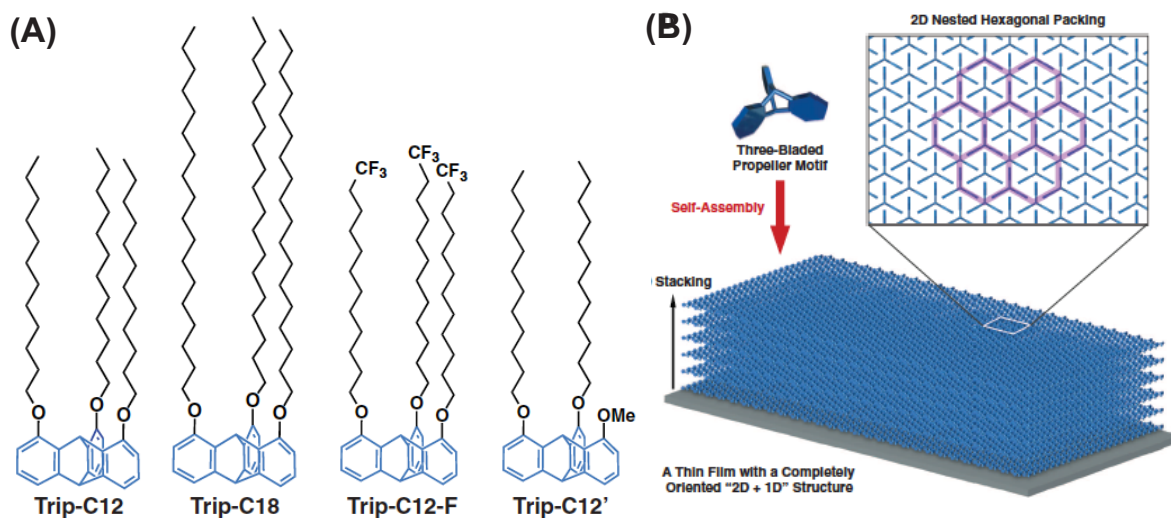


Figure 12 | The space-filling design to synthesize organic thin films with exceptional long-range structural integrity. (A) Molecular structures of a series of tripodal paraffinic triptycenes. (B) Space-filling model with a three-bladed, propeller-shaped motif, capable of forming a "2D hexagonal array + 1D multilayers" by the interpenetration of its propeller parts (nested packing).

1.4. Summary

In biological systems, long-range molecular order is crucial for the activities of living organisms. Although chemists devote to design and synthesize new architectures of material having superb features, this notion has inspired them to explore new methods to develop ordered solid-stated materials, especially in a large area, potentially utilized for the various devices and actuators. For polymers, controlling the orientation of polymer chains is processible, large-area, and high ordered in solid state, which is one of the key technologies for developing high-performance polymer-based devices. The preconceived notion has told us that polymer chains tend to lie down and be more preferably oriented horizontally on substrates. However, the physically difficult issue that how to make polymer chains vertically stand up or even homeotropic order on substrates has not been intensively explored to date, because of inherent flexibility and entanglement of polymer chains. For small molecules, their crytsals are known as an ordered strcture in solid state. However, such long-range molecular order is thermal-unstable when the constituent molecules are melted. In order to immobilize the macroscopic order in crystals, topochemical reactions in solid state is necessary to cross-link the small molecules to afford a 1D or 2D polymer.

Material science has been booming dramatically in the recent decades, benefitting by the development of solid-stated material. Under the above emergent backgrounds, the researches on cotrolled solid-stated molecular assembly up to a macroscopic order is of great significance for the basic science. In this PhD thesis, I mainly focus on the two individual works in terms of polymers and small molecules.

In Chapter 2 and 3, I proposed a design principle of polymers processable into a 2D homeotropic order. And in chapter 4, I present a topochemical cycloaddition of phthalonitriles to autocatalytically convert the crystalline fibers formed by the high pure metal-free phthalocyanines in one step.

Chapter

2

Solid-state Assembly Of Bottlebrush Polymers To 2D lattices

2D Rectangular, and hexagonal lattices are uncommon structures for polymer chains packing. Here, we found that the cylindrical polymers can be designed to possess oppositely oriented local dipoles in their cross section. The interaction of such local dipoles possibly forces cylindrical polymers to tightly connect bilaterally, affording a 2D rectangular lattice.

2.1 Introduction

As a linear configuration, the flexible or stereoregular polymer chains fold into 1D ordered lamellar lattice, in which folded chains in a lattice cell is isometric (I). However, 2D or 3D ordered lattices such as tetragonal, orthorhombic, and hexagonal system are very scarce for ordered polymer structures. Inspiring by the self-assembly of small molecules, design for a particular structure of polymer backbone or modification of the pendent groups in the side chains to construct a columnar structure are effective strategies to obtain 2D ordered lattices (2–18).

One of classical polymers with 2D ordered lattice is brush-like macromolecule with liquid crystalline columnar phase. It has been reported that n -alkyl substituted siloxane polymer exhibited a hexagonal columnar phase even if it has no discotic or rod-like mesogenic cores at all (2,3). Percec's group designed brush-like polymers carrying dendritic side groups, having a hexagonal columnar phase (4,5). In that work, he highlighted the huge steric

[1] See *Chapter 1, 1.1*.

[2] G. Ungar. *Mol. Cryst. Liq. Cryst.* **396**, 155 (2003).

[3] K. Okoshi *et al.* *Macromolecules* **35**, 4556 (2002).

[4] See *Chapter 1, 1.5*.

[5] B. M. Rosen *et al.* *Chem. Rev.* **109**, 6275 (2009).

[6] G. N. Mol, K. D. Harris, C. W. M. Bastiaansen, D. J. Broer. *Adv. Funct. Mater.* **15**, 1153 (2005).

[7] Y. Yu, M. Nakano, T. Ikeda. *Nature* **425**, 145 (2003).

[8] T. Ikeda, J. -I. Mamiya, Y. Yu. *Angew. Chem. Int. Ed.* **46**, 506 (2007).

[9] Y. Ohseido, I. Imae, Y. Shirota. *J. Polym. Sci., B: Polym. Phys.* **41**, 2471 (2003).

- [10] H. -L. Tu *et al.* *Macromolecules* **33**, 6315 (2000).
 [11] X. -Y. Yin *et al.* *J. Am. Chem. Soc.* **125**, 6854 (2003).
 [12] C. Ye *et al.* *Macromolecules* **37**, 7188 (2004).
 [13] C. -P. Chai *et al.* *Macromolecules* **40**, 9361 (2007).
 [14] H. -L. Xie *et al.* *J. Am. Chem. Soc.* **132**, 8071 (2010).

hindrance effect derived from dendritic side groups to induce this 2D columnar structure.

To directly introduce small liquid crystalline (LC) molecules into the side chains is a design method widespread used to enhance the organizing ability of polymer to form ordered structures. Furthermore, thermal-, photo-, and electric responsive behavior of these functional mesogens can be amplified in the side-chain LC polymers, which provide many possibilities to develop active soft materials (6–9). For 2D lattices, such molecular design is also available. Cheng's group firstly reported that a thermotropic LC polymer consisting of polyethylene (PE) backbone and phenyl lateral substituents showed a supramolecular hexagonal columnar LC phase (Figure 1A) (10,11). Afterwards, Zhou's group deeply investigated the phase structures of a series of side-chain LC polymers wrapped by “mesogen jacket” and discovered a hierarchical 2D rectangular lattices with biaxial orientation, in which semirigid backbones

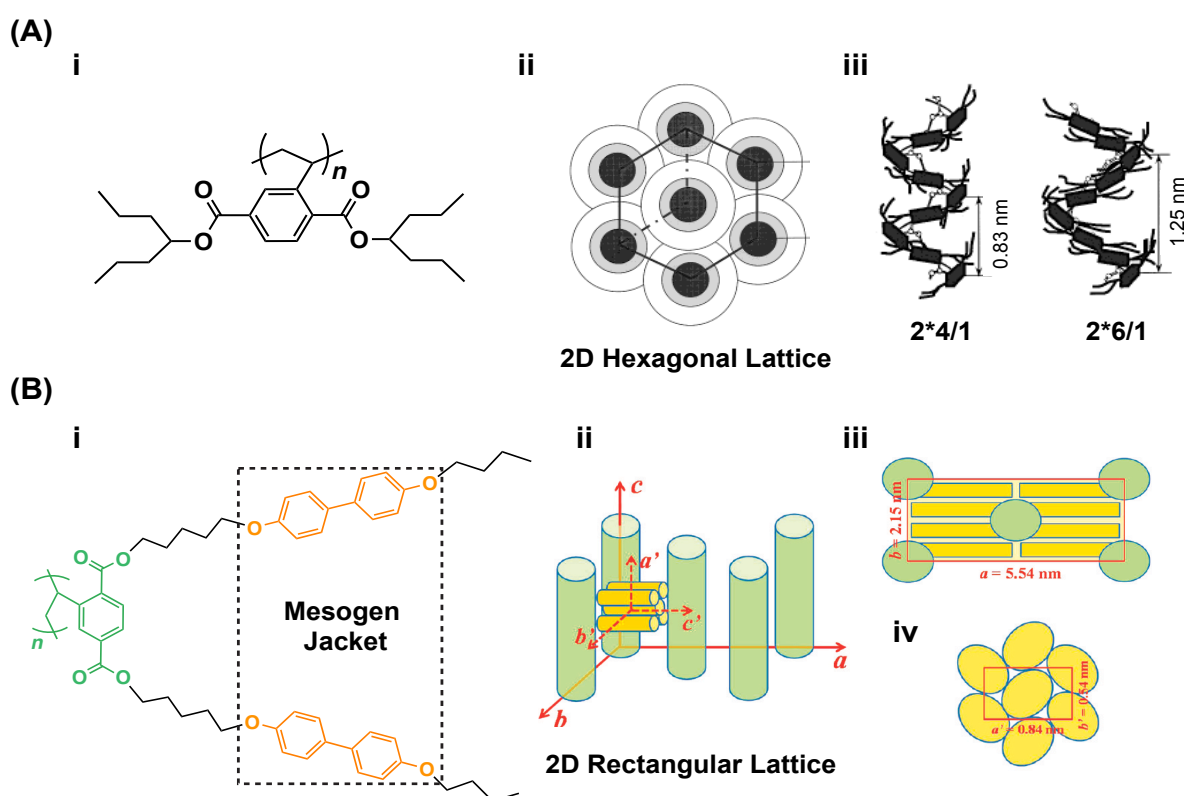


Figure 1 | 2D lattices of side-chain LC polymer. (A) Molecular structure (i) of the polymer pendent with phenyl lateral substituents and its schematic drawing (ii) of supramolecular hexagonal packing model. Polymer chains possibly display 2*4/1 and 2*6/1 helical conformations in a hexagonal lattice (iii).¹⁰ (B) Molecular structure (i) of the polymer wrapped by biphenyl “mesogen jacket” and its schematic drawing (ii–iv) of 2D rectangular packing model. Side view (ii) of the model shows a biaxial orientation, in which the backbones are parallel to the *c* axis (iii) while side chains are packed along to the *c'* axis (iv).¹⁴

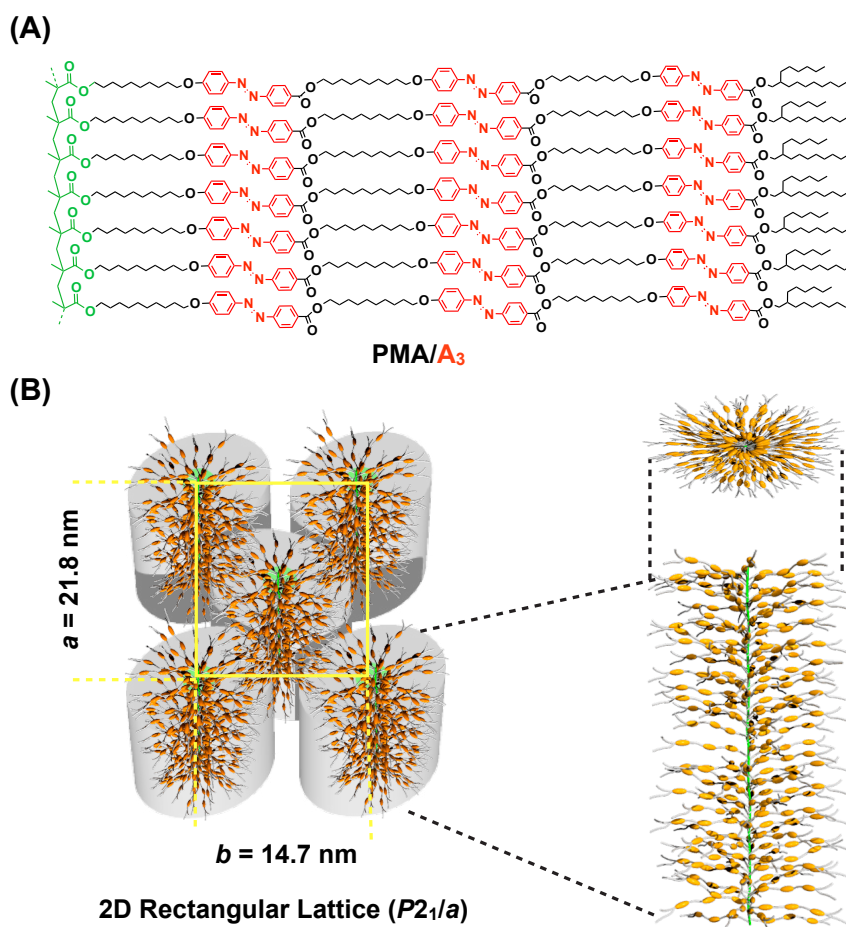


Figure 2 | 2D rectangular lattice formed by a bottlebrush polymer bearing mesogenic side chains.¹⁸ (A) Molecular formulae of the brush polymer (**PMA/A₃**) carrying three azobenzene units in the side chains. (B) Schematic illustration of a 2D rectangular lattice of **PMA/A₃**. The space group of this rectangular lattice is $P2_1/a$ with lattice parameters a and b of 21.8 nm and 14.7 nm, respectively, indicating that the polymer molecules adopt an elliptically cylindrical shape.

packed into a 2D rectangular lattice while side chains also formed a rectangular lattice, perpendicular attached to the backbones (Figure 1B) (12–14). In addition, some polymers containing discotic LC molecules in the side chains also can exhibit the 2D columnar phase (15–17).

In my work, the biggest difference from the known side-chain LC polymers is that the multi-mesogens instead of one are introduced into the side chains linked by aliphatic chains (Figure. 2A). Such particular bottlebrush-like molecular design not only enhances the intermolecular interaction but also affords a cylindrical shape, benefiting for the formation of 2D lattice. In pioneering work, we found that brush polymer (**PMA/A₃**) spontaneously packed into a 2D rectangular lattice ($P2_1/a$) on cooling from its isotropic state (Figure.

[15] P. Kohn, M *et al.* *Macromolecules* **45**, 5676 (2012).

[16] I. Tahar-Djebbar *et al.* *Chem. Mater.* **23**, 4653 (2011).

[17] Y. -F. Zhu *et al.* *Macromolecules* **45**, 3346 (2012).

[18] N. Hosono *et al.* *Science* **330**, 808 (2010).

2B), suggesting that brush polymer molecule adopts a cylindrical shape in bulk (18). Judging from the magnitudes of lattice parameters, a and b , the cylinders of **PMA/A₃** most likely deform elliptically to some extent and align parallel to one another without entanglement of their side chains. Inhere, there are still two questions we do not figure out:

(1) Why dose this bottlebrush polymer adopt a deformed cylindrical shape even in bulk?

(2) Why dose this bottlebrush polymer pack into a 2D rectangular lattice?

In this chapter, I will answer the above two questions. Followed by the previous design principle, we similarly designed several new polymers by tuning the types and number of mesogen in side chains, and the structure of polymer backbone. Through a systematic study on their lattice structures, we deeply analyze the mechanism of self-assembly behavior of these bottlebrush polymers in bulk.

2.2. Results and Discussion

2.2.1. Design and Synthesis of Polymers

In light of the previous molecular structure (**PMA/A₃**), we can easily tune the structures of mesogens and polymer backbones. Inhere, three kinds of polymer backbones, polymethacrylate (**PMA**), polyacrylate (**PA**) as well as polyphenylacetylene (**PPA**) and three new kinds of mesogens, biphenyl (**B**), tolan (**T**), and azobenzene (**A**) are rearranged and combined into these polymers (Figures. 3B and 3C). Without α -methyl group, **PA** chain is more flexible than **PMA** chain. As one of typical helical polymers, **PPA** is composed of conjugated polyacetylene and phenyl side groups (19). Meanwhile, biphenyl is one of basic mesogenic cores to establish the rod-like LC molecules. Tolani, two phenyl rings connected by a carbon triple-bond, has a larger aspect ratio than biphenyl and azobenzene. For the purpose of investigating possible effects of dipoles in the side chains,

[19] E. Yashima, K. Maeda, H. Iida, Y. Furusho, K. Nagai. *Chem. Rev.* **109**, 6102 (2009).

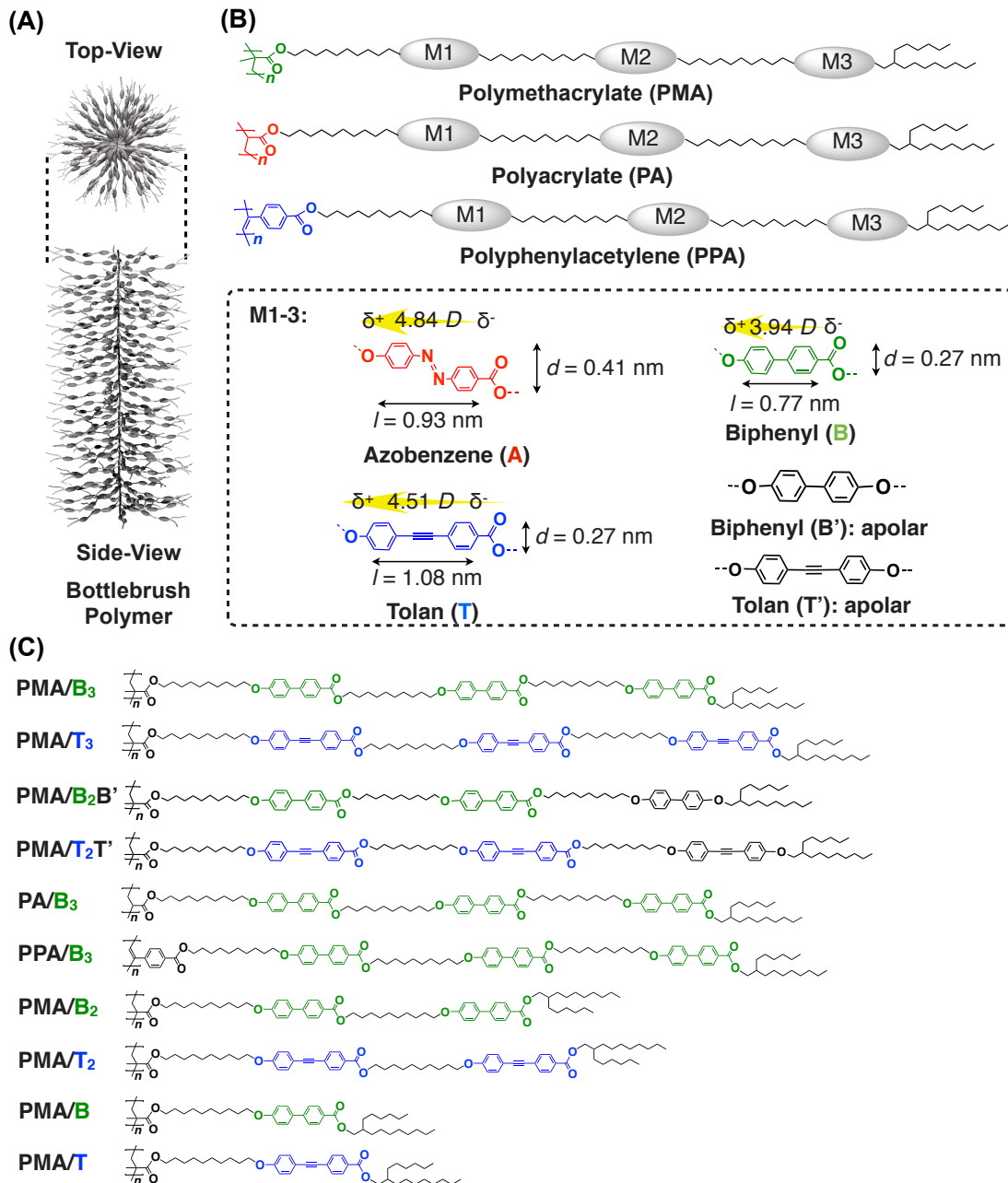


Figure 3 | Molecular structures of bottlebrush polymers bearing different mesogenic side chains. (A) Schematic illustration of a bottlebrush polymer adopting a cylindrical shape. (B) Three kinds of polymer backbone and four kinds of mesogenic core with different aspect ratio. l and d refers to the length of long and short axis of a mesogen, respectively. Yellow arrows denote direction of dipole moment of a mesogen. (C) Molecular formulae of polymers bearing different mesogenic side chains.

[20] B. -Z. Tang, W. -H. Poon, S. -M. Leung, W. -H. Leung, H. Peng. *Macromolecules* **30**, 2209 (1997).

[21] S. Abe *et al.* *J. Am. Chem. Soc.* **131**, 6958 (2009).

[22] See 2.4 Supporting Informations.

we prepared **PMA/B₂B'** and **PMA/T₂T'** as references where the outermost mesogenic unit (M3 in Figure. 3B) is connected at its both sides by ether oxygen atoms unlike other cases such as **PMA/B₃** and **PMA/T₃**, where an electronically push-pull structure is utilized for the incorporation of all mesogenic units (Figure. 3C). Additionally, we also investigated side-chain length effect by decreasing the number of mesogens in the side chains.

In this work, monomers were prepared by stepwise condensation of mesogen-containing precursory acids (Scheme S1–S4 in Supporting Information). To obtain polymeric compounds, **PMA** and **PA** derivatives were synthesized by free radical polymerization of the corresponding monomers in the presence of 2,2'-azobis(isobutyronitrile) (AIBN) in benzene solution, while a **PPA** derivative was obtained by olefin metathesis polymerization using Rh(nbd)BPh₄ as a catalyst in chloroform medium (20,21). After polymerization, the raw products were purified by recycling preparative size-exclusion chromatography (*re*-SEC) to remove unreacted monomers. The yield, molecular weight, degree of polymerization and polydistribution of the synthesized polymers are summarized in Table S1 (22), as determined by size-exclusion chromatography (SEC) analysis based on polystyrene standards.

2.2.2. Thermal Properties of Polymers

Thermal properties of polymers were studied by differential scanning calorimetry (DSC) and summarized in Table S2. Figure 4 presents their phase transition behavior. As shown in DSC traces of the second heating and cooling circulation (Figure. S1), apart from **PA/B₃** and **PMA/B₂B'**, residual bottlebrush polymers with three mesogens displayed two exothermic peaks on cooling from isotropic state indicating the presence of mesophase (Figure. S1), which is consistent with the previous **PMA/A₃**. By contrast, polymers bearing shorter

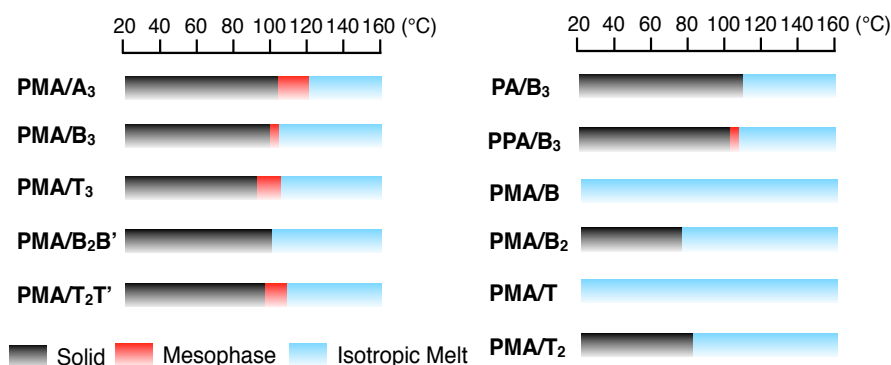


Figure 4 | Phase transition behavior of polymers. Thermal properties are characterized by DSC, recorded the second heating/cooling cycles. The scan rate is 5 °C/min.

side chains did not show a mesophase (Figures. S1A, S1B and S1D, S1E). It is worthy of noting that the phase transition behaviors of the bottlebrush polymers are mainly determined by the types of mesogens rather than that of the polymer backbone. For example, **PMA/B₃**, **PA/B₃** and **PPA/B₃** upon cooling from their isotropic melt underwent a phase transition at nearly the same temperature (Figures. S1C, S1I and S1J), whereas the mesophase temperature range of **PMA/A₃** with only the azobenzene side chains (120–103 °C) was apparently higher than those of **PMA/B₃** (104–99 °C, see Figure. S1C) and **PMA/T₃** (105–92 °C, see Figure. S1F).

2.2.3. X-Ray Scattering Analysis of Polymers

2.2.3.1. Mesogen Effects

In the pioneering work, **PMA/A₃** spontaneously packed into a 2D rectangular lattice ($P2_1/a$) on cooling from its isotropic state (18). In accordance with previous **PMA/A₃**, synchrotron radiation small-angle X-ray scattering (SAXS) pattern of a bulk sample of **PMA/B₃**, measured at 100 °C (mesophase) in a glass capillary displayed clear diffraction peaks (Figure. 5A, i) assignable to a 2D rectangular lattice (space group; $P2_1/a$) with lattice parameters a and b of 19.9 nm and 14.2 nm, respectively (Table. S3), suggesting that **PMA/B₃**

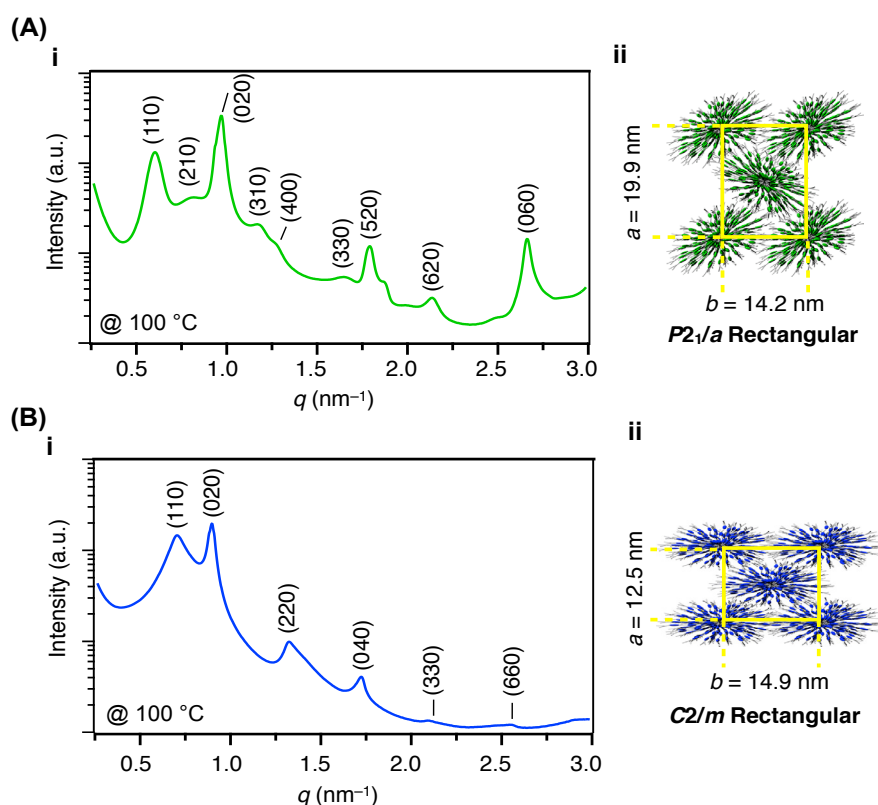


Figure 5 | Self-assembled structures of bottlebrush polymers carrying three mesogens in bulk. 1D SAXS patterns (i) and schematic illustrations of 2D rectangular lattices (ii) of bulk samples of (A) **PMA/B₃** and (B) **PMA/T₃** in a glass capillary ($\phi = 1.5$ mm), measured at 100 °C (mesophase) on cooling from their isotropic melts. Miller indices are given in parentheses.

adopts a cylindrical shape but deforms elliptically and its long axis of cylinder inclines with respect to a and b axes of lattice to some extent (Figure. 5A, ii). On the other hand, the diffraction peaks in the SAXS pattern of a bulk sample of **PMA/T₃** at its mesophase (100 °C) (Figure. 5B, i) were well assigned to a $C2/m$ rectangular lattice with lattice parameters a and b of 12.5 nm and 14.9 nm, respectively (Table. S4). Although **PMA/T₃** similarly adopts an elliptical cylinder, its long axis aligns parallel to the b axis of lattice (Figure. 5B, ii). Temperature-dependent SAXS patterns (Figures. S2A and S3A) indicated that such 2D rectangular lattices were formed initially in mesophase and solidified to room temperature. In the wide-angle X-ray diffraction (WAXD) profiles of **PMA/B₃** and **PMA/T₃** (Figures. S2B and S3B), a broad peak (halo) with d -spacing of 0.44 nm above mesophase temperature was observed. However, when cooling to the room temperature, the broad peak of **PMA/T₃** split into a trapezoidal scattering peak between 13–16 nm⁻¹ in q value, suggesting that tolans perform a better organizing ability than biphenyls.

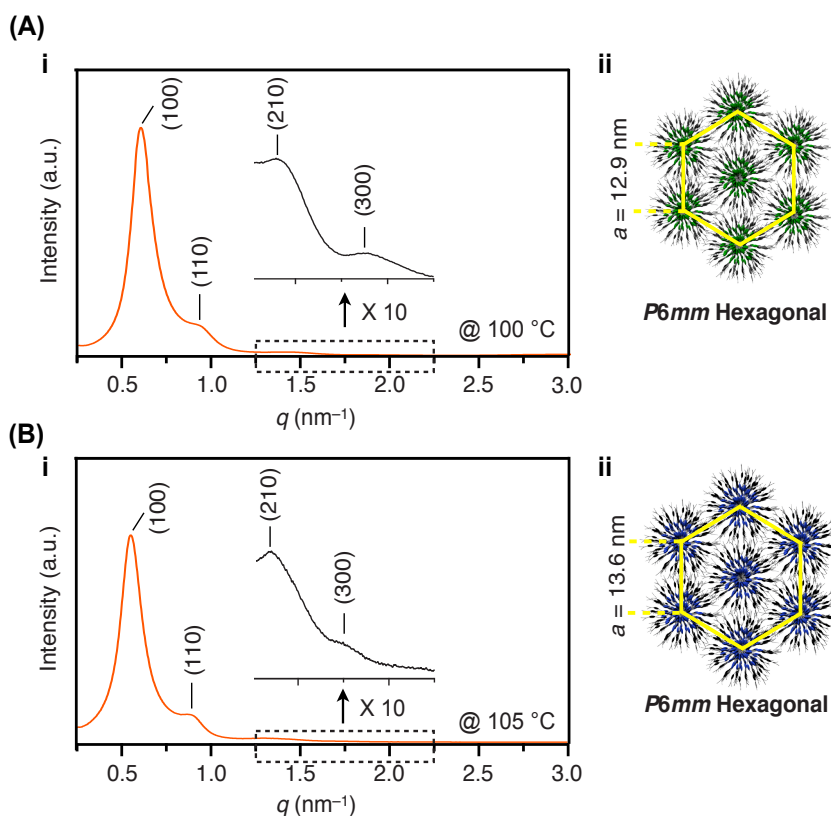


Figure 6 | Self-assembled structures of brush polymers containing an apolar mesogen in bulk. 1D SAXS patterns (i) and schematic illustrations of 2D lattices (ii) of bulk samples of (A) **PMA/B₂B'** and (B) **PMA/T₂T'** in a glass capillary ($\phi = 1.5$ mm), measured at 100 °C (mesophase) on cooling from their isotropic melts. Miller indices are given in parentheses.

Later on, we evaluated the self-assembled structures of two bottlebrush polymers containing an apolar mesogen at outmost position (M3 in Figure 3B) by SAXS (Figure. 6, Figures. S4 and S5). To our big surprise, diffraction peaks corresponding to (100), (110), (210) and (300) planes of lattice clearly demonstrated that independent on the nature of mesogens, **PMA/B₂B'** and **PMA/T₂T'** packed into a highly symmetric *P6mm* hexagonal lattice with lattice parameter a of 12.7 nm and 13.6 nm in their mesophase, respectively (Tables. S5 and S6), which means that a regular cylinder is adopted by their brush molecules (Figure. 6, ii).

Here, why do the 2D lattices of bottlebrush polymers transform from rectangular to hexagonal lattice, by merely replacing the ester group in the outmost mesogen (M3 in Figure 3B) with ether oxygen atoms? In many similar cases of polar liquid crystals with a rod-like shape, they tend to align parallel and form layered structure (smectic) in such way that their dipoles are cancelled out antiparallely in layers

- [23] P. J. Sebastiao, P. S. Carvalho, M. R. Chaves, H. T. Nguyen, A. C. Ribeiro. *Eur. Phys. J. E.* 10119-2 (2006).
- [24] L. Longa, W. H. de Jeu. *Phys. Rev. A* **28**, 2380 (1983).
- [25] Y. Lansac, M. A. Glaser, N. A. Clark. *Phys. Rev. E* **64**, 051703 (2001).
- [26] E. J. Foster, R. B. Jones, C. Lavigueur, V. E. Williams. *J. Am. Chem. Soc.* **128**, 8569 (2006).
- [27] T. Osawa *et al.* *Angew. Chem. Int. Ed.* **51**, 7990 (2012).

(23–25). Inspired from this notion, I highlighted a dipole-dipole interaction of polar mesogens. Taking **PMA/T₃** as an example, all three mesogenic units in its individual side chains are polarized along the same direction by the attachment with an electron-withdrawing ester carbonyl group and an electron-donating ether oxygen atom (Figure. 3B). Consequently, its individual side chains bear a large dipole from the terminus to the backbone core (Figure. 7A).

Further to note, **PMA/T₃**, which assembles into a 2D rectangular lattice, is deformed ellipsoidally in its cross section, where oppositely-oriented local dipoles are supposed to emanate from the terminus (Figure. 7B). Although these local dipoles are cancelled with one another within each cylinder, they can be locally interactive with those of neighboring columns. Namely, such ellipsoidally deformed cylinders are tightly connected bilaterally *via* a dipole–dipole interaction and form a 2D assembly with a rectangular geometry (Figure. 7B). The similar effect has been also observed in the columnar liquid crystal consisting of triphenylenehexacboxyester derivative (26,27).

To the contrary, without a dipole-dipole interaction, **PMA/B₂B'** and **PMA/T₂T'** containing an apolar **B** or **T** at the outmost did not follow the above scenario. As a result, the side chains of both two polymers weakly interact with one another and extend isotropically to form an entropically favored round shape, which stably packs into a more symmetric hexagonal lattice rather than anisotropic rectangular lattice (Figure. 7C). A tiny structural discrepancy such as a substituent group, to induce totally different lattices is beyond our expectations.

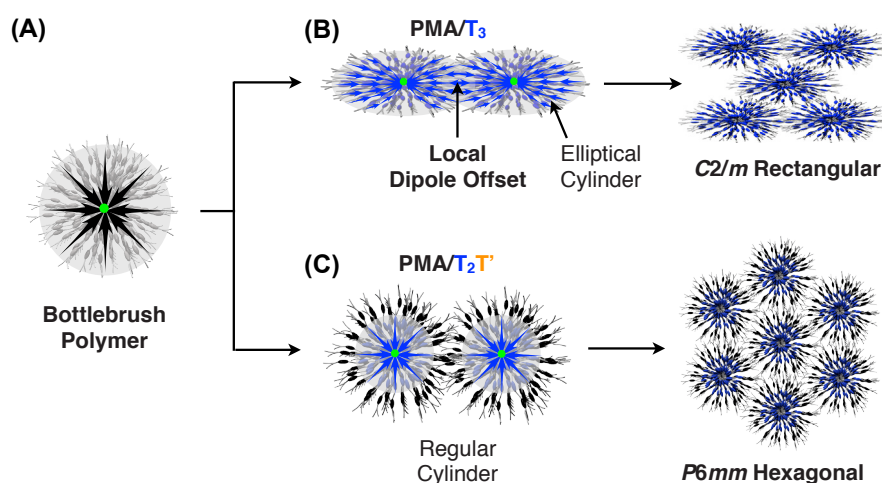


Figure 7 | Schematic illustrations of formation mechanism for 2D rectangular and hexagonal lattices.

2.2.3.2. Side-chain Length Effect

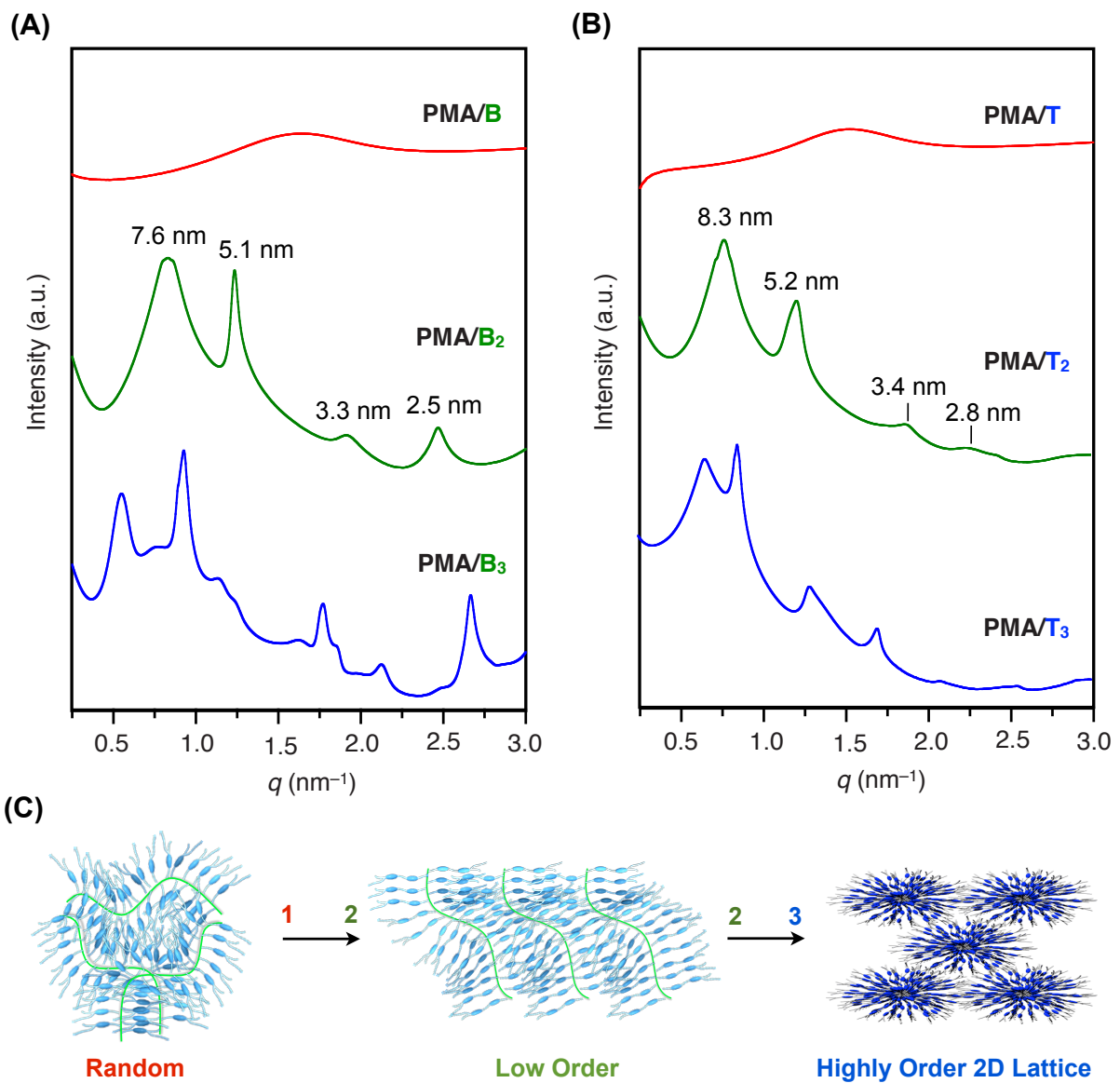


Figure 8 | Solid-stated structures of polymers bearing shorter side chains. 1D SAXS patterns of bulk samples of (A) PMA/B_n ($n = 1, 2, 3$) and (B) PMA/T_n ($n = 1, 2, 3$) in a glass capillary ($\phi = 1.5$ mm), measured at 25 °C (solid) on cooling from their isotropic melts. A reasonable structure ascribable to the diffraction peaks could not be determined in the cases of PMA/B₂ and PMA/T₂. (C) Schematic illustrations of solid-stated structures of polymers bearing one, two, and three mesogens.

Polymers bearing shorter side chains show another organizing behavior in the solid state. **PMA/B** and **PMA/T** with only one mesogen showed a glass state at room temperature. In their SAXS patterns (Figure. 8A and 8B), no diffraction peak was observed, implying a randomly amorphous structure (Figure. 8C). In the cases of solid-stated **PMA/B₂** and **PMA/T₂**, all of the observed diffraction peaks were broad and failed to assign to a possible model structure. This result further indicated that the polymer with less than three mesogenic units in their side chains gave ill-defined structures. As previous discussion, unidirectional dipole repulsion provided by polar mesogens plays a key role on the formation of cylindrical shape. Therefore, it is reasonable to speculate that insufficient expelled force is afforded by the dipole-dipole interaction of mesogens in the side chains if the number of mesogen is less than three.

¹H NMR spectroscopy of polymers in CDCl₃ solution can well reflect the conformation of single polymer molecule. ¹H NMR spectra range from 6.5–8.5 ppm of monomer and polymers are given in Figure 9. In ¹H NMR spectrum of monomer (Figure. 9A), four well split peaks attributed to four kinds of protons in an asymmetric biphenyl group were observed. After polymerization, peaks shifted and became overlapped in the case of **PMA/B** (Figure. 9B), which is very common for polymer systems. But, to our surprised, it is unusual that the peaks of biphenyl groups in **PMA/B₂** did not become broader but instead, further split into two groups, which are identical to those peaks of monomer (**MA/B**) and polymer (**PMA/B**) (Figure. 9C). Furthermore, more distinctly split peaks appeared in the spectrum of **PMA/B₃** (Figure. 9D), in which the integrated ratio between the split peaks and overlapped peaks was 2/1. It is clear that there are two environments for biphenyl units in the side chains of **PMA/B₃**. Due to a crowded surrounding, the ones closest to the backbone (dark green region in Figure 9D) display overlapped peaks, same to the **PMA/B**. But, the ones far from the backbone (light green region in Figure 9D) are likely located in the least congests environment, and show split peaks, which are identical to the peaks of monomer. Judging from the ratio of crowded and free ones, **PMA/B₃** most likely adopts a regular cylindrical shape as shown in Figure 9D. The NMR results further confirm that a cylindrical structure is so essential to form a 2D lattice.

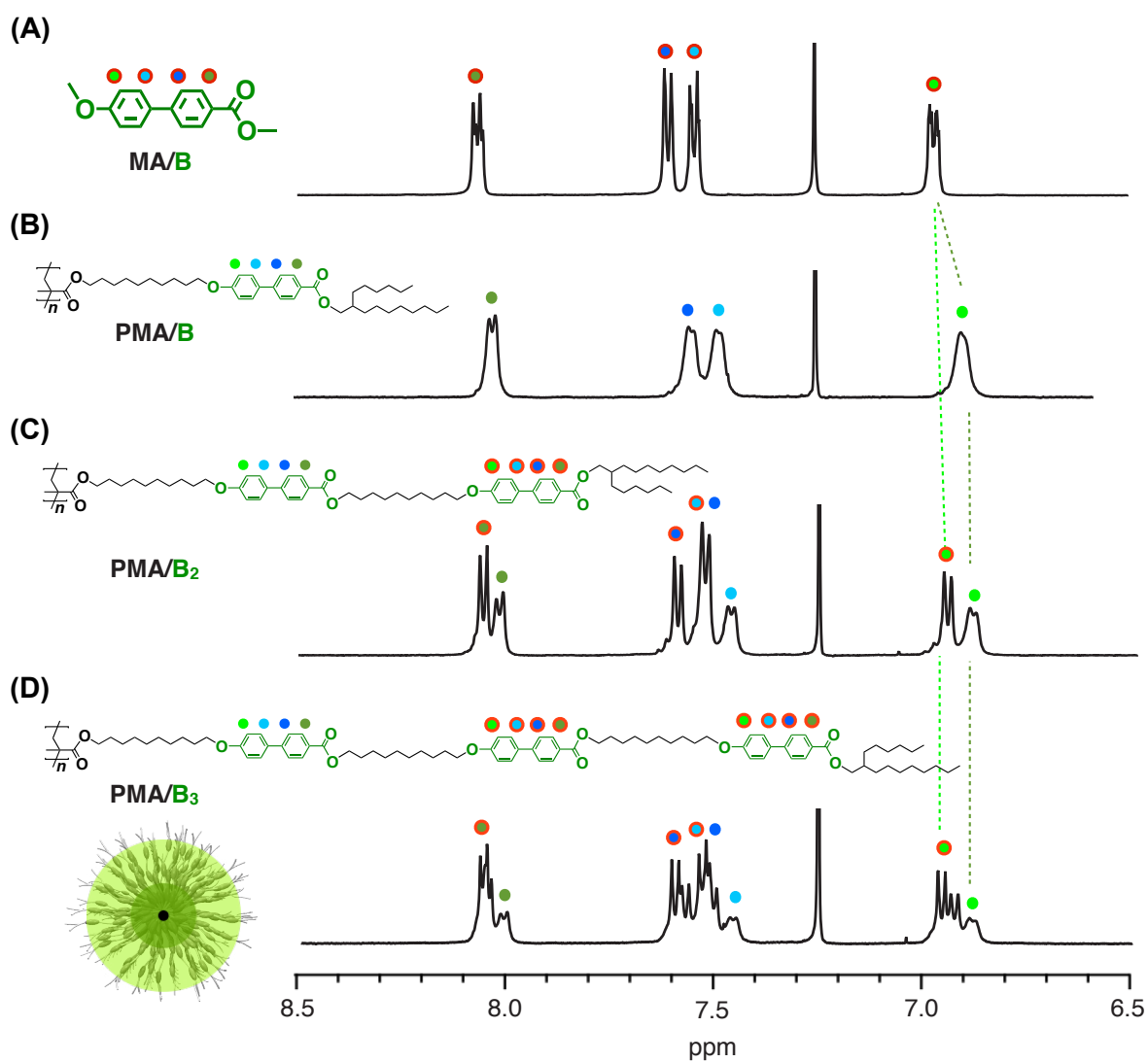


Figure 9 | ^1H NMR spectra of biphenyl units of monomer and polymers in CDCl_3 solution. (A) MA/B, (B) PMA/B, (C) PMA/B₂, and (D) PMA/B₃ are selected from 6.5 to 8.5 ppm. In a cylindrical shape, side chains of PMA/B₃ extend isotropically without entanglement.

2.2.3.3. Polymer Backbone Effect

[28] K. Ishitake et al. *Angew. Chem. Int. Ed.* **48**, 1991 (2009).

[29] K. Ishitake et al. *Macromolecules* **44**, 9108 (2011).

[30] J. G. Rudick. *Acc. Chem. Res.* **41**, 1641 (2008).

[31] Jacky. W. Y. Lam, B. -Z. Tang. *Acc. Chem. Res.* **38**, 745 (2005).

Despite such a high sensitivity to the side-chain structure, the polymer backbone does not play an essential role for lattice structures. In the SAXS pattern of **PA/B₃** (Figures. 10A and S6), the observed diffraction peaks were assignable to *P2/a* rectangular lattice and the lattice parameters *a* and *b* were of 13.8 nm and 14.3 nm, respectively (Table. S7). However, in the case of **PPA/B₃** (Figures. 10B and S7), the diffraction peaks well agreed with a *C2/m* rectangular lattice (lattice parameters; *a* = 11.2 nm and *b* = 13.8 nm, Table. S8). By contrasting the configurations of *P2/a* and *C2/m* lattices along with *P2₁/a* lattice of **PMA/B₃**, it is found that the cylinders of polymer deform more elliptically from **PMA/B₃**, **PPA/B₃**, to **PA/B₃**, possibly resulted from the various configurations of polymer backbones. It has been reported that a highly isotactic polymethacrylate (**PMA**) pendent bulky groups were obtained just by free radical polymerization (28,29). Also, polyphenylacetylene (**PPA**) generally performs *trans-cis* and *cis-cis* configurations in its backbone (30,31).

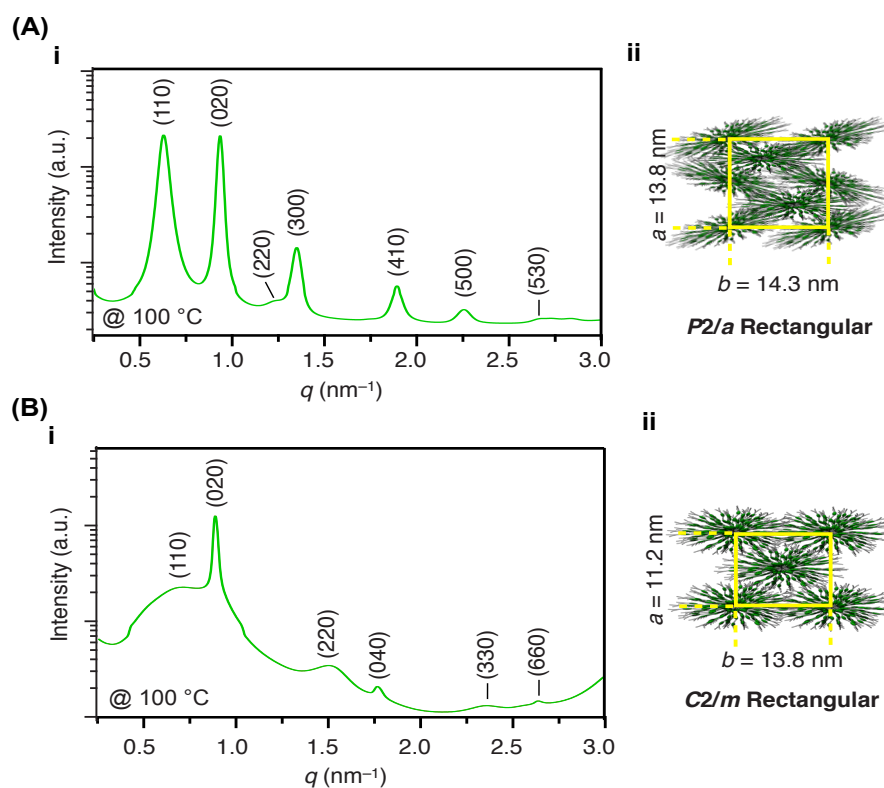


Figure 10 | Self-assembled structures of brush polymers with different backbones in bulk. 1D SAXS patterns (i) and schematic illustrations of 2D rectangular lattices (ii) of bulk samples of (A) **PA/B₃** and (B) **PPA/B₃** in a glass capillary ($\phi = 1.5$ mm), measured at 100 °C on cooling from their isotropic melts. Miller indices are given in parentheses.

2.3. Conclusion

It is well known that a columnar structure is essential for constructing 2D ordered lattices. In 2010, our group reported that a bottlebrush polymer self-assembled into a 2D rectangular lattice. Behind this interesting self-assembled phenomenon, there is a basic question need to make clear: why dose this brush polymer adopt a cylindrical shape and pack into a 2D rectangular lattice?

In order to search for the answers, I design several similar brush polymers consisted of different mesogens, side-chain length, and backbones. Through a deep investigation, I found that the side-chain length and the structure of backbone are two inherent elements to determinate the shape of polymer molecule in solution. Three mesogens are needed to afford sufficient expelled force and make backbone straightly extended (Figure. 11A). A regular cylindrical polymer grafted isotropically extended side chains is composed of polymethacrylate as a backbone and three mesogens in side chains (Figure. 11B).

On the other hand, mesogen and dipole-dipole interaction are two acquired characters to tune the cylindrical shape of polymer in bulk and induce different 2D lattices such as rectangular and hexagonal lattice (Figures. 11C and D). More elliptical cylinders manipulated by dipole-dipole interaction tend to pack into different rectangular lattices but without a dipole, a hexagonal lattice is dominated. I believe that these molecular design principles provide a new insight not only on the self-assembly of polymers but also on the homeotropic orientation in the next chapter.

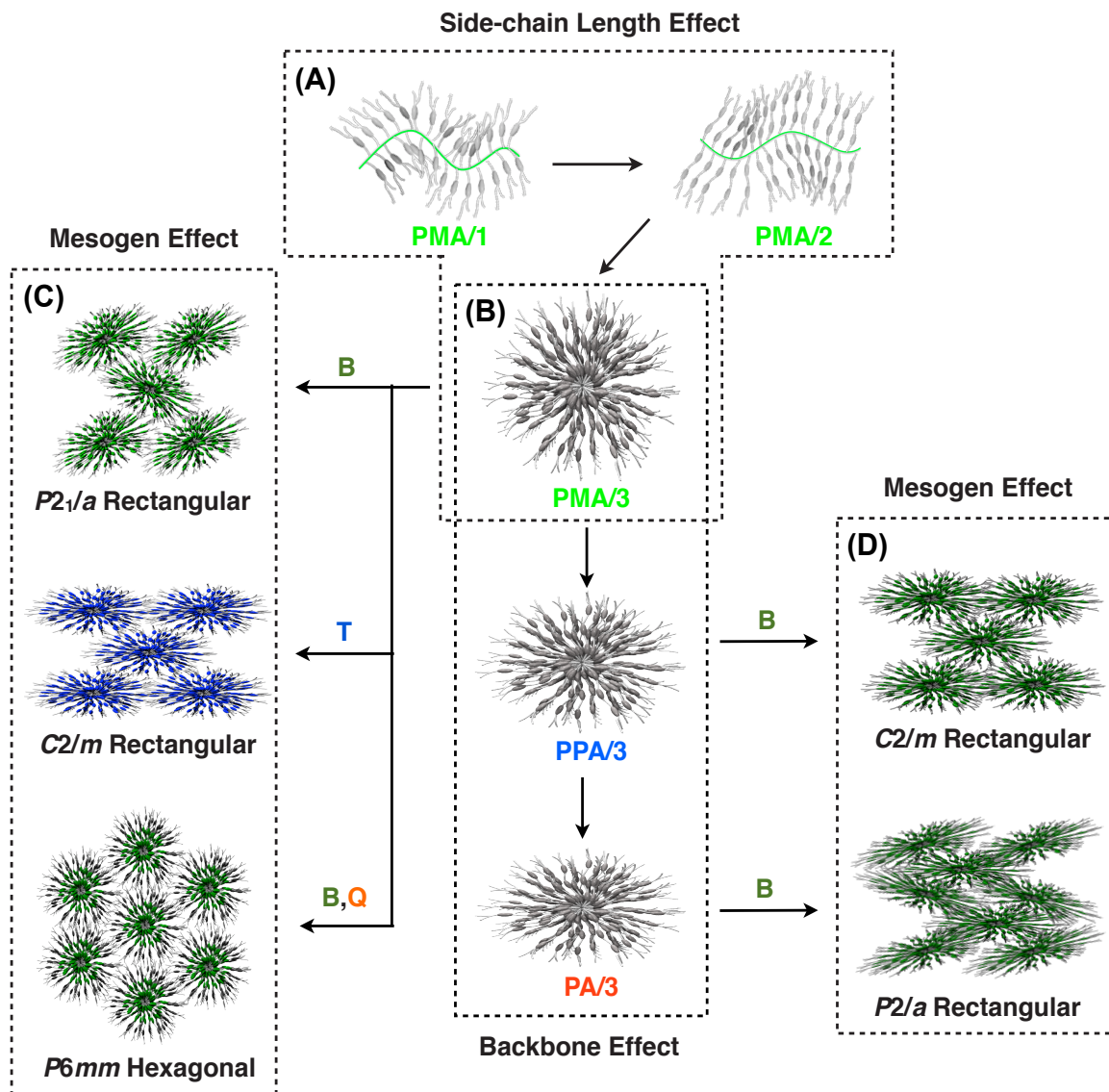


Figure 11 | Schematic illustrations of 2D rectangular and hexagonal lattices formed by cylindrical brush polymers. Three main factors, side-chain length (A), backbone (B), and mesogen (C and D) affect lattice structures. PMA, PPA, and PA refer to polymethacrylate, polyacrylate and polyphenylacetylene, respectively. B, T, and Q refer to biphenyl, tolan, and quaterthiophene, respectively.

2.4. Supporting Information

2.4.1. Materials and Methods

Materials Unless otherwise noted, reagents were used as received from Aldrich Chemical [2-hexyl-1-decanol, and ethyl 4-hydroxy-4'-biphenylcarboxylate], Tokyo Chemical Industry [10-bromo-1-decanol, tert-butyldimethylchlorosilane (TBDMSCl), trimethylsilylacetylene, and tetrabutylammonium fluoride (TBAF, 1 M in tetrahydrofuran (THF)), and tetrakis(triphenylphosphine)palladium], and Wako Pure Chemical Industries [N,N'-diisopropylcarbodiimide (DIPC), *p*-toluenesulfonic acid monohydrate, 4-dimethylaminopyridine (DMAP), triethylamine, 4,4'-biphenol, 2,2'-azobisisobutyronitrile (AIBN), 4-iodophenol, methacryloyl chloride, acryloyl chloride, imidazole, CuI, Cs₂CO₃, Na₂CO₃ and KOH]. 4-(Dimethylamino)pyridinium 4-toluenesulfonate (DPTS) (32), 10-Bromodecyl tert-butyldimethylsilyl ether (18), 1-bromo-2-hexyldecane (33), 4-ethynylbenzoic acid (34), Rh(nbd)BPh₄ (35), were prepared according to reported procedures. CH₂Cl₂ was dried over CaH₂ and freshly distilled prior to use. THF was refluxed over a mixture of Na and benzophenone and freshly distilled before use. Other dehydrated solvents were purchased from Wako Pure Chemical Industries or Kanto Chemicals.

General Column chromatography was carried out with Wakogel silica C-300 (particle size: 45–75 μm). Recycling preparative size-exclusion chromatography (SEC) was performed using JAIGEL 2H and 2.5H columns on a JAI model LC-9201 recycling HPLC system equipped with a JASCO model MD-2010 Plus variable-wavelength UV-Vis detector with CHCl₃/MeOH (100/1 v/v) as an eluent. Analytical SEC was performed at 40 °C on a TOSOH model HLC-8220 GPC system equipped with a refractive index (RI) detector, using CHCl₃ as an eluent at a flow rate of 0.35 mL min⁻¹ on linearly connected two polystyrene gel columns (TSKgel SuperHM-M, TOSOH). The molecular weight calibration curve was obtained by using standard polystyrenes (Shodex STANDARD SM-105, Showa Denko). ¹H and ¹³C NMR spectra were recorded on a JEOL model JNM-ECA500 spectrometer, operating at 500 and 125 MHz, respectively, where chemical shifts (δ in ppm) were determined with respect to tetramethylsilane as an internal reference. Matrix-assisted laser desorption ionization time-of-flight (MALDI-TOF) mass spectrometry was performed on an Applied Biosystems model MDS SCIEX 4800 Plus MALDI TOF/TOF™ Analyzer using dithranol as a matrix. Infrared (IR) spectra were recorded at 25 °C on a JASCO model FT/IR-4100 Fourier transform infrared spectrometer with an attenuated total reflection (ATR) equipment (ATR PRO450-S). Differential scanning calorimetry (DSC) was performed on a Mettler–Toledo model DSC differential scanning calorimeter, where temperature and enthalpy were calibrated

[32] J. S. Moore, S. I. Stupp. *Macromolecules* **23**, 65 (1990).

[33] S. Stas, S. Sergeev, Y. Geerts. *Tetrahedron* **66**, 1837 (2010).

[34] E. Yashima, T. Matsushima, Y. Okamoto. *J. Am. Chem. Soc.* **119**, 6345 (1997).

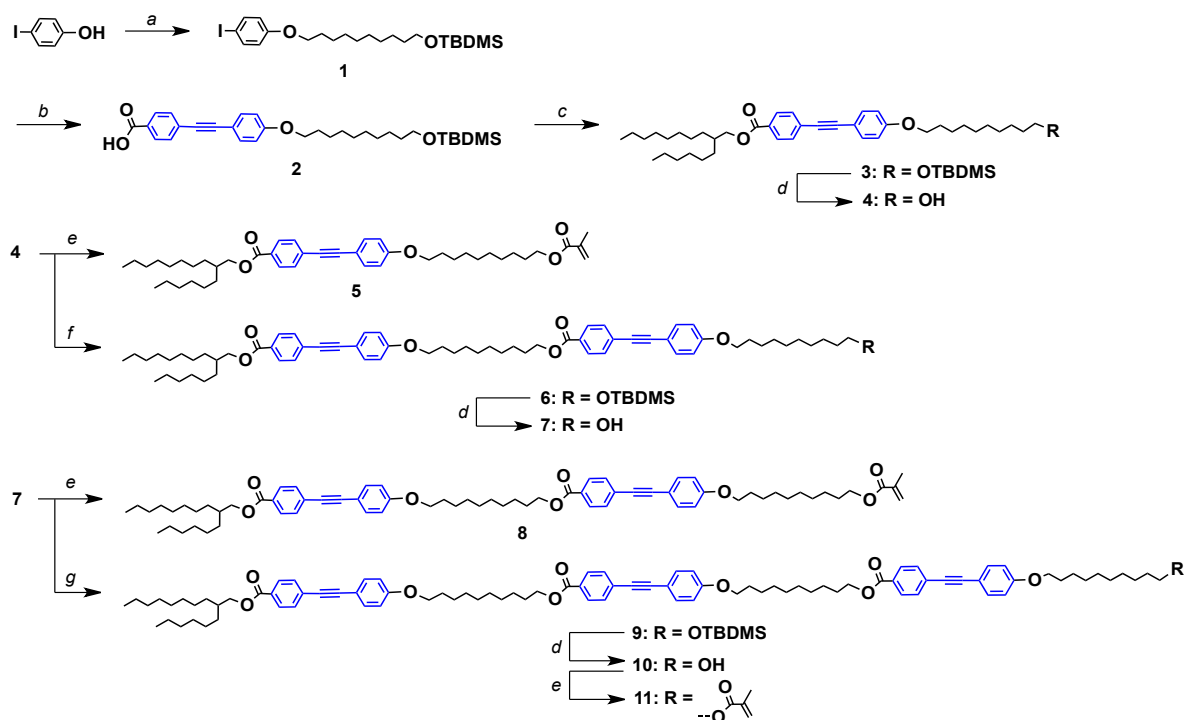
[35] R. Schrock, J. A. Osborn. *Inorg. Chem.* **9**, 2339 (1970).

[36] <http://www.esrf.eu/computing/scientific/FIT2D/>
 [37] http://homepage2.nifty.com/~hsc/soft/cellcalc_e.html.

[38] M. J. Frisch *et al.* Gaussian 03, Gaussian, Inc., Wallingford CT (2004).

with In (430 K , 3.3 J mol^{-1}) and Zn (692.7 K , 12 J mol^{-1}) standard samples using sealed Al pans. Cooling and heating profiles were recorded and analyzed using the Mettler–Toledo STARE software system. Small-angle X-ray scattering (SAXS) and wide-angle X-ray diffraction (WAXD) experiments were carried out at BL45XU in SPring-8 (Hyogo, Japan) with an imaging plate area detector, a R-Axis IV++ (Rigaku). Scattering vector, $q = 4\pi\sin\theta/\lambda$, and position of incident X-ray on the detector were calibrated using several orders of layer reflections from silver behenate ($d = 58.380\text{ \AA}$), where 2θ and λ are scattering angle and wavelength of X-ray (1.0 \AA), respectively. The sample-to-detector distances for SAXS and WAXD measurements were 2.0 and 0.4 m , respectively. The scattering/diffraction images recorded were integrated along the Debye-Scherrer ring, affording one-dimensional intensity data using the FIT2D software (36). The cell parameters were refined using the CellCalc ver. 2.10 software (37). Bulky samples were placed into a $1.5\text{ mm-}\phi$ glass capillary in a temperature-controlled heating block and once heated to isotropic melt. The resultant samples were then exposed to an X-ray beam for 10 (WAXD) or 100 (SAXS) seconds at given temperatures. Dipole moments of three mesogens **A**, **B** and **T** were calculated with the density functional theory (DFT) method at the B3LYP/6-31G(d) level using a Gaussian 03 packageS8 (38).

2.4.2. Synthesis



Scheme S1 I Synthesis of **5**, **8** and **11**. Reagents and conditions: (a) 10-bromodecyl tert-butyldimethylsilyl ether, Cs_2CO_3 , DMF, $70\text{ }^\circ\text{C}$; (b) 4-ethynylbenzoic acid, CuI, triethylamine, tetrakis(triphenylphosphine) palladium, THF, reflux; (c) 2-hexyl-1-decanol, DPTS, DIPC, CH_2Cl_2 , $25\text{ }^\circ\text{C}$; (d) TBAF, THF, $25\text{ }^\circ\text{C}$; (e) methacryloyl chloride, triethylamine, CH_2Cl_2 , $25\text{ }^\circ\text{C}$; (f) **2**, DPTS, DIPC, CH_2Cl_2 , $25\text{ }^\circ\text{C}$; (g) **2**, DPTS, DIPC, CH_2Cl_2 , $40\text{ }^\circ\text{C}$.

Compound 1. 10-Bromodecyl tert-butyldimethylsilyl ether (6.9 g, 19.7 mmol) and Cs_2CO_3 (7.3 g, 22.5 mmol) were added to a DMF solution (45 mL) of 4-iodophenol (4.1 g, 18.6 mmol), and the mixture was stirred at 70 °C for 18 h under N_2 . The reaction mixture was poured into a saturated aqueous solution of NH_4Cl and extracted with AcOEt. The combined organic extract was washed successively with water and brine, and an organic phase separated was dried over anhydrous MgSO_4 and then evaporated to dryness under a reduced pressure. The residue was subjected to column chromatography (SiO_2 , hexane/AcOEt 10/1 v/v) to allow isolation of **1** as colorless oil (7.5 g, 15.3 mmol) in 82% yield. ^1H NMR (500 MHz, CDCl_3): δ (ppm) 7.51 (d, $J = 9.2$ Hz, 2H), 6.65 (d, $J = 9.2$ Hz, 2H), 3.88 (t, $J = 6.6$ Hz, 2H), 3.58 (t, $J = 6.6$ Hz, 2H), 1.74 (m, 2H), 1.49 (m, 2H), 1.41 (m, 2H), 1.27 (br, 10H), 0.88 (s, 9H), 0.03 (s, 6H). ^{13}C NMR (125 MHz, CDCl_3): δ (ppm) 159.16, 138.28, 117.08, 82.52, 68.25, 63.46, 33.03, 29.69, 29.63, 29.55, 29.49, 29.28, 26.14, 25.94, 18.53, -5.10. MALDI-TOF mass: calcd. for $\text{C}_{22}\text{H}_{39}\text{INaO}_2\text{Si}$ [$\text{M} + \text{Na}$] $^+$: $m/z = 513.17$; found: 513.19.

Compound 2. To a THF solution (30 mL) of **1** (5.2 g, 10.7 mmol) was successively added 4-ethynylbenzoic acid (1.9 g, 12.8 mmol), CuI (0.051 g, 0.3 mmol), triethylamine (30 mL) and tetrakis(triphenylphosphine)palladium (0.616 g, 0.5 mmol), and the mixture was purged with N_2 for 20 min and then refluxed for 18 h under N_2 . The reaction mixture was poured into a saturated aqueous solution of NH_4Cl and extracted with AcOEt, CH_2Cl_2 and ether. The combined organic extract was evaporated to dryness under a reduced pressure. The residue was recrystallized from MeOH, affording **2** as pale yellow solid (3.9 g, 7.6 mmol) in 71% yield. ^1H NMR (500 MHz, $\text{DMSO}-d_6$, 60 °C): δ (ppm) 7.90 (d, $J = 8.1$ Hz, 2H), 7.51–7.47 (m, 4H), 6.96 (d, $J = 8.6$ Hz, 2H), 4.01 (t, $J = 6.6$ Hz, 2H), 3.57 (t, $J = 6.3$ Hz, 2H), 1.72 (m, 2H), 1.43 (m, 4H), 1.32–1.28 (br, 10H), 0.87 (s, 9H), 0.02 (s, 6H). ^{13}C NMR (125 MHz, $\text{DMSO}-d_6$, 60 °C): δ (ppm) 166.38, 159.19, 132.87, 130.94, 130.01, 129.23, 126.91, 114.77, 113.41, 92.13, 87.12, 67.56, 62.23, 31.99, 28.63, 28.56, 28.40, 28.30, 25.55, 25.15, 24.97, 17.64, -5.56. MALDI-TOF mass: calcd. for $\text{C}_{31}\text{H}_{43}\text{Na}_2\text{O}_4\text{Si}$ [$\text{M} - \text{H} + 2\text{Na}$] $^+$: $m/z = 553.27$; found: 553.37.

Compound 3. To a CH_2Cl_2 solution (20 mL) of **2** (1.50 g, 2.95 mmol) was successively added DPTS (0.17 g, 0.59 mmol) and DIPC (0.48 g, 3.81 mmol), and the mixture was stirred at 25 °C under Ar until all the reagents were dissolved. 2-Hexyl-1-decanol (0.75 g, 3.09 mmol) was added to the resulting solution, and the mixture was stirred at 25 °C for 12 h under Ar. The reaction mixture was poured into water and extracted with CHCl_3 . The combined organic extract was washed successively with water and brine, and an organic phase separated was dried over anhydrous MgSO_4 and then evaporated to dryness under a reduced pressure. The residue was subjected to column chromatography (SiO_2 , CHCl_3) to allow isolation of **3** as colorless oil (2.10 g, 2.86 mmol) in 97% yield. ^1H NMR (500 MHz, CDCl_3): δ (ppm) 8.00 (d, $J = 8.0$ Hz, 2H), 7.55 (d, $J = 8.0$ Hz, 2H), 7.47 (d, $J = 8.6$ Hz, 2H), 6.88 (d, $J = 8.6$ Hz, 2H), 4.23 (d, $J = 5.8$ Hz, 2H), 3.97 (t, $J = 6.3$ Hz, 2H), 3.60 (t, $J = 6.3$ Hz, 2H), 1.82–1.76 (m, 3H), 1.54–1.22 (m, 38H), 0.90–0.86 (m, 15H), 0.05 (s, 6H). ^{13}C NMR (125 MHz, CDCl_3): δ (ppm) 166.31, 159.63, 133.24, 131.28, 129.53, 129.44, 128.34, 114.63, 114.55, 92.62, 87.50, 68.11, 67.94, 63.08, 37.47, 32.81, 31.92, 31.83, 31.47, 29.96, 29.63, 29.57, 29.53, 29.48, 29.42, 29.36, 29.32, 29.19, 26.78, 26.76, 26.01, 25.74, 25.66, 22.69, 22.66, 18.39, 14.11, -5.23. MALDI-TOF mass: calcd. for $\text{C}_{47}\text{H}_{77}\text{O}_4\text{Si}$ [$\text{M} + \text{H}$] $^+$: $m/z = 733.56$; found: 733.56.

Compound 4. TBAF (1.0 M in THF, 6.0 mL, 6.0 mmol) was added to a THF solution (20 mL) of **3** (2.0 g, 2.84 mmol), and the mixture was stirred at 25 °C for 12 h under Ar. The reaction mixture was evaporated to dryness under a reduced pressure, and a CHCl_3 solution of the residue was washed with a saturated aqueous solution of NH_4Cl . An organic phase separated was dried over anhydrous MgSO_4 and evaporated to dryness under a reduced pressure. The residue was subjected to

column chromatography (SiO₂, CHCl₃) to allow isolation of **4** as colorless oil (1.77 g, 2.58 mmol) in 91% yield. ¹H NMR (500 MHz, CDCl₃): δ (ppm) 8.00 (d, *J* = 8.0 Hz, 2H), 7.55 (d, *J* = 8.0 Hz, 2H), 7.47 (d, *J* = 8.6 Hz, 2H), 6.88 (d, *J* = 8.6 Hz, 2H), 4.23 (d, *J* = 5.8 Hz, 2H), 3.97 (t, *J* = 6.3 Hz, 2H), 3.64 (m, 2H), 1.82–1.76 (m, 3H), 1.60–1.54 (m, 2H), 1.47–1.19 (m, 37H), 0.89–0.86 (m, 6H). ¹³C NMR (125 MHz, CDCl₃): δ (ppm) 166.22, 159.54, 133.15, 131.20, 129.53, 129.44, 128.34, 114.60, 114.55, 92.63, 87.51, 68.11, 67.94, 63.06, 37.47, 32.81, 31.92, 31.83, 31.47, 29.96, 29.63, 29.57, 29.53, 29.48, 29.41, 29.36, 29.32, 29.20, 26.78, 26.76, 26.01, 25.75, 25.66, 22.68, 22.66, 14.11. MALDI-TOF mass: calcd. for C₄₁H₆₃O₄ [M + H]⁺: *m/z* = 619.47; found: 619.47.

Compound 5. To a CH₂Cl₂ solution (15 mL) of **4** (0.70 g, 1.13 mmol) was successively added methacryloyl chloride (0.24 g, 2.21 mmol) and triethylamine (0.21 g, 2.20 mmol), and the mixture was stirred at 25 °C for 10 h under Ar. The reaction mixture was poured into water and extracted with CHCl₃. The combined organic extract was washed successively with a saturated aqueous solution of NaHCO₃, water and brine, and an organic phase separated was dried over anhydrous MgSO₄ and then evaporated to dryness under a reduced pressure. The residue was subjected to column chromatography (SiO₂, CHCl₃/hexane 1/1 v/v) to allow isolation of **5** as colorless oil (0.63 g, 0.91 mmol) in 80% yield. ¹H NMR (500 MHz, CDCl₃): δ (ppm) 8.00 (d, *J* = 8.0 Hz, 2H), 7.55 (d, *J* = 8.0 Hz, 2H), 7.47 (d, *J* = 8.6 Hz, 2H), 6.87 (d, *J* = 8.6 Hz, 2H), 6.10 (s, 1H), 5.54 (t, *J* = 1.7 Hz, 1H), 4.23 (d, *J* = 5.8 Hz, 2H), 4.13 (t, *J* = 6.9 Hz, 2H), 3.97 (t, *J* = 6.3 Hz, 2H), 1.94 (br, 3H), 1.82–1.76 (m, 3H), 1.70–1.64 (m, 2H), 1.51–1.28 (m, 36H), 0.89–0.86 (m, 6H). ¹³C NMR (125 MHz, CDCl₃): δ (ppm) 167.56, 166.28, 159.61, 136.58, 133.23, 131.27, 129.53, 129.44, 128.33, 125.13, 114.61, 114.54, 92.61, 87.50, 68.09, 67.92, 64.81, 37.46, 31.91, 31.82, 31.46, 29.96, 29.56, 29.45, 29.44, 29.34, 29.31, 29.23, 29.18, 28.62, 26.77, 26.76, 26.00, 25.97, 22.68, 22.65, 18.33, 14.12. MALDI-TOF mass: calcd. for C₄₅H₆₇O₅ [M + H]⁺: *m/z* = 687.50; found: 687.45.

Compound 6. By a procedure similar to that for **3**, compound **6** was obtained in 75% yield (2.16 g, 1.95 mmol) from **2** (1.40 g, 2.75 mmol), **4** (1.61 g, 2.60 mmol), DPTS (0.15 g, 0.54 mmol) and DIPC (0.48 g, 3.81 mmol). ¹H NMR (500 MHz, CDCl₃): δ (ppm) 8.00 (d, *J* = 8.0 Hz, 4H, overlapped), 7.55 (d, *J* = 8.0 Hz, 4H), 7.46 (d, *J* = 8.6 Hz, 4H), 6.87 (d, *J* = 8.6 Hz, 4H, overlapped), 4.32 (t, *J* = 6.6 Hz, 2H), 4.22 (d, *J* = 5.8 Hz, 2H), 3.96 (t, *J* = 6.3 Hz, 4H), 3.60 (t, *J* = 6.6 Hz, 2H), 1.81–1.74 (m, 7H), 1.59–1.28 (m, 50H), 0.91–0.86 (m, 15H), 0.05 (s, 6H). ¹³C NMR (125 MHz, CDCl₃): δ (ppm) 166.30, 166.23, 159.62, 133.23, 131.27, 129.52, 129.44, 128.36, 114.62, 114.53, 92.66, 92.63, 87.50, 68.10, 67.94, 65.27, 63.08, 37.46, 32.79, 31.91, 31.82, 31.46, 29.95, 29.62, 29.56, 29.52, 29.47, 29.45, 29.43, 29.40, 29.35, 29.23, 29.18, 26.77, 26.75, 26.00, 25.73, 25.66, 22.68, 22.66, 18.39, 14.11, –5.23. MALDI-TOF mass: calcd. for C₇₂H₁₀₅O₇Si [M + H]⁺: *m/z* = 1109.76; found: 1109.70.

Compound 7. By a procedure similar to that for **4**, compound **7** was obtained in 88% yield (1.65 g, 1.66 mmol) from **6** (2.10 g, 1.89 mmol) and TBAF (1.0 M in THF, 4.0 mL, 4.0 mmol). ¹H NMR (500 MHz, CDCl₃): δ (ppm) 8.00 (d, *J* = 8.0 Hz, 2H), 7.99 (d, *J* = 8.0 Hz, 2H), 7.55 (d, *J* = 8.0 Hz, 4H, overlapped), 7.46 (d, *J* = 8.6 Hz, 4H), 6.87 (d, *J* = 8.6 Hz, 4H, overlapped), 4.32 (t, *J* = 6.6 Hz, 2H), 4.23 (d, *J* = 5.8 Hz, 2H), 3.96 (t, *J* = 6.3 Hz, 4H), 3.64 (t, *J* = 6.6 Hz, 2H), 1.81–1.74 (m, 7H), 1.59–1.54 (m, 2H), 1.45–1.28 (m, 49H), 0.91–0.86 (m, 6H). ¹³C NMR (125 MHz, CDCl₃): δ (ppm) 166.31, 166.22, 159.63, 133.22, 131.27, 129.51, 129.44, 128.37, 114.63, 114.53, 92.66, 92.64, 87.51, 68.11, 67.94, 65.27, 63.08, 37.47, 32.79, 31.92, 31.82, 31.46, 29.96, 29.63, 29.56, 29.51, 29.48, 29.45, 29.43, 29.40, 29.36, 29.23, 29.18, 26.77, 26.74, 26.00, 25.73, 25.66, 22.68, 22.66, 14.11. MALDI-TOF mass: calcd. for C₆₆H₉₁O₇ [M + H]⁺: *m/z* = 995.68; found: 995.70.

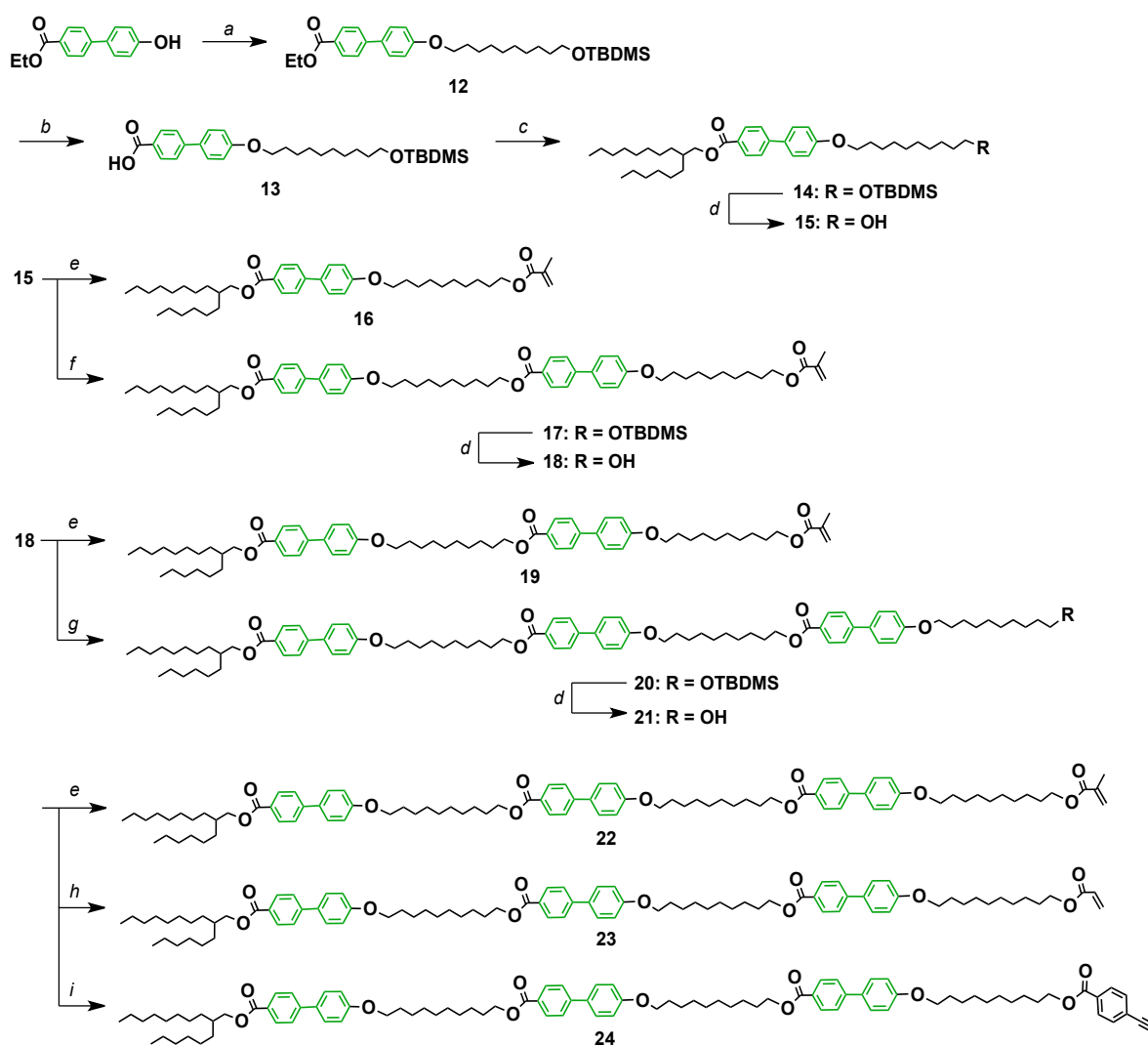
Compound 8. By a procedure similar to that for **5**, compound **8** was obtained in

70% yield (0.46 g, 0.43 mmol) from **7** (0.61 g, 0.61 mmol), methacryloyl chloride (0.16 g, 1.21 mmol) and triethylamine (0.16 g, 1.20 mmol). ^1H NMR (500 MHz, CDCl_3): δ (ppm) 8.00 (d, $J = 8.0$ Hz, 2H), 7.99 (d, $J = 8.0$ Hz, 2H), 7.55 (d, $J = 8.6$ Hz, 4H), 7.47 (d, $J = 8.6$ Hz, 4H), 6.87 (d, $J = 8.6$ Hz, 4H), 6.10 (m, 1H), 5.54 (m, 1H), 4.32 (t, $J = 6.7$ Hz, 2H), 4.23 (d, $J = 5.7$ Hz, 2H), 4.14 (t, $J = 6.6$ Hz, 2H), 3.97 (t, $J = 6.3$ Hz, 4H, overlapped), 1.94 (br, 3H), 1.84–1.76 (m, 7H), 1.70–1.64 (m, 2H), 1.46–1.28 (m, 48H), 0.89–0.86 (m, 6H). ^{13}C NMR (125 MHz, CDCl_3): δ (ppm) 167.56, 166.35, 159.61, 136.65, 133.23, 131.27, 129.50, 129.44, 128.35, 125.17, 114.62, 114.54, 92.60, 87.59, 68.10, 65.26, 64.82, 37.50, 31.91, 31.82, 31.46, 29.96, 29.56, 29.46, 29.43, 29.34, 29.31, 29.24, 29.18, 28.73, 28.62, 26.77, 26.01, 25.97, 22.68, 22.65, 18.33, 14.13, 14.11. MALDI-TOF mass: calcd. for $\text{C}_{70}\text{H}_{95}\text{O}_8$ [$\text{M} + \text{H}$] $^+$: $m/z = 1063.70$; found: 1063.68.

Compound 9. By a procedure similar to that for **3**, except that the reaction temperature was 40 °C, compound **9** was obtained in 81% yield (1.20 g, 0.81 mmol) from **2** (0.55 g, 1.10 mmol), **7** (1.0 g, 1.0 mmol), DPTS (0.061 g, 0.21 mmol) and DIPC (0.25 g, 2.01 mmol). ^1H NMR (500 MHz, CDCl_3): δ (ppm) 8.00 (d, $J = 8.0$ Hz, 6H, overlapped), 7.55 (d, $J = 8.0$ Hz, 6H), 7.46 (d, $J = 8.6$ Hz, 6H, overlapped), 6.87 (d, $J = 8.6$ Hz, 6H, overlapped), 4.32 (t, $J = 6.9$ Hz, 4H, overlapped), 4.22 (d, $J = 5.8$ Hz, 2H), 3.98–3.95 (m, 6H), 3.60 (t, $J = 6.6$ Hz, 2H), 1.81–1.74 (m, 11H), 1.59–1.28 (m, 62H), 0.91–0.86 (m, 15H), 0.05 (s, 6H). ^{13}C NMR (125 MHz, CDCl_3): δ (ppm) 166.28, 166.21, 159.62, 133.23, 131.26, 129.52, 129.44, 128.38, 114.61, 114.53, 92.68, 92.63, 87.50, 68.12, 67.94, 65.27, 63.08, 37.47, 32.79, 31.91, 31.82, 31.45, 29.95, 29.61, 29.55, 29.52, 29.48, 29.44, 29.43, 29.40, 29.35, 29.23, 29.18, 26.77, 26.75, 26.00, 25.73, 25.66, 22.68, 22.66, 18.39, 14.11, –5.23. MALDI-TOF mass: calcd. for $\text{C}_{97}\text{H}_{133}\text{O}_{10}\text{Si}$ [$\text{M} + \text{H}$] $^+$: $m/z = 1485.97$; found: 1485.95.

Compound 10. By a procedure similar to that for **4**, compound **10** was obtained in 91% yield (0.92 g, 0.67 mmol) from **9** (1.10 g, 0.74 mmol) and TBAF (1.0 M in THF, 1.50 mL, 1.50 mmol). ^1H NMR (500 MHz, CDCl_3): δ (ppm) 8.00 (d, $J = 8.0$ Hz, 4H, overlapped), 7.98 (d, $J = 8.0$ Hz, 2H), 7.55 (d, $J = 8.0$ Hz, 6H), 7.46 (d, $J = 8.6$ Hz, 6H, overlapped), 6.87 (d, $J = 8.6$ Hz, 6H, overlapped), 4.32 (t, $J = 6.9$ Hz, 4H, overlapped), 4.22 (d, $J = 5.8$ Hz, 2H), 3.98–3.95 (m, 6H), 3.63 (br, 2H), 1.81–1.74 (m, 11H), 1.58–1.54 (m, 2H), 1.41–1.28 (m, 61H), 0.89–0.86 (m, 6H). ^{13}C NMR (125 MHz, CDCl_3): δ (ppm) 166.27, 166.20, 159.61, 133.23, 131.25, 129.51, 129.45, 129.43, 114.61, 114.52, 114.49, 92.63, 92.64, 87.50, 68.15, 68.08, 67.91, 65.24, 37.45, 32.80, 31.91, 31.88, 31.45, 30.37, 29.95, 29.62, 29.55, 29.47, 29.42, 29.33, 29.24, 29.18, 28.93, 28.70, 26.77, 26.75, 26.01, 22.68, 22.65, 14.12. MALDI-TOF mass: calcd. for $\text{C}_{91}\text{H}_{119}\text{O}_{10}$ [$\text{M} + \text{H}$] $^+$: $m/z = 1371.88$; found: 1371.90.

Compound 11. By a procedure similar to that for **5**, compound **11** was obtained in 60% yield (0.57 g, 0.39 mmol) from **10** (0.90 g, 0.66 mmol), methacryloyl chloride (0.14 g, 1.31 mmol) and triethylamine (0.14 g, 1.35 mmol). ^1H NMR (500 MHz, CDCl_3): δ (ppm) 8.00 (d, $J = 8.0$ Hz, 4H, overlapped), 7.99 (d, $J = 8.0$ Hz, 2H), 7.55 (d, $J = 8.6$ Hz, 6H), 7.47 (d, $J = 8.6$ Hz, 2H), 7.46 (d, $J = 8.6$ Hz, 4H, overlapped), 6.87 (d, $J = 8.6$ Hz, 6H, overlapped), 6.10 (s, 1H), 5.54 (t, $J = 1.7$ Hz, 1H), 4.32 (t, $J = 6.7$ Hz, 4H), 4.23 (d, $J = 5.7$ Hz, 2H), 4.14 (t, $J = 6.6$ Hz, 2H), 3.97 (t, $J = 6.3$ Hz, 6H, overlapped), 1.94 (s, 3H), 1.83–1.74 (m, 11H), 1.70–1.64 (m, 2H), 1.46–1.28 (m, 60H), 0.89–0.86 (m, 6H). ^{13}C NMR (125 MHz, CDCl_3): δ (ppm) 167.56, 166.35, 159.60, 136.65, 133.22, 131.26, 129.50, 129.44, 128.35, 125.18, 114.62, 114.54, 92.61, 87.59, 68.10, 65.27, 64.83, 37.50, 31.91, 31.82, 31.46, 29.97, 29.55, 29.45, 29.42, 29.34, 29.31, 29.24, 29.18, 28.73, 28.62, 26.77, 26.01, 25.97, 22.69, 22.65, 18.33, 14.13, 14.11. MALDI-TOF mass: calcd. for $\text{C}_{95}\text{H}_{123}\text{O}_{11}$ [$\text{M} + \text{H}$] $^+$: $m/z = 1439.91$; found: 1440.01.



Scheme S2 I Synthesis of 16, 19, 22, 23 and 24. Reagents and conditions: (a) 10-bromodecyl tert-butylidimethylsilyl ether, Cs_2CO_3 , DMF, 70 °C; (b) KOH, THF, 50 °C; (c) 2-hexyl-1-decanol, DPTS, DIPC, CH_2Cl_2 , 25 °C; (d) TBAF, THF, 25 °C; (e) methacryloyl chloride, triethylamine, CH_2Cl_2 , 25 °C; (f) **13**, DPTS, DIPC, CH_2Cl_2 , 25 °C; (g) **13**, DPTS, DIPC, CH_2Cl_2 , 40 °C; (h) acryloyl chloride, triethylamine, CH_2Cl_2 , 25 °C; (i) 4-ethynylbenzoic acid, DPTS, DIPC, CH_2Cl_2 , 25 °C.

Compound 12. To a DMF solution (110 mL) of ethyl 4-hydroxy-4'-biphenylcarboxylate (10.8 g, 44.5 mmol) was successively added 10-bromodecyl tert-butylidimethylsilyl ether (16.4 g, 46.7 mmol) and Cs_2CO_3 (17.4 g, 53.4 mmol), and the mixture was stirred at 70 °C for 15 h under N_2 . The reaction mixture was allowed to cool to 25 °C and filtrated off from an insoluble fraction. The filtrate was diluted with AcOEt, washed successively with a saturated aqueous solution of NH_4Cl , water and brine, and an organic phase separated was dried over anhydrous MgSO_4 and then evaporated to dryness under a reduced pressure. The residue was recrystallized from a mixture of AcOEt/MeOH, affording **12** as white solid (19.0 g, 37.0 mmol) in 83% yield. ^1H NMR (500 MHz, CDCl_3): δ (ppm) 8.06 (d, $J = 8.6$ Hz, 2H), 7.59 (d, $J = 8.6$ Hz, 2H), 7.54 (d, $J = 8.6$ Hz, 2H), 6.96 (d, $J = 8.6$ Hz, 2H), 4.37 (q, $J = 7.1$ Hz, 2H), 3.98 (t, $J = 6.6$ Hz, 2H), 3.68 (t, $J = 6.6$ Hz, 2H), 1.79 (m, 2H), 1.49 (m, 4H), 1.39 (t, $J = 6.9$ Hz, 3H), 1.28 (br, 10H), 0.88 (s, 9H), 0.03 (s,

6H). ^{13}C NMR (125 MHz, CDCl_3): δ (ppm) 166.75, 159.55, 145.33, 132.35, 130.19, 128.67, 128.46, 126.53, 115.07, 68.28, 63.48, 61.03, 33.04, 29.72, 29.67, 29.57, 29.54, 29.40, 26.19, 26.14, 25.95, 18.54, 14.52, -5.10. MALDI-TOF mass: calcd. for $\text{C}_{27}\text{H}_{39}\text{O}_4\text{Si}$ [$\text{M} - \text{C}_4\text{H}_9$] $^+$: $m/z = 455.26$; found: 455.30.

Compound 13. To a THF solution (240 mL) of **12** (6.1 g, 12.0 mmol) was successively added EtOH (48 mL) and an aqueous solution of KOH (1 M, 24 mL), and the mixture was stirred at 50 °C for 10 h under N_2 . The reaction mixture was poured into a saturated aqueous solution of NH_4Cl and extracted with CHCl_3 . The combined organic extract was washed successively with water and brine, dried over anhydrous MgSO_4 and then evaporated to dryness under a reduced pressure. The residue was recrystallized from EtOH, affording **13** as white solid (4.5 g, 9.3 mmol) in 78% yield. ^1H NMR (500 MHz, $\text{DMSO}-d_6$, 60 °C): δ (ppm) 7.98 (d, $J = 8.1$ Hz, 2H), 7.73 (d, $J = 8.0$ Hz, 2H), 7.66 (d, $J = 8.6$ Hz, 2H), 7.03 (d, $J = 8.6$ Hz, 2H), 4.03 (t, $J = 6.3$ Hz, 2H), 3.57 (t, $J = 6.3$ Hz, 2H), 1.73 (m, 2H), 1.44 (br, 4H), 1.29 (br, 10H), 0.87 (s, 9H), 0.02 (s, 6H). ^{13}C NMR (125 MHz, $\text{DMSO}-d_6$, 60 °C): δ (ppm) 167.43, 158.72, 143.17, 131.20, 130.21, 129.60, 127.76, 125.61, 114.85, 67.47, 62.23, 31.99, 28.63, 28.58, 28.41, 25.56, 25.20, 24.97, 17.64, -5.56. MALDI-TOF mass: calcd. for $\text{C}_{29}\text{H}_{44}\text{NaO}_4\text{Si}$ [$\text{M} + \text{Na}$] $^+$: $m/z = 507.29$; found: 507.31.

Compound 14. By a procedure similar to that for **3**, compound **14** was obtained in 91% yield (2.40 g, 3.38 mmol) from **13** (1.80 g, 3.71 mmol), 2-hexyl-1-decanol (0.95 g, 3.92 mmol), DPTS (0.17 g, 0.59 mmol) and DIPC (0.51 g, 3.95 mmol). ^1H NMR (500 MHz, CDCl_3): δ (ppm) 8.08 (d, $J = 8.6$ Hz, 2H), 7.62 (d, $J = 8.6$ Hz, 2H), 7.55 (d, $J = 8.6$ Hz, 2H), 6.98 (d, $J = 8.6$ Hz, 2H), 4.24 (d, $J = 5.7$ Hz, 2H), 4.01 (t, $J = 6.8$ Hz, 2H), 3.60 (t, $J = 6.7$ Hz, 2H), 1.79–1.77 (m, 4H), 1.56–1.12 (m, 37H), 0.89–0.86 (m, 15H), 0.05 (s, 6H). ^{13}C NMR (125 MHz, CDCl_3): δ (ppm) 166.71, 159.43, 145.24, 132.26, 130.06, 129.04, 128.38, 126.34, 122.34, 114.96, 68.18, 67.64, 63.34, 37.52, 32.92, 31.96, 31.83, 31.47, 29.96, 29.66, 29.56, 29.45, 29.43, 29.41, 29.35, 29.24, 29.20, 28.72, 26.80, 26.76, 26.05, 25.98, 25.76, 22.68, 22.66, 18.42, 14.11, -5.24. MALDI-TOF mass: calcd. for $\text{C}_{45}\text{H}_{77}\text{O}_4\text{Si}$ [$\text{M} + \text{H}$] $^+$: $m/z = 709.56$; found: 709.55.

Compound 15. By a procedure similar to that for **4**, compound **15** was obtained in 96% yield (1.85 g, 3.11 mmol) from **14** (2.30 g, 3.24 mmol) and TBAF (1.0 M in THF, 6.0 mL, 6.0 mmol). ^1H NMR (500 MHz, CDCl_3): δ (ppm) 8.08 (d, $J = 8.6$ Hz, 2H), 7.61 (d, $J = 8.6$ Hz, 2H), 7.55 (d, $J = 8.6$ Hz, 2H), 6.99 (d, $J = 8.6$ Hz, 2H), 4.24 (d, $J = 5.7$ Hz, 2H), 4.01 (t, $J = 6.8$ Hz, 2H), 3.65 (br, 2H), 1.83–1.77 (m, 4H), 1.62–1.55 (m, 2H), 1.53–1.18 (m, 36H), 0.88–0.86 (m, 6H). ^{13}C NMR (125 MHz, CDCl_3): δ (ppm) 166.71, 159.43, 145.25, 132.26, 130.06, 129.04, 128.38, 126.34, 122.33, 114.97, 68.18, 67.64, 63.33, 37.54, 32.93, 31.96, 31.83, 31.47, 29.96, 29.66, 29.56, 29.45, 29.43, 29.40, 29.35, 29.24, 29.20, 28.72, 26.80, 26.76, 26.05, 25.96, 25.76, 22.68, 22.66, 14.11. MALDI-TOF mass: calcd. for $\text{C}_{39}\text{H}_{63}\text{O}_4$ [$\text{M} + \text{H}$] $^+$: $m/z = 595.47$; found: 595.46.

Compound 16. By a procedure similar to that for **5**, compound **16** was obtained in 75% yield (0.50 g, 0.75 mmol) from **15** (0.60 g, 1.01 mmol), methacryloyl chloride (0.21 g, 2.05 mmol) and triethylamine (0.21 g, 1.98 mmol). ^1H NMR (500 MHz, CDCl_3): δ (ppm) 8.08 (d, $J = 8.0$ Hz, 2H), 7.61 (d, $J = 8.6$ Hz, 2H), 7.55 (d, $J = 8.6$ Hz, 2H), 6.98 (d, $J = 8.6$ Hz, 2H), 6.09 (s, 1H), 5.54 (d, $J = 1.7$ Hz, 1H), 4.24 (d, $J = 5.7$ Hz, 2H), 4.14 (t, $J = 6.8$ Hz, 2H), 4.01 (t, $J = 6.8$ Hz, 2H), 1.94 (s, 3H), 1.83–1.78 (m, 2H), 1.70–1.62 (m, 2H), 1.50–1.22 (m, 37H), 0.91–0.86 (m, 6H). ^{13}C NMR (125 MHz, CDCl_3): δ (ppm) 167.56, 166.72, 159.41, 145.18, 136.62, 136.58, 132.25, 130.05, 128.63, 128.31, 126.42, 125.12, 125.10, 114.94, 68.11, 67.70, 67.49, 64.81, 37.50, 37.34, 31.92, 31.84, 31.81, 31.50, 31.42, 29.98, 29.95, 29.65, 29.61, 29.57, 29.47, 29.44, 29.36, 29.32, 29.26, 29.24, 28.62, 26.79, 26.77, 26.74, 26.71, 26.05, 25.98, 25.71, 22.68, 22.66, 18.33, 14.11. MALDI-TOF mass: calcd. for $\text{C}_{43}\text{H}_{67}\text{O}_5$ [M

+ H]⁺: m/z = 663.50; found: 663.51.

Compound 17. By a procedure similar to that for **3**, compound **17** was obtained in 60% yield (1.28 g, 1.21 mmol) from **13** (1.02 g, 2.10 mmol), **15** (1.20 g, 2.02 mmol), DPTS (0.10 g, 0.33 mmol) and DIPC (0.38 g, 3.00 mmol). ¹H NMR (500 MHz, CDCl₃): δ (ppm) 8.08 (d, J = 8.6 Hz, 4H), 7.62 (d, J = 8.6 Hz, 4H), 7.55 (d, J = 8.6 Hz, 4H), 6.99 (d, J = 8.6 Hz, 4H), 4.34 (t, J = 6.9 Hz, 2H), 4.24 (d, J = 5.7 Hz, 2H), 4.01 (t, J = 6.8 Hz, 4H), 3.60 (t, J = 6.8 Hz, 2H), 1.79–1.77 (m, 7H), 1.56–1.22 (m, 50H), 0.91–0.86 (m, 15H), 0.05 (s, 6H). ¹³C NMR (125 MHz, CDCl₃): δ (ppm) 167.53, 166.76, 159.47, 145.18, 136.62, 132.27, 130.05, 128.62, 128.31, 126.42, 125.12, 114.94, 68.11, 67.70, 67.49, 64.83, 37.50, 37.34, 31.92, 31.84, 31.80, 31.52, 31.42, 29.98, 29.95, 29.65, 29.60, 29.57, 29.48, 29.44, 29.36, 29.32, 29.26, 29.24, 28.62, 26.79, 26.77, 26.74, 26.71, 26.06, 25.98, 25.74, 22.68, 22.66, 18.34, 14.11, –5.24. MALDI-TOF mass: calcd. for C₆₈H₁₀₅O₇Si [M + H]⁺: m/z = 1061.76; found: 1061.77.

Compound 18. By a procedure similar to that for **4**, compound **18** was obtained in 90% yield (1.02 g, 1.08 mmol) from **17** (1.20 g, 1.13 mmol) and TBAF (1.0 M in THF, 2.0 mL, 2.0 mmol). ¹H NMR (500 MHz, CDCl₃): δ (ppm) 8.08 (d, J = 8.6 Hz, 4H), 7.62 (d, J = 8.6 Hz, 4H), 7.55 (d, J = 8.6 Hz, 4H), 6.98 (d, J = 8.6 Hz, 4H), 4.33 (t, J = 6.9 Hz, 2H), 4.24 (d, J = 5.7 Hz, 2H), 4.01 (t, J = 6.8 Hz, 4H), 3.65 (t, J = 6.9 Hz, 2H), 1.83–1.77 (m, 7H), 1.62–1.55 (m, 2H), 1.53–1.22 (m, 49H), 0.90–0.86 (m, 6H). ¹³C NMR (125 MHz, CDCl₃): δ (ppm) 167.53, 166.75, 159.48, 145.18, 136.63, 132.27, 130.05, 128.64, 128.32, 126.42, 126.12, 114.98, 68.11, 67.70, 65.02, 63.04, 37.50, 37.34, 31.92, 31.84, 31.80, 31.52, 31.42, 29.98, 29.95, 29.65, 29.60, 29.57, 29.48, 29.45, 29.36, 29.32, 29.27, 29.24, 28.62, 26.79, 26.78, 26.74, 26.71, 26.06, 25.98, 25.74, 22.68, 22.66, 14.11. MALDI-TOF mass: calcd. for C₆₂H₉₁O₇ [M + H]⁺: m/z = 947.68; found: 947.67.

Compound 19. By a procedure similar to that for **5**, compound **19** was obtained in 76% yield (0.41 g, 0.40 mmol) from **18** (0.50 g, 0.53 mmol), methacryloyl chloride (0.11 g, 1.01 mmol) and triethylamine (0.11 g, 1.09 mmol). ¹H NMR (500 MHz, CDCl₃): δ (ppm) 8.08 (d, J = 8.6 Hz, 2H), 8.07 (d, J = 8.6 Hz, 2H), 7.61 (d, J = 8.6 Hz, 4H), 7.55 (d, J = 8.6 Hz, 4H, overlapped), 6.98 (d, J = 8.6 Hz, 4H, overlapped), 6.09 (s, 1H), 5.54 (t, J = 1.7 Hz, 1H), 4.33 (d, J = 6.8 Hz, 2H), 4.24 (d, J = 5.7 Hz, 2H), 4.14 (t, J = 6.8 Hz, 2H), 4.00 (t, J = 6.8 Hz, 4H), 1.94 (s, 3H), 1.83–1.75 (m, 7H), 1.70–1.64 (m, 2H), 1.50–1.25 (m, 48H), 0.89–0.85 (m, 6H). ¹³C NMR (125 MHz, CDCl₃): δ (ppm) 167.81, 166.73, 159.41, 145.19, 136.58, 132.22, 130.05, 128.63, 128.31, 126.41, 125.13, 114.94, 68.12, 67.70, 65.06, 64.82, 37.50, 31.92, 31.83, 31.49, 29.97, 29.65, 29.57, 29.47, 29.44, 29.36, 29.32, 29.25, 29.24, 28.76, 28.62, 26.77, 26.05, 25.97, 22.68, 22.66, 18.34, 14.11. MALDI-TOF mass: calcd. for C₆₆H₉₅O₈ [M + H]⁺: m/z = 1015.70; found: 1015.68.

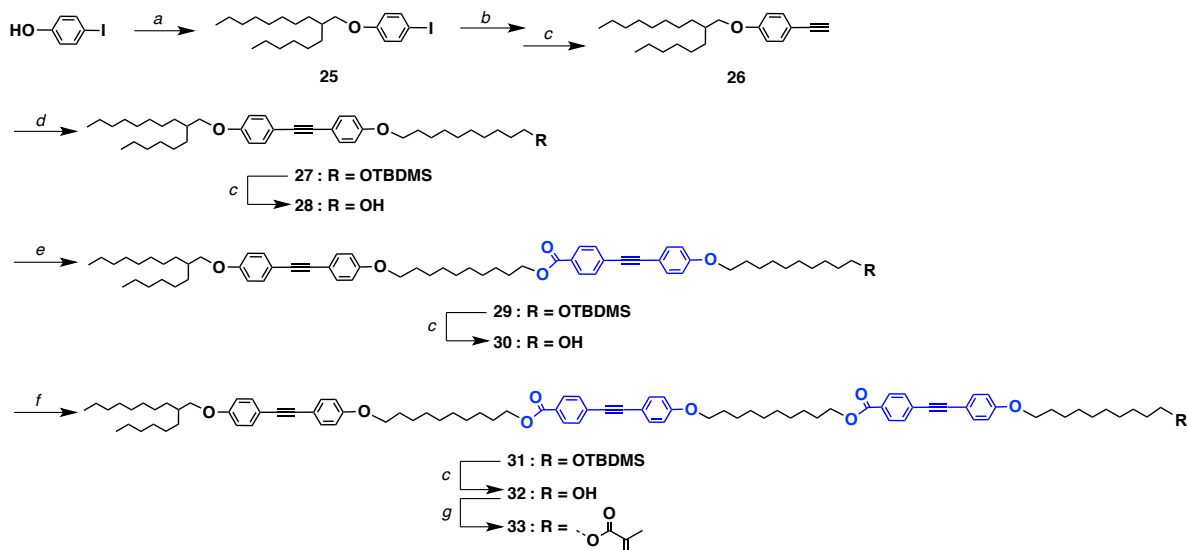
Compound 20. By a procedure similar to that for **3**, except that the reaction temperature was 40 °C, compound **20** was obtained in 93% yield (0.69 g, 0.49 mmol) from **18** (0.50 g, 0.53 mmol), **13** (0.33 g, 0.68 mmol), DPTS (0.10 g, 0.33 mmol) and DIPC (0.31 g, 2.42 mmol). ¹H NMR (500 MHz, CDCl₃): δ (ppm) 8.08 (d, J = 8.6 Hz, 4H), 8.07 (d, J = 8.6 Hz, 2H), 7.61 (d, J = 8.6 Hz, 6H), 7.55 (d, J = 8.6 Hz, 6H, overlapped), 6.98 (d, J = 8.6 Hz, 6H, overlapped), 4.34 (t, J = 6.9 Hz, 4H), 4.24 (d, J = 5.7 Hz, 2H), 4.00 (t, J = 6.8 Hz, 6H), 3.60 (t, J = 6.8 Hz, 2H), 1.84–1.75 (m, 11H), 1.56–1.22 (m, 62H), 0.91–0.86 (m, 15H), 0.05 (s, 6H). ¹³C NMR (125 MHz, CDCl₃): δ (ppm) 167.51, 166.76, 159.43, 145.18, 136.62, 132.27, 130.05, 128.62, 128.30, 126.42, 125.12, 114.94, 68.12, 67.70, 67.49, 64.84, 37.50, 37.38, 31.92, 31.84, 31.80, 31.54, 31.42, 29.98, 29.95, 29.64, 29.60, 29.56, 29.48, 29.44, 29.34, 29.32, 29.26, 29.24, 28.62, 26.79, 26.77, 26.74, 26.71, 26.06, 25.98, 25.74, 22.68, 22.66, 18.34, 14.11, –5.24. MALDI-TOF mass: calcd. for C₉₁H₁₃₃O₁₀Si [M + H]⁺: m/z = 1413.97; found: 1413.96.

Compound 21. By a procedure similar to that for **4**, compound **21** was obtained in 94% yield (0.56 g, 0.43 mmol) from **20** (0.65 g, 0.46 mmol) and TBAF (1.0 M in THF, 1.0 mL, 1.0 mmol). ^1H NMR (500 MHz, CDCl_3): δ (ppm) 8.08 (d, $J = 8.6$ Hz, 4H), 8.07 (d, $J = 8.6$ Hz, 2H), 7.61 (d, $J = 8.6$ Hz, 6H), 7.55 (d, $J = 8.6$ Hz, 6H, overlapped), 6.98 (d, $J = 8.6$ Hz, 6H, overlapped), 4.34 (t, $J = 6.9$ Hz, 4H), 4.24 (d, $J = 5.7$ Hz, 2H), 4.00 (t, $J = 6.8$ Hz, 6H), 3.65 (t, $J = 6.8$ Hz, 2H), 1.83–1.77 (m, 11H), 1.62–1.55 (m, 2H), 1.53–1.22 (m, 61H), 0.91–0.86 (m, 6H). ^{13}C NMR (125 MHz, CDCl_3): δ (ppm) 167.52, 166.75, 159.48, 145.18, 136.63, 132.27, 130.06, 128.64, 126.44, 126.12, 114.98, 68.12, 67.70, 65.04, 63.04, 37.50, 37.35, 31.92, 31.85, 31.52, 31.42, 29.98, 29.95, 29.65, 29.61, 29.57, 29.48, 29.45, 29.37, 29.32, 29.27, 28.62, 26.79, 26.78, 26.74, 26.71, 26.06, 25.98, 25.74, 22.68, 22.66, 14.11. MALDI-TOF mass: calcd. for $\text{C}_{85}\text{H}_{119}\text{O}_{10}$ $[\text{M} + \text{H}]^+$: $m/z = 1299.88$; found: 1299.90.

Compound 22. By a procedure similar to that for **5**, compound **22** was obtained in 60% yield (0.35 g, 0.25 mmol) from **21** (0.55 g, 0.42 mmol), methacryloyl chloride (0.10 g, 1.0 mmol) and triethylamine (0.12 g, 1.10 mmol). ^1H NMR (500 MHz, CDCl_3): δ (ppm) 8.08 (d, $J = 8.6$ Hz, 2H), 8.07 (d, $J = 8.6$ Hz, 4H, overlapped), 7.61 (d, $J = 8.6$ Hz, 6H), 7.55 (d, $J = 8.6$ Hz, 6H, overlapped), 6.98 (d, $J = 8.6$ Hz, 6H, overlapped), 6.09 (s, 1H), 5.54 (t, $J = 1.7$ Hz, 1H), 4.33 (t, $J = 6.8$ Hz, 4H), 4.24 (d, $J = 5.7$ Hz, 2H), 4.14 (t, $J = 6.8$ Hz, 2H), 4.00 (t, $J = 6.8$ Hz, 6H, overlapped), 1.94 (s, 3H), 1.83–1.75 (m, 11H), 1.70–1.64 (m, 2H), 1.48–1.27 (m, 60H), 0.89–0.86 (m, 6H). ^{13}C NMR (125 MHz, CDCl_3): δ (ppm) 167.82, 166.73, 159.42, 145.19, 136.58, 132.24, 130.05, 128.63, 128.31, 126.41, 125.13, 114.94, 68.12, 67.71, 65.06, 64.85, 37.52, 31.92, 31.83, 31.49, 29.96, 29.65, 29.58, 29.47, 29.44, 29.36, 29.32, 29.25, 29.25, 28.77, 28.62, 26.74, 26.05, 25.97, 22.68, 22.66, 14.13, 14.11. MALDI-TOF mass: calcd. for $\text{C}_{89}\text{H}_{123}\text{O}_{11}$ $[\text{M} + \text{H}]^+$: $m/z = 1367.91$; found: 1367.88.

Compound 23. By a procedure similar to that for **5**, compound **23** was obtained in 67% yield (0.70 g, 0.52 mmol) from **21** (1.00 g, 0.77 mmol), acryloyl chloride (0.42 g, 4.6 mmol) and triethylamine (0.50 g, 4.6 mmol). ^1H NMR (500 MHz, CDCl_3): δ (ppm) 8.05 (d, $J = 8.6$ Hz, 6H), 7.60 (d, $J = 8.6$ Hz, 6H), 7.53 (d, $J = 8.6$ Hz, 6H), 6.92 (d, $J = 8.6$ Hz, 6H), 6.34 (dd, $J = 1.8$ and 17.8 Hz, 1H), 6.07 (dd, $J = 10.9$ and 17.8 Hz, 1H), 5.75 (dd, $J = 1.8$ and 10.9 Hz, 1H), 4.28 (t, $J = 5.7$ Hz, 4H), 4.19 (d, $J = 5.7$ Hz, 2H), 4.10 (t, $J = 6.8$ Hz, 2H), 3.94 (m, 6H), 1.78–1.74 (m, 10H), 1.53–1.25 (m, 63H), 0.85–0.81 (m, 6H). ^{13}C NMR (125 MHz, CDCl_3): δ (ppm) 166.95, 166.91, 159.62, 145.44, 138.10, 132.01, 130.64, 130.28, 128.87, 128.54, 126.61, 126.30, 115.18, 68.44, 67.88, 65.32, 64.89, 37.73, 32.12, 32.04, 31.72, 29.91, 29.87, 29.73, 29.68, 29.61, 29.53, 29.49, 29.45, 29.04, 28.91, 27.04, 26.98, 26.32, 26.14, 22.90, 22.88, 14.31. MALDI-TOF mass: calcd. for $\text{C}_{88}\text{H}_{120}\text{NaO}_{11}$ $[\text{M} + \text{Na}]^+$: $m/z = 1375.87$; found: 1375.82.

Compound 24. By a procedure similar to that for **3**, except that the reaction temperature was 40 °C, compound **24** was obtained in 93% yield (0.41 g, 0.29 mmol) from **21** (0.40 g, 0.31 mmol), 4-ethynylbenzoic acid (0.14 g, 1.00 mmol), DPTS (0.05 g, 0.16 mmol) and DIPC (0.10 g, 0.72 mmol). ^1H NMR (500 MHz, CDCl_3): δ (ppm) 8.07 (d, $J = 8.6$ Hz, 6H), 7.99 (d, $J = 8.6$ Hz, 2H), 7.61 (d, $J = 8.6$ Hz, 6H), 7.54 (d, $J = 8.6$ Hz, 8H), 6.97 (d, $J = 8.6$ Hz, 6H), 4.33 (t, $J = 5.7$ Hz, 6H), 4.23 (d, $J = 5.7$ Hz, 2H), 3.98 (t, $J = 6.8$ Hz, 6H), 3.22 (s, 1H), 1.79–1.73 (m, 10H), 1.46–1.28 (m, 63H), 0.88–0.86 (m, 6H). ^{13}C NMR (125 MHz, CDCl_3): δ (ppm) 166.54, 159.46, 145.06, 132.23, 132.03, 130.51, 130.03, 129.38, 128.51, 128.26, 126.62, 126.38, 126.35, 114.91, 79.94, 68.07, 67.91, 65.04, 64.92, 37.47, 31.90, 31.87, 31.78, 31.48, 29.98, 29.92, 29.53, 29.43, 29.41, 29.32, 29.28, 29.23, 28.76, 28.71, 28.63, 26.77, 26.01, 22.62, 14.07. MALDI-TOF mass: calcd. for $\text{C}_{94}\text{H}_{122}\text{NaO}_{11}$ $[\text{M} + \text{Na}]^+$: $m/z = 1449.89$; found: 1449.87.



Scheme S3 I Synthesis of 33. Reagents and conditions: (a) 1-bromo-2-hexyldecane, Cs₂CO₃, DMF, 70 °C; (b) Trimethylsilylacetylene, CuI, triethylamine, tetrakis(triphenylphosphine)palladium, THF, reflux; (c) TBAF, THF, 25 °C; (d) **1**, CuI, triethylamine, tetrakis(triphenylphosphine)palladium, THF, reflux; (e) **2**, DPTS, DIPIC, CH₂Cl₂, 25 °C; (f) **2**, DPTS, DIPIC, CH₂Cl₂, 40 °C; (g) methacryloyl chloride, triethylamine, CH₂Cl₂, 25 °C.

Compound 25. By a procedure similar to that for **1**, compound **25** was obtained in 72% yield (3.2 g, 7.2 mmol) from 4-iodophenol (2.2 g, 10.0 mmol), 1-bromo-2-hexyldecane (3.1 g, 10.0 mmol) and Cs₂CO₃ (3.6 g, 11.2 mmol). ¹H NMR (500 MHz, CDCl₃): δ (ppm) 7.51 (d, *J* = 9.2 Hz, 2H), 6.65 (d, *J* = 9.2 Hz, 2H), 3.78 (d, *J* = 5.8 Hz, 2H), 1.75 (m, 1H), 1.43–1.27 (m, 24H), 0.88 (m, 6H). ¹³C NMR (125 MHz, CDCl₃): δ (ppm) 158.51, 132.12, 116.32, 112.43, 71.17, 37.88, 31.89, 31.31, 31.29, 29.99, 29.66, 29.57, 29.31, 26.80, 26.78, 22.67, 14.09. MALDI-TOF mass: calcd. for C₂₂H₃₈IO [M + H]⁺: *m/z* = 444.43; found: 444.40.

Compound 26. To a THF solution (30 mL) of **25** (3.0 g, 6.8 mmol) were successively added trimethylsilylacetylene (2 mL, 14.5 mmol), CuI (0.051 g, 0.3 mmol), triethylamine (30 mL) and tetrakis(triphenylphosphine)palladium (0.616 g, 0.5 mmol), and the mixture was purged with N₂ for 20 min and then refluxed for 18 h under N₂. The reaction mixture was poured into a saturated aqueous solution of NH₄Cl and extracted with AcOEt, CH₂Cl₂ and ether. The combined organic extract was evaporated to dryness under a reduced pressure, and then TBAF (1.0 M in THF, 6.0 mL, 6.0 mmol) was added to a THF solution (20 mL) of the above crude product, and the mixture was stirred at 25 °C for 12 h under Ar. The reaction mixture was evaporated to dryness under a reduced pressure, and a CHCl₃ solution of the residue was washed with a saturated aqueous solution of NH₄Cl. An organic phase separated was dried over anhydrous MgSO₄ and evaporated to dryness under a reduced pressure. The residue was subjected to column chromatography (SiO₂, *n*-hexane) to allow isolation of **26** as colorless oil (1.5 g, 4.4 mmol) in 65% yield. ¹H NMR (500 MHz, CDCl₃): δ (ppm) 7.41 (d, *J* = 9.2 Hz, 2H), 6.83 (d, *J* = 9.2 Hz, 2H), 3.82 (d, *J* = 5.7 Hz, 2H), 2.99 (s, 1H), 1.76 (m, 1H), 1.47–1.27 (br, 22H), 0.88 (m, 6H). ¹³C NMR (125 MHz, CDCl₃): δ (ppm) 159.79, 133.51, 132.12, 116.32, 114.49, 113.74, 112.43, 83.81, 75.57, 71.17, 70.97, 37.86, 31.88, 31.83, 31.30, 29.99, 29.65, 29.56, 29.31, 26.81, 26.78, 22.67, 14.09. MALDI-TOF mass: calcd. for C₂₄H₃₉O [M + H]⁺: *m/z* = 342.56; found: 342.52.

Compound 27. By a procedure similar to that for **2**, compound **27** was obtained in 73% yield (2.3 g, 3.2 mmol) from **26** (1.5 g, 4.4 mmol), **1** (2.2 g, 4.4 mmol), CuI (0.051 g, 0.3 mmol), tetrakis(triphenylphosphine)palladium (0.616 g, 0.5 mmol) and triethylamine (30 mL). ^1H NMR (500 MHz, CDCl_3): δ (ppm) 7.42 (d, $J = 8.6$ Hz, 4H), 6.84 (d, $J = 8.6$ Hz, 4H), 3.96 (t, $J = 6.6$ Hz, 2H), 3.83 (d, $J = 5.8$ Hz, 2H), 3.60 (t, $J = 6.6$ Hz, 2H), 1.77 (m, 4H), 1.52–1.27 (br, 37H), 0.89–0.86 (m, 15H), 0.05 (s, 6H). ^{13}C NMR (125 MHz, CDCl_3): δ (ppm) 159.51, 136.23, 133.26, 132.78, 132.74, 132.21, 131.33, 129.78, 114.77, 114.73, 71.02, 68.10, 63.32, 38.03, 32.89, 31.91, 31.87, 31.76, 31.40, 30.03, 29.80, 29.72, 29.58, 29.51, 29.49, 29.47, 29.44, 29.42, 29.36, 29.33, 29.26, 26.87, 26.83, 26.46, 26.43, 26.07, 25.98, 25.80, 22.67, 22.62, 22.59, 14.10, –5.26. MALDI-TOF mass: calcd. for $\text{C}_{46}\text{H}_{77}\text{O}_3\text{Si}$ [$\text{M} + \text{H}$] $^+$: $m/z = 705.18$; found: 705.20.

Compound 28. By a procedure similar to that for **4**, compound **28** was obtained in 89% yield (1.10 g, 1.9 mmol) from **27** (1.5 g, 2.1 mmol) and TBAF (1.0 M in THF, 3.0 mL, 3.0 mmol). ^1H NMR (500 MHz, CDCl_3): δ (ppm) 7.42 (d, $J = 8.6$ Hz, 4H), 6.85 (d, $J = 8.6$ Hz, 4H), 3.96 (t, $J = 6.6$ Hz, 2H), 3.83 (d, $J = 5.8$ Hz, 2H), 3.64 (br, 2H), 1.77 (m, 4H), 1.58–1.55 (br, 2H), 1.52–1.20 (br, 36H), 0.89–0.86 (m, 6H). ^{13}C NMR (125 MHz, CDCl_3): δ (ppm) 159.19, 136.34, 133.39, 132.23, 132.11, 129.67, 114.76, 114.73, 71.01, 68.06, 63.10, 37.99, 32.79, 31.84, 31.82, 31.47, 30.01, 29.69, 29.58, 29.53, 29.47, 29.36, 29.33, 29.30, 26.82, 26.78, 26.04, 25.67, 25.61, 22.68, 14.09. MALDI-TOF mass: calcd. for $\text{C}_{40}\text{H}_{63}\text{O}_3$ [$\text{M} + \text{H}$] $^+$: $m/z = 590.92$; found: 590.90.

Compound 29. By a procedure similar to that for **3**, compound **29** was obtained in 80% yield (0.80 g, 0.74 mmol) from **28** (0.55 g, 0.93 mmol), **2** (0.5 g, 1.0 mmol), DPTS (0.061 g, 0.2 mmol) and DIPC (0.144 g, 1.2 mmol). ^1H NMR (500 MHz, CDCl_3): δ (ppm) 8.00 (d, $J = 8.0$ Hz, 2H), 7.55 (d, $J = 8.6$ Hz, 2H), 7.46 (d, $J = 8.6$ Hz, 2H), 7.42 (d, $J = 8.6$ Hz, 4H), 6.87 (d, $J = 8.6$ Hz, 2H), 6.85 (d, $J = 8.6$ Hz, 4H), 4.32 (t, $J = 6.6$ Hz, 2H), 3.96 (t, $J = 6.6$ Hz, 2H), 3.96 (t, $J = 6.6$ Hz, 2H), 3.83 (d, $J = 5.8$ Hz, 2H), 3.60 (t, $J = 6.6$ Hz, 2H), 1.78 (m, 7H), 1.55–1.22 (br, 50H), 0.89–0.87 (m, 15H), 0.05 (s, 6H). ^{13}C NMR (125 MHz, CDCl_3): δ (ppm) 167.53, 166.20, 159.59, 136.51, 133.21, 132.81, 132.77, 131.23, 129.44, 114.60, 114.51, 114.47, 92.61, 87.46, 70.98, 68.09, 68.01, 65.26, 63.31, 37.90, 32.88, 31.89, 31.84, 31.34, 31.32, 30.00, 29.67, 29.55, 29.49, 29.44, 29.41, 29.36, 29.32, 29.22, 29.19, 29.17, 28.69, 26.82, 26.80, 26.00, 25.98, 25.79, 22.67, 18.38, 14.10, –5.26. MALDI-TOF mass: calcd. for $\text{C}_{71}\text{H}_{105}\text{O}_6\text{Si}$ [$\text{M} + \text{H}$] $^+$: $m/z = 1081.67$; found: 1081.65.

Compound 30. By a procedure similar to that for **4**, compound **30** was obtained in 85% yield (0.55 g, 0.55 mmol) from **29** (0.70 g, 0.65 mmol) and TBAF (1.0 M in THF, 1 mL, 1 mmol). ^1H NMR (500 MHz, CDCl_3): δ (ppm) 8.00 (d, $J = 8.0$ Hz, 2H), 7.55 (d, $J = 8.6$ Hz, 2H), 7.46 (d, $J = 8.6$ Hz, 2H), 7.42 (d, $J = 8.6$ Hz, 4H), 6.87 (d, $J = 8.6$ Hz, 2H), 6.85 (d, $J = 8.6$ Hz, 4H), 4.32 (t, $J = 6.6$ Hz, 2H), 3.96 (t, $J = 6.6$ Hz, 2H), 3.96 (t, $J = 6.6$ Hz, 2H), 3.83 (d, $J = 5.8$ Hz, 2H), 3.64 (m, 2H), 1.78 (m, 7H), 1.59–1.56 (m, 2H), 1.45–1.21 (m, 49H), 0.90–0.87 (m, 6H). ^{13}C NMR (125 MHz, CDCl_3): δ (ppm) 166.78, 159.21, 158.92, 133.22, 132.81, 132.77, 131.23, 129.44, 128.31, 115.51, 115.37, 114.60, 114.52, 114.48, 87.99, 87.89, 87.47, 70.98, 68.08, 68.02, 65.24, 63.07, 37.90, 32.79, 31.89, 31.84, 31.34, 31.32, 30.00, 29.67, 29.57, 29.50, 29.46, 29.44, 29.41, 29.38, 29.34, 29.32, 29.22, 29.19, 29.16, 28.69, 26.82, 26.80, 26.00, 25.72, 22.67, 14.10. MALDI-TOF mass: calcd. for $\text{C}_{65}\text{H}_{91}\text{O}_6$ [$\text{M} + \text{H}$] $^+$: $m/z = 997.41$; found: 997.38.

Compound 31. By a procedure similar to that for **3**, except that the reaction temperature was 40 °C, compound **31** was obtained in 92% yield (0.71 g, 0.49 mmol) from **30** (0.50 g, 0.50 mmol), **2** (0.30 g, 0.59 mmol), DPTS (0.060 g, 0.21 mmol) and DIPC (0.12 g, 1.00 mmol). ^1H NMR (500 MHz, CDCl_3): δ (ppm) 8.00 (d, $J = 8.0$ Hz, 4H), 7.55 (d, $J = 8.6$ Hz, 4H), 7.46 (d, $J = 8.6$ Hz, 4H), 7.42 (d, $J = 8.6$

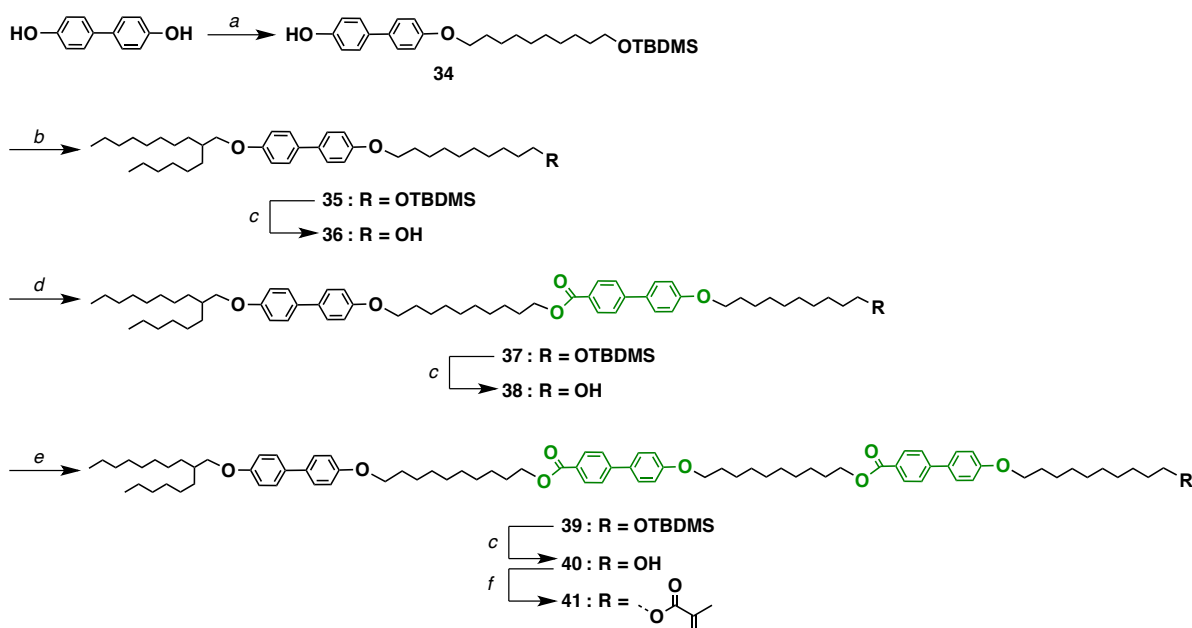
Hz, 4H), 6.87 (d, $J = 8.6$ Hz, 4H), 6.85 (d, $J = 8.6$ Hz, 4H), 4.32 (t, $J = 6.6$ Hz, 4H), 3.96 (t, $J = 6.6$ Hz, 6H), 3.83 (d, $J = 5.8$ Hz, 2H), 3.60 (t, $J = 6.6$ Hz, 2H), 1.82–1.75 (m, 11H), 1.56–1.21 (m, 62H), 0.89–0.87 (m, 15H), 0.05 (s, 6H). ^{13}C NMR (125 MHz, CDCl_3): δ (ppm) 167.55, 166.21, 159.59, 136.50, 133.23, 132.81, 131.21, 131.19, 129.43, 114.60, 114.48, 114.47, 92.62, 87.46, 70.94, 68.92, 68.11, 65.26, 63.31, 37.91, 32.88, 31.89, 31.85, 31.34, 31.32, 30.01, 29.67, 29.55, 29.50, 29.43, 29.40, 29.36, 29.32, 29.23, 29.19, 29.15, 28.62, 26.82, 26.80, 26.02, 25.98, 25.79, 22.67, 18.37, 14.10, –5.26. MALDI-TOF mass: calcd. for $\text{C}_{96}\text{H}_{133}\text{O}_9\text{Si}$ [$\text{M} + \text{H}$] $^+$: $m/z = 1458.16$; found: 1458.13.

Compound 32. By a procedure similar to that for **4**, compound **32** was obtained in 91% yield (0.60 g, 0.45 mmol) from **31** (0.70 g, 0.49 mmol) and TBAF (1.0 M in THF, 1 mL, 1 mmol). ^1H NMR (500 MHz, CDCl_3): δ (ppm) 8.00 (d, $J = 8.0$ Hz, 4H), 7.55 (d, $J = 8.6$ Hz, 4H), 7.46 (d, $J = 8.6$ Hz, 4H), 7.42 (d, $J = 8.6$ Hz, 4H), 6.87 (d, $J = 8.6$ Hz, 4H), 6.85 (d, $J = 8.6$ Hz, 4H), 4.32 (t, $J = 6.6$ Hz, 4H), 3.96 (t, $J = 6.6$ Hz, 6H), 3.83 (d, $J = 5.8$ Hz, 2H), 3.64 (m, 2H), 1.83–1.75 (m, 11H), 1.57–1.52 (m, 2H), 1.48–1.21 (m, 61H), 0.89–0.87 (m, 6H). ^{13}C NMR (125 MHz, CDCl_3): δ (ppm) 166.76, 159.21, 158.92, 133.21, 132.84, 132.73, 131.21, 129.44, 128.31, 115.51, 115.35, 114.60, 114.52, 114.46, 87.99, 87.85, 70.98, 68.09, 68.02, 65.26, 63.10, 37.92, 32.79, 31.86, 31.84, 31.32, 31.28, 30.01, 29.67, 29.57, 29.50, 29.44, 29.43, 29.39, 29.36, 29.34, 29.32, 29.22, 29.19, 29.15, 28.69, 26.82, 26.78, 26.00, 25.72, 22.65, 14.10. MALDI-TOF mass: calcd. for $\text{C}_{90}\text{H}_{119}\text{O}_9$ [$\text{M} + \text{H}$] $^+$: $m/z = 1344.89$; found: 1344.85.

Compound 33. By a procedure similar to that for **5**, compound **33** was obtained in 86% yield (0.45 g, 0.32 mmol) from **32** (0.50 g, 0.37 mmol), methacryloyl chloride (0.26 mL, 2.7 mmol) and triethylamine (0.38 mL, 2.7 mmol). ^1H NMR (500 MHz, CDCl_3): δ (ppm) 8.00 (d, $J = 8.0$ Hz, 4H), 7.55 (d, $J = 8.6$ Hz, 4H), 7.46 (d, $J = 8.6$ Hz, 4H), 7.42 (d, $J = 8.6$ Hz, 4H), 6.87 (d, $J = 8.6$ Hz, 2H), 6.84 (d, $J = 8.6$ Hz, 4H), 6.10 (s, 1H), 5.54 (t, $J = 1.7$ Hz, 1H), 4.32 (t, $J = 6.6$ Hz, 4H), 4.14 (t, $J = 6.6$ Hz, 2H), 3.96 (t, $J = 6.6$ Hz, 6H), 3.83 (d, $J = 5.8$ Hz, 2H), 1.94 (s, 3H), 1.80–1.76 (m, 11H), 1.70–1.54 (m, 2H), 1.45–1.27 (m, 60H), 0.89–0.86 (m, 6H). ^{13}C NMR (125 MHz, CDCl_3): δ (ppm) 167.54, 166.18, 159.59, 136.55, 133.21, 132.80, 132.76, 131.23, 129.43, 128.32, 125.12, 114.59, 114.51, 114.47, 92.61, 87.46, 70.97, 68.06, 68.01, 65.23, 64.79, 37.89, 31.88, 31.83, 31.33, 29.99, 29.66, 29.57, 29.43, 29.40, 29.32, 29.21, 29.16, 28.68, 28.58, 26.82, 26.79, 25.99, 25.94, 22.66, 18.32, 14.09. MALDI-TOF mass: calcd. for $\text{C}_{94}\text{H}_{123}\text{O}_{10}$ [$\text{M} + \text{H}$] $^+$: $m/z = 1411.97$; found: 1411.99.

Compound 34. By a procedure similar to that for **1**, compound **34** was obtained in 40% yield (1.8 g, 3.9 mmol) from 4,4'-biphenol (4.0 g, 21.0 mmol), 10-bromodecyl tert-butyldimethylsilyl ether (3.5 g, 10.0 mmol) and Cs_2CO_3 (7.3 g, 22.5 mmol). ^1H NMR (500 MHz, CDCl_3): δ (ppm) 7.43 (d, $J = 8.6$ Hz, 4H), 6.93 (d, $J = 8.6$ Hz, 2H), 6.87 (d, $J = 8.6$ Hz, 2H), 4.99 (s, 1H), 3.98 (t, $J = 6.6$ Hz, 2H), 3.61 (t, $J = 6.9$ Hz, 2H), 1.77 (m, 2H), 1.53–1.43 (m, 4H), 1.34–1.23 (br, 12H), 0.89 (s, 9H), 0.05 (s, 6H). ^{13}C NMR (125 MHz, CDCl_3): δ (ppm) 158.25, 154.59, 133.71, 133.19, 127.91, 127.65, 115.56, 114.74, 68.10, 63.40, 32.84, 29.56, 29.51, 29.41, 29.38, 29.29, 26.05, 25.99, 25.78, 18.40, –5.24. MALDI-TOF mass: calcd. for $\text{C}_{28}\text{H}_{45}\text{O}_3\text{Si}$ [$\text{M} + \text{H}$] $^+$: $m/z = 456.73$; found: 456.73.

Compound 35. By a procedure similar to that for **1**, compound **35** was obtained in 61% yield (0.62 g, 0.91 mmol) from **34** (0.70 g, 1.5 mmol), 1-bromo-2-hexyldecane (0.62 g, 2.0 mmol) and Cs_2CO_3 (0.72 g, 2.2 mmol). ^1H NMR (500 MHz, CDCl_3): δ (ppm) 7.45 (d, $J = 8.6$ Hz, 4H), 6.93 (d, $J = 8.6$ Hz, 4H), 3.98 (t, $J = 6.6$ Hz, 2H), 3.85 (d, $J = 5.8$ Hz, 2H), 3.60 (t, $J = 6.6$ Hz, 2H), 1.81–1.76 (m, 4H), 1.59–1.14 (br, 37H), 0.89–0.86 (m, 15H), 0.05 (s, 6H). ^{13}C NMR (125 MHz, CDCl_3): δ (ppm) 158.51, 158.22, 133.39, 133.26, 133.22, 127.93, 127.65, 127.61, 114.77, 114.74,



Scheme S4 I Synthesis of 41. Reagents and conditions: (a) 10-bromodecyl tert-butyldimethylsilyl ether, Cs₂CO₃, DMF, 70 °C; (b) 1-bromo-2-hexyldecane, Cs₂CO₃, DMF, 70 °C; (c) TBAF, THF, 25 °C; (d) **13**, DPTS, DIPC, CH₂Cl₂, 25 °C; (e) **13**, DPTS, DIPC, CH₂Cl₂, 40 °C; (f) methacryloyl chloride, triethylamine, CH₂Cl₂, 25 °C.

71.02, 68.09, 63.32, 38.00, 32.89, 31.91, 31.87, 31.73, 31.40, 30.03, 29.79, 29.70, 29.59, 29.57, 29.52, 29.48, 29.44, 29.42, 29.39, 29.33, 29.26, 26.85, 26.83, 26.46, 26.41, 26.07, 25.99, 25.80, 22.67, 22.65, 22.60, 14.09, 14.01, -5.26. MALDI-TOF mass: calcd. for C₄₄H₇₇O₃Si [M + H]⁺: *m/z* = 681.16; found: 681.13.

Compound 36. By a procedure similar to that for **4**, compound **36** was obtained in 90% yield (0.45 g, 0.79 mmol) from **35** (0.60 g, 0.88 mmol) and TBAF (1.0 M in THF, 1 mL, 1 mmol). ¹H NMR (500 MHz, CDCl₃): δ (ppm) 7.45 (d, *J* = 8.6 Hz, 4H), 6.94 (d, *J* = 8.6 Hz, 4H), 3.98 (t, *J* = 6.6 Hz, 2H), 3.85 (d, *J* = 5.8 Hz, 2H), 3.65 (br, 2H), 1.81–1.76 (m, 4H), 1.59–1.14 (br, 38H), 0.89–0.86 (m, 6H). ¹³C NMR (125 MHz, CDCl₃): δ (ppm) 158.51, 158.19, 133.39, 133.23, 127.63, 127.59, 114.76, 114.73, 71.01, 68.06, 63.06, 37.98, 32.79, 31.89, 31.85, 31.40, 30.01, 29.68, 29.58, 29.51, 29.47, 29.38, 29.35, 29.30, 26.84, 26.81, 26.04, 25.71, 25.63, 22.66, 14.09. MALDI-TOF mass: calcd. for C₃₈H₆₃O₃ [M + H]⁺: *m/z* = 566.90; found: 566.92.

Compound 37. By a procedure similar to that for **3**, compound **37** was obtained in 87% yield (0.71 g, 0.69 mmol) from **36** (0.45 g, 0.79 mmol), **13** (0.40 g, 0.83 mmol), DPTS (0.031 g, 0.1 mmol) and DIPC (0.144 g, 1.2 mmol). ¹H NMR (500 MHz, CDCl₃): δ (ppm) 8.07 (d, *J* = 8.0 Hz, 2H), 7.61 (d, *J* = 8.6 Hz, 2H), 7.55 (d, *J* = 8.6 Hz, 2H), 7.45 (d, *J* = 8.6 Hz, 4H), 6.97 (d, *J* = 8.6 Hz, 2H), 6.94 (d, *J* = 8.6 Hz, 4H), 4.33 (t, *J* = 6.6 Hz, 2H), 3.97 (t, *J* = 6.6 Hz, 2H), 3.97 (t, *J* = 6.6 Hz, 2H), 3.85 (d, *J* = 5.8 Hz, 2H), 3.60 (t, *J* = 6.6 Hz, 2H), 1.78 (m, 7H), 1.55–1.25 (br, 50H), 0.89–0.86 (m, 15H), 0.05 (s, 6H). ¹³C NMR (125 MHz, CDCl₃): δ (ppm) 166.67, 159.40, 158.68, 158.32, 145.19, 143.92, 130.04, 128.30, 127.61, 126.39, 114.93, 114.77, 114.74, 71.03, 68.16, 68.04, 65.06, 63.32, 38.01, 32.89, 31.90, 31.86, 31.44, 29.98, 29.69, 29.59, 29.56, 29.51, 29.43, 29.38, 29.36, 29.32, 28.77, 26.85, 26.77, 26.04, 25.98, 25.80, 25.79, 22.67, 14.22, 14.09, -5.26. MALDI-TOF mass: calcd.

for $C_{67}H_{105}O_6Si$ $[M + H]^+$: $m/z = 1033.62$; found: 1033.65.

Compound 38. By a procedure similar to that for **4**, compound **38** was obtained in 94% yield (0.60 g, 0.65 mmol) from **37** (0.70 g, 0.69 mmol) and TBAF (1.0 M in THF, 1 mL, 1 mmol). 1H NMR (500 MHz, $CDCl_3$): δ (ppm) 8.07 (d, $J = 8.0$ Hz, 2H), 7.61 (d, $J = 8.6$ Hz, 2H), 7.55 (d, $J = 8.6$ Hz, 2H), 7.45 (d, $J = 8.6$ Hz, 4H), 6.97 (d, $J = 8.6$ Hz, 2H), 6.94 (d, $J = 8.6$ Hz, 4H), 4.33 (t, $J = 6.6$ Hz, 2H), 3.97 (t, $J = 6.6$ Hz, 2H), 3.85 (d, $J = 5.8$ Hz, 2H), 3.64 (br, 2H), 1.78 (m, 7H), 1.59–1.55 (m, 2H), 1.52–1.28 (m, 49H), 0.89–0.86 (m, 6H). ^{13}C NMR (125 MHz, $CDCl_3$): δ (ppm) 166.68, 159.43, 158.68, 158.35, 145.19, 143.92, 130.04, 128.34, 127.62, 126.39, 114.91, 114.77, 71.05, 68.16, 68.10, 65.06, 63.22, 38.00, 32.82, 31.90, 31.86, 31.46, 29.98, 29.69, 29.59, 29.57, 29.51, 29.43, 29.40, 29.36, 29.32, 28.73, 26.85, 26.75, 26.04, 25.94, 25.80, 25.73, 22.67, 14.09. MALDI-TOF mass: calcd. for $C_{61}H_{91}O_6$ $[M + H]^+$: $m/z = 919.36$; found: 919.34.

Compound 39. By a procedure similar to that for **3**, except that the reaction temperature was 40 °C, compound **39** was obtained in 82% yield (0.68 g, 0.49 mmol) from **38** (0.55 g, 0.60 mmol), **13** (0.35 g, 0.70 mmol), DPTS (0.060 g, 0.21 mmol) and DIPC (0.12 g, 1.00 mmol). 1H NMR (500 MHz, $CDCl_3$): δ (ppm) 8.07 (d, $J = 8.0$ Hz, 4H), 7.61 (d, $J = 8.6$ Hz, 4H), 7.55 (d, $J = 8.6$ Hz, 4H), 7.45 (d, $J = 8.6$ Hz, 4H), 6.97 (d, $J = 8.6$ Hz, 4H), 6.94 (d, $J = 8.6$ Hz, 4H), 4.33 (t, $J = 6.6$ Hz, 4H), 3.97 (t, $J = 6.6$ Hz, 6H), 3.85 (d, $J = 5.8$ Hz, 2H), 3.60 (t, $J = 6.6$ Hz, 2H), 1.83–1.75 (m, 11H), 1.56–1.28 (m, 62H), 0.89–0.86 (m, 15H), 0.05 (s, 6H). ^{13}C NMR (125 MHz, $CDCl_3$): δ (ppm) 166.67, 159.40, 158.70, 158.32, 145.19, 143.91, 130.04, 128.30, 127.61, 126.39, 114.95, 114.77, 114.71, 71.03, 68.16, 68.04, 65.08, 63.35, 38.22, 32.82, 31.90, 31.86, 31.44, 29.98, 29.65, 29.59, 29.54, 29.51, 29.48, 29.38, 29.36, 29.31, 28.76, 26.85, 26.77, 26.01, 25.98, 25.84, 25.79, 22.67, 14.21, 14.09, –5.26. MALDI-TOF mass: calcd. for $C_{90}H_{133}O_9Si$ $[M + H]^+$: $m/z = 1386.09$; found: 1386.11.

Compound 40. By a procedure similar to that for **4**, compound **40** was obtained in 91% yield (0.55 g, 0.45 mmol) from **39** (0.65 g, 0.47 mmol) and TBAF (1.0 M in THF, 1 mL, 1 mmol). 1H NMR (500 MHz, $CDCl_3$): δ (ppm) 8.07 (d, $J = 8.0$ Hz, 4H), 7.61 (d, $J = 8.6$ Hz, 4H), 7.55 (d, $J = 8.6$ Hz, 4H), 7.45 (d, $J = 8.6$ Hz, 4H), 6.97 (d, $J = 8.6$ Hz, 4H), 6.94 (d, $J = 8.6$ Hz, 4H), 4.33 (t, $J = 6.6$ Hz, 4H), 3.97 (t, $J = 6.6$ Hz, 6H), 3.85 (d, $J = 5.8$ Hz, 2H), 3.64 (m, 2H), 1.87–1.77 (m, 11H), 1.58–1.52 (m, 2H), 1.46–1.20 (m, 61H), 0.89–0.86 (m, 6H). ^{13}C NMR (125 MHz, $CDCl_3$): δ (ppm) 166.71, 166.68, 159.44, 158.65, 158.32, 145.19, 143.92, 130.10, 128.36, 127.62, 126.40, 114.91, 114.77, 71.07, 68.16, 68.12, 65.06, 63.24, 38.00, 32.82, 31.95, 31.86, 31.46, 29.94, 29.69, 29.56, 29.57, 29.51, 29.43, 29.39, 29.33, 29.30, 28.73, 26.85, 26.73, 26.04, 25.94, 25.80, 25.71, 22.67, 14.09. MALDI-TOF mass: calcd. for $C_{84}H_{119}O_9$ $[M + H]^+$: $m/z = 1271.83$; found: 1271.85.

Compound 41. By a procedure similar to that for **5**, compound **41** was obtained in 95% yield (0.50 g, 0.32 mmol) from **40** (0.50 g, 0.39 mmol), methacryloyl chloride (0.26 mL, 2.7 mmol) and triethylamine (0.38 mL, 2.7 mmol). 1H NMR (500 MHz, $CDCl_3$): δ (ppm) 8.07 (d, $J = 8.0$ Hz, 4H), 7.61 (d, $J = 8.6$ Hz, 4H), 7.55 (d, $J = 8.6$ Hz, 4H), 7.45 (d, $J = 8.6$ Hz, 4H), 6.97 (d, $J = 8.6$ Hz, 2H), 6.94 (d, $J = 8.6$ Hz, 4H), 6.10 (s, 1H), 5.54 (t, $J = 1.7$ Hz, 1H), 4.33 (t, $J = 6.6$ Hz, 4H), 4.14 (t, $J = 6.6$ Hz, 2H), 3.98 (t, $J = 6.6$ Hz, 6H), 3.86 (d, $J = 5.8$ Hz, 2H), 1.94 (s, 3H), 1.80–1.78 (m, 11H), 1.70–1.53 (m, 2H), 1.46–1.28 (m, 60H), 0.89–0.86 (m, 6H). ^{13}C NMR (125 MHz, $CDCl_3$): δ (ppm) 167.52, 166.61, 159.37, 158.48, 145.14, 136.53, 133.34, 133.19, 132.15, 130.02, 128.52, 128.27, 127.61, 127.58, 126.36, 125.11, 114.89, 114.73, 114.70, 70.95, 68.07, 68.02, 65.02, 64.78, 37.96, 31.88, 31.85, 31.36, 30.01, 29.68, 29.58, 29.44, 29.41, 29.33, 29.22, 28.73, 28.58, 26.83, 26.80, 26.01, 25.94, 25.69, 22.66, 18.32, 14.10. MALDI-TOF mass: calcd. for $C_{88}H_{123}O_{10}$ $[M + H]^+$: $m/z = 1339.90$; found: 1339.92.

Polymer PMA/T. Monomer **5** (0.31 g, 0.45 mmol) was placed in a Schlenk flask (25 mL), and the inner atmosphere was strictly purged with Ar. A stock solution of AIBN (13.3 mM) in anhydrous benzene was degassed by freeze-pump-thaw cycles (three times). This stock solution (0.45 mL) was introduced using a syringe into the flask containing **5**, and the mixture was stirred at 70 °C for 24 h. The reaction mixture was subjected to preparative SEC with CHCl₃ as an eluent, to allow separation of a polymeric fraction from **5**. The polymeric fraction was dried at 50 °C under a reduced pressure to give **PMA/T** (295 mg) as colorless oil in 95% yield. ¹H NMR (500 MHz, CDCl₃): δ (ppm) 8.00–7.91 (m), 7.55–7.38 (m), 6.87–6.77 (m), 4.21–4.17 (m), 4.01–3.85 (br), 1.78–1.68 (br), 1.60–1.54 (br), 1.48–1.18 (br), 0.88–0.81 (m). FT-IR (ATR): ν (cm⁻¹) 2927, 2853, 2212, 1715, 1601, 1514, 1468, 1400, 1273, 1251, 1174, 1142, 1107, 1018. SEC analysis (CHCl₃, polystyrene standards): number-average molecular weight (M_n) = 7.0×10^4 g mol⁻¹ (DP = 113), polydispersity index (M_w/M_n) = 4.0.

Polymer PMA/T₂. Monomer **8** (0.32 g, 0.30 mmol) was placed in a Schlenk flask (25 mL), and the inner atmosphere was strictly purged with Ar. A stock solution of AIBN (8.92 mM) in anhydrous benzene was degassed by freeze-pump-thaw cycles (three times). This stock solution (0.45 mL) was introduced using a syringe into the flask containing **8**, and the mixture was stirred at 70 °C. After 24 h, the reaction mixture was poured into MeOH (150 mL), and a white precipitate formed was collected by filtration and subjected to preparative SEC with CHCl₃ as an eluent, to allow separation of a polymeric fraction from **8**. The polymeric fraction was concentrated (~5 mL) under a reduced pressure to a small volume, which was then added dropwise to MeOH (150 mL). A precipitate thus formed was collected by filtration and dried at 25 °C under a reduced pressure to give **PMA/T₂** (282 mg) as white solid in 88% yield. ¹H NMR (500 MHz, CDCl₃): δ (ppm) 8.04–7.94 (m), 7.58–7.38 (m), 6.88–6.76 (m), 4.31–4.17 (br), 3.98–3.85 (br), 1.81–1.70 (br), 1.68–1.55 (br), 1.48–1.18 (br), 0.88–0.84 (m). FT-IR (ATR): ν (cm⁻¹) 2928, 2852, 2212, 1714, 1598, 1514, 1467, 1402, 1273, 1250, 1176, 1140, 1107, 1018. SEC analysis (CHCl₃, polystyrene standards): M_n = 7.6×10^4 g mol⁻¹ (DP = 71), M_w/M_n = 3.1.

Polymer PMA/T₃. By a procedure similar to that for **PMA/T₂**, **PMA/T₃** was obtained in 80% yield (192 mg) from monomer **11** (0.24 g, 0.17 mmol) and AIBN in anhydrous benzene (6.13 mM, 0.36 mL). ¹H NMR (500 MHz, CDCl₃): δ (ppm) 8.03–7.93 (m), 7.57–7.38 (m), 6.89–6.77 (m), 4.33–4.21 (br), 3.98–3.86 (m), 1.81–1.68 (br), 1.67–1.55 (br), 1.48–1.18 (br), 0.88–0.84 (m). FT-IR (ATR): ν (cm⁻¹) 2927, 2852, 2212, 1714, 1599, 1514, 1468, 1400, 1273, 1250, 1174, 1140, 1107, 1018. SEC analysis (CHCl₃, polystyrene standards): M_n = 7.7×10^4 g mol⁻¹ (DP = 54), M_w/M_n = 3.0.

Polymer PMA/B. By a procedure similar to that for **PMA/T**, **PMA/B** was obtained in 92% yield (276 mg) from monomer **16** (0.30 g, 0.45 mmol) and AIBN in anhydrous benzene (13.3 mM, 0.45 mL). ¹H NMR (500 MHz, CDCl₃): δ (ppm) 8.05–7.98 (m), 7.60–7.45 (m), 6.97–6.87 (br), 4.23–4.18 (m), 4.03–3.87 (br), 1.80–1.68 (br), 1.72–1.51 (br), 1.48–1.18 (br), 0.91–0.82 (m). FT-IR (ATR): ν (cm⁻¹) 2927, 2854, 1714, 1605, 1525, 1496, 1472, 1396, 1275, 1191, 1109, 1039. SEC analysis (CHCl₃, polystyrene standards): M_n = 5.1×10^4 g mol⁻¹ (DP = 88), M_w/M_n = 3.8.

Polymer PMA/B₂. By a procedure similar to that for **PMA/T₂**, **PMA/B₂** was obtained in 90% yield (270 mg) from monomer **19** (0.30 g, 0.30 mmol) and AIBN in anhydrous benzene (8.91 mM, 0.45 mL). ¹H NMR (500 MHz, CDCl₃): δ (ppm) 8.08–7.96 (m), 7.62–7.42 (m), 6.96–6.85 (m), 4.31–4.20 (br), 3.98–3.86 (br), 1.81–1.70 (br), 1.68–1.55 (br), 1.48–1.18 (br), 0.88–0.83 (m). FT-IR (ATR): ν (cm⁻¹) 2927, 2854, 1715, 1605, 1525, 1497, 1475, 1396, 1276, 1191, 1109, 1039. SEC

analysis (CHCl_3 , polystyrene standards): $M_n = 1.6 \times 10^5 \text{ g mol}^{-1}$ (DP = 169), $M_w/M_n = 3.4$.

Polymer PMA/B₃. By a procedure similar to that for **PMA/T₂**, **PMA/B₃** was obtained in 90% yield (225 mg) from monomer **22** (0.25 g, 0.18 mmol) and AIBN in anhydrous benzene (6.13 mM, 0.40 mL). ¹H NMR (500 MHz, CDCl_3): δ (ppm) 8.08–7.96 (m), 7.62–7.42 (m), 6.96–6.85 (m), 4.31–4.20 (br), 3.98–3.86 (br), 1.81–1.70 (br), 1.68–1.55 (br), 1.48–1.18 (br), 0.90–0.83 (m). FT-IR (ATR): ν (cm^{-1}) 2924, 2854, 1714, 1604, 1525, 1496, 1471, 1396, 1275, 1190, 1109, 1039. SEC analysis (CHCl_3 , polystyrene standards): $M_n = 7.6 \times 10^4 \text{ g mol}^{-1}$ (DP = 54), $M_w/M_n = 3.8$.

Polymer PA/B₃. By a procedure similar to that for **PMA/T₂**, **PA/B₃** was obtained in 47% yield (94 mg) from monomer **23** (0.20 g, 0.15 mmol) and AIBN in anhydrous benzene (6.13 mM, 0.32 mL). ¹H NMR (500 MHz, CDCl_3): δ (ppm) 8.03 (br), 7.59–7.51 (br), 6.94 (br), 4.28 (br), 4.20–4.10 (br), 3.94 (br), 1.78–1.74 (br), 1.53–1.25 (br), 0.86 (br). FT-IR (ATR): ν (cm^{-1}) 2925, 2854, 1716, 1603, 1525, 1498, 1472, 1396, 1275, 1191, 1108, 1039. SEC analysis (CHCl_3 , polystyrene standards): $M_n = 3.8 \times 10^4 \text{ g mol}^{-1}$ (DP = 28), $M_w/M_n = 1.4$.

Polymer PPA/B₃. Monomer **24** (0.20 g, 0.14 mmol) was placed in a Schlenk flask (25 mL), and the inner atmosphere was strictly purged with Ar. A stock solution of $\text{Rh}(\text{nbd})\text{BPh}_4$ (1.2 mM) in anhydrous CHCl_3 was degassed by freeze-pump-thaw cycles (three times). This stock solution (2.3 mL) was introduced using a syringe into the flask containing **24**, and the mixture was stirred at 25 °C. After 24 h, triphenylphosphine (7.9 mg, 0.03 mmol) was added into the reaction mixture. The mixture was poured into MeOH, and a precipitate formed was collected by filtration and reprecipitated twice from MeOH. A precipitate thus formed was dried at 25 °C under a reduced pressure, and then subjected to preparative SEC with CHCl_3 as an eluent, to allow separation of a polymeric fraction from **24** as yellow solid (140 mg) in 70% yield. ¹H NMR (500 MHz, CDCl_3): δ (ppm) 8.06–7.94 (m), 7.62–7.41 (m), 6.96–6.86 (m), 6.72 (br), 5.74 (br), 4.30–4.23 (br), 3.98–3.84 (br), 1.82–1.65 (br), 1.48–1.20 (br), 0.90–0.83 (m). FT-IR (ATR): ν (cm^{-1}) 2925, 2854, 1714, 1604, 1525, 1496, 1469, 1396, 1277, 1188, 1108, 1039. SEC analysis (CHCl_3 , polystyrene standards): $M_n = 6.2 \times 10^4 \text{ g mol}^{-1}$ (DP = 43), $M_w/M_n = 2.0$.

Polymer PMA/T₂T'. By a procedure similar to that for **PMA/T₂**, **PMA/T₂T'** was obtained in 80% yield (176 mg) from monomer **33** (0.22 g, 0.16 mmol) and AIBN in anhydrous benzene (4.5 mM, 0.35 mL). ¹H NMR (500 MHz, CDCl_3): δ (ppm) 7.98–7.96 (m), 7.52–7.49 (m), 7.43–7.39 (m), 6.82 (m), 4.28 (br), 3.91 (br), 3.80 (m), 1.74–1.55 (m), 1.40–1.26 (br), 0.87–0.85 (m). FT-IR (ATR): ν (cm^{-1}) 2925, 2854, 2214, 1714, 1601, 1566, 1516, 1469, 1404, 1281, 1248, 1173, 1142, 1107, 1020. SEC analysis (CHCl_3 , polystyrene standards): $M_n = 1.2 \times 10^5 \text{ g mol}^{-1}$ (DP = 85), $M_w/M_n = 2.7$.

Polymer PMA/B₂B'. By a procedure similar to that for **PMA/T₂**, **PMA/B₂B'** was obtained in 53% yield (105 mg) from monomer **41** (0.21 g, 0.16 mmol) and AIBN in anhydrous benzene (4.5 mM, 0.35 mL). ¹H NMR (500 MHz, CDCl_3): δ (ppm) 8.04–8.00 (m), 7.57–7.41 (m), 6.91 (m), 4.29 (br), 3.94 (br), 3.82 (m), 1.76–1.51 (m), 1.42–1.28 (br), 0.86 (m). FT-IR (ATR): ν (cm^{-1}) 2924, 2854, 1714, 1604, 1527, 1498, 1469, 1396, 1281, 1244, 1192, 1111, 1041. SEC analysis (CHCl_3 , polystyrene standards): $M_n = 7.3 \times 10^4 \text{ g mol}^{-1}$ (DP = 54), $M_w/M_n = 2.2$.

2.4.3. Supporting Figures

2.4.3.1. DSC Profiles

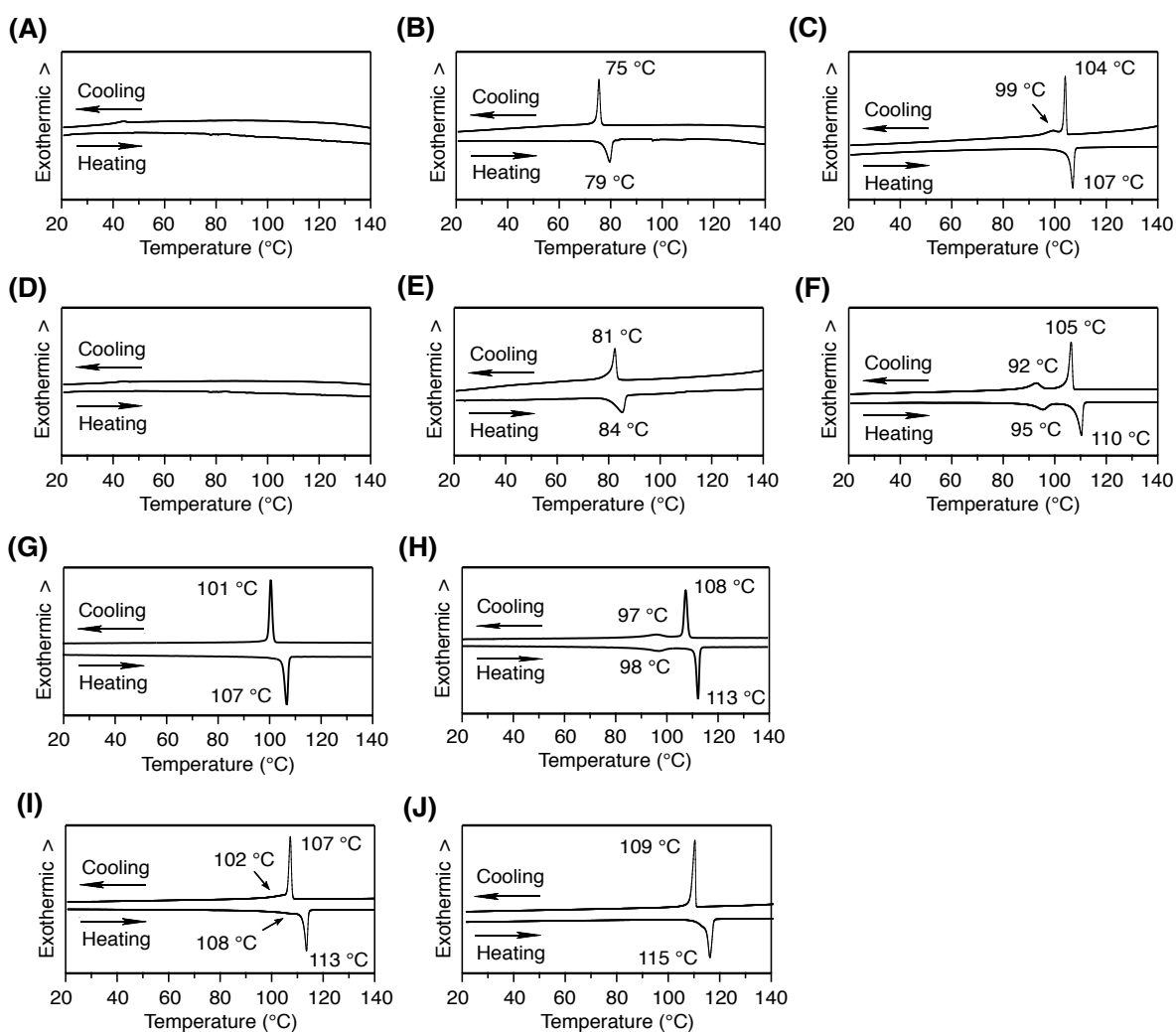


Figure S1 | DSC traces in a second heating/cooling cycle. (A) PMA/B, (B) PMA/B₂, (C) PMA/B₃, (D) PMA/T, (E) PMA/T₂, (F) PMA/T₃, (G) PMA/B₂B', (H) PMA/T₂T', (I) PPA/B₃, and (J) PA/B₃. Scan rate is 5 °C min⁻¹.

2.4.3.2. SAXS and WAXD Profiles

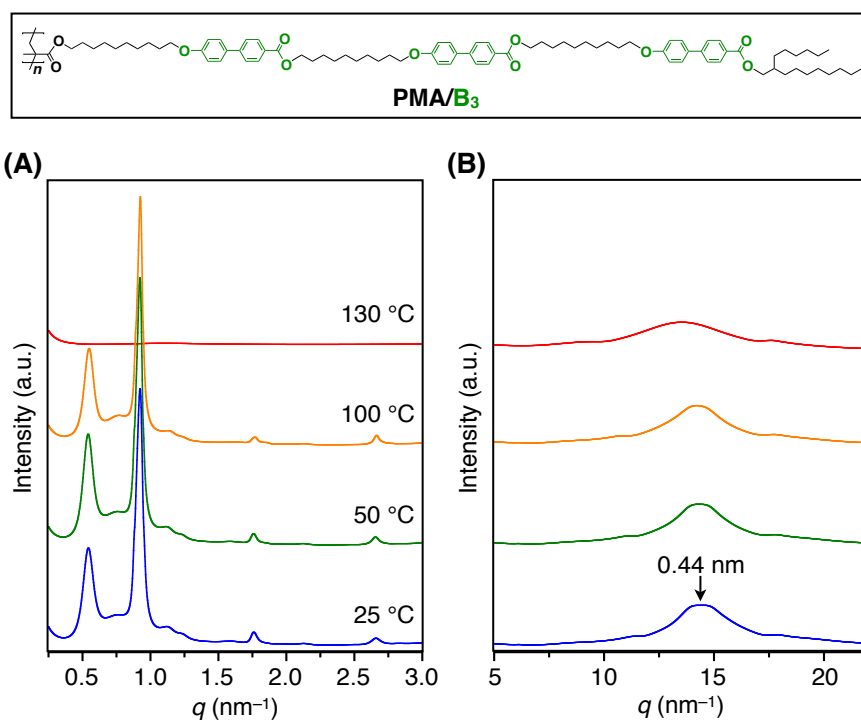


Figure S2 | (A) SAXS and (B) WAXD patterns of a bulk sample of PMA/B₃ at different temperatures on cooling from its isotropic melt in a glass capillary ($\phi = 1.5$ mm).

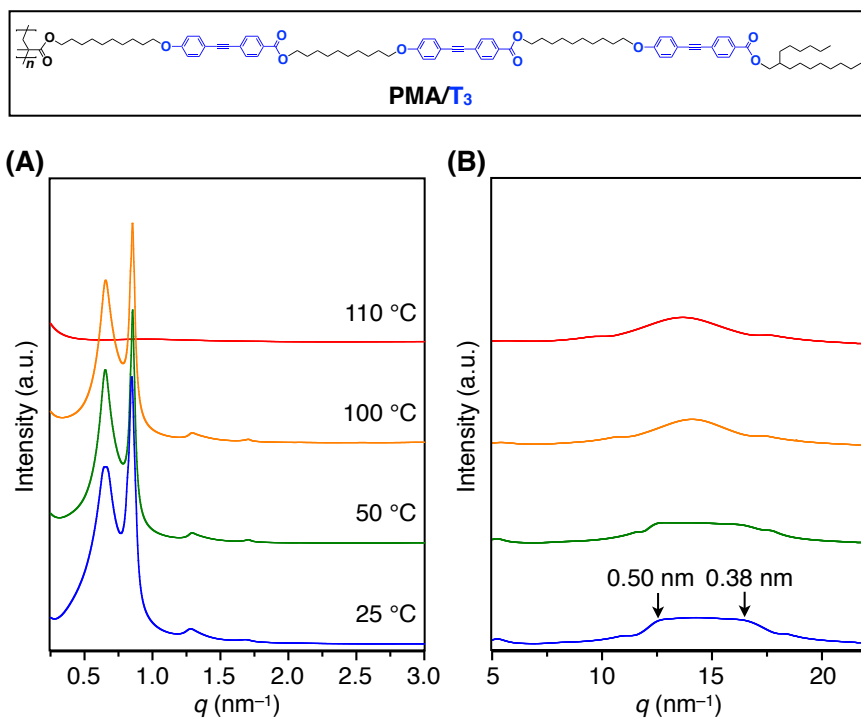


Figure S3 | (A) SAXS and (B) WAXD patterns of a bulk sample of PMA/T₃ at different temperatures on cooling from its isotropic melt in a glass capillary ($\phi = 1.5$ mm).

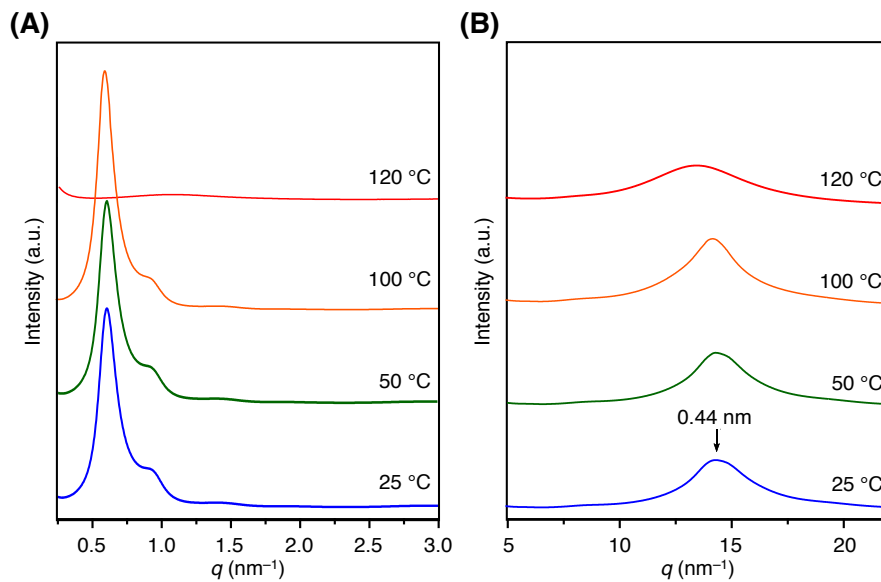


Figure S4 | (A) SAXS and (B) WAXD patterns of a bulk sample of PMA/B₂B' at different temperatures on cooling from its isotropic melt in a glass capillary ($\phi = 1.5$ mm).

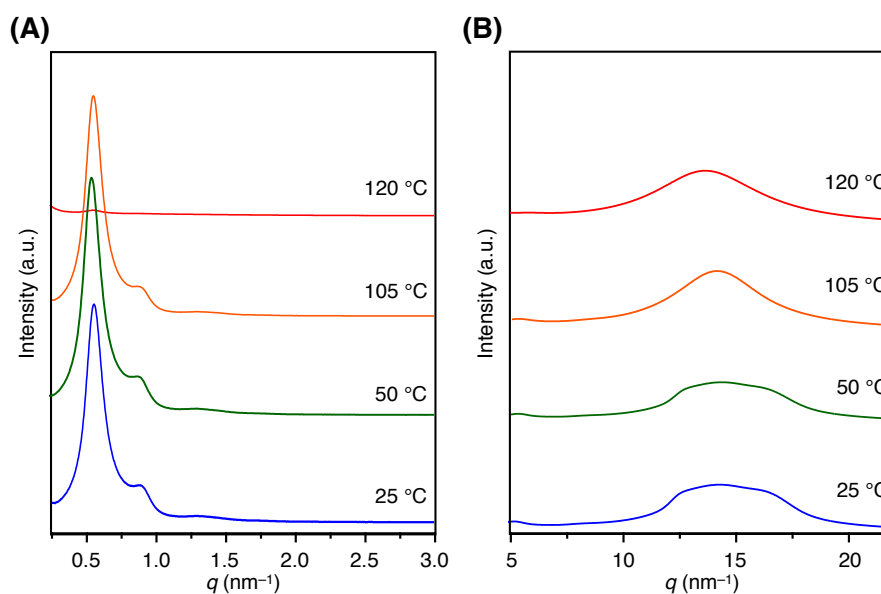


Figure S5 | (A) SAXS and (B) WAXD patterns of a bulk sample of PMA/T₂T' at different temperatures on cooling from its isotropic melt in a glass capillary ($\phi = 1.5$ mm).

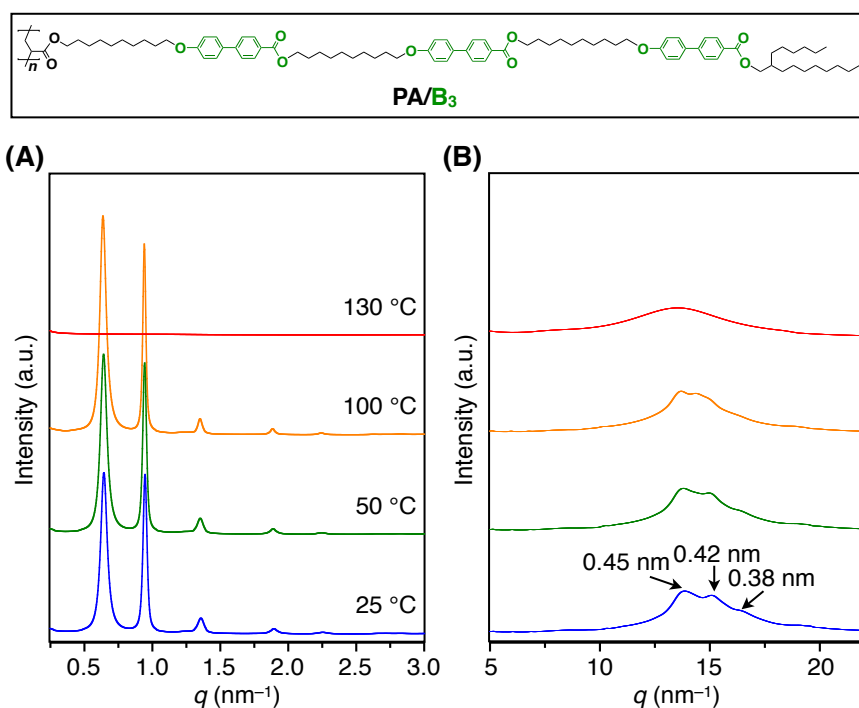


Figure S6 | (A) SAXS and (B) WAXD patterns of a bulk sample of PA/B₃ at different temperatures on cooling from its isotropic melt in a glass capillary ($\phi = 1.5$ mm).

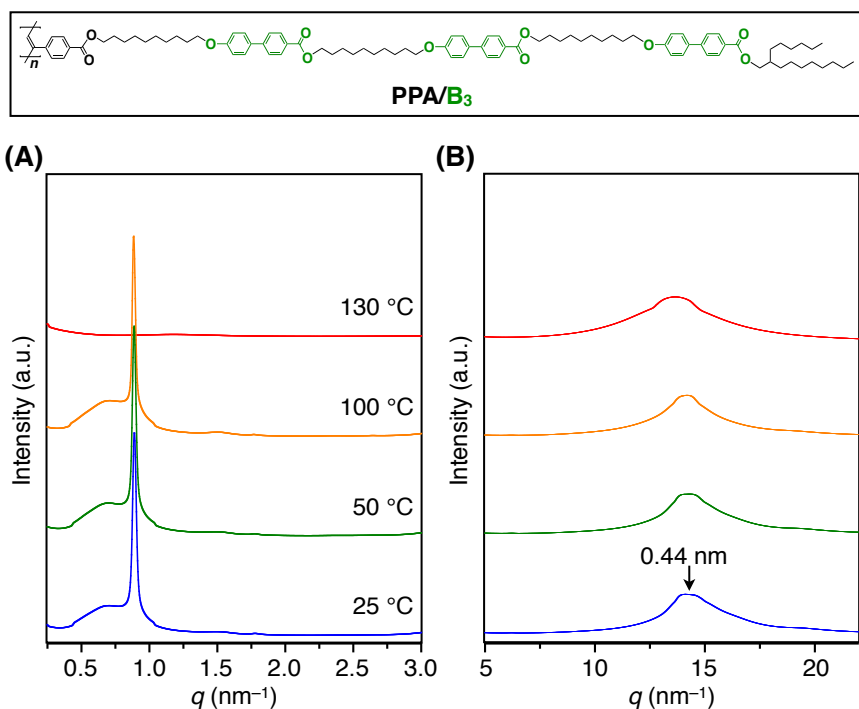


Figure S7 | (A) SAXS and (B) WAXD patterns of a bulk sample of PPA/B₃ at different temperatures on cooling from its isotropic melt in a glass capillary ($\phi = 1.5$ mm).

2.4.4. Supporting Tables

Table S1 | Polymerization Results of Macromonomers.

Polymer	Yield (%)	$M_n \times 10^{-4}^a$	M_w/M_n^a	DP ^a
PMA/B	92	5.1	3.8	88
PMA/B ₂	90	16.0	3.4	169
PMA/B ₃	90	7.6	3.8	54
PMA/T	95	7.0	4.0	113
PMA/T ₂	88	7.6	3.1	71
PMA/T ₃	80	7.7	3.0	54
PMA/B ₂ B'	53	7.3	2.2	54
PMA/T ₂ T'	80	12.0	2.7	85
PA/B ₃	47	3.8	1.4	28
PPA/B ₃	70	6.2	2.0	43

^a Determined by SEC (polystyrene standards) with CHCl₃ as an eluent.

Table S2 | Phase Transition Temperatures (*T*) and Enthalpy Changes (ΔH) of Polymers.

Polymers	Phase Sequence (Space Group) ^a		<i>T</i> (°C)		ΔH (J g ⁻¹)
			heat	cool	heat/cool
PMA/B	– ^c		no	/ no	no / no
PMA/B ₂	S (–) ^b	/ Iso	79	/ 75	9.0 / 9.4
PMA/B ₃	S (<i>P2₁/a</i>)	/ M (<i>P2₁/a</i>)	no	/ 99	no / 1.9
	S (<i>P2₁/a</i>)	/ Iso	107	/ no	20.4 / no
	M (<i>P2₁/a</i>)	/ Iso	no	/ 104	no / 18.8
PMA/T	– ^c		no	/ no	no / no
PMA/T ₂	S (–) ^b	/ Iso	84	/ 81	8.9 / 9.6
PMA/T ₃	S (<i>C2/m</i>)	/ M (<i>C2/m</i>)	95	/ 92	6.2 / 5.8
	M (<i>C2/m</i>)	/ Iso	110	/ 105	14.1 / 14.8
PMA/B ₂ B'	S (<i>P6mm</i>)	/ Iso	107	/ 101	24.1 / 24.6
PMA/T ₂ T'	S (<i>P6mm</i>)	/ M (<i>P6mm</i>)	98	/ 97	4.7 / 3.9
	M (<i>P6mm</i>)	/ Iso	113	/ 108	17.0 / 17.4
PA/B ₃	S (<i>P2/a</i>)	/ Iso	115	/ 109	33.6 / 33.8
PPA/B ₃	S (<i>C2/m</i>)	/ M (<i>C2/m</i>)	108	/ 102	– / –
	M (<i>C2/m</i>)	/ Iso	113	/ 107	19.6 / 19.0

^a S: solid, M: mesophase, Iso: isotropic melt, *P2₁/a*, *C2/m*, *P2/a*: rectangular lattice, *P6mm*: hexagonal lattice. ^b Not determined from SAXS pattern. ^c No phase transition.

Table S3 | SAXS Data of a Bulk Sample of PMA/B₃.

Temp. (°C)	q (nm ⁻¹)	$d_{\text{obs.}}$ (nm)	$d_{\text{calc.}}$ (nm)	hkl	Temp. (°C)	q (nm ⁻¹)	$d_{\text{obs.}}$ (nm)	$d_{\text{calc.}}$ (nm)	hkl
25	0.543	11.58	11.55	110	100	0.548	11.45	11.31	110
(P2 ₁ /a) ^a	0.765	8.21	8.14	210	(P2 ₁ /a) ^a	0.770	8.15	8.16	210
	0.923	6.81	7.09	020		0.926	6.78	6.79	020
	1.120	5.61	6.00	310		1.129	5.56	5.65	310
	1.241	5.06	4.97	400		1.245	5.04	5.01	400
	1.587	3.96	3.85	330		1.620	3.88	3.77	330
	1.762	3.57	3.47	520		1.770	3.55	3.50	520
	2.128	2.95	3.00	620		1.853	3.39	3.39	040
	2.658	2.36	2.36	060		2.122	2.96	3.04	620
						2.664	2.36	2.36	060

^a P2₁/a rectangular lattice parameters $a = 19.9$ and $b = 14.2$ nm at 25 °C and $a = 20.4$ and $b = 13.6$ nm at 100 °C.

Table S4 | SAXS Data of a Bulk Sample of PMA/T₃.

Temp. (°C)	q (nm ⁻¹)	$d_{\text{obs.}}$ (nm)	$d_{\text{calc.}}$ (nm)	hkl	Temp. (°C)	q (nm ⁻¹)	$d_{\text{obs.}}$ (nm)	$d_{\text{calc.}}$ (nm)	hkl
25	0.657	9.57	9.58	110	100	0.650	9.66	9.65	110
(C2/m) ^a	0.849	7.40	7.46	020	(C2/m) ^a	0.855	7.35	7.36	020
	1.281	4.90	4.79	220		1.292	4.86	4.82	220
	1.683	3.73	3.73	040		1.705	3.68	3.68	040
	1.976	3.18	3.19	330		2.011	3.12	3.21	330
						2.547	2.47	2.47	060

^a C2/m rectangular lattice parameters $a = 12.5$ and $b = 14.9$ nm at 25 °C and $a = 12.8$ and $b = 14.7$ nm at 100 °C.

Table S5 | SAXS Data of a Bulk Sample of PMA/B₂B'.

Temp. (°C)	q (nm ⁻¹)	$d_{\text{obs.}}$ (nm)	$d_{\text{calc.}}$ (nm)	hkl	Temp. (°C)	q (nm ⁻¹)	$d_{\text{obs.}}$ (nm)	$d_{\text{calc.}}$ (nm)	hkl
25	0.581	10.81	11.05	100	100	0.571	11.00	11.21	100
(P6mm) ^a	0.968	6.49	6.38	110	(P6mm) ^a	0.954	6.58	6.47	110
	1.455	4.32	4.20	210		1.460	4.30	4.26	210
	1.751	3.59	3.68	300		1.707	3.68	3.74	300

^a P6mm hexagonal lattice parameter $a = 12.7$ nm at 25 °C and $a = 12.9$ nm at 100 °C.

Table S6 | SAXS Data of a Bulk Sample of PMA/T₂T'.

Temp. (°C)	q (nm ⁻¹)	$d_{\text{obs.}}$ (nm)	$d_{\text{calc.}}$ (nm)	hkl	Temp. (°C)	q (nm ⁻¹)	$d_{\text{obs.}}$ (nm)	$d_{\text{calc.}}$ (nm)	hkl
25	0.540	11.63	11.78	100	100	0.537	11.69	11.80	100
(P6mm) ^a	0.918	6.84	6.80	110	(P6mm) ^a	0.913	6.88	6.81	110
	1.392	4.51	4.45	210		1.371	4.58	4.46	210
	1.622	3.88	3.93	300		1.622	3.88	3.93	300

^a P6mm hexagonal lattice parameter $a = 13.6$ nm at 25 °C and $a = 13.6$ nm at 105 °C.

Table S7 | SAXS Data of a Bulk Sample of PA/B₃.

Temp. (°C)	q (nm ⁻¹)	$d_{\text{obs.}}$ (nm)	$d_{\text{calc.}}$ (nm)	hkl	Temp. (°C)	q (nm ⁻¹)	$d_{\text{obs.}}$ (nm)	$d_{\text{calc.}}$ (nm)	hkl
25	0.645	9.74	9.38	110	100	0.636	9.87	9.91	110
(P2/a) ^a	0.947	6.64	6.93	200	(P2/a) ^a	0.942	6.67	6.89	200
	1.357	4.63	4.63	300		1.261	4.98	4.96	220
	1.895	3.32	3.34	410		1.352	4.65	4.59	300
	2.253	2.79	2.78	500		1.884	3.34	3.35	410
						2.242	2.80	2.75	500
						2.630	2.39	2.38	530

^a P2₁/a rectangular lattice parameters $a = 13.9$ and $b = 12.4$ nm at 25 °C and $a = 13.8$ and $b = 14.3$ nm at 100 °C.

Table S8 | SAXS Data of a Bulk Sample of PPA/B₃.

Temp. (°C)	q (nm ⁻¹)	$d_{\text{obs.}}$ (nm)	$d_{\text{calc.}}$ (nm)	hkl	Temp. (°C)	q (nm ⁻¹)	$d_{\text{obs.}}$ (nm)	$d_{\text{calc.}}$ (nm)	hkl
25	0.706	8.90	9.32	110	100	0.702	8.95	8.68	110
(C2/m) ^a	0.889	7.07	7.07	020	(C2/m) ^a	0.911	6.90	6.91	020
	1.329	4.73	4.71	220		1.384	4.54	4.34	220
	1.776	3.54	3.54	040		1.815	3.46	3.45	040
						2.191	2.87	2.89	330
						2.730	2.30	2.30	060

^a C2/m rectangular lattice parameters $a = 12.6$ and $b = 14.2$ nm at 25 °C and $a = 11.2$ and $b = 13.8$ nm at 100 °C.

Chapter 3 Controlling Bottlebrush Polymers Assemble To 2D Homeotropic Order

3

Vertical alignment of polymers on surfaces is challenging. Here, I proposed a design principle allowing polymers to be arranged into 2D homeotropic orientations by using long-range dipole-dipole interactions in conjunction with hot-pressing on Teflon sheets.

3.1 Introduction

Macroscopic alignment of molecules is of considerable practical significance, since it is promising for developing high-performance organic materials and devices (1,2). For example, two-dimensional (2D) homeotropic alignment of columnar liquid crystalline (*c*-LC) molecules exhibited the excellent charge mobility, which is essential for organic photovoltaic cell (3). In fact, there are two distinct alignments of *c*-LCs: homogeneous, (column axis parallel to a substrate) and homeotropic (column axis perpendicular to a substrate) (4). For *c*-LC polymers, merely homogeneous examples have been reported (5–7). Cheng *et al.* found that a 2D hexagonal columnar lattice formed by poly[di(4-heptyl) vinylterephthalate] (PDHVPT) is homogeneously aligned by shearing in light of a six-fold symmetry of (100) diffractions in 2D WAXD image when X-ray beam was parallel to the shearing direction (Figure. 1A) (5). Zhou *et al.* chose a *c*-LC polymer with “mesogenic jacket” (molecular structure is shown in Chapter 2.1 as a candidate and demonstrated that homogeneous alignment was successfully obtained not only by shearing but also by electric field (*E*-field) (Figure. 2B)

[1] See Chapter 1

[2] G. M. Whitesides, B. Grzybowski. *Science* **295**, 2418 (2002).

[3] L. Schmidt-Mende, A. Fechtenkötter, K. Müllen, E. Moons, R. H. Friend, J. D. MacKenzie. *Science* **293**, 1119 (2001).

[4] B. R. Kaafarani. *Chem. Mater.* **23**, 378 (2011).

[5] X. -Y. Yin *et al.* *J. Am. Chem. Soc.* **125**, 6854 (2003).

[6] H. -L. Xie *et al.* *J. Am. Chem. Soc.* **132**, 8071 (2010).

[7] M. Defaux *et al.* *Macromolecules* **42**, 3500 (2009).

[8] J. C. Wittmann *et al.* *Nature* **352**, 414 (1991).

[9] A. M. van de Craats *et al.* *Adv. Mater.* **15**, 495 (2003).

[10] R. I. Gearba *et al.* *Adv. Mater.* **19**, 815 (2007).

[11] T. Takahashi, F. Teraoka, I. Tsujimoto. *J. Macromol. Sci. Phys.* **B12**, 303 (1976).

[12] N. Hosono *et al.* *Science* **330**, 808 (2010).

(6). Defaux *et al.* fabricated a anisotropic thin film of poly(di-*n*-propylsiloxane) (PDPS) with homogeneous alignment by using a polytetrafluoroethylene (PTFE)-rubbed substrate (Figure. 2C) (7).

As an aligner, patterned PTFE surface was originally proposed by Wittmann and Smith (8), and shown to have a remarkable orienting capability for many CLCs and few polymers (9–11). Although the detailed mechanism is unclear to now, the surface-topology-induced epitaxy (surfaced patterns such as grooves) combined with a molecular epitaxy (molecular oriented axis of ordered structure) is generally accepted for realizing macroscopic alignment on the PTFE substrate (Figure. 2A). Therefore, in most cases, a homogeneous orientation is usually obtained by this strategy, especial for polymers. As an unprecedented discovery, we accidentally fabricated a 2D ordered thin film composed of a bottlebrush polymer upon hot-pressed by groove-pattern Teflon sheets (PTFE), in which polymer backbones align homeotropically to the film plane, while their side chains align horizontally along the direction of grooves on Teflon surface (Figure. 2B) (12). A possible mechanism is that a 2D rectangular lattice formed by bottlebrush polymer translated 1D structured order of Teflon surface and the propagated from the interface macroscopically to the deep region of the hot-pressed film.

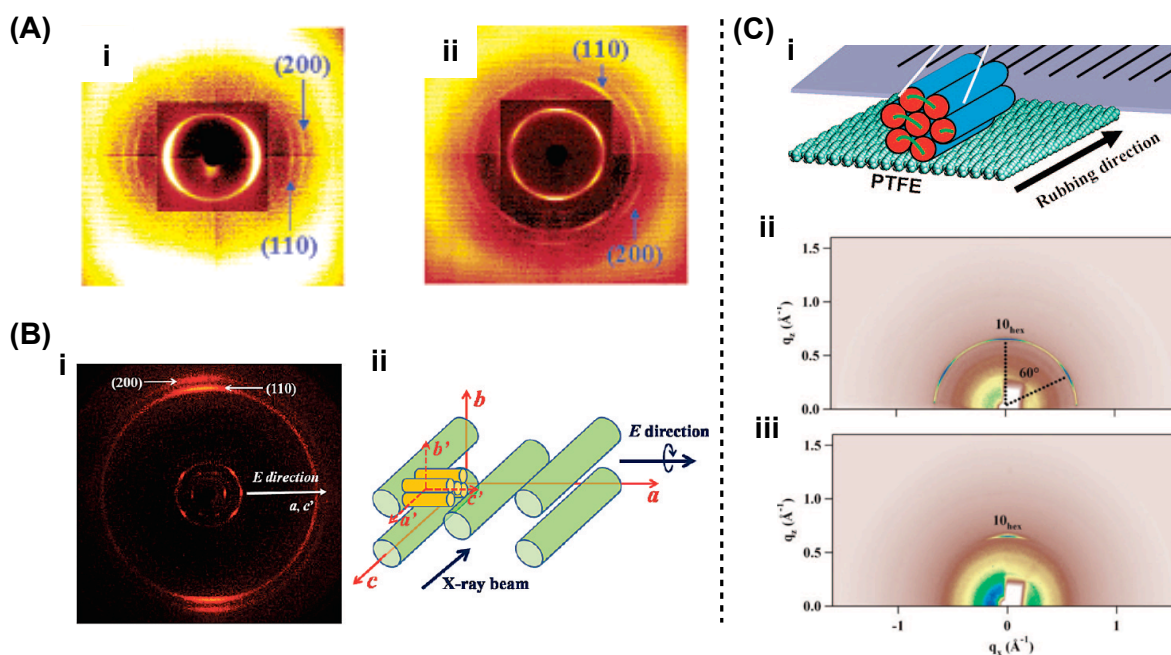


Figure 1 | Homogeneous alignment of columnar liquid crystalline (CLC) polymers. (A) 2D WAXD images of aligned PDHVPT obtained with X-ray beam perpendicular (i) and parallel (ii) to the shear direction.⁵ (B) 2D WAXD pattern (i) and schematic illustration (ii) of a CLC polymer with “mesogenic jacket” oriented by applied E-field.⁶ (C) Schematic illustration (i) and GIXD patterns (ii, iii) of a PDPS thin film on a PTFE-rubbed surface. X-ray beam is directed parallel (ii) or perpendicular (iii) to the rubbing direction.⁷

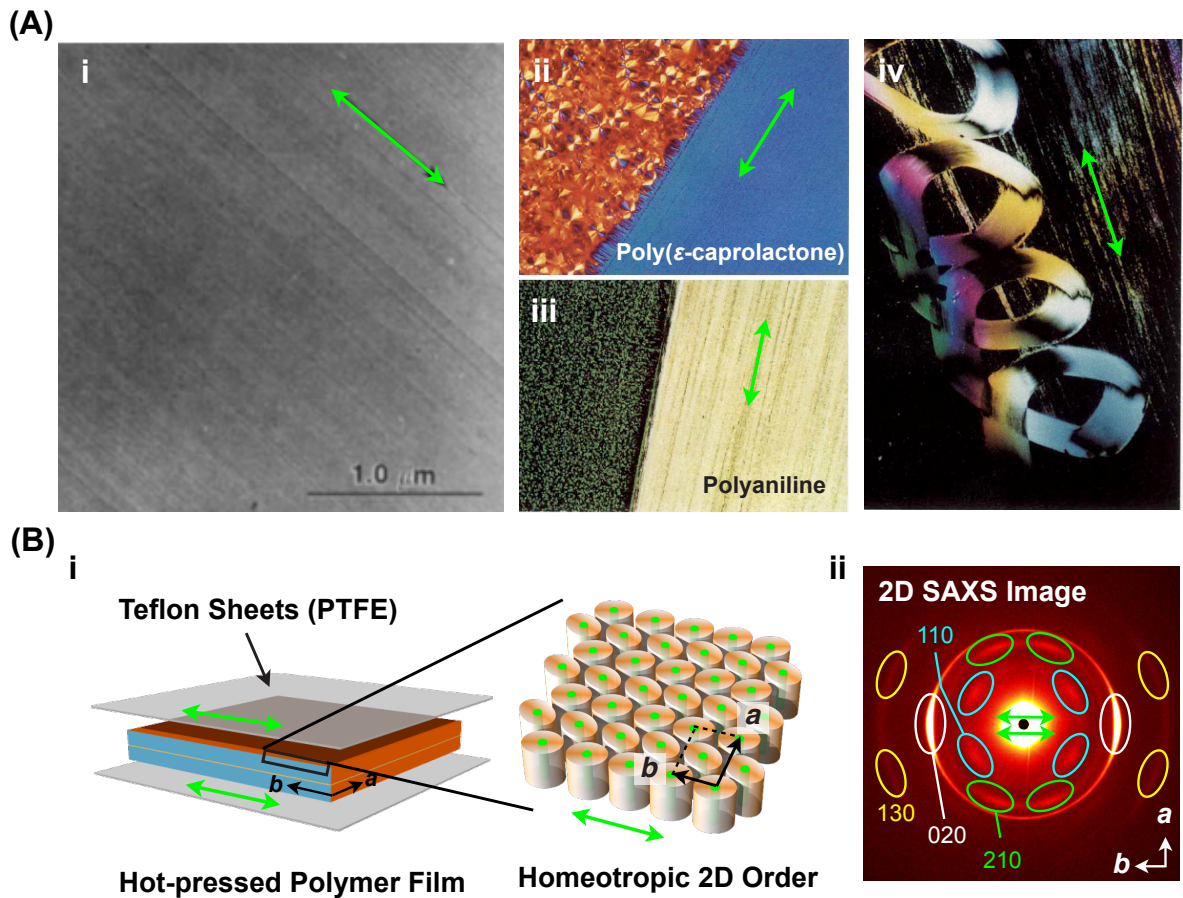


Figure 2 | Polytetrafluoroethylene (PTFE) with pattern surface as an aligner for alignment. (A) PTFE as a substrate for homogeneously oriented growth of materials.⁸ (i) TEM image of a PTFE thin layer treated by mechanical rubbing. POM images taken on (ii) poly(ε-caprolactone), (iii) polyaniline and (iv) rod-like liquid crystalline molecule grown on a glass slide coated with oriented PTFE. (B) Stretched PTFE as a substrate for homeotropic orientation of a brush polymer by hot-pressing.¹² (i) Schematic illustration of hot-pressed polymer film and a molecular arrangement in the film surface region. (ii) Through-view 2D SAXS image of hot-pressed film prepared by hot-pressing with two Teflon sheets.

In the previous chapter, I synthesized several similar brush polymers and study the formation mechanism of their self-assembled 2D lattices. Because of dipole-dipole interaction, three main 2D lattices were obtained: $P2_1/a$, $C2/m$ rectangular and $P6mm$ hexagonal. In this chapter, I will focus on the following questions:

- 1) What kinds of 2D lattice are processable into homeotropic 2D order and why?
- 2) What is the driving force for vertical propagation from the interface between Teflon surface and polymer bulk?

3.2. Results and Discussion

3.2.1. New Bottlebrush Polymers

In order to detail investigate the macroscopic orientation behavior of bottlebrush polymers, I newly synthesized 7 hybrid polymers carrying three mesogenic units in side chains (Schemes. S1–3 and Table S1 in Supporting Information). Figure 3 presents the their molecular structures and phase transition behaviors. All polymers were prepared by free radical polymerization and their thermal properties were characterized by differential scanning calorimetry (DSC, Figure. S1). As we expected, all bottlebrush polymers exhibited an obvious mesophase, but the phase transition temperatures were various based on the nature of mesogens rather than their sequences. For example, **PMA/A₃** showed higher phase transition temperatures than **PMA/B₃** and **PMA/T₃**, accordingly, bottlebrush polymers such as **PMA/T₂A**, **PMA/B₂A**, **PMA/TA₂** and **PMA/BA₂**, which contain at least one azobenzene unit, displayed a higher mesophase temperature range than those having no azobenzene such as **PMA/B₃** and **PMA/T₃** (Figures. 3B and S1). On the other hand, **PMA/T₂B**, **PMA/TBT**, and **PMA/BT₂** underwent a phase transition at nearly the same temperature, although the sequences of mesogens are different (Figures. 3B and S1).

The self-assembly behaviors of new bottlebrush polymers were evaluated by synchrotron radiation small-angle X-ray scattering (SAXS) (Figures. S2–S8 and Tables. S3–S9) and their lattice structures are summarized in Table 1. Of further note on the **PMA** family, the 2D rectangular lattices of **PMA/A₃** and **PMA/B₃** and those of their hybrids such as **PMA/B₂A** (Figure. S2 and Table. S3) and **PMA/BA₂** (Figure. S3 and Table. S5) commonly belong to the symmetry group of $P2_1/a$ irrespective of the ratio of mesogens **A** to **B**. Meanwhile, the 2D rectangular lattice of **PMA/T₃** belongs to the symmetry group of $C2/m$ and is different from the above series having

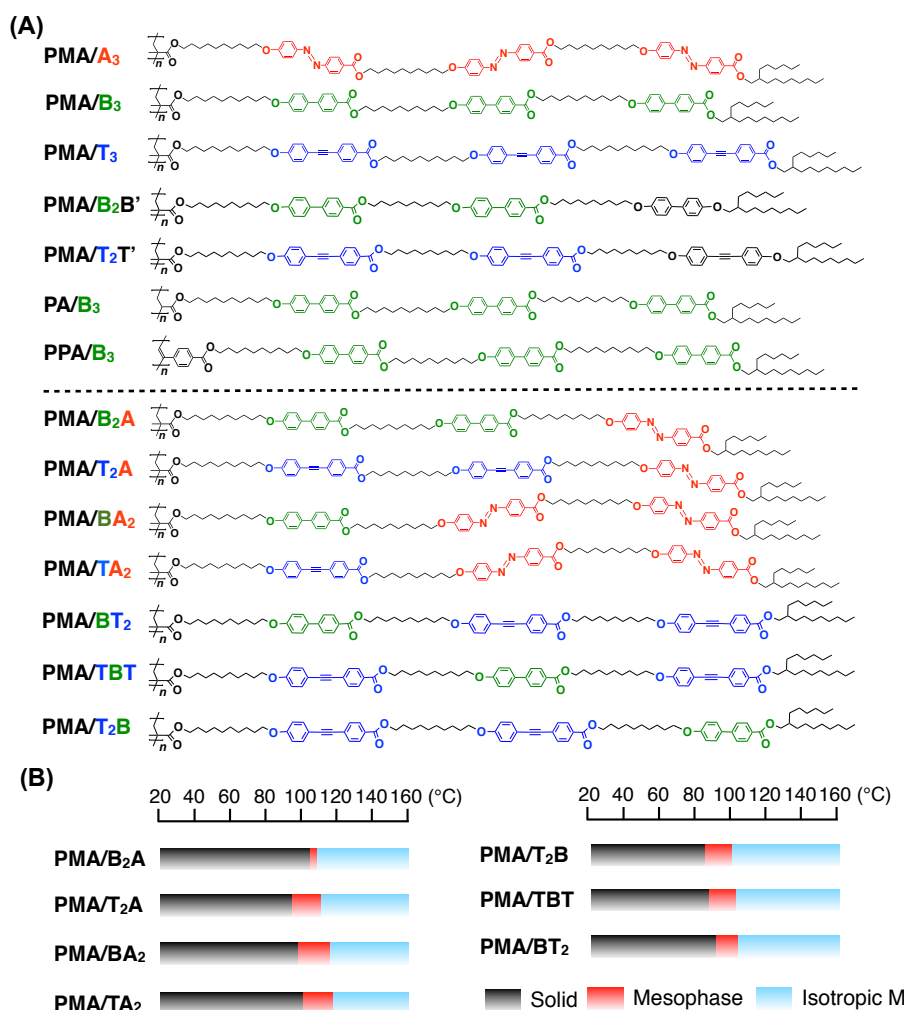


Figure 3 | (A) Molecular formulae of existing (up) and newly synthesized (down) brush polymers. (B) Phase transition behavior of newly synthesized (down) brush polymers. Thermal properties are characterized by DSC, recorded the second heating/cooling cycles. The scan rate is 5 °C /min. Black arrows denote the shifted direction of phase transition temperatures.

mesogens **A** and/or **B** exclusively. However, when mesogen **A** or **B** is combined with mesogen **T** for the side-chain motif, the preferred symmetry group of the resulting 2D rectangular lattice is determined by the major mesogen. Namely, **PMA/T₂A** (Figure. S4 and Table. S5) and **PMA/TA₂** (Figure. S5 and Table. S6) prefer *C2/m* and *P2₁/a*, respectively. Accordingly, irrespective of the sequence of three mesogenic units in the side chains, **PMA/T₂B**, **PMA/TBT** and **PMA/BT₂**, the same as **PMA/T₂A**, all prefer *C2/m* because **T** is the major mesogen in these three bottlebrush polymers (Figures. S6–S8 and Tables. S7–S9).

Table 1 | Structural Parameters of Brush Polymers in Bulk.

Polymer	Aspect Ratio ^a	Temp. (°C)	Space Group ^b	Lattice Parameter	
				a (nm)	b (nm)
PMA/A ₃	2.27	115	<i>P2₁/a</i>	21.8	14.7
PMA/B ₃	2.85	100	<i>P2₁/a</i>	20.4	13.6
PMA/BA ₂	2.40	110	<i>P2₁/a</i>	22.2	14.2
PMA/TA ₂	2.70	110	<i>P2₁/a</i>	21.8	14.7
PMA/B ₂ A	2.60	105	<i>P2₁/a</i>	23.0	13.8
PMA/T ₃	4.00	100	<i>C2/m</i>	12.8	14.7
PMA/T ₂ A	3.25	105	<i>C2/m</i>	11.9	14.7
PMA/T ₂ B	3.62	100	<i>C2/m</i>	12.6	14.5
PMA/TBT	3.62	100	<i>C2/m</i>	12.8	14.6
PMA/BT ₂	3.62	100	<i>C2/m</i>	12.7	14.4

^aAspect Ratio = l/d , l and d refers to the length of long and short axis of a mesogen, respectively. ^b*P2₁/a*, *C2/m*: rectangular lattice.

3.2.2. 2D Homeotropic Orientation of Bottlebrush Polymers

As in our previous study (12), we hot-pressed these bottlebrush polymers between two Teflon sheets. Each Teflon sheet on its one side generally possesses unidirectionally oriented surface grooves. During hot-pressing, Teflon sheets were arranged such that their surface grooves were parallel to one another for sandwiching the bottlebrush polymers. Individual samples were allowed to cool from their isotropic melts to a temperature lower by 5 °C than the phase transition temperature to the ordered phase and pressed at 8.0 MPa, and then slowly cooled to room temperature. Consequently, 6–10 μm thick self-standing films were obtained (see Methods). In a through-view 2D SAXS image of the hot-pressed PMA/B₃ (*P2₁/a*) film, arc-

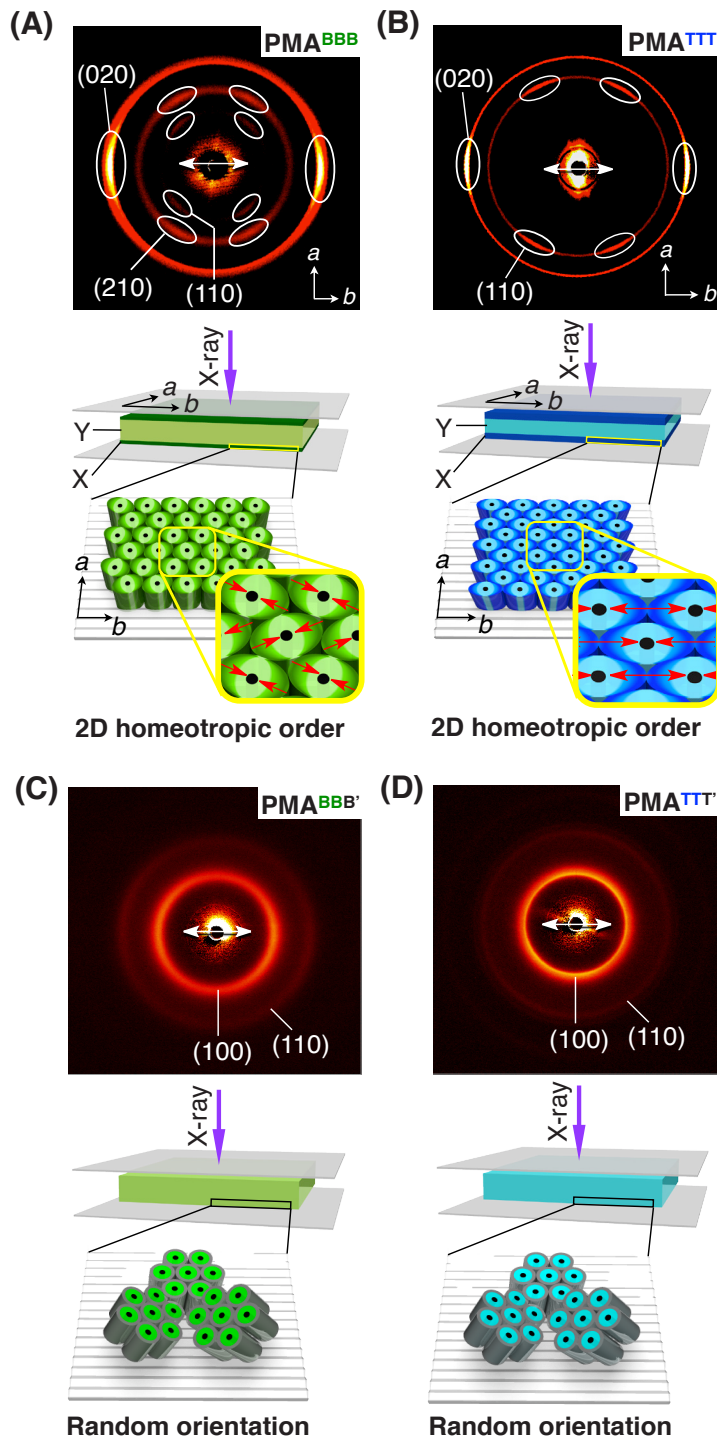


Figure 4 | Orientation of bottlebrush polymers in their hot-pressed films. Through-view 2D SAXS images (upper) at 25 °C of hot-pressed films of (A) **PMA/B₃**, (B) **PMA/T₃**, (C) **PMA/B₂B'** and (D) **PMA/T₂T'** and schematic representations (lower) of their molecular arrangements. The surface grooves on the Teflon sheets are depicted by black lines, whose directions are highlighted by white arrows. Red arrows denote the directions of the oppositely oriented local dipoles in the side chains. X and Y indicate the homeotropic ordered and disordered domains in hot-pressed films, respectively.

shaped diffractions assignable to the (110) , (210) , and (020) planes were clearly observed (Figure. 4A), suggesting that the (001) plane of the 2D lattice is oriented parallel to the surface of the Teflon sheets. Furthermore, the diffraction spots indexed to the (020) plane appeared only in a parallel direction to the surface grooves on the Teflon sheets. Consistent with the results of through-view 2D SAXS imaging, only (020) spots were observed in the equatorial direction of the edge-view 2D SAXS image (Figure. 7A). These results clearly indicate that the b -axis of the 2D lattice, as illustrated in Figure. 4A (lower), is oriented parallel to the surface grooves on the Teflon sheets. In other words, **PMA/B₃** adopts a homeotropic order in the hot-pressed film. Consistently, in polarizing optical microscopy (POM), the hot-pressed **PMA/B₃** under crossed polarizers exhibited a contrast at every 45° on rotation, giving bright and dark views when the azimuthal angles between the polarizing direction of the incident light and the b -axis of the 2D lattice were 45° and 0° (90°), respectively (Figure. 5A). Likewise, polarized infrared (IR) spectroscopy of the film gave polar plots with a clear dichroic feature (Figure. 5E) in which the stretching vibration bands attributable to the aromatic ether ($C_{Ar}-O$) and ester ($C-O$) groups, as well as those of the aromatic rings ($C_{Ar}-C_{Ar}$), of the mesogens displayed a maximum absorbance in the direction parallel (0°) to the surface grooves on the Teflon sheets. The same held true for the hot-pressed **PMA/T₃** in 2D XRD (Figures. 4B and S10B), although its preferred symmetry group of the 2D lattice was $C2/m$ and different. Again, POM (Figure. 5B) and polarized IR (Figure. 5F) unambiguously supported the homeotropic order of cylindrical **PMA/T₃** in the hot-pressed film.

Most importantly, not only **PMA/B₃** and **PMA/T₃** but also all the other **PMA**-based bottlebrush polymers, adopting a rectangular 2D lattice, displayed the same orientation behavior upon being hot-pressed in the Teflon sheets. Namely, such polymer cylinders align homeotropically with respect to the Teflon sheets when their surface grooves are arranged parallel to one another (Figures. 6–9). In contrast, when the bottlebrush polymers such as **PMA/B₂B'** and **PMA/T₂T'**, which adopt a hexagonal columnar lattice, were likewise hot-pressed in the Teflon sheets, only isotropic circles emerged in their through-view 2D-XRD profiles (Figures. 4C,D, upper). Together with the results of POM (Figures. 5C,D) and polarized IR (Figures. 5G,H), these 2D-XRD profiles clearly indicate the absence of any macroscopic structural order in the hot-pressed **PMA/B₂B'** and **PMA/T₂T'** films (Figures. 4C,D, lower). Despite such a high sensitivity to the side-chain structure, the polymer backbone does not play an essential role. In fact, analogous to the **PMA** series, **PA/B₃** and **PPA/B₃** having polyacrylate and polyphenylacetylene backbones, respectively, adopt a 2D rectangular lattice in bulk and align homeotropically in their hot-pressed films (Figures. 6H,I and 7J,K).

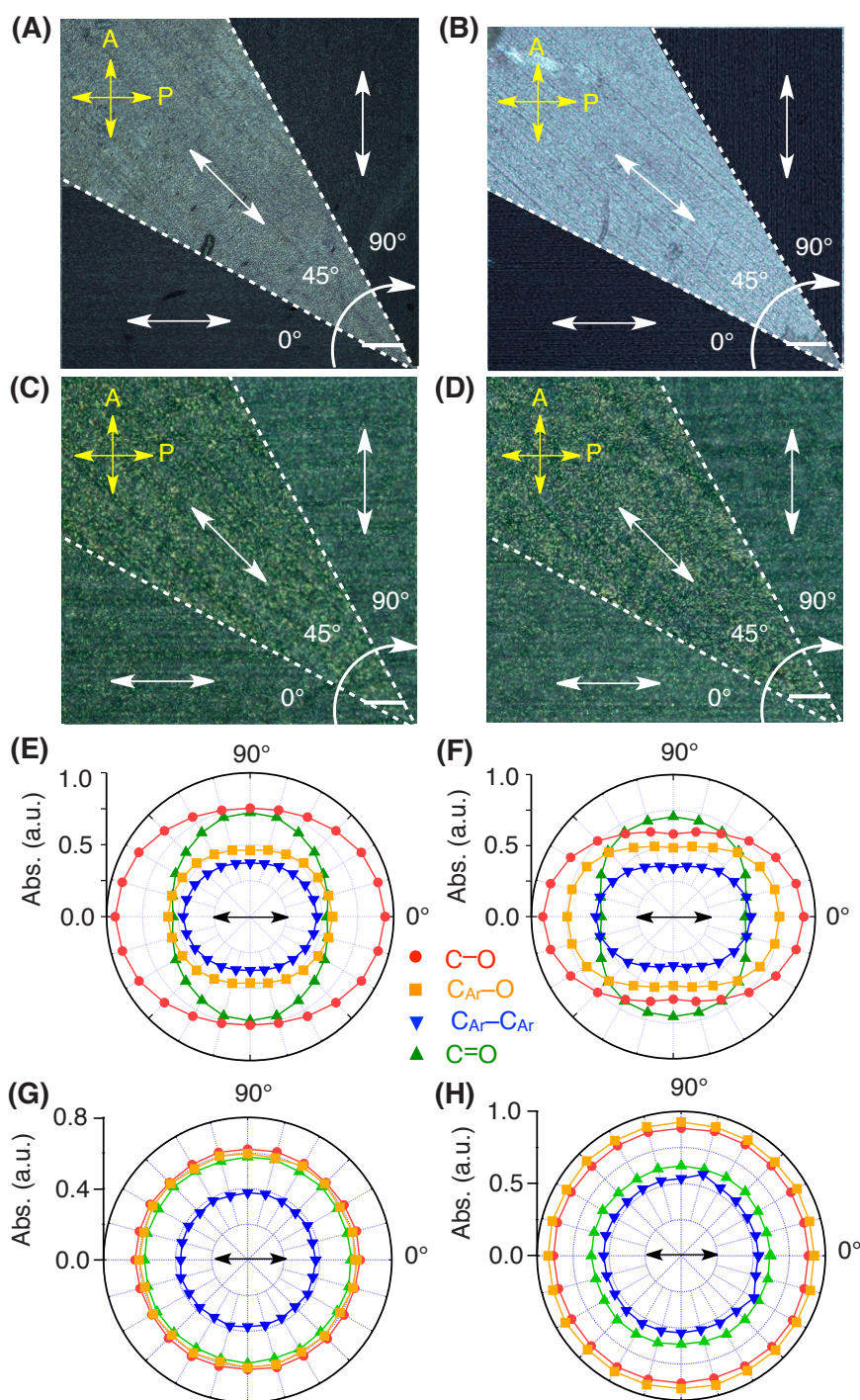


Figure 5 | Anisotropic orientation of side-chain mesogenic units of bottlebrush polymers in their hot-pressed films. (A-D) POM micrographs of hot-pressed films of (A) PMA/B₃, (B) PMA/T₃, (C) PMA/B₂B', and (D) PMA/T₂T' under crossed polarizers, recorded at 0° (lower regions), 45° (diagonal regions) and 90° (upper regions) relative to the transmission axis of the polarizer (P, yellow arrow) upon clockwise rotation of the film (white circular arrow). All of the scale bars represent 50 μm. White arrows in all of the images denote directions of the surface grooves on the Teflon sheets. (E-H) Polar plots of the infrared absorption intensities, recorded upon rotation of a polarizer at every 15°, of hot-pressed films of (E) PMA/B₃, (F) PMA/T₃, (G) PMA/B₂B', and (H) PMA/T₂T'. The azimuthal angle is defined as 0° when the polarizing direction of the incident light is parallel to the surface grooves on the Teflon sheets (black arrows).

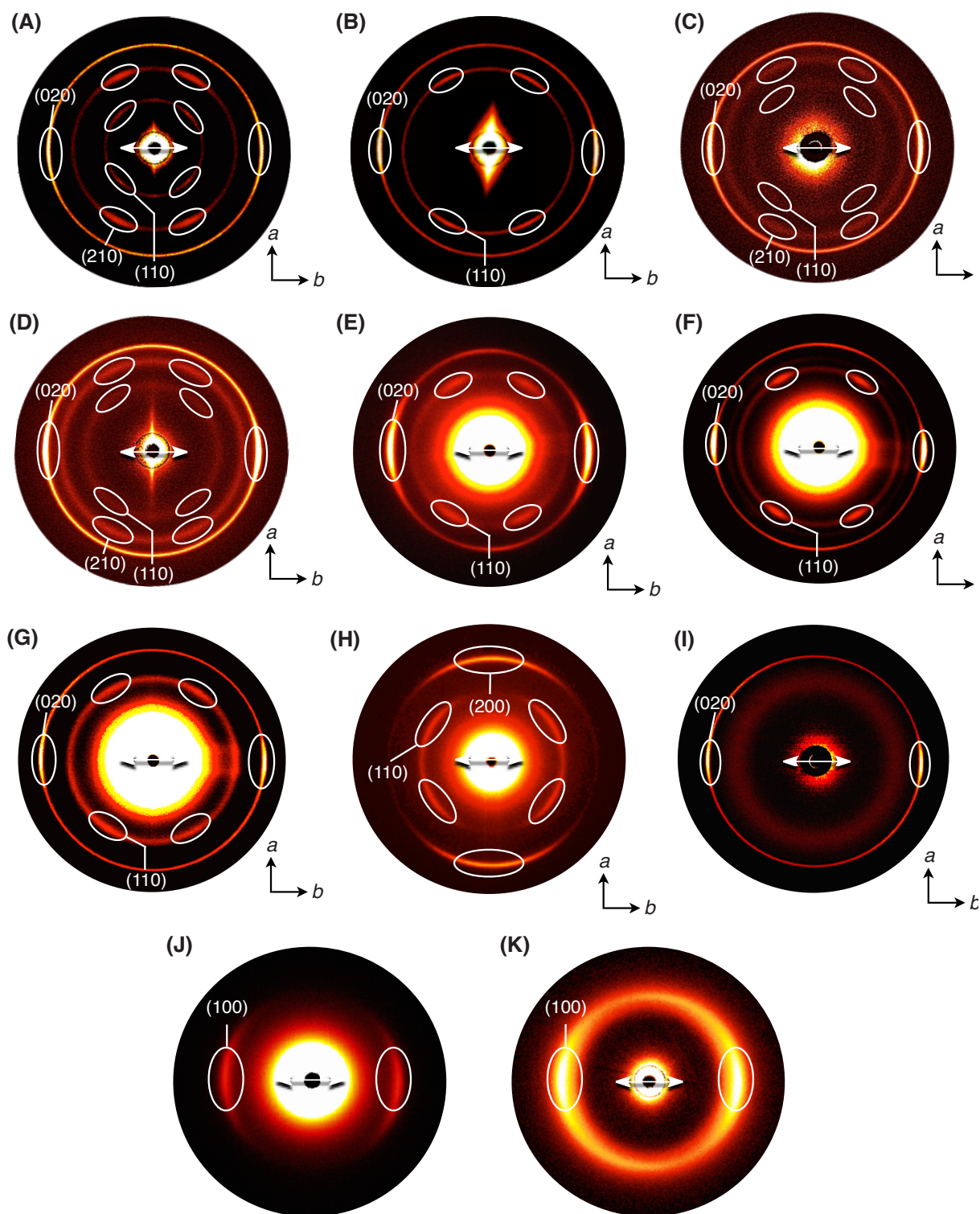
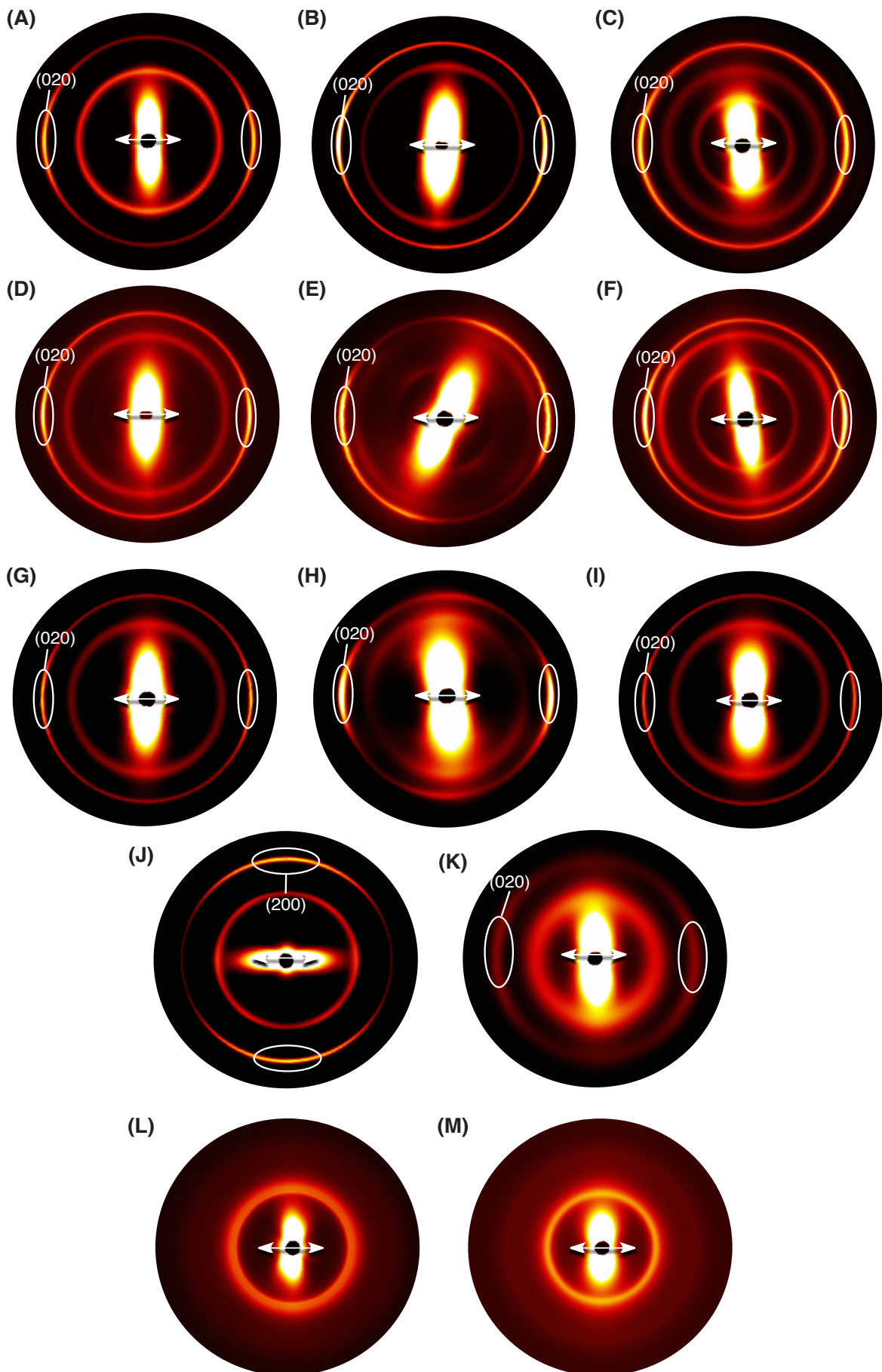


Figure 6 | Through-view 2D SAXS images at 25 °C of hot-pressed films of (A) PMA/B₂A, (B) PMA/BA₂, (C) PMA/T₂A, (D) PMA/TA₂, (E) PMA/T₂B, (F) PMA/TBT, (G) PMA/BT₂, (H) PA/B₃, (I) PPA/B₃, (J) MA/B₃, and (K) MA/T₃ prepared with parallel arranged Teflon sheets. White arrows denote the directions of grooves on the Teflon sheets.

Figure 7 | Edge-view 2D SAXS images at 25 °C of hot-pressed films of (A) PMA/B₃, (B) PMA/T₃, (C) PMA/B₂A, (D) PMA/T₂A, (E) PMA/BA₂, (F) PMA/TA₂, (G) PMA/T₂B, (H) PMA/TBT, (I) PMA/BT₂, (J) PA/B₃, (K) PPA/B₃, (L) PMA/B₂B', and (M) PMA/T₂T' prepared with parallel arranged Teflon sheets. White arrows denote the directions of grooves on the Teflon sheets.



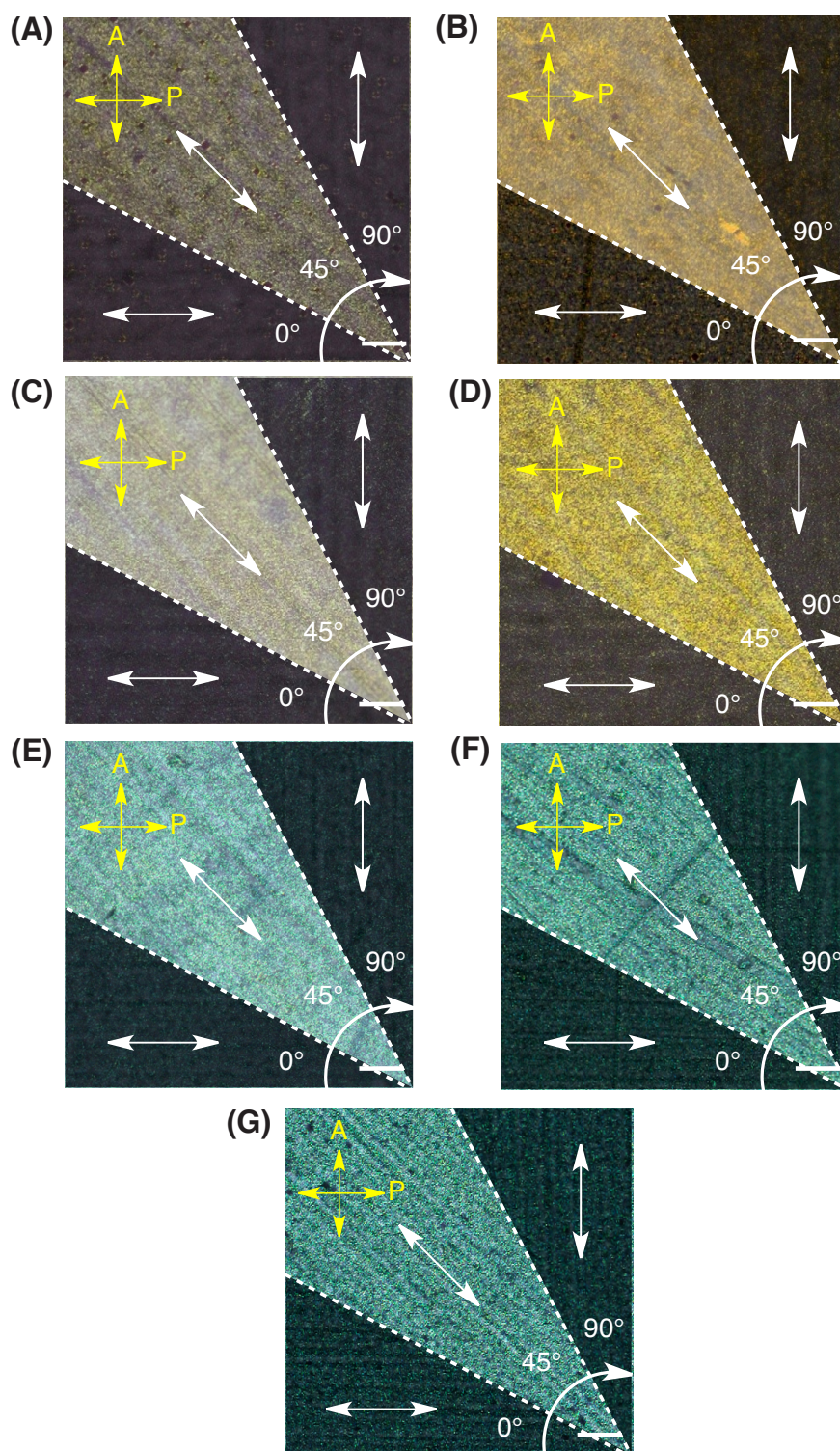


Figure 8 | POM micrographs of hot-pressed films of (A) PMA/B₂A, (B) PMA/BA₂, (C) PMA/T₂A, (D) PMA/TA₂, (E) PMA/T₂B, (F) PMA/TBT, and (G) PMA/BT₂ under crossed polarizers, recorded at 0° (lower regions), 45° (diagonal regions) and 90° (upper regions) relative to the transmission axis of the polarizer (P, yellow arrow) upon clockwise rotation of the film (white circular arrow). All of the scale bars represent 50 μm. White arrows in all of the images denote directions of the surface grooves on the Teflon sheets.

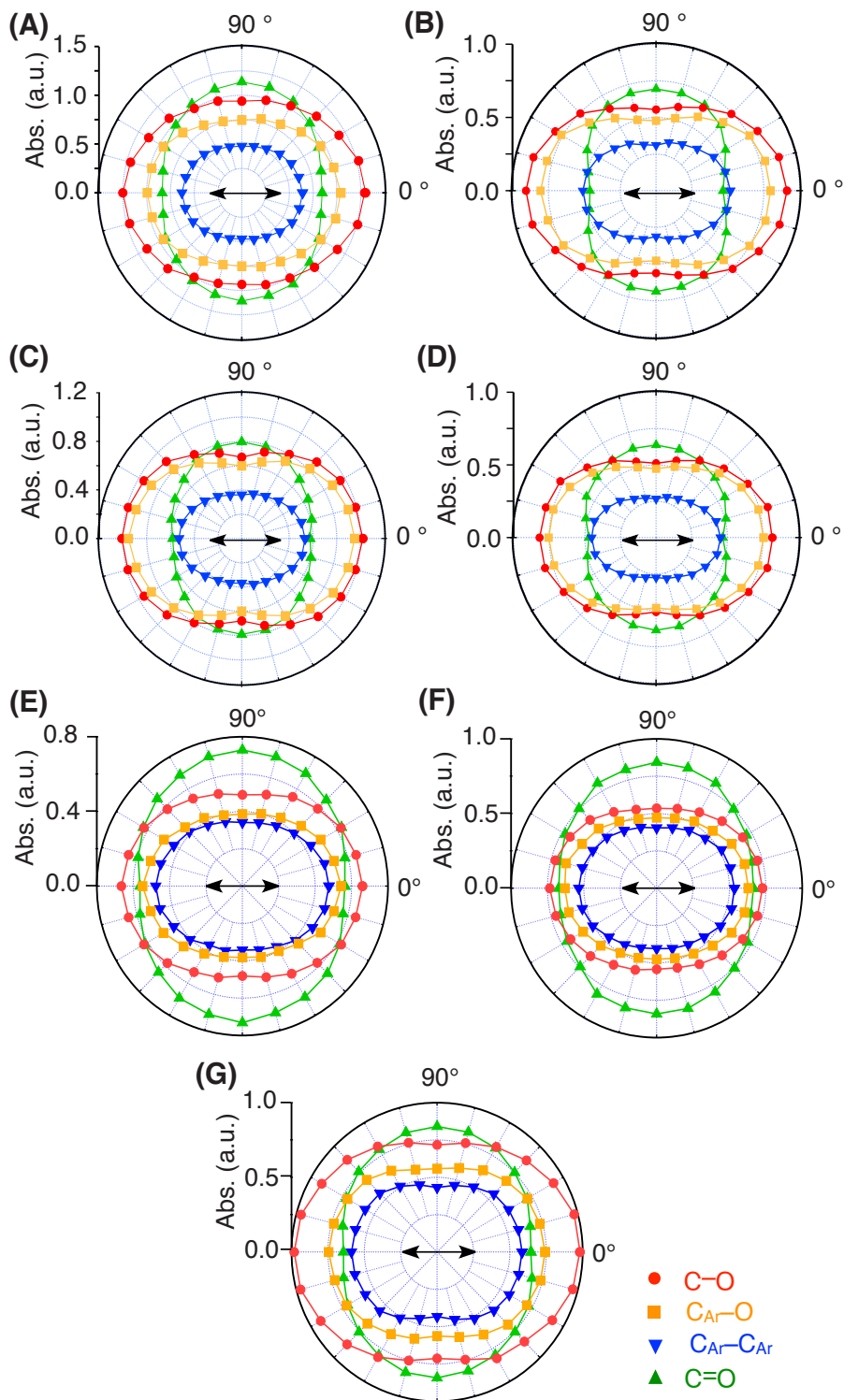


Figure 9 | Polar plots of the infrared absorption intensities, recorded upon rotation of a polarizer at every 15°, of hot-pressed films of (A) PMA/B₂A, (B) PMA/BA₂, (C) PMA/T₂A, (D) PMA/TA₂, (E) PMA/T₂B, (F) PMA/TBT, and (G) PMA/BT. The azimuthal angle is defined as 0° when the polarizing direction of the incident light is parallel to the surface grooves on the Teflon sheets (black arrows).

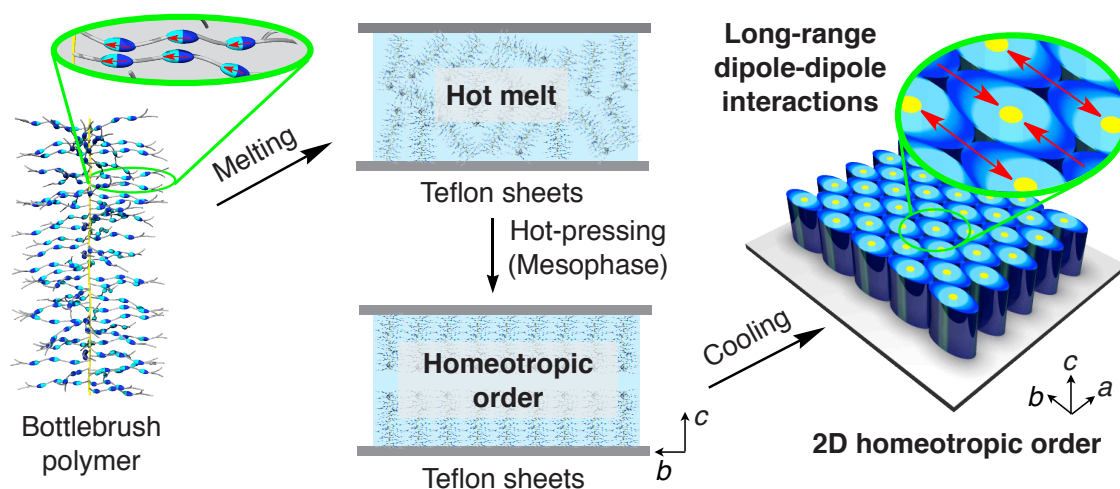


Figure 10 | Schematic illustrations of formation mechanism for homeotropic 2D order. Schematic representations of the self-assembly of a cylindrical bottlebrush polymer into a 2D homeotropic order. The polymer carries three polarized mesogenic units in its individual side chains and self-assembles into a 2D rectangular geometry, where constituent cylinders are deformed to have an ellipsoidal cross section featuring oppositely oriented local dipoles. The interaction between these dipoles forces the cylinders to tightly connect bilaterally. With a physical assistance of the surface grooves on the Teflon sheets, nucleation for homeotropic ordering can be induced and propagate efficiently upon hot-pressing toward the interior of the film, wherein consistent polymer molecules align homeotropically.

Through the aforementioned systematic study using 14 newly designed bottlebrush polymers with long mesogenic side chains, we found that whether the polymer assembles into a 2D rectangular lattice or not is crucial for the homeotropic orientation of the polymer backbone on the Teflon sheets. As discussed for the monomer of **PMA/A₃** in our previous manuscript (12), those of **PMA/B₃** and **PMA/T₃**, when hot-pressed, orient their mesogenic units along the surface grooves of Teflon sheets (Figures. 6J,K). Also noteworthy, the corresponding bottlebrush polymers orient their mesogenic side chains mainly along the *b*-axis of the 2D rectangular lattice. Consequently, polymer domains are oriented unidirectionally in such a way that the *ab* planes of their individual 2D rectangular lattices align parallel to the surface of the Teflon sheets. Hence, their *c*-axis align homeotropically with respect to the surface of the Teflon sheets (Figure. 10). This represents how the homeotropic orientation of particular bottlebrush polymers such as **PMA/B₃** and **PMA/T₃** as well as **PMA/A₃** is nucleated. In contrast, in the case of highly symmetric hexagonal columnar lattice, where constituent cylindrical polymer objects adopt an entropically favored round shape with isotropically extended mesogenic units, the surface grooves on the Teflon sheets upon hot-pressing are surely unable to nucleate the assembly of bottlebrush polymers such as **PMA/B₂B'** and **PMA/T₂T'** to a macroscopic order (Figures. 4C,D, lower).

3.2.3. Orientation of Mesogens in Polymers at Their Cross Section

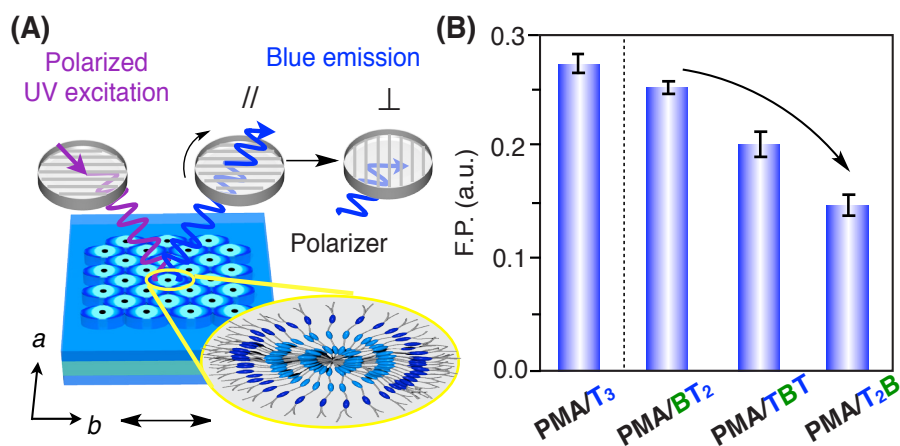


Figure 11 | Orientation of mesogens in polymers at their cross section characterized by polarized fluorescence method. (A) Schematic representation of anisotropic fluorescence experiments and orientation of mesogens in the side chains (top view). When a film sample is excited by polarized UV light (310 nm, purple line) parallel to the surface grooves on the Teflon sheets (black arrows), a polarized blue emission (420 nm, blue line) appears. The outermost mesogens are oriented more parallel to the surface grooves on the Teflon sheets than those of inner mesogens. (B), Fluorescence anisotropy $(I_{0^\circ} - I_{90^\circ}) / (I_{0^\circ} + I_{90^\circ})$ of hot-pressed films of **PMA/T₃**, **PMA/BT₂**, **PMA/TBT** and **PMA/T₂B**, where I_{0° and I_{90° are the fluorescence intensities in the polarized emission spectra when the excitation and emission polarizers form angles of 0 and 90°, respectively.

Polarized fluorescence spectroscopy is a useful tool for investigating the orientation of fluorophores (14,15). The fluorescent intensity of **PMA/T₃** under UV irradiation was sufficiently strong to be detected by the naked eye, even in its film state, whereas **PMA/B₃** was barely emissive (Figure. S11). In fact, the fluorescence spectral patterns of **PMA/BT₂**, **PMA/TBT** and **PMA/T₂B** are almost identical

[14] M. Y. Berezin, S. Achilefu. *Chem. Rev.* **110**, 2641 (2010).

[15] M. Glasbeek, H. Zhang. *Chem. Rev.* **104**, 1929 (2004).

to that of **PMA/T₃** either in solution or in the film state, indicating that the contribution of mesogen **B** is negligibly small (Figures. S12 and S13). Therefore, comparison of the fluorescence anisotropies of the hot-pressed films of **PMA/BT₂**, **PMA/TBT** and **PMA/T₂B** possibly allows for evaluating the degrees of orientation of mesogen **T** at different positions in the side chains. As explained schematically in Figure. 11A, we investigated the degrees of fluorescence anisotropy of three hot-pressed polymer films **PMA/BT₂**, **PMA/TBT** and **PMA/T₂B** using a polarized light parallel to the surface grooves on the Teflon sheets. As a result, when mesogen **B** is further displaced from the backbone (**PMA/BT₂** → **PMA/TBT** → **PMA/T₂B**), the fluorescence anisotropy decreases from 0.25 (**PMA/BT₂**) to 0.20 (**PMA/TBT**) and then to 0.15 (**PMA/T₂B**) (Figure. 11B). These results suggest that the outermost mesogen units, which are likely located in the least congested environment, align more parallel to the surface grooves on the Teflon sheets, whereas the innermost mesogen units are oriented more radially and therefore more isotropically (Figure. 11A).

3.2.4. Evaluation of Order Parameters of the Hot-pressed Films

Finally, we investigated order parameters of the hot-pressed films. Because the 2D assembly with a rectangular geometry is nucleated at the polymer/Teflon sheet interface, the order parameter of a bottlebrush polymer generally decreases as the film thickness increases. We noticed an interesting relationship between the thickness of the homeotropically ordered domain (X in Figures. 4A,B, lower) and total π -plane surface area of all the mesogens ($^{\text{all}}S_{\pi}$) in its individual side chains. Value X was estimated by integrating the scattering peak of the (020) plane in its 2D SAXS data (Figures. S9 and S10), while the total π -plane surface area $^{\text{all}}S_{\pi}$ was obtained in Table 2 by sum of the π -plane surface areas of all mesogens $^{\text{B}}S_{\pi}$ (0.21 nm^2), $^{\text{T}}S_{\pi}$ (0.29 nm^2), and/or $^{\text{A}}S_{\pi}$ (0.38 nm^2) involved in the side chains ($S_{\pi} = l \times d$, Figure. 12C). As shown in Figure 12B, the

Table 2 | Structural Parameters of Bottlebrush Polymers in Hot-pressed Films.

Polymers	Space Group ^a	Lattice Parameter		^{all} S_{π}^b (nm ²)	Hot-pressed Film	
		<i>a</i> (nm)	<i>b</i> (nm)		<i>X</i> (μ m) ^c	<i>Y</i> (μ m) ^d
PMA/A ₃	<i>P2₁/a</i>	21.8	14.7	1.14	2.6	4.9
PMA/TA ₂	<i>P2₁/a</i>	21.8	14.7	1.05	1.6	4.8
PMA/BA ₂	<i>P2₁/a</i>	22.2	14.2	0.97	1.3	5.4
PMA/T ₂ A	<i>C2/m</i>	11.9	14.7	0.96	1.1	4.8
PMA/T ₃	<i>C2/m</i>	12.8	14.7	0.87	1.0	5.0
PMA/B ₂ A	<i>P2₁/a</i>	23.0	13.8	0.80	0.6	4.8
PMA/B ₃	<i>P2₁/a</i>	20.4	13.6	0.62	0.5	6.0
PMA/B ₂ B'	<i>P6mm</i>	12.7	–	0.86	RO ^e	
PMA/T ₂ T'	<i>P6mm</i>	13.6	–	1.03	RO ^e	
PA/B ₃	<i>P2/a</i>	13.8	14.3	0.62	1.1	3.8
PPA/B ₃	<i>C2/m</i>	11.2	13.8	0.62	0.6	4.8

^a*P2₁/a*, *C2/m*, *P2/a*: rectangular lattice, *P6mm*: hexagonal lattice (in mesophase).
^{all} S_{π} : Sum of plane area of mesogens in a side chain. ^cThickness of homeotropic orientation of the polymer. ^dThickness of random orientation of the polymer. ^eRO: Random orientation.

plots of *X* against ^{all} S_{π} clearly showed that the order parameter of the film increases with increasing ^{all} S_{π} . In all of the bottlebrush polymers examined, PMA/A₃ with the largest ^{all} S_{π} gave the highest order parameter (*X* = 2.5 μ m), where the cylindrical polymer objects located in a 2.5- μ m thick area from the polymer/Teflon sheet interface were homeotropically oriented (12). This trend indicates a large contribution of the π -stacking interaction along the cylindrical polymer axis to the orientational integrity of the hot-pressed film (Figure. 12A).

Wide-angle x-ray diffraction (WAXD) profiles (Figure. 12D) of bulk samples of PMA/B₃, PMA/T₃, and PMA/TA₂ at 25 °C support this trend. In the case of PMA/TA₂ with a large order parameter (*X* = 1.6 μ m), two peaks at 0.50 and 0.38 nm periodic distances were observed, corresponding to diameter of molten chain and π - π distance of aromatic cores. By contrast, polymer with a smaller order parameter

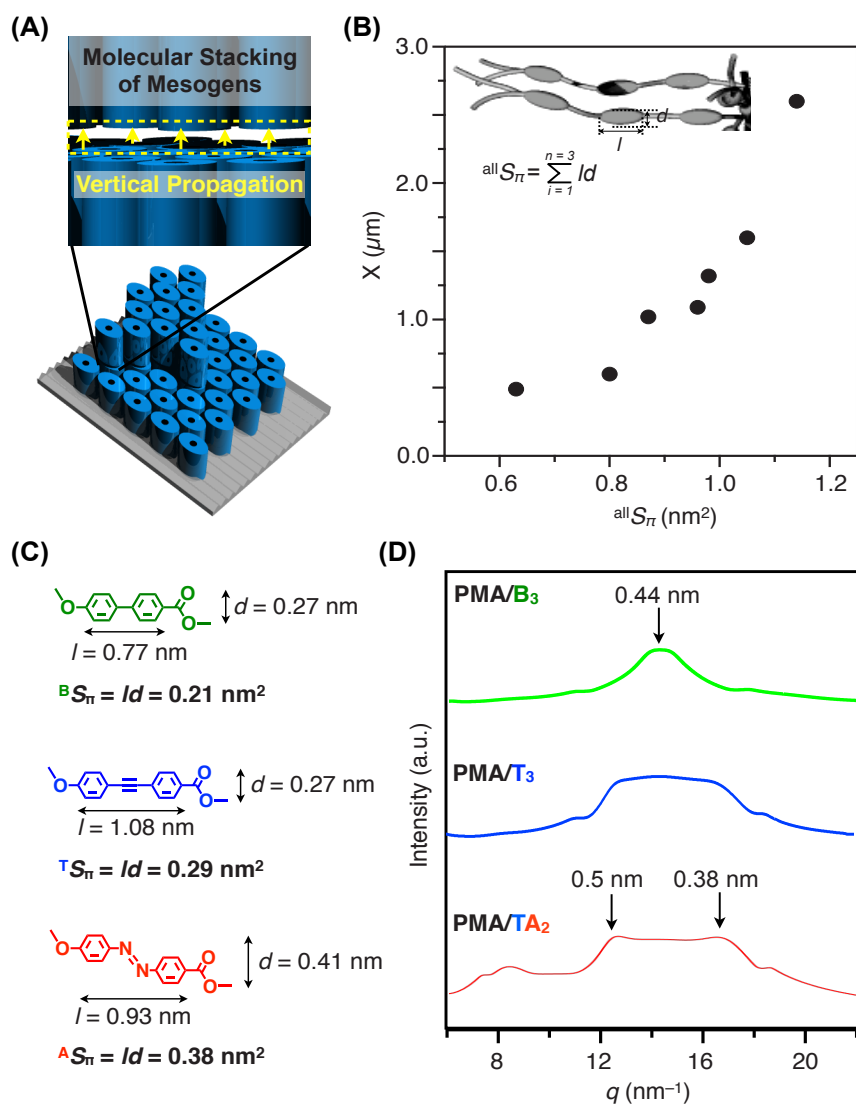


Figure 12 | Driving force for the vertical propagation in hot-pressed film. (A) Schematic illustrations of vertical propagation from the interface of Teflon/polymer towards the deep region of hot-pressed film. Yellow arrows denote the direction of propagation. (B) Plots of sum of π -plane area of mesogen skeletons in a side chain ($^{all}S_{\pi}$) vs the thickness of the homeotropically ordered domain (X). (C) Sizes of π -plane of biphenyl, tolan and azobenzene, which refer to the product of long (l) and short axis (d) of molecular skeleton. (D) Wide-angle X-ray diffraction (WAXD) profiles of bulk samples of **PMA/B₃**, **PMA/T₃**, and **PMA/TA₂** at 25 °C.

showed broad trapezoidal scattering peaks between 13 – 16 nm^{-1} in q value (**PMA/T₃**) or even a broad peak at 14 nm^{-1} in q value (**PMA/B₃**). It is clear that the mesogens in side chains pile up with periodic orders along polymer backbones in solid state.

3.3. Conclusion

To realize homeotropic orientation of polymer in large area is unprecedented challenge but one of essential structural requisites for organic devices. Recently, our group demonstrated the first example of homeotropic orientation of a particular brush polymer. In deeper, two mechanism queries for this 2D homeotropic order is remained. What kinds of polymer lattice are suited to homeotropic 2D order and why? And what is the driving force for vertical molecular arrangement?

In this chapter, I synthesized several new brush polymers and got the answers based on three kinds of polymer lattices and their orientations in hot-pressed film. It is revealed that homeotropic orientation is not determined by the structure of polymer backbones. However, an anisotropic rectangular lattice ($P2_1/a$ or $C2/m$) is essential to achieve macroscopic alignment of polymer backbones homeotropically to the surface of Teflon sheet, because it can translate the 1D structural information of Teflon sheet with a groove-patterned surface. Basically speaking, such macroscopic orientation is a destined result of dipole neutralization and lowest energy node. The driving force of vertical molecular arrangement likely stem from the π - π stacking of rod-like mesogens, because a large π -plane area of mesogen benefits for the structuring of side chains and the surface event is more efficiently transmitted to the inside of polymer films.

3.4. Supporting Information

3.4.1. Materials and Methods

Materials Unless otherwise noted, reagents were used as received from Tokyo Chemical Industry [tetrabutylammonium fluoride (TBAF, 1 M in tetrahydrofuran (THF)), and Wako Pure Chemical Industries [N,N'-diisopropylcarbodiimide (DIPC), p-toluenesulfonic acid monohydrate, 4-dimethylaminopyridine (DMAP), triethylamine, 2,2'-azobisisobutyronitrile (AIBN), methacryloyl chloride], 4-(Dimethylamino)pyridinium 4-toluenesulfonate (DPTS) (13), compounds **1** (12), **2** (16), **8** (12), **12** (16), **21** (16), **27** (16), and **31** (16) were prepared according to reported procedures. CH₂Cl₂ was dried over CaH₂ and freshly distilled prior to use. THF was refluxed over a mixture of Na and benzophenone and freshly distilled before use. Other dehydrated solvents were purchased from Wako Pure Chemical Industries or Kanto Chemicals. Uniaxially stretched polytetrafluoroethylene (PTFE, Teflon™) sheets (300 mm × 10 m × 0.1 mm) were purchased from Flon Industry and cut into a proper size before use.

General Column chromatography was carried out with Wakogel silica C-300 (particle size: 45–75 μm). Recycling preparative size-exclusion chromatography (SEC) was performed using JAIGEL 2H and 2.5H columns on a JAI model LC-9201 recycling HPLC system equipped with a JASCO model MD-2010 Plus variable-wavelength UV-vis detector with CHCl₃/MeOH (100/1 v/v) as an eluent. Analytical SEC was performed at 40 °C on a TOSOH model HLC-8220 GPC system equipped with a refractive index (RI) detector, using CHCl₃ as an eluent at a flow rate of 0.35 mL min⁻¹ on linearly connected two polystyrene gel columns (TSKgel SuperHM-M, TOSOH). The molecular weight calibration curve was obtained by using standard polystyrenes (Shodex STANDARD SM-105, Showa Denko). ¹H and ¹³C NMR spectra were recorded on a JEOL model JNM-ECA500 spectrometer, operating at 500 and 125 MHz, respectively, where chemical shifts (δ in ppm) were determined with respect to tetramethylsilane as an internal reference. Matrix-assisted laser desorption ionization time-of-flight (MALDI-TOF) mass spectrometry was performed on an Applied Biosystems model MDS SCIEX 4800 Plus MALDI TOF/TOF™ Analyzer using dithranol as a matrix. Infrared (IR) spectra were recorded at 25 °C on a JASCO model FT/IR-4100 Fourier transform infrared spectrometer with an attenuated total reflection (ATR) equipment (ATR PRO450-S). Polarized IR spectra were recorded at 25 °C on a JASCO model FT/IR-4100 Fourier transform infrared spectrometer connected to an Irtron IRT-5000 microscope unit. Differential scanning calorimetry (DSC) was performed on a Mettler–Toledo model DSC 1 differential scanning calorimeter, where temperature

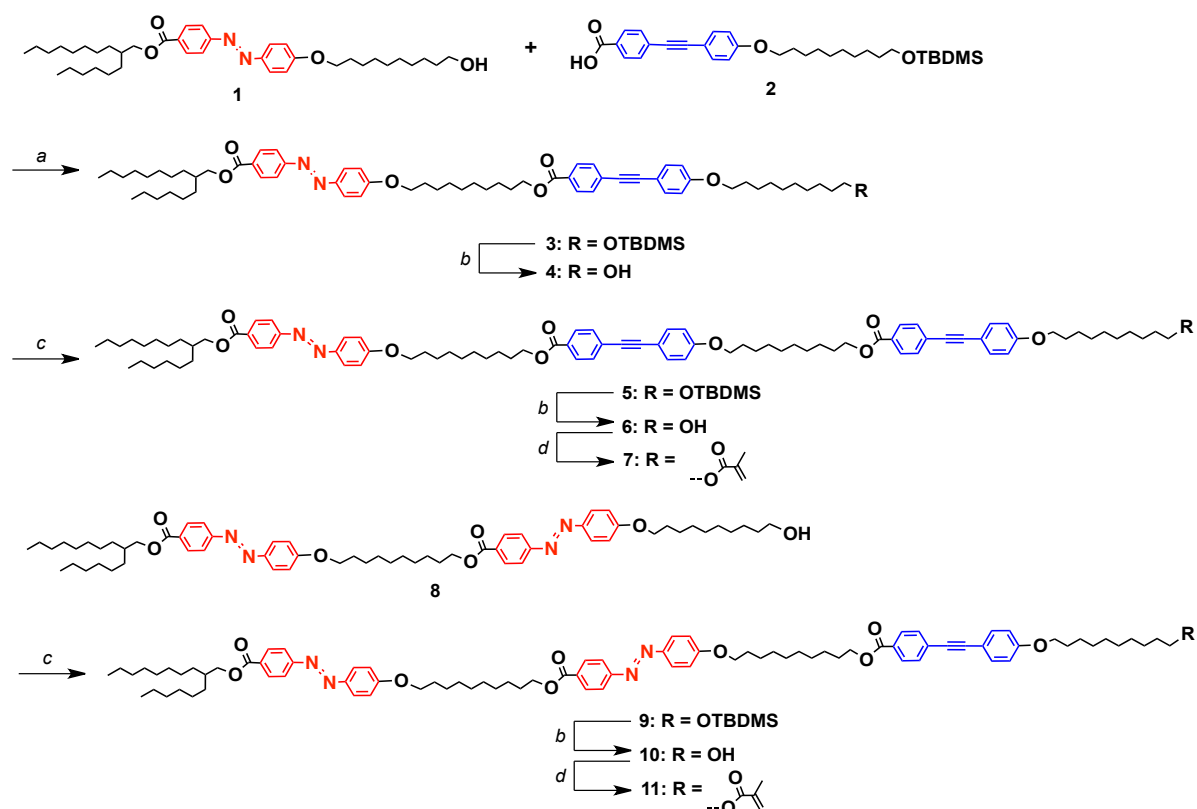
and enthalpy were calibrated with In (430 K, 3.3 J mol⁻¹) and Zn (692.7 K, 12 J mol⁻¹) standard samples using sealed Al pans. Cooling and heating profiles were recorded and analyzed using the Mettler–Toledo STARE software system. Polarized optical microscopy (POM) was performed on a Nikon model Eclipse LV100POL optical polarizing microscope equipped with a Mettler–Toledo model FP90 controller attached to a FP82HT hot stage. Polarized emission spectra were recorded on JASCO model FP-6500 spectrofluorometer installed with one UV/VIS polarizer and one VIS polarizer. Polarity of light can be tuned parallel or vertically by rotating the polarizers. Hot press was performed on an Imoto Machinery model IMC-180C compact press. Film thicknesses were measured using a Mitutoyo model MDQ-30M micrometer. Small-angle X-ray scattering (SAXS) and wide-angle X-ray diffraction (WAXD) experiments were carried out at BL45XU in SPring-8 (Hyogo, Japan) with an imaging plate area detector, a R-Axis IV++ (Rigaku). Scattering vector, $q = 4\pi\sin\theta/\lambda$, and position of incident X-ray on the detector were calibrated using several orders of layer reflections from silver behenate ($d = 58.380 \text{ \AA}$), where 2θ and λ are scattering angle and wavelength of X-ray (0.90 \AA), respectively. The sample-to-detector distances for SAXS and WAXD measurements were 2.5 and 0.5 m, respectively. The scattering/diffraction images recorded were integrated along the Debye-Scherrer ring, affording one-dimensional intensity data using the FIT2D software (17). The cell parameters were refined using the CellCalc ver. 2.10 software (18). Powdery samples were placed into a 1.5 mm- ϕ glass capillary in a temperature-controlled heating block and once heated to isotropic melt. The resultant samples were then exposed to an X-ray beam for 10 (WAXD) or 100 (SAXS) seconds at given temperatures. Film samples were clipped with tweezers or sandwiched by sapphire glasses and exposed at 25 °C to an X-ray beam for 300 seconds. The resulting SAXS profiles indicate that the lattice structures of the polymers in the films are essentially identical to those in the bulk samples.

[17] <http://www.esrf.eu/computing/scientific/FIT2D/>
 [18] http://homepage2.nifty.com/~hsc/soft/cellcalc_e.html.

Hot-pressing A cast polymer film prepared from its CHCl₃ solution (1 mg/mL) was sandwiched by two anisotropic Teflon sheets (10 cm × 10 cm) such that their surface grooves were parallel to one another. The hot-pressing was conducted under 8.0 MPa in a mesophase temperature range for 1 hour (5 °C lower than the phase transition temperature from the isotropic melt to an ordered phase) after heating to an isotropic state shortly (10 °C higher than the melting temperature) for complete melting. Then, the sample was allowed to cool to 25 °C. A self-standing polymer film was peeled from the Teflon sheet using a blade.

3.4.2. Synthesis

Compound 3. To a CH₂Cl₂ solution (20 mL) of **2** (0.81 g, 1.60 mmol) was successively added DPTS (0.10 g, 0.33 mmol) and DIPC (0.40 g, 3.20 mmol), and the mixture was stirred at 25 °C under Ar until all the reagents were dissolved. **1** (1.0 g, 1.60 mmol) was added to the resulting solution, and the mixture was stirred at 25 °C for 12 h under Ar. The reaction mixture was poured into water and extracted with CHCl₃. The combined organic extract was washed successively with water



Scheme S11 | Synthesis of 7 and 11. Reagents and conditions: (a) **2**, DPTS, DIPC, CH_2Cl_2 , 25 °C; (b) TBAF, THF, 25 °C; (c) **2**, DPTS, DIPC, CH_2Cl_2 , 40 °C; (d) methacryloyl chloride, triethylamine, CH_2Cl_2 , 25 °C.

and brine, and an organic phase separated was dried over anhydrous MgSO_4 and then evaporated to dryness under a reduced pressure. The residue was subjected to column chromatography (SiO_2 , CHCl_3) to allow isolation of **3** as orange solid (1.50 g, 1.34 mmol) in 84% yield. ^1H NMR (500 MHz, CDCl_3): δ (ppm) 8.16 (d, $J = 8.6$ Hz, 2H), 8.00 (d, $J = 8.6$ Hz, 2H), 7.93 (d, $J = 8.6$ Hz, 2H), 7.91 (d, $J = 8.6$ Hz, 2H), 7.55 (d, $J = 8.0$ Hz, 2H), 7.46 (d, $J = 8.6$ Hz, 2H), 7.01 (d, $J = 8.6$ Hz, 2H), 6.86 (d, $J = 8.6$ Hz, 2H), 4.31 (t, $J = 6.9$ Hz, 2H), 4.25 (d, $J = 5.8$ Hz, 2H), 4.04 (t, $J = 6.3$ Hz, 2H), 3.96 (t, $J = 6.3$ Hz, 2H), 3.60 (t, $J = 6.6$ Hz, 2H), 1.85–1.75 (m, 7H), 1.52–1.30 (m, 50H), 0.89–0.86 (m, 15H), 0.05 (s, 6H). ^{13}C NMR (125 MHz, CDCl_3): δ (ppm) 166.29, 166.21, 162.33, 159.65, 155.40, 146.91, 133.37, 133.23, 131.67, 131.60, 131.26, 130.51, 129.46, 128.39, 125.20, 122.35, 114.81, 114.71, 114.64, 114.52, 92.68, 87.49, 68.44, 68.13, 68.03, 65.25, 63.32, 37.50, 32.90, 31.92, 31.83, 31.51, 29.98, 29.64, 29.57, 29.51, 29.46, 29.44, 29.38, 29.34, 29.32, 29.24, 29.20, 28.72, 26.80, 26.77, 26.01, 25.82, 24.63, 22.68, 22.66, 18.39, 14.34, 14.12, -5.24 . MALDI-TOF mass: calcd. for $\text{C}_{70}\text{H}_{105}\text{N}_2\text{O}_7\text{Si}$ [$\text{M} + \text{H}$] $^+$: $m/z = 1113.77$; found: 1113.79.

Compound 4. TBAF (1.0 M in THF, 6.0 mL, 6.0 mmol) was added to a THF solution (20 mL) of **3** (1.40 g, 1.26 mmol), and the mixture was stirred at 25 °C for 12 h under Ar. The reaction mixture was evaporated to dryness under a reduced pressure, and a CHCl_3 solution of the residue was washed with a saturated aqueous solution of NH_4Cl . An organic phase separated was dried over anhydrous MgSO_4 and evaporated to dryness under a reduced pressure. The residue was subjected to column chromatography (SiO_2 , CHCl_3) to allow isolation of **4** as orange solid (1.22 g, 1.22 mmol) in 97% yield. ^1H NMR (500 MHz, CDCl_3): δ (ppm) 8.16 (d, $J = 8.6$ Hz,

2H), 8.00 (d, $J = 8.6$ Hz, 2H), 7.93 (d, $J = 8.6$ Hz, 2H), 7.90 (d, $J = 8.6$ Hz, 2H), 7.55 (d, $J = 8.0$ Hz, 2H), 7.46 (d, $J = 8.6$ Hz, 2H), 7.01 (d, $J = 8.6$ Hz, 2H), 6.86 (d, $J = 8.6$ Hz, 2H), 4.31 (t, $J = 6.9$ Hz, 2H), 4.25 (d, $J = 5.8$ Hz, 2H), 4.05 (t, $J = 6.3$ Hz, 2H), 3.96 (t, $J = 6.3$ Hz, 2H), 3.64 (t, $J = 6.6$ Hz, 2H), 1.85–1.78 (m, 7H), 1.59–1.54 (m, 2H), 1.48–1.29 (m, 49H), 0.88–0.86 (m, 6H). ^{13}C NMR (125 MHz, CDCl_3): δ (ppm) 166.31, 166.22, 162.33, 159.64, 155.40, 146.91, 133.23, 131.59, 131.26, 130.51, 129.46, 128.38, 125.20, 122.34, 114.82, 114.64, 114.53, 92.66, 87.49, 68.44, 68.12, 68.04, 65.26, 63.07, 37.49, 32.81, 31.92, 31.82, 31.50, 29.97, 29.64, 29.56, 29.52, 29.47, 29.45, 29.41, 29.35, 29.31, 29.24, 29.18, 28.71, 26.80, 26.79, 26.01, 25.74, 23.50, 22.68, 22.66, 14.11. MALDI-TOF mass: calcd. for $\text{C}_{64}\text{H}_{91}\text{N}_2\text{O}_7\text{Si}$ [$\text{M} + \text{H}$] $^+$: $m/z = 999.68$; found: 999.67.

Compound 5. By a procedure similar to that for **3**, except that the reaction temperature was 40 °C, compound **5** was obtained in 90% yield (1.34 g, 0.90 mmol) from **4** (1.0 g, 1.0 mmol), **2** (0.55 g, 1.10 mmol), DPTS (0.061 g, 0.21 mmol) and DIPC (0.25 g, 2.01 mmol). ^1H NMR (500 MHz, CDCl_3): δ (ppm) 8.16 (d, $J = 8.6$ Hz, 2H), 8.00 (d, $J = 8.6$ Hz, 4H), 7.94 (d, $J = 8.6$ Hz, 2H), 7.90 (d, $J = 8.6$ Hz, 2H), 7.55 (d, $J = 8.6$ Hz, 4H), 7.46 (d \times 2, $J = 8.6$ Hz, 4H, overlapped), 7.01 (d, $J = 8.6$ Hz, 2H), 6.87 (d, $J = 8.6$ Hz, 4H), 4.32 (t, $J = 6.6$ Hz, 4H), 4.26 (d, $J = 5.8$ Hz, 2H), 4.05 (t, $J = 6.6$ Hz, 2H), 3.96 (t, $J = 6.6$ Hz, 4H), 3.60 (t, $J = 6.6$ Hz, 2H), 1.85–1.76 (m, 11H), 1.52–1.30 (m, 62H), 0.90–0.86 (m, 15H), 0.05 (s, 6H). ^{13}C NMR (125 MHz, CDCl_3): δ (ppm) 166.29, 166.21, 162.33, 159.65, 155.40, 146.92, 133.24, 131.60, 131.26, 130.51, 129.46, 128.38, 125.20, 122.35, 114.82, 114.64, 114.53, 92.67, 87.49, 68.44, 68.11, 68.03, 65.25, 63.32, 37.50, 32.90, 31.92, 31.83, 31.51, 29.97, 29.64, 29.57, 29.51, 29.45, 29.43, 29.37, 29.34, 29.32, 29.24, 29.20, 28.72, 26.80, 26.77, 26.02, 25.82, 22.68, 22.66, 18.39, 14.12, –5.24. MALDI-TOF mass: calcd. for $\text{C}_{95}\text{H}_{133}\text{N}_2\text{O}_{10}\text{Si}$ [$\text{M} + \text{H}$] $^+$: $m/z = 1489.97$; found: 1489.94.

Compound 6. By a procedure similar to that for **4**, compound **6** was obtained in 90% yield (1.24 g, 0.90 mmol) from **5** (1.20 g, 0.81 mmol) and TBAF (1.0 M in THF, 2.0 mL, 2.0 mmol). ^1H NMR (500 MHz, CDCl_3): δ (ppm) 8.16 (d, $J = 8.6$ Hz, 2H), 8.00 (d, $J = 8.6$ Hz, 4H), 7.94 (d, $J = 8.6$ Hz, 2H), 7.90 (d, $J = 8.6$ Hz, 2H), 7.55 (d, $J = 8.0$ Hz, 4H), 7.46 (d \times 2, $J = 8.6$ Hz, 4H, overlapped), 7.01 (d, $J = 8.6$ Hz, 2H), 6.87 (d, $J = 8.0$ Hz, 4H), 4.32 (t, $J = 6.6$ Hz, 4H), 4.25 (d, $J = 5.8$ Hz, 2H), 4.05 (t, $J = 6.3$ Hz, 2H), 3.96 (t, $J = 6.6$ Hz, 4H), 3.64 (br, $J = 6.6$ Hz, 2H), 1.84–1.75 (m, 11H), 1.58–1.55 (m, 2H), 1.46–1.22 (m, 61H), 0.88–0.86 (m, 6H). ^{13}C NMR (125 MHz, CDCl_3): δ (ppm) 166.29, 166.21, 162.33, 159.64, 155.42, 146.91, 133.24, 131.61, 131.26, 130.51, 129.46, 128.38, 125.20, 122.34, 114.82, 114.64, 114.53, 92.67, 87.50, 68.44, 68.12, 68.04, 65.26, 63.08, 37.50, 32.92, 31.92, 31.83, 31.50, 29.97, 29.64, 29.57, 29.52, 29.45, 29.43, 29.41, 29.35, 29.24, 29.19, 28.72, 26.80, 26.77, 26.02, 25.74, 22.68, 22.66, 14.10. MALDI-TOF mass: calcd. for $\text{C}_{89}\text{H}_{119}\text{N}_2\text{O}_{10}$ [$\text{M} + \text{H}$] $^+$: $m/z = 1375.89$; found: 1375.82.

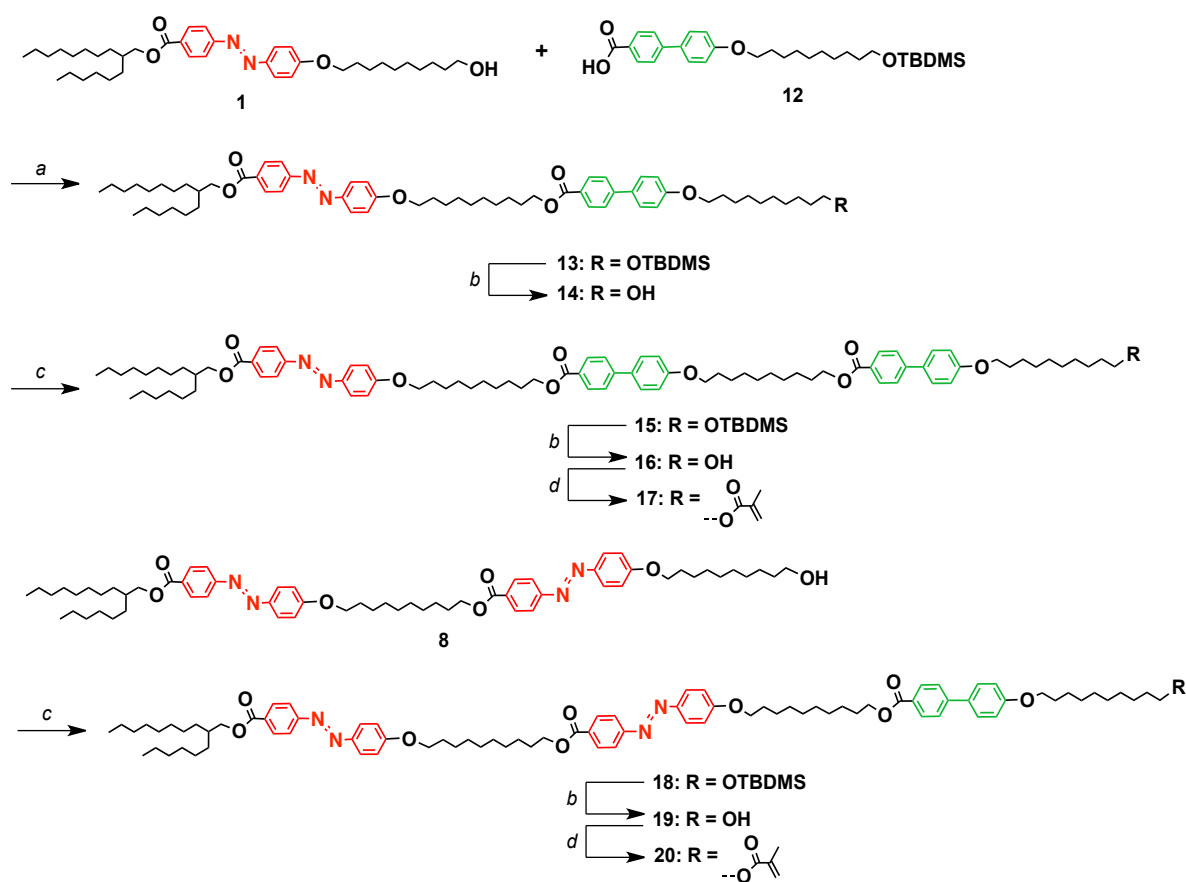
Compound 7. To a CH_2Cl_2 solution (15 mL) of **6** (1.0 g, 0.73 mmol) was successively added methacryloyl chloride (0.15 g, 1.50 mmol) and triethylamine (0.16 g, 1.50 mmol), and the mixture was stirred at 25 °C for 10 h under Ar. The reaction mixture was poured into water and extracted with CHCl_3 . The combined organic extract was washed successively with a saturated aqueous solution of NaHCO_3 , water and brine, and an organic phase separated was dried over anhydrous MgSO_4 and then evaporated to dryness under a reduced pressure. The residue was subjected to column chromatography (SiO_2 , CHCl_3 /hexane 1/1 v/v) to allow isolation of **7** as orange solid (0.63 g, 0.44 mmol) in 60% yield. ^1H NMR (500 MHz, CDCl_3): δ (ppm) 8.16 (d, $J = 8.6$ Hz, 2H), 8.00 (d, $J = 8.0$ Hz, 4H), 7.93 (d, $J = 8.6$ Hz, 2H), 7.90 (d, $J = 8.6$ Hz, 2H), 7.55 (d, $J = 8.0$ Hz, 4H), 7.46 (d \times 2, $J = 8.6$ Hz, 4H, overlapped), 7.01 (d, $J = 8.6$ Hz, 2H), 6.87 (d, $J = 8.0$ Hz, 4H), 6.10 (s, 1H), 5.54 (t, $J = 1.7$ Hz, 1H), 4.32 (t, $J = 6.6$ Hz, 4H), 4.25 (d, $J = 5.8$ Hz, 2H), 4.14 (t, $J = 6.3$ Hz, 2H), 4.05 (t, $J = 6.3$ Hz, 2H), 3.97 (t, $J = 6.6$ Hz, 4H), 1.94 (s, 3H), 1.85–1.76 (m,

11H), 1.70–1.64 (m, 2H), 1.45–1.29 (m, 60H), 0.88–0.86 (m, 6H). ^{13}C NMR (125 MHz, CDCl_3): δ (ppm) 166.30, 166.21, 162.33, 159.65, 155.42, 146.91, 136.60, 133.24, 131.62, 131.26, 130.51, 129.47, 128.38, 125.21, 122.34, 114.82, 114.64, 114.53, 92.67, 87.50, 68.44, 68.12, 68.04, 65.26, 63.09, 37.50, 32.92, 31.92, 31.83, 31.50, 29.97, 29.64, 29.58, 29.52, 29.46, 29.43, 29.41, 29.35, 29.25, 29.19, 28.72, 26.80, 26.77, 26.02, 25.74, 22.68, 22.66, 14.11. MALDI-TOF mass: calcd. for $\text{C}_{93}\text{H}_{123}\text{N}_2\text{O}_{11}$ $[\text{M} + \text{H}]^+$: $m/z = 1443.91$; found: 1443.89.

Compound 9. By a procedure similar to that for **3**, except that the reaction temperature was 40 °C, compound **9** was obtained in 95% yield (1.42 g, 0.95 mmol) from **8** (1.0 g, 1.0 mmol), **2** (0.55 g, 1.10 mmol), DPTS (0.060 g, 0.210 mmol) and DIPC (0.25 g, 1.98 mmol). ^1H NMR (500 MHz, CDCl_3): δ (ppm) 8.17 (d, $J = 8.6$ Hz, 2H), 8.16 (d, $J = 8.6$ Hz, 2H), 8.00 (d, $J = 8.6$ Hz, 2H), 7.93 (d \times 2, $J = 8.6$ Hz, 4H, overlapped), 7.90 (d \times 2, $J = 8.6$ Hz, 4H, overlapped), 7.55 (d, $J = 8.0$ Hz, 2H), 7.46 (d, $J = 8.6$ Hz, 2H), 7.00 (d \times 2, $J = 8.6$ Hz, 4H, overlapped), 6.87 (d, $J = 8.6$ Hz, 2H), 4.35 (t, $J = 6.9$ Hz, 2H), 4.32 (t, $J = 6.6$ Hz, 2H), 4.26 (d, $J = 5.8$ Hz, 2H), 4.04 (t \times 2, $J = 6.6$ Hz, 4H, overlapped), 3.96 (t, $J = 6.6$ Hz, 2H), 3.60 (t, $J = 6.6$ Hz, 2H), 1.81–1.78 (m, 11H), 1.56–1.22 (m, 62H), 0.90–0.86 (m, 15H), 0.05 (s, 6H). ^{13}C NMR (125 MHz, CDCl_3): δ (ppm) 166.32, 166.21, 162.38, 159.65, 155.40, 146.98, 133.23, 131.60, 130.53, 130.51, 129.45, 128.38, 125.20, 122.34, 122.32, 114.82, 114.64, 92.70, 87.52, 68.44, 68.14, 65.25, 63.32, 37.50, 32.90, 31.83, 31.50, 29.97, 29.64, 29.56, 29.50, 29.45, 29.43, 29.37, 29.34, 29.31, 29.24, 29.19, 28.72, 26.77, 26.02, 25.82, 22.68, 22.65, 18.39, 14.11, –5.24. MALDI-TOF mass: calcd. for $\text{C}_{93}\text{H}_{133}\text{N}_4\text{O}_{10}\text{Si}$ $[\text{M} + \text{H}]^+$: $m/z = 1493.98$; found: 1493.90.

Compound 10. By a procedure similar to that for **4**, compound **10** was obtained in 84% yield (1.01 g, 0.73 mmol) from **9** (1.30 g, 0.87 mmol) and TBAF (1.0 M in THF, 2.0 mL, 2.0 mmol). ^1H NMR (500 MHz, CDCl_3): δ (ppm) 8.17 (d, $J = 8.6$ Hz, 2H), 8.16 (d, $J = 8.6$ Hz, 2H), 8.00 (d, $J = 8.6$ Hz, 2H), 7.93 (d \times 2, $J = 8.6$ Hz, 4H, overlapped), 7.90 (d \times 2, $J = 8.6$ Hz, 4H, overlapped), 7.55 (d, $J = 8.6$ Hz, 2H), 7.46 (d, $J = 8.6$ Hz, 2H), 7.01 (d \times 2, $J = 8.6$ Hz, 4H, overlapped), 6.87 (d, $J = 8.6$ Hz, 2H), 4.34 (t, $J = 6.9$ Hz, 2H), 4.32 (t, $J = 6.6$ Hz, 2H), 4.26 (d, $J = 5.8$ Hz, 2H), 4.04 (t \times 2, $J = 6.6$ Hz, 4H, overlapped), 3.97 (t, $J = 6.6$ Hz, 2H), 3.64 (q, $J = 5.8$ Hz, 2H), 1.82–1.77 (m, 11H), 1.48–1.45 (m, 2H), 1.44–1.22 (m, 61H), 0.90–0.86 (m, 6H). ^{13}C NMR (125 MHz, CDCl_3): δ (ppm) 166.28, 166.21, 162.36, 159.66, 155.45, 146.95, 133.24, 131.27, 130.54, 130.52, 129.46, 128.37, 125.20, 124.38, 122.35, 122.33, 114.83, 114.65, 92.67, 87.49, 68.46, 68.14, 65.25, 63.10, 37.55, 32.82, 31.92, 31.83, 31.51, 29.57, 29.52, 29.48, 29.46, 29.35, 29.32, 29.24, 29.19, 28.72, 26.78, 26.02, 25.75, 22.68, 22.66, 14.10. MALDI-TOF mass: calcd. for $\text{C}_{87}\text{H}_{119}\text{N}_4\text{O}_{10}$ $[\text{M} + \text{H}]^+$: $m/z = 1379.89$; found: 1379.86.

Compound 11. By a procedure similar to that for **7**, compound **11** was obtained in 65% yield (0.61 g, 0.42 mmol) from **10** (0.90 g, 0.65 mmol), methacryloyl chloride (0.14 g, 1.30 mmol) and triethylamine (0.14 g, 1.36 mmol). ^1H NMR (500 MHz, CDCl_3): δ (ppm) 8.17 (d, $J = 8.6$ Hz, 2H), 8.16 (d, $J = 8.6$ Hz, 2H), 8.00 (d, $J = 8.0$ Hz, 2H), 7.93 (d \times 2, $J = 8.6$ Hz, 4H), 7.90 (d \times 2, $J = 8.6$ Hz, 4H), 7.55 (d, $J = 8.6$ Hz, 2H), 7.46 (d, $J = 8.6$ Hz, 2H), 7.01 (d \times 2, $J = 8.6$ Hz, 4H, overlapped), 6.87 (d, $J = 8.6$ Hz, 2H), 6.10 (s, 1H), 5.54 (t, $J = 1.7$ Hz, 1H), 4.35 (t, $J = 6.6$ Hz, 2H), 4.32 (t, $J = 6.7$ Hz, 2H), 4.25 (d, $J = 5.7$ Hz, 2H), 4.14 (t, $J = 6.3$ Hz, 2H), 4.05 (t \times 2, $J = 6.3$ Hz, 4H), 3.97 (t, $J = 6.6$ Hz, 2H), 1.94 (s, 3H), 1.82–1.76 (m, 11H), 1.70–1.64 (m, 2H), 1.47–1.27 (m, 60H), 0.89–0.86 (m, 6H). ^{13}C NMR (125 MHz, CDCl_3): δ (ppm) 166.30, 166.22, 162.33, 159.65, 155.43, 146.91, 136.58, 133.24, 131.62, 131.26, 130.51, 129.49, 128.38, 125.21, 122.33, 114.82, 114.64, 114.54, 92.67, 87.51, 68.44, 68.12, 68.04, 65.26, 63.11, 37.50, 32.92, 31.94, 31.83, 31.50, 29.95, 29.64, 29.58, 29.52, 29.46, 29.43, 29.43, 29.35, 29.27, 29.19, 28.72, 26.81, 26.77, 26.02, 25.73, 22.68, 22.66, 14.11. MALDI-TOF mass: calcd. for $\text{C}_{91}\text{H}_{123}\text{N}_4\text{O}_{11}$ $[\text{M} + \text{H}]^+$: $m/z = 1447.92$; found: 1447.93.



Scheme S2 I Synthesis of 17 and 20. Reagents and conditions: (a) **12**, DPTS, DIPC, CH_2Cl_2 , 25 °C; (b) TBAF, THF, 25 °C; (c) **12**, DPTS, DIPC, CH_2Cl_2 , 40 °C; (d) methacryloyl chloride, triethylamine, CH_2Cl_2 , 25 °C.

Compound 13. By a procedure similar to that for **3**, compound **13** was obtained in 84% yield (1.46 g, 1.34 mmol) from **1** (1.0 g, 1.60 mmol), **12** (0.78 g, 1.60 mmol), DPTS (0.10 g, 0.33 mmol) and DIPC (0.40 g, 3.20 mmol). ^1H NMR (500 MHz, CDCl_3): δ (ppm) 8.16 (d, $J = 8.6$ Hz, 2H), 8.08 (d, $J = 8.6$ Hz, 2H), 7.93 (d, $J = 8.6$ Hz, 2H), 7.90 (d, $J = 8.6$ Hz, 2H), 7.61 (d, $J = 8.0$ Hz, 2H), 7.55 (d, $J = 8.6$ Hz, 2H), 7.01 (d, $J = 8.6$ Hz, 2H), 6.98 (d, $J = 8.6$ Hz, 2H), 4.33 (t, $J = 6.6$ Hz, 2H), 4.25 (d, $J = 5.7$ Hz, 2H), 4.04 (t, $J = 6.3$ Hz, 2H), 4.00 (t, $J = 6.8$ Hz, 2H), 3.60 (t, $J = 6.6$ Hz, 2H), 1.84–1.75 (m, 7H), 1.55–1.30 (m, 50H), 0.89–0.86 (m, 15H), 0.05 (s, 6H). ^{13}C NMR (125 MHz, CDCl_3): δ (ppm) 166.67, 166.31, 162.35, 159.42, 155.36, 146.85, 145.20, 130.51, 130.06, 128.30, 126.41, 125.19, 122.34, 114.94, 114.80, 68.44, 68.13, 68.03, 65.05, 63.33, 37.48, 32.90, 31.92, 31.83, 31.48, 29.97, 29.64, 29.57, 29.52, 29.46, 29.44, 29.39, 29.34, 29.32, 29.25, 29.18, 28.76, 26.77, 26.05, 25.82, 22.68, 22.66, 18.39, 14.12, -5.25 . MALDI-TOF mass: calcd. for $\text{C}_{68}\text{H}_{105}\text{N}_2\text{O}_7\text{Si}$ [$\text{M} + \text{H}$] $^+$: $m/z = 1089.77$; found: 1089.73.

Compound 14. By a procedure similar to that for **4**, compound **14** was obtained in 98% yield (1.22 g, 1.25 mmol) from **13** (1.40 g, 1.28 mmol) and TBAF (1.0 M in THF, 2.5 mL, 2.5 mmol). ^1H NMR (500 MHz, CDCl_3): δ (ppm) 8.16 (d, $J = 8.6$ Hz, 2H), 8.08 (d, $J = 8.6$ Hz, 2H), 7.93 (d, $J = 8.6$ Hz, 2H), 7.90 (d, $J = 8.6$ Hz, 2H), 7.61 (d, $J = 8.0$ Hz, 2H), 7.55 (d, $J = 8.6$ Hz, 2H), 7.01 (d, $J = 8.6$ Hz, 2H), 6.97 (d, $J = 8.6$ Hz, 2H), 4.33 (t, $J = 6.8$ Hz, 2H), 4.25 (d, $J = 5.8$ Hz, 2H), 4.04 (t, $J = 6.3$ Hz, 2H), 4.00 (t, $J = 6.3$ Hz, 2H), 3.64 (t, $J = 6.6$ Hz, 2H), 1.85–1.71 (m, 7H), 1.61–1.54

(m, 2H), 1.46–1.29 (m, 49H), 0.88–0.86 (m, 6H). ^{13}C NMR (125 MHz, CDCl_3): δ (ppm) 166.67, 166.32, 162.32, 159.42, 155.37, 146.88, 145.20, 132.20, 131.58, 130.51, 130.06, 128.56, 128.30, 126.40, 125.20, 122.34, 114.94, 114.80, 114.20, 68.43, 68.12, 68.03, 65.05, 63.08, 37.48, 32.81, 31.92, 31.83, 31.48, 31.41, 29.97, 29.64, 29.57, 29.53, 29.49, 29.45, 29.44, 29.42, 29.37, 29.34, 29.32, 29.25, 29.18, 28.76, 26.79, 26.76, 26.04, 25.74, 22.68, 22.66, 14.11. MALDI-TOF mass: calcd. for $\text{C}_{62}\text{H}_{91}\text{N}_2\text{O}_7$ $[\text{M} + \text{H}]^+$: $m/z = 975.68$; found: 975.65.

Compound 15. By a procedure similar to that for **3**, except that the reaction temperature was 40 °C, compound **15** was obtained in 81% yield (1.20 g, 0.83 mmol) from **14** (1.0 g, 1.03 mmol), **12** (0.55 g, 1.10 mmol), DPTS (0.060 g, 0.21 mmol) and DIPC (0.25 g, 1.99 mmol). ^1H NMR (500 MHz, CDCl_3): δ (ppm) 8.16 (d, $J = 8.6$ Hz, 2H), 8.08 (d, $J = 8.6$ Hz, 4H), 7.94 (d, $J = 8.6$ Hz, 2H), 7.90 (d, $J = 8.6$ Hz, 2H), 7.61 (d, $J = 8.6$ Hz, 4H), 7.55 (d \times 2, $J = 8.6$ Hz, 4H, overlapped), 7.01 (d, $J = 8.6$ Hz, 2H), 6.98 (d \times 2, $J = 8.6$ Hz, 4H, overlapped), 4.33 (t, $J = 6.6$ Hz, 4H), 4.25 (d, $J = 5.7$ Hz, 2H), 4.04 (t, $J = 6.6$ Hz, 2H), 4.00 (t, $J = 6.6$ Hz, 4H), 3.60 (t, $J = 6.6$ Hz, 2H), 1.85–1.73 (m, 11H), 1.52–1.30 (m, 62H), 0.92–0.86 (m, 15H), 0.05 (s, 6H). ^{13}C NMR (125 MHz, CDCl_3): δ (ppm) 166.66, 166.23, 162.33, 159.45, 155.39, 145.22, 132.22, 131.51, 130.51, 130.06, 128.59, 128.31, 126.41, 125.19, 122.34, 114.97, 114.82, 68.45, 68.18, 68.04, 65.05, 63.33, 37.50, 32.90, 31.92, 31.83, 31.51, 29.97, 29.64, 29.57, 29.53, 29.44, 29.39, 29.36, 29.32, 29.27, 29.25, 29.19, 28.77, 26.80, 26.77, 26.05, 25.82, 22.68, 22.66, 18.39, 14.11, –5.24. MALDI-TOF mass: calcd. for $\text{C}_{91}\text{H}_{133}\text{N}_2\text{O}_{10}\text{Si}$ $[\text{M} + \text{H}]^+$: $m/z = 1441.97$; found: 1441.98.

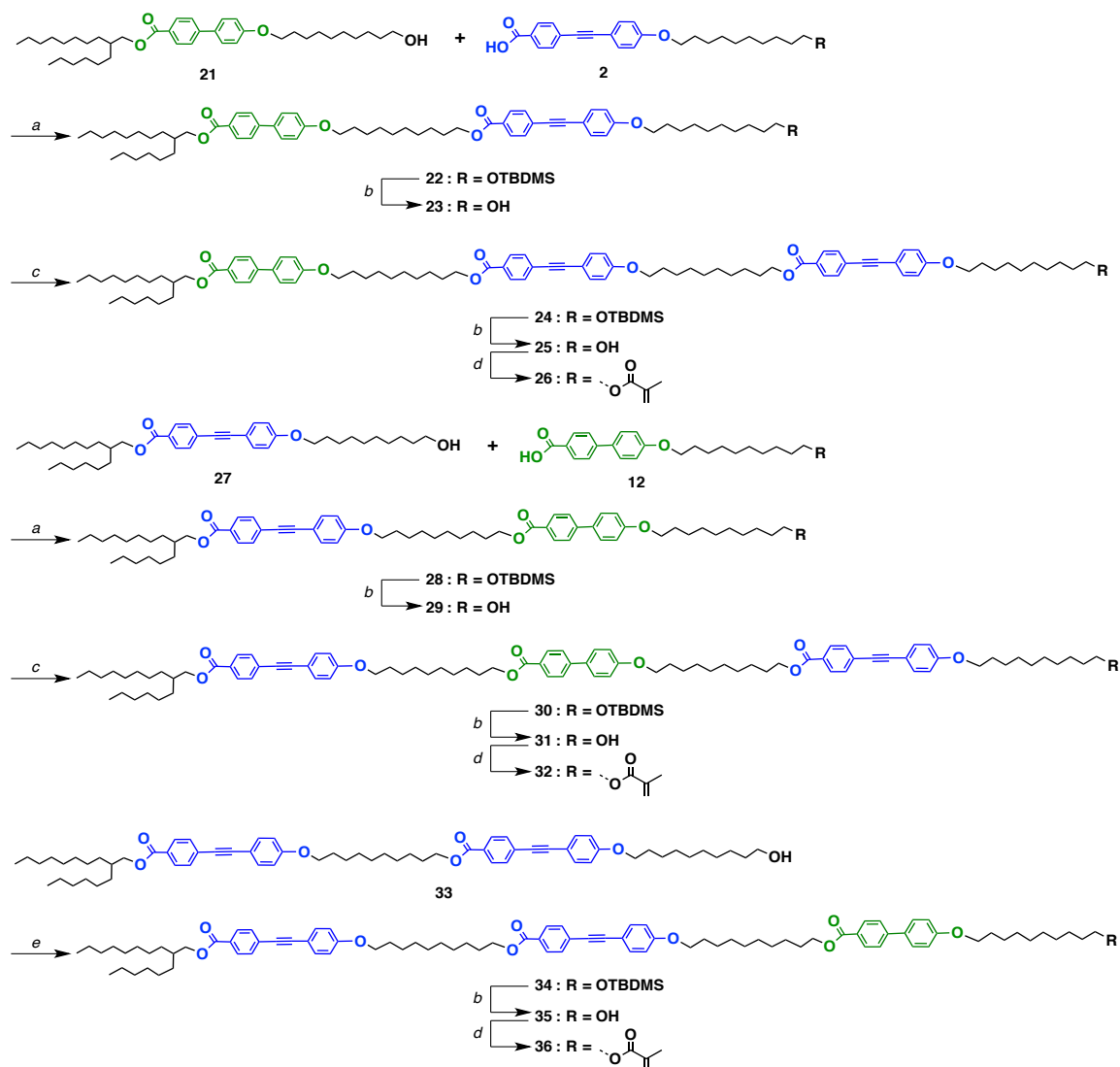
Compound 16. By a procedure similar to that for **4**, compound **16** was obtained in 94% yield (1.24 g, 0.72 mmol) from **15** (1.10 g, 0.76 mmol) and TBAF (1.0 M in THF, 2.0 mL, 2.0 mmol). ^1H NMR (500 MHz, CDCl_3): δ (ppm) 8.16 (d, $J = 8.6$ Hz, 2H), 8.08 (d, $J = 8.6$ Hz, 4H), 7.94 (d, $J = 8.6$ Hz, 2H), 7.90 (d, $J = 8.6$ Hz, 2H), 7.61 (d, $J = 8.0$ Hz, 4H), 7.55 (d \times 2, $J = 8.6$ Hz, 4H, overlapped), 7.01 (d, $J = 8.6$ Hz, 2H), 6.97 (d \times 2, $J = 8.6$ Hz, 4H, overlapped), 4.34 (t, $J = 6.6$ Hz, 4H), 4.25 (d, $J = 5.8$ Hz, 2H), 4.04 (t, $J = 6.3$ Hz, 2H), 4.00 (t, $J = 6.6$ Hz, 4H), 3.64 (br, $J = 6.6$ Hz, 2H), 1.85–1.73 (m, 11H), 1.61–1.54 (m, 2H), 1.47–1.25 (m, 61H), 0.90–0.86 (m, 6H). ^{13}C NMR (125 MHz, CDCl_3): δ (ppm) 166.66, 166.21, 162.35, 159.44, 155.40, 145.21, 132.23, 130.51, 130.06, 128.58, 128.31, 126.40, 125.20, 122.34, 114.97, 114.82, 68.45, 68.15, 68.04, 65.06, 63.08, 37.50, 32.82, 31.92, 31.83, 31.50, 29.97, 29.64, 29.57, 29.53, 29.49, 29.46, 29.44, 29.41, 29.37, 29.32, 29.26, 29.18, 28.77, 26.80, 26.77, 26.05, 25.75, 22.68, 22.66, 14.11. MALDI-TOF mass: calcd. for $\text{C}_{85}\text{H}_{119}\text{N}_2\text{O}_{10}$ $[\text{M} + \text{H}]^+$: $m/z = 1327.89$; found: 1327.81.

Compound 17. By a procedure similar to that for **7**, compound **17** was obtained in 61% yield (0.51 g, 0.37 mmol) from **16** (0.80 g, 0.60 mmol), methacryloyl chloride (0.13 g, 1.20 mmol) and triethylamine (0.13 g, 1.21 mmol). ^1H NMR (500 MHz, CDCl_3): δ (ppm) 8.16 (d, $J = 8.0$ Hz, 2H), 8.07 (d \times 2, $J = 8.6$ Hz, 4H, overlapped), 7.93 (d, $J = 8.6$ Hz, 2H), 7.90 (d, $J = 8.0$ Hz, 2H), 7.61 (d, $J = 8.6$ Hz, 4H), 7.55 (d \times 2, $J = 8.6$ Hz, 4H, overlapped), 7.00 (d, $J = 8.6$ Hz, 2H), 6.98 (d \times 2, $J = 8.6$ Hz, 4H, overlapped), 6.09 (s, 1H), 5.54 (t, $J = 1.7$ Hz, 1H), 4.33 (t, $J = 6.8$ Hz, 4H), 4.25 (d, $J = 5.7$ Hz, 2H), 4.14 (t, $J = 6.8$ Hz, 2H), 4.05 (t, $J = 6.8$ Hz, 2H), 4.00 (t \times 2, $J = 6.8$ Hz, 4H, overlapped), 1.94 (s, 3H), 1.81–1.75 (m, 11H), 1.69–1.64 (m, 2H), 1.47–1.28 (m, 60H), 0.88–0.86 (m, 6H). ^{13}C NMR (125 MHz, CDCl_3): δ (ppm) 166.68, 166.22, 162.35, 159.45, 155.40, 145.21, 136.61, 132.23, 130.51, 130.06, 128.58, 128.33, 126.40, 125.22, 122.34, 114.97, 114.82, 68.45, 68.15, 68.04, 65.06, 63.11, 37.50, 32.83, 31.92, 31.85, 31.50, 29.98, 29.66, 29.57, 29.53, 29.49, 29.45, 29.41, 29.37, 29.32, 29.26, 29.18, 28.77, 26.81, 26.77, 26.05, 25.74, 22.68, 22.66, 14.13. MALDI-TOF mass: calcd. for $\text{C}_{89}\text{H}_{123}\text{N}_2\text{O}_{11}$ $[\text{M} + \text{H}]^+$: $m/z = 1395.91$; found: 1395.94.

Compound 18. By a procedure similar to that for **3**, except that the reaction temperature was 40 °C, compound **18** was obtained in 94% yield (1.38 g, 0.94 mmol) from **8** (1.0 g, 1.0 mmol), **12** (0.53 g, 1.10 mmol), DPTS (0.06 g, 0.21 mmol) and DIPC (0.26 g, 2.00 mmol). ¹H NMR (500 MHz, CDCl₃): δ (ppm) 8.17 (d, *J* = 8.6 Hz, 2H), 8.16 (d, *J* = 8.6 Hz, 2H), 8.08 (d, *J* = 8.0 Hz, 2H), 7.93 (d × 2, *J* = 8.6 Hz, 4H, overlapped), 7.90 (d × 2, *J* = 8.6 Hz, 4H, overlapped), 7.61 (d, *J* = 8.6 Hz, 2H), 7.55 (d, *J* = 8.6 Hz, 2H), 7.00 (d × 2, *J* = 8.6 Hz, 4H, overlapped), 6.98 (d, *J* = 8.6 Hz, 2H), 4.35 (t, *J* = 6.9 Hz, 2H), 4.33 (t, *J* = 6.6 Hz, 2H), 4.25 (d, *J* = 5.7 Hz, 2H), 4.04 (t × 2, *J* = 6.6 Hz, 4H, overlapped), 4.00 (t, *J* = 6.6 Hz, 2H), 3.60 (t, *J* = 6.6 Hz, 2H), 1.83–1.76 (m, 11H), 1.50–1.25 (m, 62H), 0.90–0.86 (m, 15H), 0.05 (s, 6H). ¹³C NMR (125 MHz, CDCl₃): δ (ppm) 166.30, 166.21, 162.34, 159.47, 155.39, 145.23, 130.53, 130.51, 130.06, 128.30, 126.41, 125.19, 122.34, 114.97, 114.82, 68.49, 68.17, 65.39, 65.05, 63.33, 37.53, 32.90, 31.88, 31.51, 29.57, 29.44, 29.34, 29.27, 29.24, 29.19, 28.74, 26.84, 26.06, 26.04, 26.00, 22.68, 22.65, 18.41, 14.11, –5.24. MALDI-TOF mass: calcd. for C₉₁H₁₃₃N₄O₁₀Si [M + H]⁺: *m/z* = 1469.98; found: 1469.88.

Compound 19. By a procedure similar to that for **4**, compound **19** was obtained in 92% yield (1.10 g, 0.81 mmol) from **18** (1.30 g, 0.88 mmol) and TBAF (1.0 M in THF, 2.0 mL, 2.0 mmol). ¹H NMR (500 MHz, CDCl₃): δ (ppm) 8.17 (d, *J* = 8.6 Hz, 2H), 8.16 (d, *J* = 8.6 Hz, 2H), 8.08 (d, *J* = 8.6 Hz, 2H), 7.93 (d × 2, *J* = 8.6 Hz, 4H, overlapped), 7.90 (d × 2, *J* = 8.6 Hz, 4H, overlapped), 7.61 (d, *J* = 8.6 Hz, 2H), 7.55 (d, *J* = 8.6 Hz, 2H), 7.01 (d × 2, *J* = 8.6 Hz, 4H, overlapped), 6.98 (d, *J* = 8.6 Hz, 2H), 4.35 (t, *J* = 6.9 Hz, 2H), 4.33 (t, *J* = 6.6 Hz, 2H), 4.25 (d, *J* = 5.8 Hz, 2H), 4.04 (t × 2, *J* = 6.6 Hz, 4H, overlapped), 4.00 (t, *J* = 6.6 Hz, 2H), 3.64 (q, *J* = 5.8 Hz, 2H), 1.83–1.76 (m, 11H), 1.49–1.46 (m, 2H), 1.45–1.25 (m, 61H), 0.89–0.86 (m, 6H). ¹³C NMR (125 MHz, CDCl₃): δ (ppm) 166.32, 166.21, 162.37, 159.40, 155.46, 145.21, 132.22, 130.51, 130.06, 128.31, 126.41, 125.19, 122.34, 114.97, 114.82, 68.45, 68.15, 63.09, 37.50, 32.86, 32.81, 31.92, 31.86, 31.50, 31.43, 29.97, 29.53, 29.49, 29.44, 29.41, 29.37, 29.34, 29.31, 29.26, 29.24, 29.18, 26.77, 26.04, 26.01, 25.75, 22.68, 14.10. MALDI-TOF mass: calcd. for C₈₅H₁₁₉N₄O₁₀ [M + H]⁺: *m/z* = 1355.89; found: 1355.84.

Compound 20. By a procedure similar to that for **7**, compound **20** was obtained in 66% yield (0.55 g, 0.39 mmol) from **19** (0.80 g, 0.59 mmol), methacryloyl chloride (0.13 g, 1.22 mmol) and triethylamine (0.13 g, 1.21 mmol). ¹H NMR (500 MHz, CDCl₃): δ (ppm) 8.17 (d, *J* = 8.6 Hz, 2H), 8.16 (d, *J* = 8.6 Hz, 2H), 8.07 (d, *J* = 8.6 Hz, 2H), 7.93 (d × 2, *J* = 8.6 Hz, 4H, overlapped), 7.91 (d × 2, *J* = 8.6 Hz, 4H, overlapped), 7.61 (d, *J* = 8.6 Hz, 2H), 7.55 (d, *J* = 8.6 Hz, 2H), 7.00 (d × 2, *J* = 8.6 Hz, 4H, overlapped), 6.98 (d, *J* = 8.6 Hz, 2H), 6.10 (s, 1H), 5.54 (t, *J* = 1.7 Hz, 1H), 4.33 (t × 2, *J* = 6.7 Hz, 4H, overlapped), 4.25 (d, *J* = 5.7 Hz, 2H), 4.14 (t, *J* = 6.8 Hz, 2H), 4.05 (t × 2, *J* = 6.8 Hz, 4H, overlapped), 4.00 (t, *J* = 6.8 Hz, 2H), 1.94 (s, 3H), 1.82–1.75 (m, 11H), 1.69–1.60 (m, 2H), 1.48–1.27 (m, 60H), 0.89–0.86 (m, 6H). ¹³C NMR (125 MHz, CDCl₃): δ (ppm) 166.68, 166.22, 162.37, 159.47, 155.41, 145.21, 136.58, 132.23, 130.52, 130.07, 128.58, 128.35, 126.40, 125.23, 122.34, 114.98, 114.82, 68.45, 68.17, 68.04, 65.06, 63.11, 37.52, 32.83, 31.92, 31.85, 31.51, 29.98, 29.66, 29.57, 29.53, 29.49, 29.45, 29.41, 29.37, 29.34, 29.26, 29.18, 28.78, 26.81, 26.77, 26.07, 25.75, 22.68, 22.66, 14.12. MALDI-TOF mass: calcd. for C₈₉H₁₂₃N₄O₁₁ [M + H]⁺: *m/z* = 1423.92; found: 1423.91.



Scheme S3 I Synthesis of **26**, **32** and **36**. Reagents and conditions: (a) DPTS, DIPC, CH_2Cl_2 , 25 °C; (b) TBAF, THF, 25 °C; (c) **2**, DPTS, DIPC, CH_2Cl_2 , 40 °C; (d) methacryloyl chloride, triethylamine, CH_2Cl_2 , 25 °C; (e) **12**, DPTS, DIPC, CH_2Cl_2 , 40 °C.

Compound 22. By a procedure similar to that for **3**, compound **22** was obtained in 88% yield (1.60 g, 1.48 mmol) from **21** (1.0 g, 1.68 mmol), **2** (0.86 g, 1.70 mmol), DPTS (0.10 g, 0.33 mmol) and DIPC (0.40 g, 3.20 mmol). ^1H NMR (500 MHz, CDCl_3): δ (ppm) 8.06 (d, $J = 8.0$ Hz, 2H), 8.00 (d, $J = 8.6$ Hz, 2H), 7.61 (d, $J = 8.0$ Hz, 2H), 7.55 (d, $J = 8.6$ Hz, 4H), 7.46 (d, $J = 8.6$ Hz, 2H), 6.98 (d, $J = 8.6$ Hz, 2H), 6.86 (d, $J = 8.6$ Hz, 2H), 4.30 (t, $J = 6.9$ Hz, 2H), 4.22 (d, $J = 5.8$ Hz, 2H), 4.00 (t, $J = 6.3$ Hz, 2H), 3.96 (t, $J = 6.3$ Hz, 2H), 3.58 (t, $J = 6.6$ Hz, 2H), 1.82–1.73 (m, 7H), 1.44–1.20 (m, 50H), 0.88–0.85 (m, 15H), 0.05 (s, 6H). ^{13}C NMR (125 MHz, CDCl_3): δ (ppm) 166.68, 166.17, 159.61, 159.38, 158.98, 145.15, 138.12, 133.31, 132.20, 131.23, 130.02, 129.43, 128.59, 128.34, 128.28, 126.40, 116.90, 114.90, 114.58, 114.47, 87.45, 68.07, 67.66, 65.22, 63.30, 37.47, 32.88, 31.90, 31.82, 31.46, 29.97, 29.70, 29.63, 29.56, 29.50, 29.45, 29.41, 29.35, 29.31, 29.25, 29.22, 29.17, 29.12, 28.67, 26.77, 26.75, 26.04, 26.00, 25.98, 25.64, 22.67, 22.65, 18.37, 14.10,

Compound 22. By a procedure similar to that for **3**, compound **22** was obtained in 88% yield (1.60 g, 1.48 mmol) from **21** (1.0 g, 1.68 mmol), **2** (0.86 g, 1.70 mmol), DPTS (0.10 g, 0.33 mmol) and DIPC (0.40 g, 3.20 mmol). ^1H NMR (500 MHz, CDCl_3): δ (ppm) 8.06 (d, $J = 8.0$ Hz, 2H), 8.00 (d, $J = 8.6$ Hz, 2H), 7.61 (d, $J = 8.0$ Hz, 2H), 7.55 (d, $J = 8.6$ Hz, 4H), 7.46 (d, $J = 8.6$ Hz, 2H), 6.98 (d, $J = 8.6$ Hz, 2H), 6.86 (d, $J = 8.6$ Hz, 2H), 4.30 (t, $J = 6.9$ Hz, 2H), 4.22 (d, $J = 5.8$ Hz, 2H), 4.00 (t, $J = 6.3$ Hz, 2H), 3.96 (t, $J = 6.3$ Hz, 2H), 3.58 (t, $J = 6.6$ Hz, 2H), 1.82–1.73 (m, 7H), 1.44–1.20 (m, 50H), 0.88–0.85 (m, 15H), 0.05 (s, 6H). ^{13}C NMR (125 MHz, CDCl_3): δ (ppm) 166.68, 166.17, 159.61, 159.38, 158.98, 145.15, 138.12, 133.31, 132.20, 131.23, 130.02, 129.43, 128.59, 128.34, 128.28, 126.40, 116.90, 114.90, 114.58, 114.47, 87.45, 68.07, 67.66, 65.22, 63.30, 37.47, 32.88, 31.90, 31.82, 31.46, 29.97, 29.70, 29.63, 29.56, 29.50, 29.45, 29.41, 29.35, 29.31, 29.25, 29.22, 29.17, 29.12, 28.67, 26.77, 26.75, 26.04, 26.00, 25.98, 25.64, 22.67, 22.65, 18.37, 14.10, –5.27. MALDI-TOF mass: calcd. for $\text{C}_{70}\text{H}_{105}\text{O}_7\text{Si}$ [$\text{M} + \text{H}$] $^+$: $m/z = 1085.66$; found: 1085.66.

Compound 23. By a procedure similar to that for **4**, compound **23** was obtained in 95% yield (1.28 g, 1.31 mmol) from **22** (1.50 g, 1.38 mmol) and TBAF (1.0 M in THF, 2.60 mL, 2.60 mmol). ^1H NMR (500 MHz, CDCl_3): δ (ppm) 8.06 (d, $J = 8.0$ Hz, 2H), 8.00 (d, $J = 8.6$ Hz, 2H), 7.61 (d, $J = 8.0$ Hz, 2H), 7.55 (d, $J = 8.6$ Hz, 4H), 7.46 (d, $J = 8.6$ Hz, 2H), 6.98 (d, $J = 8.6$ Hz, 2H), 6.86 (d, $J = 8.6$ Hz, 2H), 4.32 (t, $J = 6.9$ Hz, 2H), 4.23 (d, $J = 5.8$ Hz, 2H), 4.00 (t, $J = 6.3$ Hz, 2H), 3.96 (t, $J = 6.3$ Hz, 2H), 3.64 (t, $J = 6.6$ Hz, 2H), 1.83–1.72 (m, 7H), 1.59–1.54 (m, 2H), 1.52–1.30 (m, 49H), 0.89–0.86 (m, 6H). ^{13}C NMR (125 MHz, CDCl_3): δ (ppm) 166.70, 166.17, 159.57, 159.36, 145.13, 138.10, 133.19, 132.17, 131.21, 129.99, 129.41, 128.55, 128.30, 128.26, 126.38, 116.88, 114.89, 114.57, 114.45, 92.61, 87.44, 68.07, 68.04, 67.65, 65.22, 63.02, 37.44, 32.76, 31.87, 31.79, 31.44, 29.93, 29.60, 29.53, 29.48, 29.43, 29.39, 29.37, 29.32, 29.28, 29.22, 29.20, 29.13, 28.66, 26.74, 26.72, 26.01, 25.96, 25.70, 23.46, 22.64, 14.09. MALDI-TOF mass: calcd. for $\text{C}_{64}\text{H}_{91}\text{O}_7$ [$\text{M} + \text{H}$] $^+$: $m/z = 971.67$; found: 971.62.

Compound 24. By a procedure similar to that for **3**, except that the reaction temperature was 40 °C, compound **24** was obtained in 85% yield (1.24 g, 0.85 mmol) from **23** (1.0 g, 1.0 mmol), **2** (0.55 g, 1.10 mmol), DPTS (0.061 g, 0.21 mmol) and DIPC (0.25 g, 2.01 mmol). ^1H NMR (500 MHz, CDCl_3): δ (ppm) 8.06 (d, $J = 8.6$ Hz, 2H), 8.00 (d, $J = 8.0$ Hz, 4H), 7.61 (d, $J = 8.6$ Hz, 2H), 7.54 (d, $J = 8.6$ Hz, 6H), 7.46 (d, $J = 8.6$ Hz, 2H), 7.46 (d, $J = 8.6$ Hz, 2H), 6.98 (d, $J = 8.6$ Hz, 2H), 6.87 (d, $J = 8.0$ Hz, 4H), 4.32 (t, $J = 6.6$ Hz, 4H), 4.23 (d, $J = 5.8$ Hz, 2H), 4.02 (t, $J = 6.6$ Hz, 2H), 3.96 (t, $J = 6.6$ Hz, 4H), 3.58 (t, $J = 6.6$ Hz, 2H), 1.86–1.77 (m, 11H), 1.51–1.28 (m, 62H), 0.89–0.86 (m, 15H), 0.05 (s, 6H). ^{13}C NMR (125 MHz, CDCl_3): δ (ppm) 166.65, 166.15, 159.61, 159.48, 145.11, 138.10, 133.31, 132.18, 130.12, 129.48, 128.59, 128.36, 128.28, 126.40, 114.96, 114.68, 114.41, 87.47, 68.12, 67.68, 65.22, 63.34, 37.47, 32.86, 31.93, 31.84, 31.43, 29.95, 29.70, 29.64, 29.56, 29.52, 29.47, 29.41, 29.36, 29.33, 29.25, 29.22, 29.16, 29.12, 28.67, 26.77, 26.74, 26.04, 26.01, 25.98, 25.68, 22.67, 22.63, 18.37, 14.11, –5.27. MALDI-TOF mass: calcd. for $\text{C}_{95}\text{H}_{133}\text{O}_{10}\text{Si}$ [$\text{M} + \text{H}$] $^+$: $m/z = 1461.96$; found: 1461.97.

Compound 25. By a procedure similar to that for **4**, compound **25** was obtained in 90% yield (1.00 g, 0.74 mmol) from **24** (1.20 g, 0.82 mmol) and TBAF (1.0 M in THF, 2.0 mL, 2.0 mmol). ^1H NMR (500 MHz, CDCl_3): δ (ppm) 8.06 (d, $J = 8.6$ Hz, 2H), 8.00 (d, $J = 8.0$ Hz, 4H), 7.61 (d, $J = 8.6$ Hz, 2H), 7.54 (d, $J = 8.6$ Hz, 6H), 7.46 (d, $J = 8.6$ Hz, 2H), 7.46 (d, $J = 8.6$ Hz, 2H), 6.98 (d, $J = 8.6$ Hz, 2H), 6.87 (d, $J = 8.0$ Hz, 4H), 4.33 (t, $J = 6.6$ Hz, 4H), 4.23 (d, $J = 5.8$ Hz, 2H), 4.02 (t, $J = 6.6$ Hz, 2H), 3.96 (t, $J = 6.6$ Hz, 4H), 3.64 (m, 2H), 1.85–1.76 (m, 11H), 1.56–1.53 (m, 2H), 1.46–1.21 (m, 61H), 0.88–0.86 (m, 6H). ^{13}C NMR (125 MHz, CDCl_3): δ (ppm)

166.71, 166.21, 159.57, 145.23, 138.14, 133.19, 132.18, 129.97, 129.41, 128.55, 128.32, 128.25, 126.38, 116.88, 114.89, 114.54, 114.46, 92.64, 87.47, 68.11, 68.06, 67.65, 65.21, 63.02, 37.46, 32.76, 31.87, 31.81, 31.44, 29.93, 29.62, 29.53, 29.49, 29.45, 29.39, 29.38, 29.32, 29.25, 29.21, 29.17, 29.14, 28.66, 26.74, 26.72, 26.07, 25.96, 25.74, 23.46, 22.65, 14.09. MALDI-TOF mass: calcd. for $C_{89}H_{119}O_{10}$ $[M + H]^+$: $m/z = 1347.87$; found: 1347.86.

Compound 26. By a procedure similar to that for **7**, compound **26** was obtained in 60% yield (0.63 g, 0.44 mmol) from **25** (1.00 g, 0.74 mmol), methacryloyl chloride (0.15 g, 1.50 mmol) and triethylamine (0.16 g, 1.50 mmol). 1H NMR (500 MHz, $CDCl_3$): δ (ppm) 8.06 (d, $J = 8.6$ Hz, 2H), 8.00 (d, $J = 8.0$ Hz, 4H), 7.61 (d, $J = 8.6$ Hz, 2H), 7.54 (d, $J = 8.6$ Hz, 6H), 7.46 (d, $J = 8.6$ Hz, 2H), 7.46 (d, $J = 8.6$ Hz, 2H), 6.98 (d, $J = 8.6$ Hz, 2H), 6.87 (d, $J = 8.0$ Hz, 4H), 6.09 (s, 1H), 5.54 (t, $J = 1.7$ Hz, 1H), 4.32 (t, $J = 6.6$ Hz, 4H), 4.23 (d, $J = 5.8$ Hz, 2H), 4.14 (t, $J = 6.3$ Hz, 2H), 4.01 (t, $J = 6.3$ Hz, 2H), 3.97 (t, $J = 6.6$ Hz, 4H), 1.94 (s, 3H), 1.80–1.75 (m, 11H), 1.67–1.64 (m, 2H), 1.55–1.28 (m, 60H), 0.88–0.86 (m, 6H). ^{13}C NMR (125 MHz, $CDCl_3$): δ (ppm) 167.51, 159.60, 159.39, 136.61, 136.51, 133.20, 131.23, 130.01, 129.48, 129.42, 128.51, 128.30, 128.27, 126.36, 125.12, 123.38, 117.84, 114.89, 114.57, 114.47, 92.60, 87.46, 68.07, 68.05, 67.88, 65.23, 65.01, 64.78, 37.41, 31.87, 31.79, 31.42, 29.92, 29.59, 29.53, 29.42, 29.40, 29.31, 29.28, 29.22, 29.15, 28.72, 28.67, 28.57, 26.73, 26.71, 26.01, 25.98, 25.93, 22.65, 22.62, 18.32, 14.09. MALDI-TOF mass: calcd. for $C_{93}H_{123}O_{11}$ $[M + H]^+$: $m/z = 1415.91$; found: 1415.91.

Compound 28. By a procedure similar to that for **3**, compound **28** was obtained in 85% yield (1.55 g, 1.43 mmol) from **27** (1.0 g, 1.68 mmol), **12** (0.82 g, 1.70 mmol), DPTS (0.10 g, 0.33 mmol) and DIPC (0.40 g, 3.20 mmol). 1H NMR (500 MHz, $CDCl_3$): δ (ppm) 8.06 (d, $J = 8.0$ Hz, 2H), 8.00 (d, $J = 8.6$ Hz, 2H), 7.62 (d, $J = 8.0$ Hz, 2H), 7.55 (d, $J = 8.6$ Hz, 4H), 7.46 (d, $J = 8.6$ Hz, 2H), 6.98 (d, $J = 8.6$ Hz, 2H), 6.86 (d, $J = 8.6$ Hz, 2H), 4.32 (t, $J = 6.9$ Hz, 2H), 4.23 (d, $J = 5.8$ Hz, 2H), 4.00 (t, $J = 6.3$ Hz, 2H), 3.96 (t, $J = 6.3$ Hz, 2H), 3.58 (t, $J = 6.6$ Hz, 2H), 1.81–1.72 (m, 7H), 1.45–1.21 (m, 50H), 0.88–0.86 (m, 15H), 0.05 (s, 6H). ^{13}C NMR (125 MHz, $CDCl_3$): δ (ppm) 166.69, 166.17, 159.61, 159.37, 158.98, 145.15, 138.11, 133.31, 132.20, 131.23, 130.02, 129.43, 128.59, 128.34, 128.29, 126.40, 116.90, 114.90, 114.58, 114.47, 87.45, 68.07, 67.66, 65.22, 63.30, 37.48, 32.88, 31.90, 31.82, 31.46, 29.98, 29.70, 29.63, 29.56, 29.50, 29.45, 29.41, 29.35, 29.31, 29.25, 29.22, 29.18, 29.13, 28.67, 26.79, 26.76, 26.04, 26.00, 25.96, 25.64, 22.67, 22.65, 18.32, 14.11, –5.27. MALDI-TOF mass: calcd. for $C_{70}H_{105}O_7Si$ $[M + H]^+$: $m/z = 1085.66$; found: 1085.65.

Compound 29. By a procedure similar to that for **4**, compound **29** was obtained in 95% yield (1.28 g, 1.31 mmol) from **28** (1.50 g, 1.38 mmol) and TBAF (1.0 M in THF, 2.60 mL, 2.60 mmol). 1H NMR (500 MHz, $CDCl_3$): δ (ppm) 8.06 (d, $J = 8.0$ Hz, 2H), 8.00 (d, $J = 8.6$ Hz, 2H), 7.61 (d, $J = 8.0$ Hz, 2H), 7.55 (d, $J = 8.6$ Hz, 4H), 7.46 (d, $J = 8.6$ Hz, 2H), 6.98 (d, $J = 8.6$ Hz, 2H), 6.86 (d, $J = 8.6$ Hz, 2H), 4.33 (t, $J = 6.9$ Hz, 2H), 4.23 (d, $J = 5.8$ Hz, 2H), 4.00 (t, $J = 6.3$ Hz, 2H), 3.96 (t, $J = 6.3$ Hz, 2H), 3.64 (t, $J = 6.6$ Hz, 2H), 1.82–1.70 (m, 7H), 1.58–1.55 (m, 2H), 1.52–1.28 (m, 49H), 0.89–0.86 (m, 6H). ^{13}C NMR (125 MHz, $CDCl_3$): δ (ppm) 166.71, 166.17, 159.56, 159.36, 145.13, 138.11, 133.19, 132.16, 131.21, 129.98, 129.41, 128.56, 128.30, 128.26, 126.38, 116.88, 114.88, 114.54, 114.47, 92.61, 87.44, 68.07, 68.04, 67.65, 65.24, 63.02, 37.44, 32.76, 31.88, 31.79, 31.44, 29.93, 29.61, 29.53, 29.48, 29.43, 29.38, 29.36, 29.32, 29.28, 29.25, 29.20, 29.13, 28.66, 26.71, 26.72, 26.01, 25.96, 25.72, 23.46, 22.64, 14.09. MALDI-TOF mass: calcd. for $C_{64}H_{91}O_7$ $[M + H]^+$: $m/z = 971.67$; found: 971.65.

Compound 30. By a procedure similar to that for **3**, except that the reaction temperature was 40 °C, compound **30** was obtained in 87% yield (1.27 g, 0.87

mmol) from **29** (1.0 g, 1.0 mmol), **2** (0.55 g, 1.10 mmol), DPTS (0.061 g, 0.21 mmol) and DIPC (0.25 g, 2.01 mmol). ^1H NMR (500 MHz, CDCl_3): δ (ppm) 8.06 (d, $J = 8.6$ Hz, 2H), 8.00 (d, $J = 8.0$ Hz, 4H), 7.61 (d, $J = 8.6$ Hz, 2H), 7.54 (d, $J = 8.6$ Hz, 6H), 7.46 (d, $J = 8.6$ Hz, 2H), 7.46 (d, $J = 8.6$ Hz, 2H), 6.98 (d, $J = 8.6$ Hz, 2H), 6.87 (d, $J = 8.0$ Hz, 4H), 4.33 (t, $J = 6.6$ Hz, 4H), 4.23 (d, $J = 5.8$ Hz, 2H), 4.00 (t, $J = 6.6$ Hz, 2H), 3.96 (t, $J = 6.6$ Hz, 4H), 3.58 (t, $J = 6.6$ Hz, 2H), 1.87–1.78 (m, 11H), 1.52–1.28 (m, 62H), 0.89–0.86 (m, 15H), 0.05 (s, 6H). ^{13}C NMR (125 MHz, CDCl_3): δ (ppm) 166.65, 166.15, 159.64, 159.48, 145.11, 138.13, 133.31, 132.16, 130.12, 129.48, 128.58, 128.36, 128.28, 126.42, 114.96, 114.68, 114.46, 87.47, 68.12, 67.68, 65.22, 63.34, 37.47, 32.87, 31.93, 31.84, 31.46, 29.95, 29.77, 29.64, 29.56, 29.51, 29.47, 29.40, 29.36, 29.33, 29.25, 29.25, 29.16, 29.14, 28.67, 26.78, 26.74, 26.05, 26.01, 25.98, 25.68, 22.63, 22.63, 18.37, 14.11, –5.27. MALDI-TOF mass: calcd. for $\text{C}_{95}\text{H}_{133}\text{O}_{10}\text{Si}$ $[\text{M} + \text{H}]^+$: $m/z = 1461.96$; found: 1461.97.

Compound 31. By a procedure similar to that for **4**, compound **31** was obtained in 95% yield (1.01 g, 0.75 mmol) from **30** (1.20 g, 0.82 mmol) and TBAF (1.0 M in THF, 2.0 mL, 2.0 mmol). ^1H NMR (500 MHz, CDCl_3): δ (ppm) 8.06 (d, $J = 8.6$ Hz, 2H), 8.00 (d, $J = 8.0$ Hz, 4H), 7.61 (d, $J = 8.6$ Hz, 2H), 7.54 (d, $J = 8.6$ Hz, 6H), 7.46 (d, $J = 8.6$ Hz, 2H), 7.46 (d, $J = 8.6$ Hz, 6H), 6.98 (d, $J = 8.6$ Hz, 2H), 6.87 (d, $J = 8.0$ Hz, 4H), 4.32 (t, $J = 6.6$ Hz, 4H), 4.23 (d, $J = 5.8$ Hz, 2H), 4.01 (t, $J = 6.6$ Hz, 2H), 3.96 (t, $J = 6.6$ Hz, 4H), 3.64 (br, $J = 6.6$ Hz, 2H), 1.86–1.77 (m, 11H), 1.57–1.53 (m, 2H), 1.46–1.20 (m, 61H), 0.88–0.86 (m, 6H). ^{13}C NMR (125 MHz, CDCl_3): δ (ppm) 166.71, 166.21, 159.58, 145.23, 138.16, 133.19, 132.18, 129.97, 129.45, 128.55, 128.31, 128.25, 126.38, 116.88, 114.85, 114.54, 114.47, 92.64, 87.47, 68.12, 68.06, 67.65, 65.21, 63.12, 37.46, 32.76, 31.88, 31.81, 31.46, 29.93, 29.62, 29.56, 29.49, 29.40, 29.38, 29.36, 29.32, 29.25, 29.20, 29.17, 29.13, 28.66, 26.74, 26.72, 26.07, 25.98, 25.74, 23.46, 22.61, 14.10. MALDI-TOF mass: calcd. for $\text{C}_{89}\text{H}_{119}\text{O}_{10}$ $[\text{M} + \text{H}]^+$: $m/z = 1347.87$; found: 1347.82.

Compound 32. By a procedure similar to that for **7**, compound **32** was obtained in 70% yield (0.73 g, 0.52 mmol) from **31** (1.00 g, 0.74 mmol), methacryloyl chloride (0.15 g, 1.50 mmol) and triethylamine (0.16 g, 1.50 mmol). ^1H NMR (500 MHz, CDCl_3): δ (ppm) 8.07 (d, $J = 8.6$ Hz, 2H), 8.00 (d, $J = 8.0$ Hz, 2H), 8.00 (d, $J = 8.0$ Hz, 2H), 7.61 (d, $J = 8.6$ Hz, 2H), 7.55 (d, $J = 8.6$ Hz, 6H), 7.46 (d, $J = 8.6$ Hz, 2H), 7.46 (d, $J = 8.6$ Hz, 2H), 6.98 (d, $J = 8.6$ Hz, 2H), 6.87 (d, $J = 8.0$ Hz, 4H), 6.10 (s, 1H), 5.54 (t, $J = 1.7$ Hz, 1H), 4.32 (t, $J = 6.6$ Hz, 4H), 4.23 (d, $J = 5.8$ Hz, 2H), 4.14 (t, $J = 6.3$ Hz, 2H), 4.01 (t, $J = 6.3$ Hz, 2H), 3.97 (t, $J = 6.6$ Hz, 4H), 1.94 (s, 3H), 1.82–1.76 (m, 11H), 1.69–1.64 (m, 2H), 1.50–1.28 (m, 60H), 0.89–0.87 (m, 6H). ^{13}C NMR (125 MHz, CDCl_3): δ (ppm) 167.58, 167.23, 159.64, 159.39, 136.62, 136.51, 133.21, 131.23, 130.01, 129.48, 129.42, 128.51, 128.33, 128.27, 126.36, 125.18, 123.38, 117.86, 114.89, 114.53, 114.47, 92.61, 87.46, 68.07, 68.07, 67.88, 65.26, 65.01, 64.78, 37.41, 31.89, 31.79, 31.42, 29.90, 29.59, 29.53, 29.42, 29.40, 29.33, 29.28, 29.22, 29.17, 28.72, 28.65, 28.57, 26.76, 26.71, 26.01, 25.98, 25.95, 22.65, 22.64, 18.32, 14.10. MALDI-TOF mass: calcd. for $\text{C}_{93}\text{H}_{123}\text{O}_{11}$ $[\text{M} + \text{H}]^+$: $m/z = 1415.91$; found: 1415.94.

Compound 34. By a procedure similar to that for **3**, except that the reaction temperature was 40 °C, compound **34** was obtained in 91% yield (1.33 g, 0.91 mmol) from **33** (1.0 g, 1.0 mmol), **12** (0.53 g, 1.10 mmol), DPTS (0.060 g, 0.210 mmol) and DIPC (0.25 g, 1.98 mmol). ^1H NMR (500 MHz, CDCl_3): δ (ppm) 8.06 (d, $J = 8.6$ Hz, 2H), 8.00 (d, $J = 8.0$ Hz, 4H), 7.61 (d, $J = 8.6$ Hz, 2H), 7.54 (d, $J = 8.6$ Hz, 6H), 7.46 (d, $J = 8.6$ Hz, 2H), 7.46 (d, $J = 8.6$ Hz, 2H), 6.98 (d, $J = 8.6$ Hz, 2H), 6.87 (d, $J = 8.0$ Hz, 4H), 4.32 (t, $J = 6.6$ Hz, 4H), 4.23 (d, $J = 5.8$ Hz, 2H), 4.00 (t, $J = 6.6$ Hz, 2H), 3.96 (t, $J = 6.6$ Hz, 4H), 3.58 (t, $J = 6.6$ Hz, 2H), 1.85–1.78 (m, 11H), 1.53–1.29 (m, 62H), 0.89–0.86 (m, 15H), 0.05 (s, 6H). ^{13}C NMR (125 MHz, CDCl_3): δ (ppm) 166.68, 166.17, 159.61, 159.48, 145.10, 138.11, 133.31, 132.19,

129.48, 128.59, 128.36, 128.28, 126.40, 114.96, 114.68, 114.44, 87.47, 68.20, 67.68, 65.24, 63.34, 37.47, 32.86, 31.96, 31.84, 31.43, 29.95, 29.71, 29.64, 29.57, 29.52, 29.47, 29.41, 29.37, 29.33, 29.25, 29.23, 29.16, 29.12, 28.65, 26.81, 26.78, 26.04, 26.01, 25.96, 25.68, 22.65, 22.63, 18.31, 14.11, -5.26. MALDI-TOF mass: calcd. for $C_{95}H_{133}O_{10}Si$ $[M + H]^+$: $m/z = 1461.96$; found: 1461.93.

Compound 35. By a procedure similar to that for **4**, compound **35** was obtained in 94% yield (1.13 g, 0.84 mmol) from **34** (1.30 g, 0.89 mmol) and TBAF (1.0 M in THF, 2.0 mL, 2.0 mmol). 1H NMR (500 MHz, $CDCl_3$): δ (ppm) 8.06 (d, $J = 8.6$ Hz, 2H), 8.00 (d, $J = 8.0$ Hz, 4H), 7.61 (d, $J = 8.6$ Hz, 2H), 7.54 (d, $J = 8.6$ Hz, 6H), 7.46 (d, $J = 8.6$ Hz, 2H), 7.46 (d, $J = 8.6$ Hz, 2H), 6.98 (d, $J = 8.6$ Hz, 2H), 6.87 (d, $J = 8.0$ Hz, 4H), 4.32 (t, $J = 6.6$ Hz, 4H), 4.23 (d, $J = 5.8$ Hz, 2H), 4.00 (t, $J = 6.6$ Hz, 2H), 3.96 (t, $J = 6.6$ Hz, 4H), 3.64 (br, $J = 6.6$ Hz, 2H), 1.86–1.77 (m, 11H), 1.58–1.52 (m, 2H), 1.46–1.23 (m, 61H), 0.89–0.86 (m, 6H). ^{13}C NMR (125 MHz, $CDCl_3$): δ (ppm) 166.73, 166.25, 159.56, 145.23, 138.13, 133.19, 132.16, 129.97, 129.45, 128.55, 128.32, 128.25, 126.38, 116.88, 114.89, 114.54, 114.46, 92.64, 87.47, 68.11, 68.06, 67.65, 65.21, 63.21, 37.45, 32.76, 31.87, 31.83, 31.44, 29.93, 29.67, 29.52, 29.49, 29.43, 29.35, 29.32, 29.30, 29.26, 29.24, 29.17, 29.14, 28.67, 26.73, 26.72, 26.07, 25.94, 25.74, 23.47, 22.65, 14.11. MALDI-TOF mass: calcd. for $C_{89}H_{119}O_{10}$ $[M + H]^+$: $m/z = 1347.87$; found: 1347.85.

Compound 36. By a procedure similar to that for **7**, compound **36** was obtained in 65% yield (0.68 g, 0.48 mmol) from **35** (1.0 g, 0.74 mmol), methacryloyl chloride (0.14 g, 1.30 mmol) and triethylamine (0.14 g, 1.36 mmol). 1H NMR (500 MHz, $CDCl_3$): δ (ppm) 8.07 (d, $J = 8.6$ Hz, 2H), 8.00 (d, $J = 8.0$ Hz, 2H), 8.00 (d, $J = 8.0$ Hz, 2H), 7.61 (d, $J = 8.6$ Hz, 2H), 7.55 (d, $J = 8.6$ Hz, 6H), 7.46 (d, $J = 8.6$ Hz, 2H), 7.46 (d, $J = 8.6$ Hz, 2H), 6.97 (d, $J = 8.6$ Hz, 2H), 6.87 (d, $J = 8.0$ Hz, 4H), 6.10 (s, 1H), 5.54 (t, $J = 1.7$ Hz, 1H), 4.33 (t, $J = 6.6$ Hz, 4H), 4.23 (d, $J = 5.8$ Hz, 2H), 4.14 (t, $J = 6.3$ Hz, 2H), 4.01 (t, $J = 6.3$ Hz, 2H), 3.97 (t, $J = 6.6$ Hz, 4H), 1.94 (s, 3H), 1.83–1.76 (m, 11H), 1.70–1.64 (m, 2H), 1.50–1.28 (m, 60H), 0.89–0.86 (m, 6H). ^{13}C NMR (125 MHz, $CDCl_3$): δ (ppm) 167.52, 167.48, 159.61, 159.38, 136.61, 136.54, 133.20, 131.25, 130.01, 129.48, 129.42, 128.51, 128.30, 128.27, 126.36, 125.12, 123.38, 117.84, 114.89, 114.57, 114.47, 92.60, 87.45, 68.07, 68.05, 67.86, 65.23, 65.05, 64.78, 37.41, 31.86, 31.79, 31.47, 29.91, 29.59, 29.53, 29.45, 29.41, 29.31, 29.28, 29.20, 29.17, 28.72, 28.68, 28.57, 26.78, 26.75, 26.01, 25.98, 25.93, 22.65, 22.62, 18.31, 14.09. MALDI-TOF mass: calcd. for $C_{93}H_{123}O_{11}$ $[M + H]^+$: $m/z = 1415.91$; found: 1415.88.

Polymer PMA/T₂A. Monomer **7** (0.20 g, 0.14 mmol) was placed in a Schlenk flask (25 mL), and the inner atmosphere was strictly purged with Ar. A stock solution of AIBN (6.13 mM) in anhydrous benzene was degassed by freeze-pump-thaw cycles (three times). This stock solution (0.30 mL) was introduced using a syringe into the flask containing **7**, and the mixture was stirred at 70 °C. After 24 h, the reaction mixture was poured into MeOH (150 mL), and a white precipitate formed was collected by filtration and subjected to preparative SEC with $CHCl_3$ as an eluent, to allow separation of a polymeric fraction from **7**. The polymeric fraction was concentrated (~5 mL) under a reduced pressure to a small volume, which was then added dropwise to MeOH (150 mL). A precipitate thus formed was collected by filtration and dried at 25 °C under a reduced pressure to give **PMA/T₂A** (170 mg) as orange solid in 85% yield. 1H NMR (500 MHz, $CDCl_3$): δ (ppm) 8.16–8.12 (m), 8.02–7.86 (m), 7.56–7.39 (m), 7.05–6.97 (m), 6.87–6.78 (m), 4.32–4.21 (br), 4.05–3.98 (m), 3.97–3.84 (m), 1.81–1.68 (br), 1.67–1.55 (br), 1.48–1.18 (br), 0.90–0.84 (m). FT-IR (ATR): ν (cm^{-1}) 2927, 2854, 2212, 1716, 1601, 1516, 1469, 1402, 1275, 1174, 1140, 1109, 1016. SEC analysis ($CHCl_3$, polystyrene standards): number-averaged molecular weight (M_n) = 7.9×10^4 $g\ mol^{-1}$ (degree of polymerization DP = 55), polydispersity index (M_w/M_n) = 3.3.

Polymer PMA/TA₂. By a procedure similar to that for **PMA/T₂A**, **PMA/TA₂** was obtained in 75% yield (165 mg) from monomer **11** (0.22 g, 0.15 mmol) and AIBN in anhydrous benzene (6.13 mM, 0.33 mL). ¹H NMR (500 MHz, CDCl₃): δ (ppm) 8.15–8.12 (m), 7.98–7.86 (m), 7.56–7.38 (br), 7.01–6.93 (m), 6.83–6.78 (br), 4.35–4.21 (br), 4.05–3.94 (m), 3.93–3.81 (br), 1.81–1.68 (br), 1.67–1.55 (br), 1.48–1.18 (br), 0.90–0.84 (m). FT-IR (ATR): ν (cm⁻¹) 2927, 2852, 2212, 1716, 1599, 1502, 1469, 1400, 1275, 1174, 1138, 1107, 1016. SEC analysis (CHCl₃, polystyrene standards): M_n = 6.2 × 10⁴ g mol⁻¹ (DP = 45), M_w/M_n = 2.2.

Polymer PMA/B₂A. By a procedure similar to that for **PMA/T₂A**, **PMA/B₂A** was obtained in 87% yield (165 mg) from monomer **17** (0.19 g, 0.14 mmol) and AIBN in anhydrous benzene (6.13 mM, 0.30 mL). ¹H NMR (500 MHz, CDCl₃): δ (ppm) 8.16–8.12 (m), 8.08–7.86 (m), 7.59–7.42 (m), 7.01–6.96 (m), 6.92–6.86 (m), 4.32–4.22 (br), 4.05–3.98 (m), 3.97–3.86 (br), 1.82–1.68 (br), 1.67–1.55 (br), 1.48–1.18 (br), 0.90–0.84 (m). FT-IR (ATR): ν (cm⁻¹) 2925, 2854, 1714, 1603, 1525, 1498, 1469, 1398, 1275, 1190, 1138, 1109, 1036. SEC analysis (CHCl₃, polystyrene standards): M_n = 7.7 × 10⁴ g mol⁻¹ (DP = 55), M_w/M_n = 2.9.

Polymer PMA/BA₂. By a procedure similar to that for **PMA/T₂A**, **PMA/BA₂** was obtained in 89% yield (205 mg) from monomer **20** (0.23 g, 0.15 mmol) and AIBN in anhydrous benzene (6.13 mM, 0.33 mL). ¹H NMR (500 MHz, CDCl₃): δ (ppm) 8.15–8.12 (m), 8.06–7.85 (m), 7.56–7.43 (br), 7.01–6.93 (m), 6.93–6.85 (br), 4.35–4.21 (br), 3.04–3.82 (br), 1.81–1.68 (br), 1.67–1.55 (br), 1.48–1.18 (br), 0.90–0.84 (m). FT-IR (ATR): ν (cm⁻¹) 2929, 2854, 1716, 1603, 1525, 1500, 1469, 1400, 1273, 1188, 1140, 1111, 1036, 1014. SEC analysis (CHCl₃, polystyrene standards): M_n = 8.0 × 10⁴ g mol⁻¹ (DP = 57), M_w/M_n = 3.2.

Polymer PMA/T₂B. By a procedure similar to that for **PMA/T₂A**, **PMA/T₂B** was obtained in 80% yield (184 mg) from monomer **26** (0.23 g, 0.16 mmol) and AIBN in anhydrous benzene (4.5 mM, 0.35 mL). ¹H NMR (500 MHz, CDCl₃): δ (ppm) 8.04 (d), 7.98–7.96 (br), 7.60–7.41 (m), 6.95 (d), 6.82 (br), 4.28 (br), 4.22 (br), 3.96 (br), 3.90 (br), 1.74 (br), 1.57 (br), 1.40–1.25 (br), 0.87–0.85 (m). FT-IR (ATR): ν (cm⁻¹) 2925, 2854, 2214, 1715, 1600, 1516, 1498, 1469, 1405, 1273, 1249, 1174, 1141, 1016. SEC analysis (CHCl₃, polystyrene standards): M_n = 8.4 × 10⁴ g mol⁻¹ (DP = 58), M_w/M_n = 2.3.

Polymer PMA/TBT. By a procedure similar to that for **PMA/T₂A**, **PMA/TBT** was obtained in 67% yield (154 mg) from monomer **32** (0.23 g, 0.16 mmol) and AIBN in anhydrous benzene (4.5 mM, 0.35 mL). ¹H NMR (500 MHz, CDCl₃): δ (ppm) 8.04 (d), 7.98–7.96 (br), 7.58–7.40 (m), 6.93 (br), 6.84–6.80 (m), 4.29 (br), 4.21 (br), 3.93–3.90 (br), 1.75 (br), 1.58 (br), 1.40–1.25 (br), 0.87–0.85 (m). FT-IR (ATR): ν (cm⁻¹) 2924, 2854, 2213, 1714, 1601, 1518, 1469, 1405, 1274, 1249, 1175, 1141, 1105, 1017. SEC analysis (CHCl₃, polystyrene standards): M_n = 6.5 × 10⁴ g mol⁻¹, M_w/M_n = 2.0.

Polymer PMA/BT₂. By a procedure similar to that for **PMA/T₂A**, **PMA/BT₂** was obtained in 91% yield (209 mg) from monomer **36** (0.23 g, 0.16 mmol) and AIBN in anhydrous benzene (4.5 mM, 0.35 mL). ¹H NMR (500 MHz, CDCl₃): δ (ppm) 7.98–7.96 (m), 7.54–7.41 (m), 6.85–6.81 (m), 4.28 (br), 4.21 (br), 3.94–3.89 (m), 1.74 (m), 1.56 (br), 1.40–1.26 (br), 0.87–0.85 (m). FT-IR (ATR): ν (cm⁻¹) 2924, 2854, 2215, 1715, 1600, 1517, 1498, 1469, 1404, 1277, 1250, 1175, 1141, 1107, 1017. SEC analysis (CHCl₃, polystyrene standards): M_n = 1.1 × 10⁵ g mol⁻¹, M_w/M_n = 3.3.

3.4.3. Supporting Figures

3.4.3.1. DSC Profiles

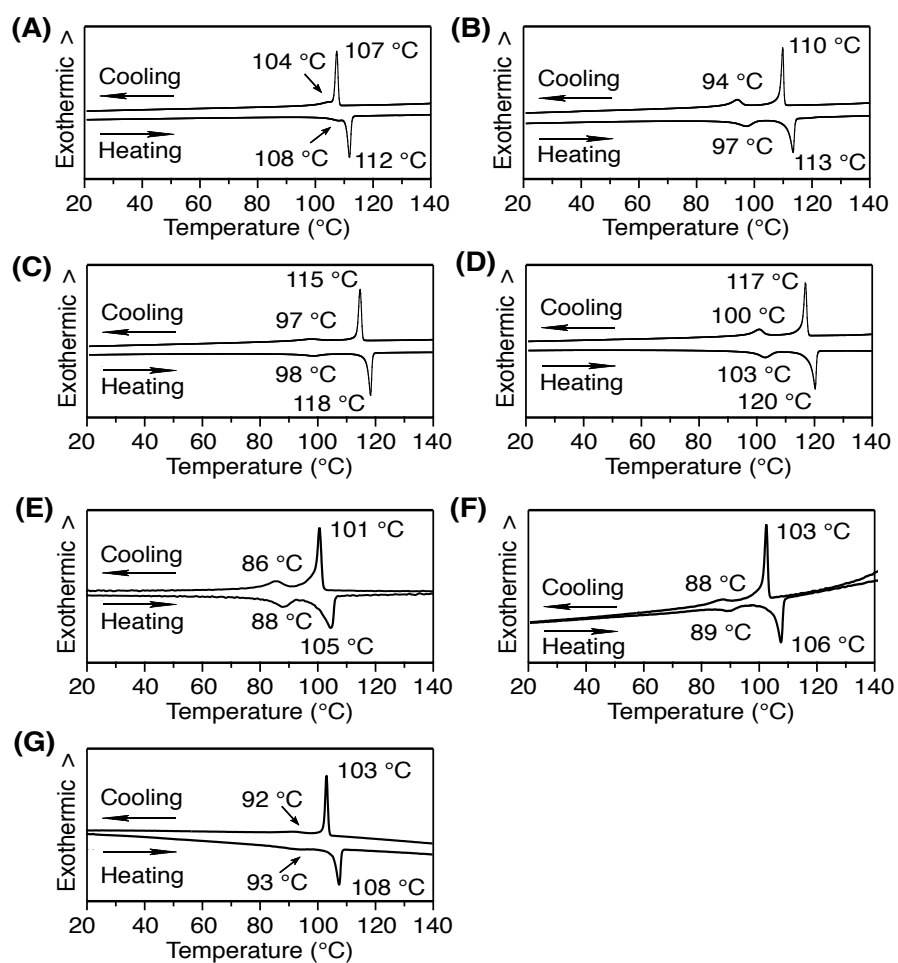


Figure S1 | DSC traces in a second heating/cooling cycle. (A) PMA/B₂A, (B) PMA/BA₂, (C) PMA/T₂A, (D) PMA/TA₂, (E) PMA/T₂B, (F) PMA/TBT, and (G) PMA/BT₂. Scan rate is 5 °C min⁻¹.

3.4.3.2. SAXS and WAXD Profiles

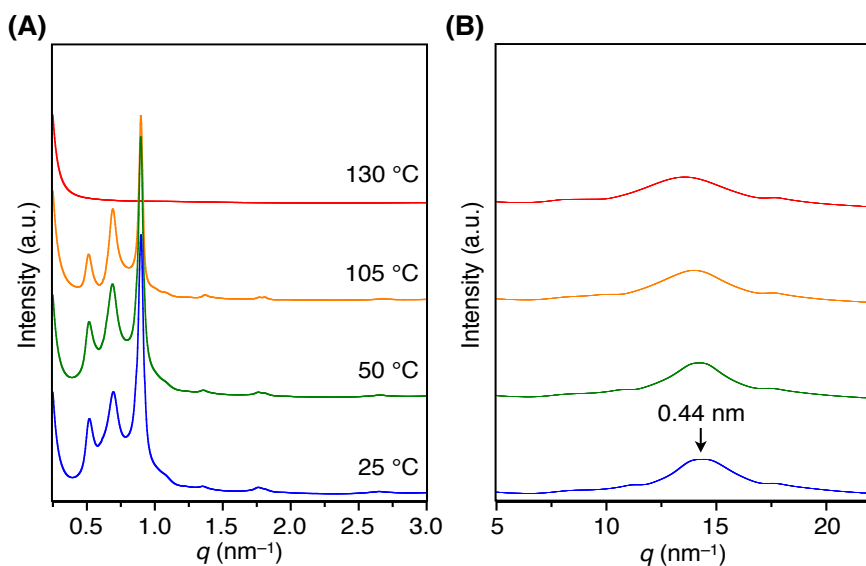
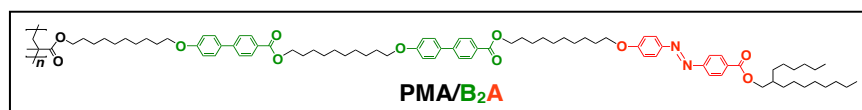


Figure S2 | (A) SAXS and (B) WAXD patterns of a bulk sample of PMA/B₂A at different temperatures on cooling from its isotropic melt in a glass capillary ($\phi = 1.5$ mm).

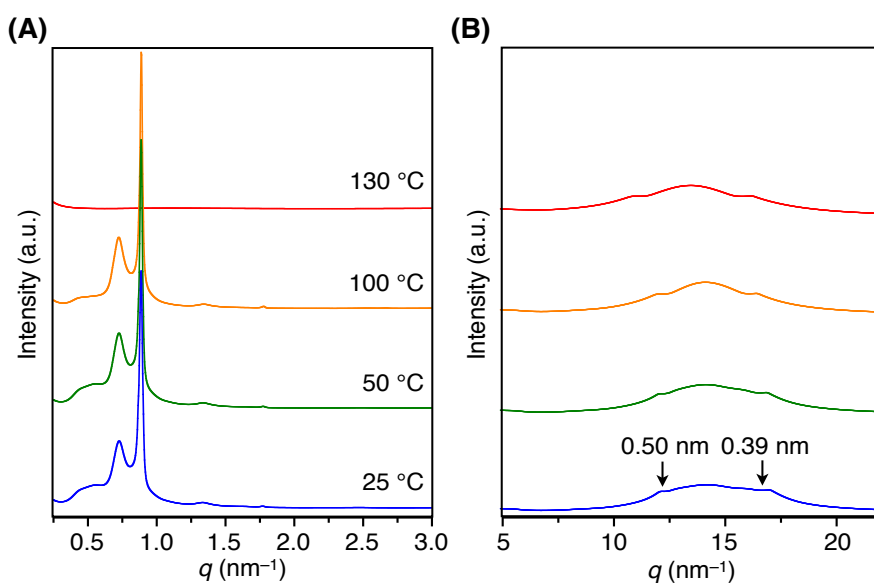


Figure S3 | (A) SAXS and (B) WAXD patterns of a bulk sample of PMA/BA₂ at different temperatures on cooling from its isotropic melt in a glass capillary ($\phi = 1.5$ mm).

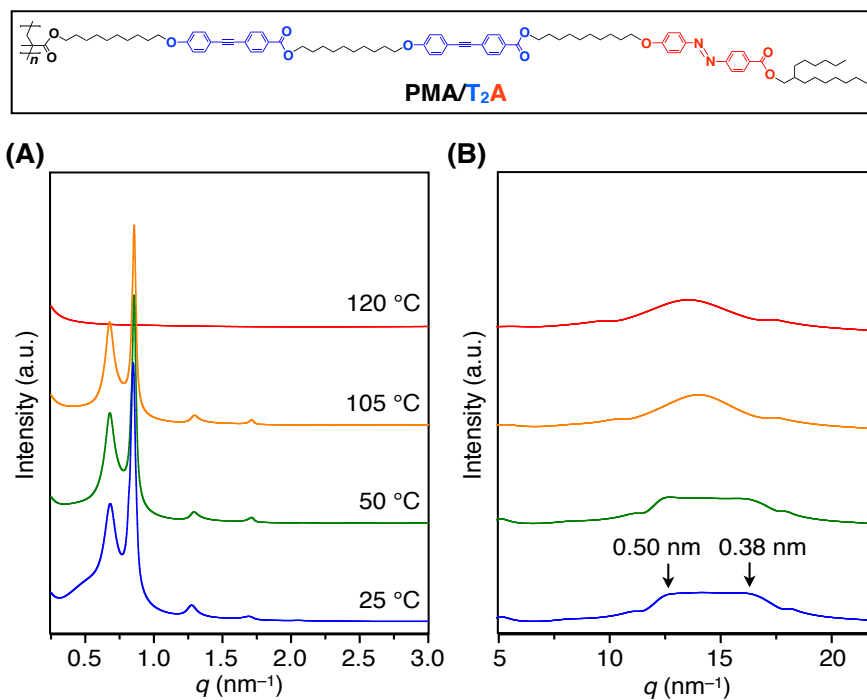


Figure S4 | (A) SAXS and (B) WAXD patterns of a bulk sample of PMA/T₂A at different temperatures on cooling from its isotropic melt in a glass capillary ($\phi = 1.5$ mm).

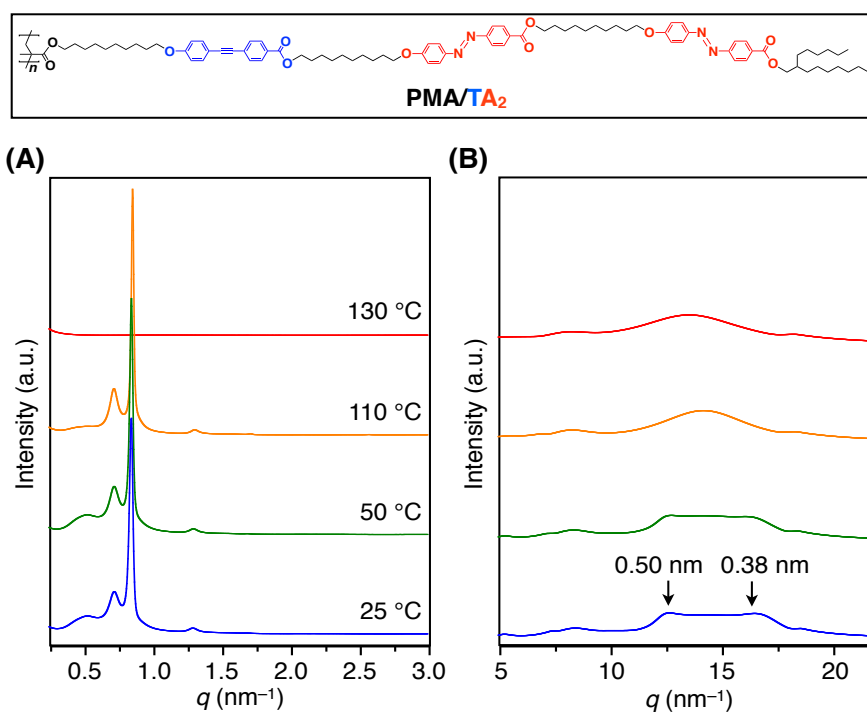


Figure S5 | (A) SAXS and (B) WAXD patterns of a bulk sample of PMA/TA₂ at different temperatures on cooling from its isotropic melt in a glass capillary ($\phi = 1.5$ mm).

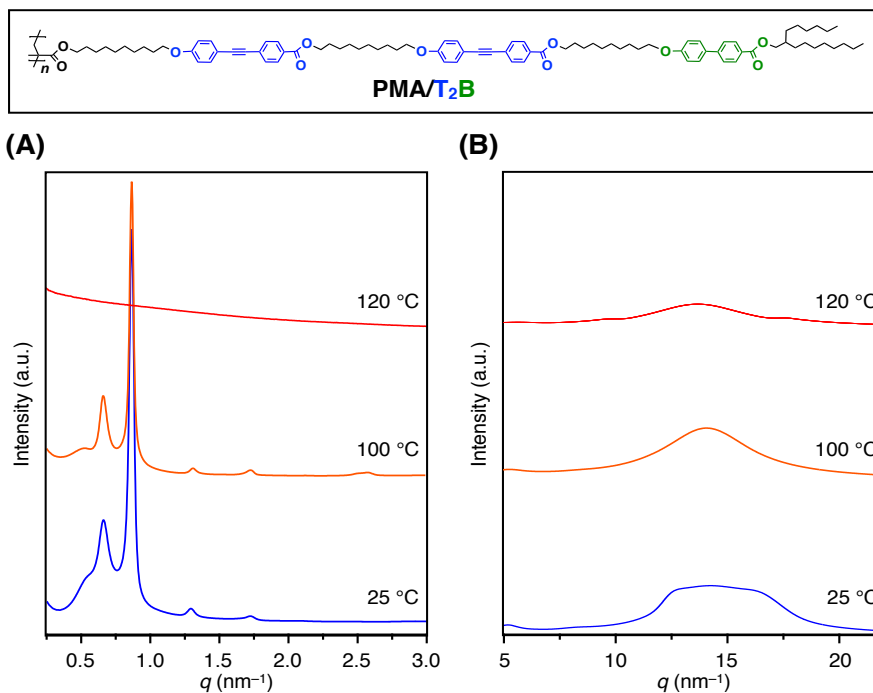


Figure S6 | (A) SAXS and (B) WAXD patterns of a bulk sample of PMA/T₂B at different temperatures on cooling from its isotropic melt in a glass capillary ($\phi = 1.5$ mm).

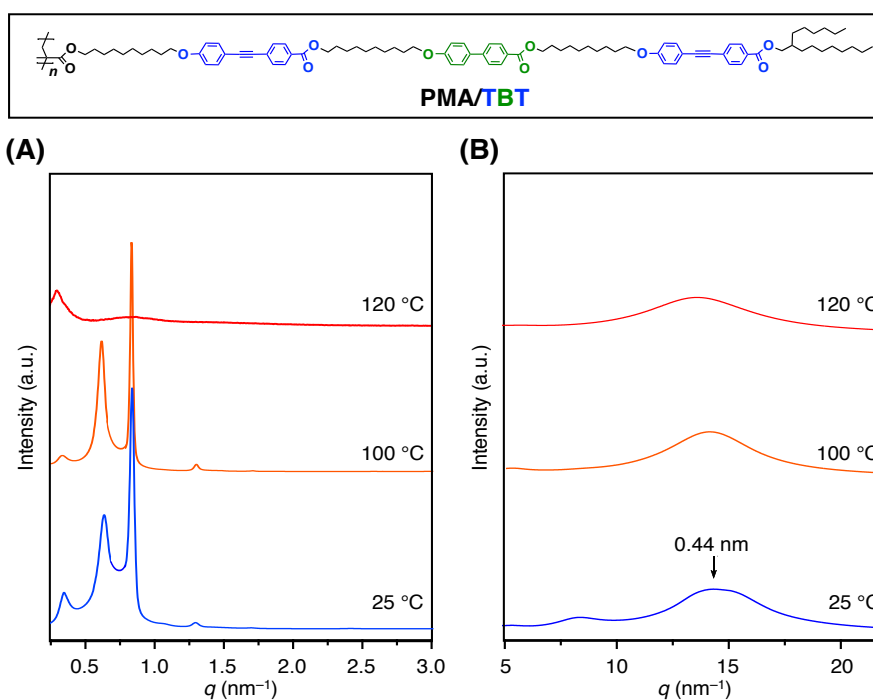


Figure S7 | (A) SAXS and (B) WAXD patterns of a bulk sample of PMA/TBT at different temperatures on cooling from its isotropic melt in a glass capillary ($\phi = 1.5$ mm).

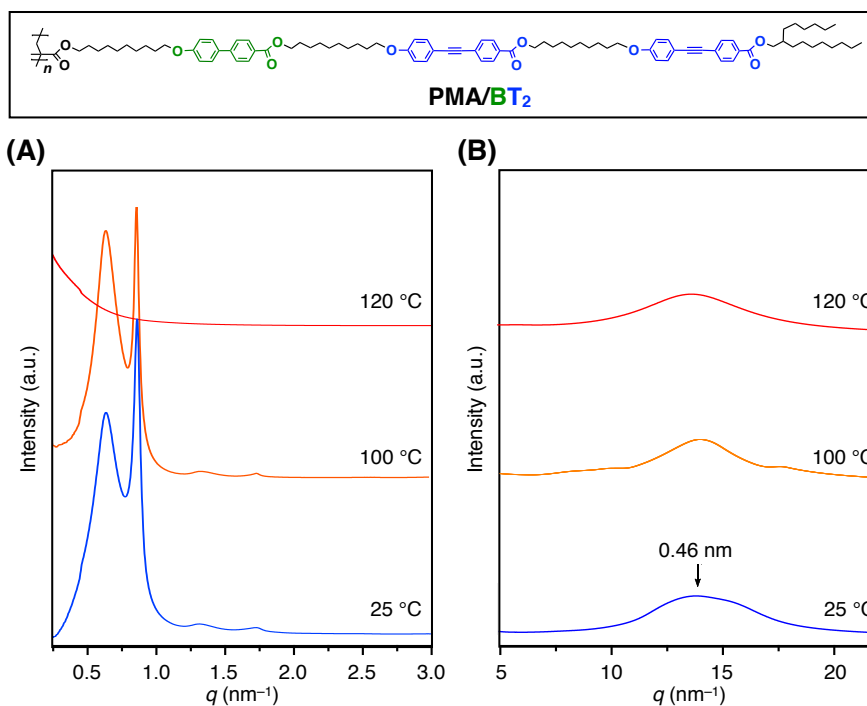


Figure S8 | (A) SAXS and (B) WAXD patterns of a bulk sample of PMA/BT₂ at different temperatures on cooling from its isotropic melt in a glass capillary ($\phi = 1.5$ mm).

3.4.3.3. 2D SAXS Results

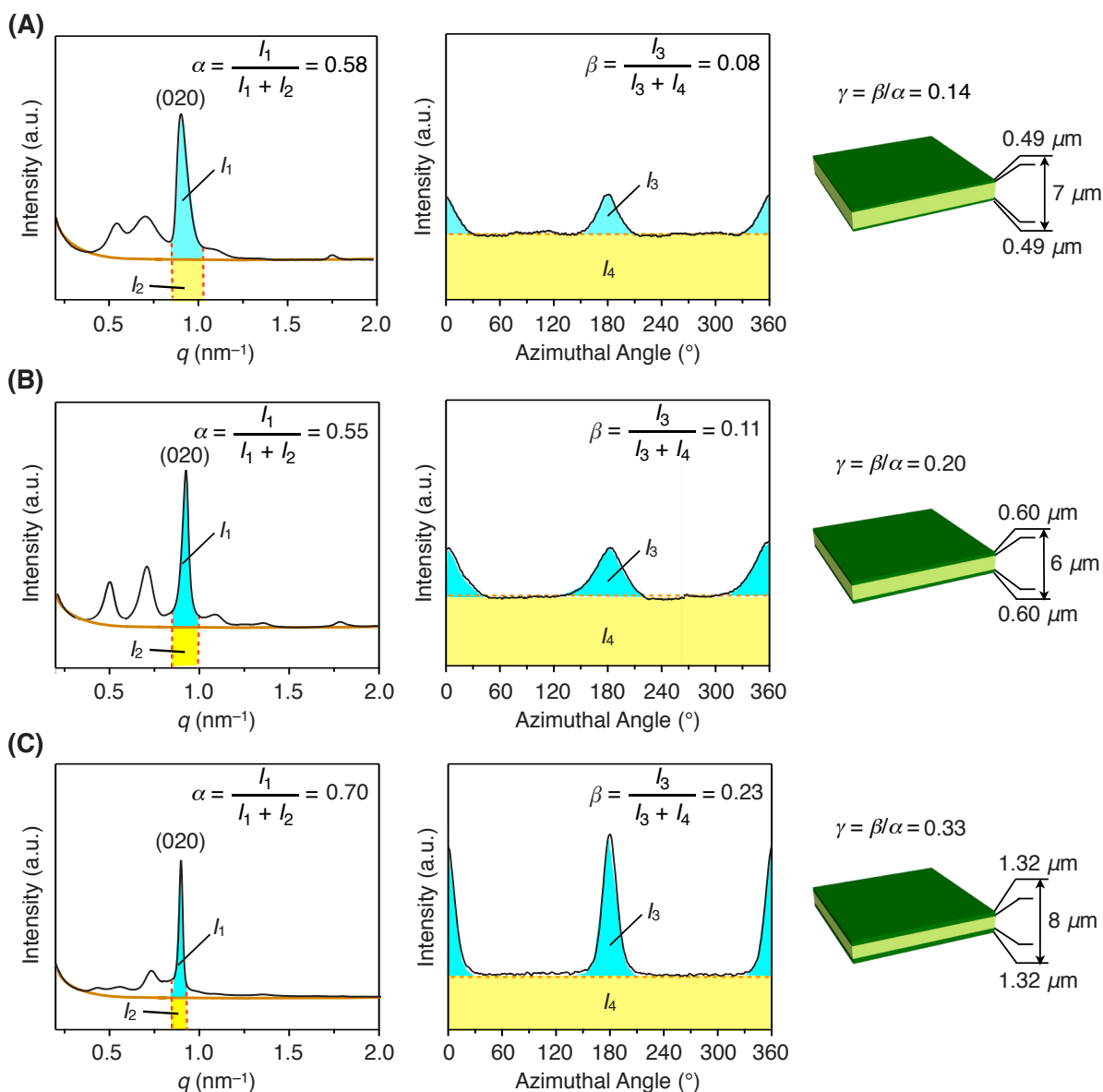


Figure S9 | Quantification of SAXS data for evaluating the degrees of lattice orientation (γ) of (A) PMA/B₃, (B) PMA/B₂A, and (C) PMA/BA₂ in 7, 6 and 8 μm -thick hot-pressed films, respectively, prepared with parallel-arranged Teflon sheets. Illustrations of the hot-pressed films show analytical data, provided that the degrees of lattice orientation on both sides of the films are identical to one another. The estimation of the degrees of lattice orientation was carried out by a method similar to that reported by Daxer and Fratzl.¹⁹ Thus, the 2D SAXS images were integrated along the Debye–Scherrer ring to obtain scattering intensity profiles as a function of scattering vector q ranging from 0.2 to 2 nm^{-1} (left), where $\alpha [= l_1/(l_1+l_2)$; l_1 and l_2 donate integrals of the blue and yellow parts, respectively] represents contribution of both oriented and non-oriented polymer to the total scattering corresponding to the scattering from the (020) plane. Then, the scattering intensities were plotted against azimuthal angle θ (right), where $\beta [= l_3/(l_3+l_4)$; l_3 and l_4 donate integrals of the blue and yellow parts, respectively] represents contribution of oriented polymer alone to the total scattering. The degree of lattice orientation is defined as $\gamma = \beta/\alpha$. If all polymer molecules are randomly oriented in the film, γ should be zero. On the other hand, if all of them align unidirectionally, γ should be unity.

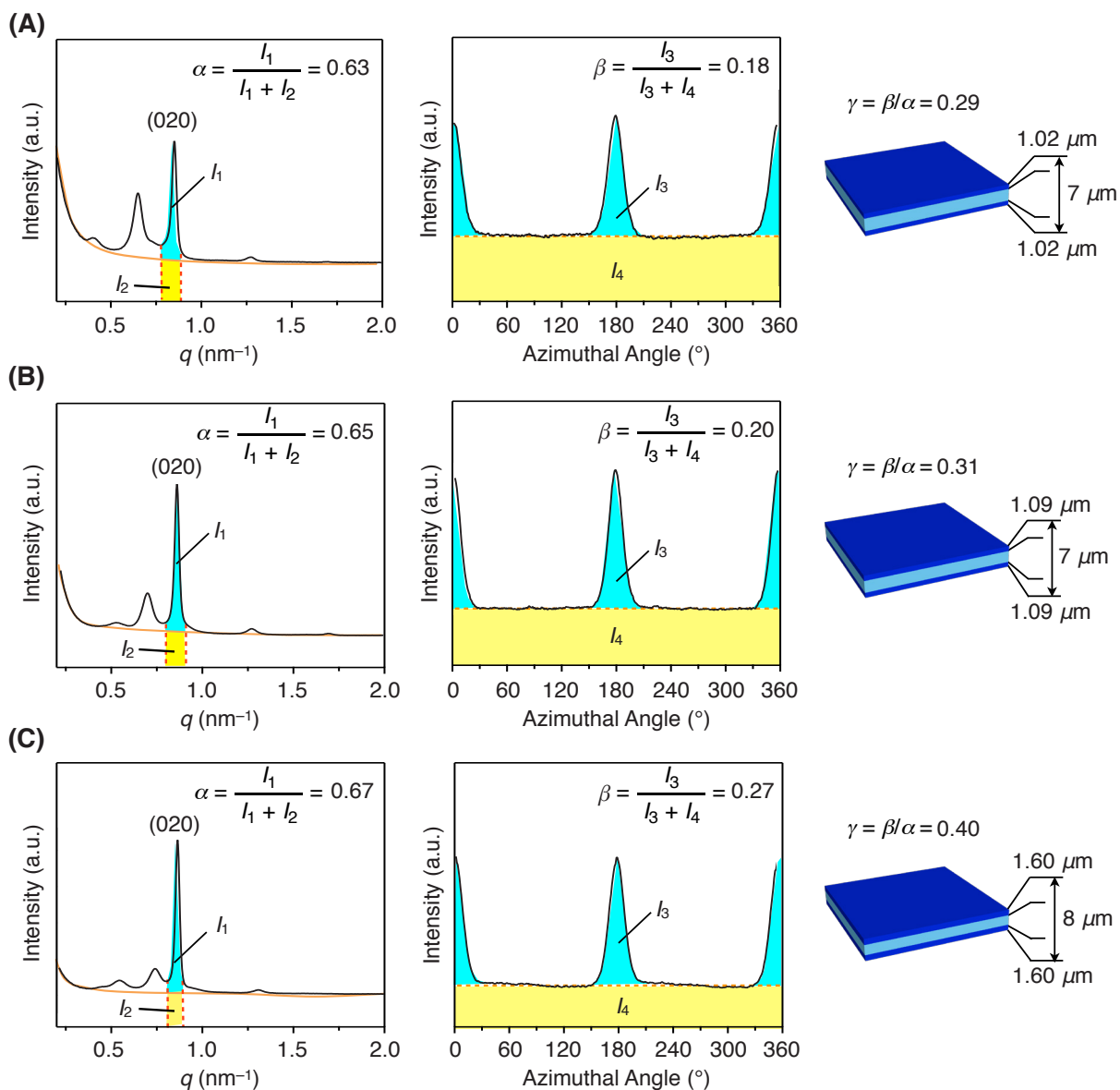


Figure S10 | Quantification of SAXS data for evaluating the degrees of lattice orientation (γ) of (A) PMA/ T_3 , (B) PMA/ T_2A , and (C) PMA/ TA_2 in 7, 7 and 8 μm -thick hot-pressed films, respectively, prepared with parallel-arranged Teflon sheets. Illustrations of the hot-pressed films show analytical data, provided that the degrees of lattice orientation on both sides of the films are identical to one another. The estimation of the degrees of lattice orientation was carried out by a method similar to that reported by Daxer and Fratzl.¹⁹ Thus, the 2D SAXS images were integrated along the Debye–Scherrer ring to obtain scattering intensity profiles as a function of scattering vector q ranging from 0.2 to 2 nm^{-1} (left), where $\alpha = [l_1/(l_1+l_2)]$; l_1 and l_2 donate integrals of the blue and yellow parts, respectively] represents contribution of both oriented and non-oriented polymer to the total scattering corresponding to the scattering from the (020) plane. Then, the scattering intensities were plotted against azimuthal angle θ (right), where $\beta = [l_3/(l_3+l_4)]$; l_3 and l_4 donate integrals of the blue and yellow parts, respectively] represents contribution of oriented polymer alone to the total scattering. The degree of lattice orientation is defined as $\gamma = \beta/\alpha$. If all polymer molecules are randomly oriented in the film, γ should be zero. On the other hand, if all of them align unidirectionally, γ should be unity.

[19] A. Daxer, P. Fratzl. *Invest. Ophthalmol. Vis. Sci.* **38**, 121 (1997).

3.4.3.4 Polarized Fluorescence Spectra

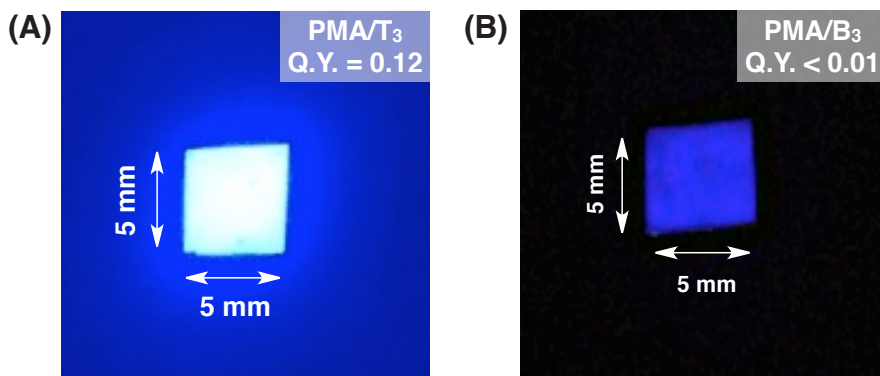


Figure S11 | Photographs of hot-pressed films (5 mm × 5 mm) of (A) PMA/T₃ and (B) PMA/B₃ irradiated by UV light (365 nm). The fluorescence quantum yield of hot-pressed PMA/T₃ film was 0.12, while that of hot-pressed PMA/B₃ film was only less than 0.01.

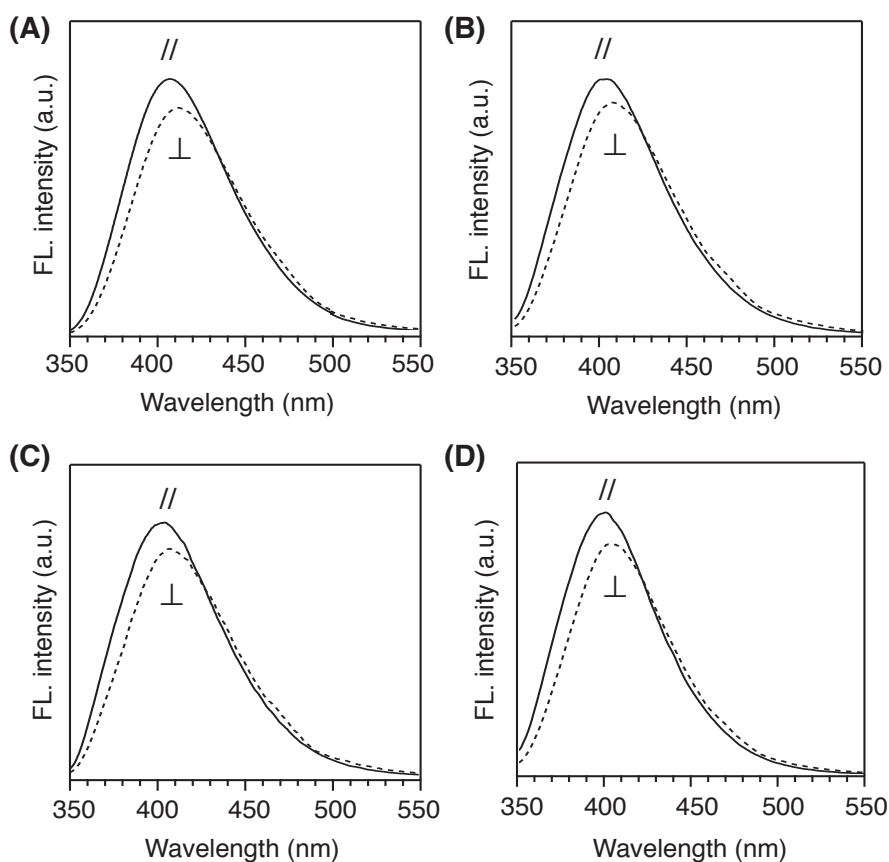


Figure S12 | Polarized emission spectra of (A) PMA/T₃, (B) PMA/BT₂, (C) PMA/T₂B, and (D) PMA/T₃B in CHCl₃ (0.1 g/L). The excitation polarizer is parallel (//) and perpendicular (⊥) to the emission polarizer, respectively.

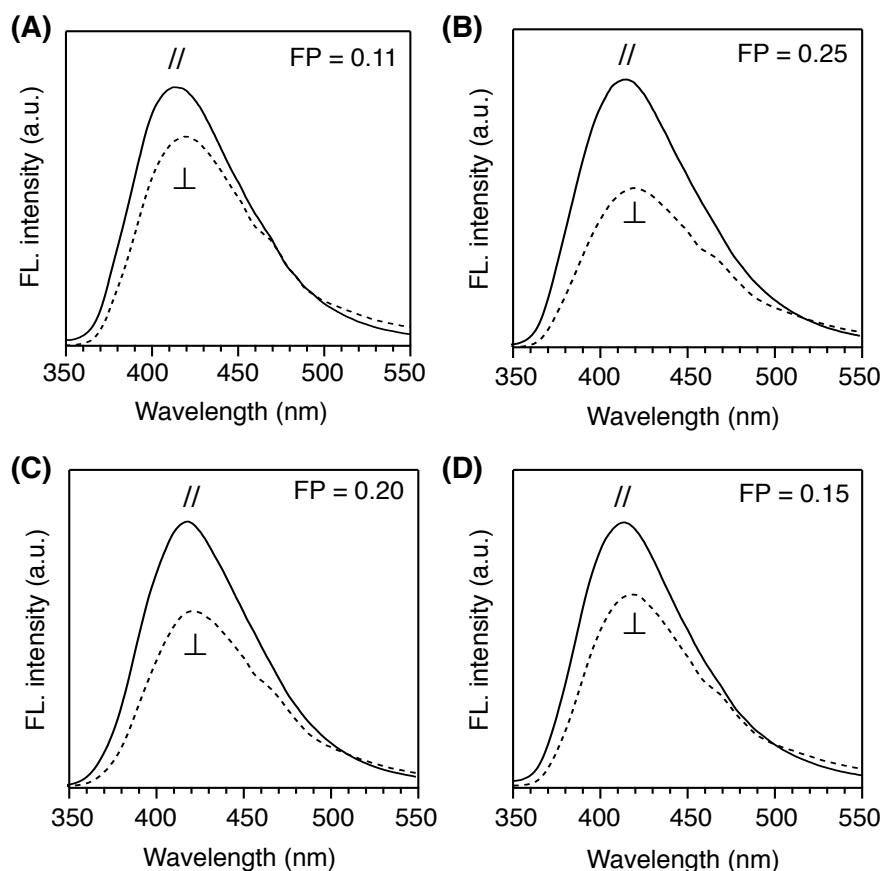


Figure S13 | Polarized emission spectra of hot-pressed films of (A) PMA/T₂T₁, (B) PMA/BT₂, (C) PMA/TBT, and (D) PMAT₂B under the reflection mode. When the polarizing direction of the excitation light is parallel to the surface grooves on the Teflon sheets, the excitation polarizer is parallel (//) and perpendicular (⊥) to the emission polarizer, respectively. Fluorescence polarization (FP) was computed by the formula $FP = (I_{//} - I_{\perp}) / (I_{//} + I_{\perp})$, where $I_{//}$ and I_{\perp} are the fluorescence intensities in the polarized emission spectra.

3.4.4. Supporting Tables

Table S1 | Polymerization Results of Macromonomers.

Polymer	Yield (%)	$M_n \times 10^{-4}^a$	M_w/M_n^a	DP^a
PMA/BA ₂	89	8.0	3.2	57
PMA/B ₂ A	87	7.7	2.9	55
PMA/TA ₂	75	6.2	2.2	45
PMA/T ₂ A	85	7.9	3.3	55
PMA/T ₂ B	80	8.4	2.3	58
PMA/TBT	67	6.5	2.0	45
PMA/BT ₂	91	11.0	3.3	76

^a Determined by SEC (polystyrene standards) with CHCl₃ as an eluent.

Table S2 | Phase Transition Temperatures (T) and Enthalpy Changes (ΔH) of Polymers.

Polymer	Phase Sequence (Space Group) ^a		T (°C)		ΔH (J g ⁻¹)
			heat	cool	heat/cool
PMA/B ₂ A	S ($P2_1/a$)	/ M ($P2_1/a$)	108	/ 104	– / –
	M ($P2_1/a$)	/ Iso	112	/ 107	18.2 / 20.2
PMA/BA ₂	S ($P2_1/a$)	/ M ($P2_1/a$)	98	/ 97	2.4 / 2.0
	M ($P2_1/a$)	/ Iso	118	/ 115	16.0 / 16.4
PMA/T ₂ A	S ($C2/m$)	/ M ($C2/m$)	97	/ 94	5.2 / 4.8
	M ($C2/m$)	/ Iso	113	/ 110	14.5 / 15.4
PMA/TA ₂	S ($P2_1/a$)	/ M ($P2_1/a$)	103	/ 100	5.6 / 5.0
	M ($P2_1/a$)	/ Iso	120	/ 117	15.2 / 16.5
PMA/T ₂ B	S ($C2/m$)	/ M ($C2/m$)	88	/ 86	3.0 / 2.7
	M ($C2/m$)	/ Iso	105	/ 101	11.9 / 12.7
PMA/BTB	S ($C2/m$)	/ M ($C2/m$)	89	/ 88	1.8 / 1.7
	M ($C2/m$)	/ Iso	106	/ 103	13.4 / 13.5
PMA/BT ₂	S ($C2/m$)	/ M ($C2/m$)	93	/ 92	1.7 / 1.4
	M ($C2/m$)	/ Iso	108	/ 103	14.4 / 14.7

^a S: solid, M: mesophase, Iso: isotropic melt, $P2_1/a$, $C2/m$: rectangular lattice

Table S3 | SAXS Data of a Bulk Sample of PMA/B₂A.

Temp. (°C)	q (nm ⁻¹)	$d_{\text{obs.}}$ (nm)	$d_{\text{calc.}}$ (nm)	hkl	Temp. (°C)	q (nm ⁻¹)	$d_{\text{obs.}}$ (nm)	$d_{\text{calc.}}$ (nm)	hkl
25	0.520	12.09	11.96	110	105	0.503	12.01	11.84	110
(P2 ₁ /a) ^a	0.695	9.04	8.78	210	(P2 ₁ /a) ^a	0.712	8.82	8.84	210
	0.899	6.99	7.07	020		0.919	6.84	6.90	020
	1.083	5.80	5.60	400		1.091	5.75	5.75	400
	1.231	5.10	5.13	320		1.251	5.02	5.13	320
	1.350	4.65	4.61	130		1.390	4.52	4.51	130
	1.760	3.57	3.61	430		1.789	3.51	3.59	430
	1.814	3.46	3.53	040		1.828	3.44	3.45	040
	1.978	3.17	3.19	340		1.992	3.15	3.15	340
	2.650	2.37	2.36	060		2.134	2.94	2.96	440
						2.250	2.79	2.74	150
				2.692	2.33	2.30	060		

^a $P2_1/a$ rectangular lattice parameters $a = 22.4$ and $b = 14.1$ nm at 25 °C and $a = 23.0$ and $b = 13.8$ nm at 105 °C.

Table S4 | SAXS Data of a Bulk Sample of PMA/BA₂.

Temp. (°C)	q (nm ⁻¹)	$d_{\text{obs.}}$ (nm)	$d_{\text{calc.}}$ (nm)	hkl	Temp. (°C)	q (nm ⁻¹)	$d_{\text{obs.}}$ (nm)	$d_{\text{calc.}}$ (nm)	hkl
25	0.549	11.44	11.83	110	100	0.540	11.65	11.72	110
(P2 ₁ /a) ^a	0.726	8.65	8.52	210	(P2 ₁ /a) ^a	0.723	8.68	8.73	210
	0.887	7.08	7.12	020		0.887	7.08	7.09	020
	1.334	4.71	4.63	130		1.342	4.68	4.62	130
	1.648	3.81	3.94	330		1.659	3.79	3.91	330
	1.770	3.55	3.56	040		1.778	3.53	3.54	040
	2.481	2.53	2.51	450		2.174	2.89	2.81	150
	2.653	2.37	2.37	060		2.525	2.49	2.53	450
						2.667	2.35	2.36	060

^a P2₁/a rectangular lattice parameters $a = 21.2$ and $b = 14.3$ nm at 25 °C and $a = 22.2$ and $b = 14.2$ nm at 100 °C.

Table S5 | SAXS Data of a Bulk Sample of PMA/T₂A.

Temp. (°C)	q (nm ⁻¹)	$d_{\text{obs.}}$ (nm)	$d_{\text{calc.}}$ (nm)	hkl	Temp. (°C)	q (nm ⁻¹)	$d_{\text{obs.}}$ (nm)	$d_{\text{calc.}}$ (nm)	hkl
25	0.682	9.22	9.23	110	105	0.679	9.25	9.23	110
(C2/m) ^a	0.849	7.40	7.44	020	(C2/m) ^a	0.855	7.35	7.32	020
	1.326	4.74	4.61	220		1.312	4.63	4.61	220
	1.691	3.72	3.72	040		1.713	3.67	3.66	040
	2.051	3.06	3.08	330		2.087	3.01	3.07	330
						2.569	2.44	2.44	060

^a C2/m rectangular lattice parameters $a = 11.8$ and $b = 14.9$ nm at 25 °C and $a = 11.9$ and $b = 14.7$ nm at 105 °C.

Table S6 | SAXS Data of a Bulk Sample of PMA/TA₂.

Temp. (°C)	q (nm ⁻¹)	$d_{\text{obs.}}$ (nm)	$d_{\text{calc.}}$ (nm)	hkl	Temp. (°C)	q (nm ⁻¹)	$d_{\text{obs.}}$ (nm)	$d_{\text{calc.}}$ (nm)	hkl
25	0.519	12.10	12.46	110	110	0.522	12.02	12.07	110
(P2 ₁ /a) ^a	0.723	8.69	8.84	210	(P2 ₁ /a) ^a	0.720	8.72	8.75	210
	0.848	7.41	7.61	020		0.857	7.33	7.33	020
	1.295	4.85	4.94	130		1.309	4.80	4.77	130
	1.548	4.06	4.15	330		1.587	3.96	4.06	330
	1.687	3.73	3.80	040		1.714	3.66	3.67	040
	2.064	3.04	3.01	150		2.086	3.01	2.95	150
	2.353	2.67	2.65	450		2.431	2.58	2.58	450
						2.575	2.44	2.44	060

^a P2₁/a rectangular lattice parameters $a = 21.7$ and $b = 15.2$ nm at 25 °C and $a = 21.8$ and $b = 14.7$ nm at 110 °C.

Table S7 | SAXS Data of a Bulk Sample of PMA/T₂B.

Temp. (°C)	q (nm ⁻¹)	$d_{\text{obs.}}$ (nm)	$d_{\text{calc.}}$ (nm)	hkl	Temp. (°C)	q (nm ⁻¹)	$d_{\text{obs.}}$ (nm)	$d_{\text{calc.}}$ (nm)	hkl
25	0.659	9.53	9.63	110	100	0.662	9.49	9.53	110
(C2/m) ^a	0.864	7.27	7.29	020	(C2/m) ^a	0.868	7.24	7.25	020
	1.291	4.86	4.82	220		1.313	4.78	4.77	220
	1.721	3.65	3.64	040		1.730	3.63	3.63	040
	2.089	3.01	3.21	330		2.132	2.95	3.18	330
						2.528	2.48	2.42	060

^a C2/m rectangular lattice parameters $a = 12.8$ and $b = 14.6$ nm at 25 °C and $a = 12.6$ and $b = 14.5$ nm at 100 °C.

Table S8 | SAXS Data of a Bulk Sample of PMA/TBT.

Temp. (°C)	q (nm ⁻¹)	$d_{\text{obs.}}$ (nm)	$d_{\text{calc.}}$ (nm)	hkl	Temp. (°C)	q (nm ⁻¹)	$d_{\text{obs.}}$ (nm)	$d_{\text{calc.}}$ (nm)	hkl
25	0.653	9.62	9.63	110	100	0.646	9.72	9.62	110
(C2/m) ^a	0.852	7.35	7.38	020	(C2/m) ^a	0.858	7.32	7.31	020
	1.304	4.82	4.82	220		1.319	4.76	4.81	220
	1.699	3.70	3.69	040		1.721	3.65	3.66	040

^a C2/m rectangular lattice parameters $a = 12.7$ and $b = 14.8$ nm at 25 °C and $a = 12.8$ and $b = 14.6$ nm at 100 °C.

Table S9 | SAXS Data of a Bulk Sample of PMA/BT₂.

Temp. (°C)	q (nm ⁻¹)	$d_{\text{obs.}}$ (nm)	$d_{\text{calc.}}$ (nm)	hkl	Temp. (°C)	q (nm ⁻¹)	$d_{\text{obs.}}$ (nm)	$d_{\text{calc.}}$ (nm)	hkl
25	0.649	9.68	9.59	110	100	0.649	9.68	9.54	110
(C2/m) ^a	0.874	7.19	7.22	020	(C2/m) ^a	0.874	7.19	7.20	020
	1.322	4.75	4.80	220		1.335	4.70	4.77	220
	1.737	3.65	3.61	040		1.746	3.60	3.60	040
	1.963	3.20	3.20	330		1.960	3.20	3.18	330
						2.622	2.40	2.40	060

^a C2/m rectangular lattice parameters $a = 12.9$ and $b = 14.4$ nm at 25 °C and $a = 12.7$ and $b = 14.4$ nm at 100 °C.

Chapter

4

Solid-state Self-replication Of
Phthalocyanines Driven By
Supramolecular Polymerization

To exploit a self-replicating supramolecular system for the construction, selection, and amplification of large molecular and assemblies is a big challenge. Here, we proposed a supramolecular polymerization process enabled to accurately control the solid-state self-replication of phthalocyanines featuring with a high yield and selectivity.

4.1 Introduction

The talent to self-replicate is so essential for the evolution of a living organism, yet the underlying mechanism of self-replication during the origin of life remains an unanswered question to biochemists (1–3). The recent experimental approaches on this issue have largely focused on the controllable autocatalysis systems, in which molecules enable to catalyze its own formation from many precursors (4). The successful autocatalytic examples include the biomacromolecules, such as DNA (5,6), RNA (7) and peptides (8,9), and some organic small molecules (10–13). However, these relatively simple chemical systems are far from the complex self-organization exhibited by living organisms. To exploit self-replicating systems in construction, selection and amplification at the supramolecular level is still a big challenge. Until now, the only case of self-replicating supramolecular system is constructed by Otto group, demonstrating that two self-replicating peptide-derived macrocycles were capable of promoting their own formation driven by assembly of supramolecular fibers and showed selectivity to

- [1] L. E. Orgel. *Nature* **358**, 203 (1992).
- [2] L. E. Orgel. *Acc. Chem. Res.* **28**, 109 (1995).
- [3] E. Szathmary, J. M. Smith. *J. Theor. Biol.* **187**, 555 (1997).
- [4] S. N. Semenov. *Nature* **537**, 656 (2016).
- [5] G. von. Kiedrowski. *Angew. Chem. Int. Engl.* **25**, 932 (1986).
- [6] G. von. Kiedrowski *et al.* *Angew. Chem. Int. Engl.* **30**, 423 (1991).
- [7] N. Paul, G. F. Joyce. *Proc. Natl. Acad. Sci.* **99**, 12733 (2002).
- [8] D. H. Lee *et al.* *Nature* **382**, 525 (1996).
- [9] S. Yao *et al.* *J. Am. Chem. Soc.* **119**, 10559 (1997).
- [10] T. Tjivikua, P. Ballester, J. Rebek. *J. Am. Chem. Soc.* **112**, 1249 (1990).

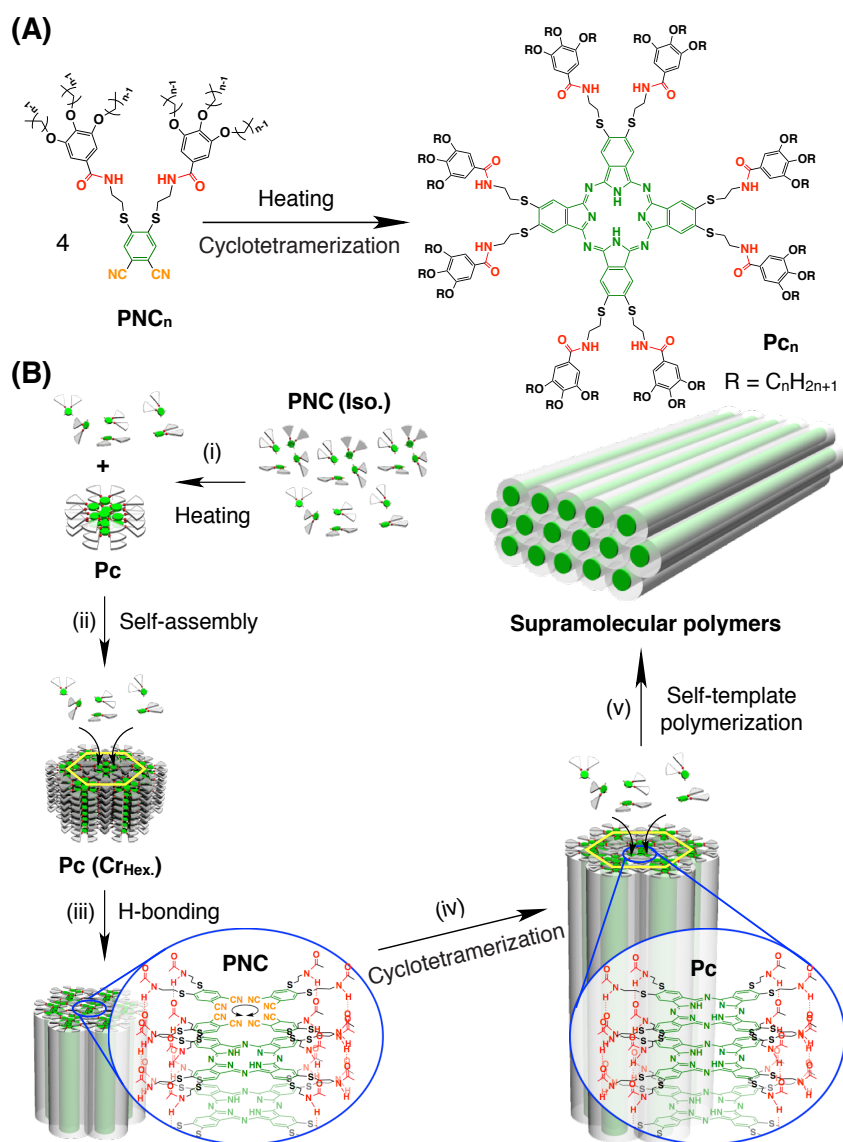


Figure 1 | Self-replicating supramolecular polymerization. (A) Cyclotetramerization reaction of 4,5-dithiophthalonitrile derivatives (PNC_n) autocatalyzed to form metal-free phthalocyanines (Pc) upon heating. (B), schematic illustrations of solid-state self-replication of phthalocyanines in conjugation with a supramolecular polymerization. (i) Upon heating, tiny Pc were formed initially by the isotropic PNC and self-assembled into a columnar crystal nucleus with a 2D hexagonal geometry (ii). (iii) The rest PNC preferred to paste on the template Pc molecules on the cross-section surface of columnar nucleus through the H-bonding interactions of amide groups and spontaneously cyclized to form a macrocyclic Pc in a molecular distance (iv). (v) When self-replicating polymerization kept rolling, PNC self-assembled into a crystalline fiber composed of highly pure Pc .

[11] V. Rotello, J. Hong, J. Rebek. *J. Am. Chem. Soc.* **113**, 9422 (1999).

[12] A. Terfort, G. von Kiedrowski. *Angew. Chem. Int. Engl.* **31**, 654 (1992).

[13] E. Kassianidis, D. Philp. *Angew. Chem. Int. Ed.* **45**, 6344 (2006).

[14] J. M. Carnall. *Science* **327**, 1502 (2010).

[15] A. Pal *et al.* *Angew. Chem. Int. Ed.* **54**, 7852 (2015).

[16] J. W. Sadownik *et al.* *Nature Chem.* **8**, 264 (2016).

mechanical stimulation (14–16).

In this chapter, I show that a novel self-replicating supramolecular polymerization process accurately controls the autocatalytic cyclotetramerization of 4,5-dithiophthalonitrile derivatives (**PNC_n**, Figure. 1A) to convert metal-free phthalocyanines (**Pc_n**, Figure. 1A) featuring a high yield (> 80%) and selectivity. In general, it is necessary to add the base or metal catalysts with phthalonitriles to produce phthalocyanines (17–19). In our system, however, no additional catalysts were doped but only heating was necessary. Upon heating at suitable temperature to keep **PNC** as an isotropic state but its corresponding **Pc** as a solid state, tiny **Pc** were formed initially but self-assembled to a columnar crystal nucleus with a 2D hexagonal geometry (Figure. 1B, i and ii). Due to the H-bonding interactions of amide groups, the rest **PNC** preferred to paste on the template **Pc** molecules on the cross-section surface of columnar nucleus and autocatalyzed to form a new macrocyclic **Pc** within a molecular distance (Figure. 1B, iii and iv). When such “template pasting and then cyclotetramerization” process kept rolling repeatedly, **PNC** were supramolecularly polymerized to assemble the crystalline fibers consisting of highly pure **Pc** in one step (Figure. 1B, v). Our finding not only presents a new synthetic methodology towards a high yield and selectivity, but also provides a one-pot strategy to design self-synthesizing materials.

[17] M. Mayukh *et al.* *J. Org. Chem.* **75**, 7893 (2010).

[18] T. Kimura *et al.* *J. Org. Chem.* **69**, 4716 (2004).

[19] J. Leclaires *et al.* *J. Am. Chem. Soc.* **127**, 15762 (2005).

4.2. Results and Discussion

4.2.1. Crystalline Fibers Formed by **Pc₄**

Previously, a 4,5-dithiophthalonitrile derivative, carrying three dodecyl chains by the amide groups (**PNC₁₂**, Figure. 1A), was elaborately designed to develop a novel ferroelectric liquid crystalline system (20,21). By mistake, I accidentally found that the color of liquid crystal cell filled with **PNC₁₂** turned to green after heating at its isotropic state for overnight (Figure. S1), probably suggesting

[20] D. Miyajima *et al.* *J. Am. Chem. Soc.* **132**, 8530 (2010).

[21] D. Miyajima *et al.* *Science* **336**, 209 (2012).

the present of phthalocyanines. Such serendipity pushed me to explore the underlying reasons. For this purpose, other phthalonitrile derivatives, PNC_n ($n = 2 \sim 6$), with the different lengths of side chains were synthesized following reported strategy (Scheme. S1) (20). Meanwhile, their corresponding metal-free phthalocyanine Pc_n were also prepared as a standard sample by refluxing the PNC_n with 1,8-Diazabicyclo[5.4.0]undec-7-ene (DBU) as catalyst in 1-pentanol to afford a poorly soluble dark-green powder with a low yield (Scheme. S2) (19).

Of a particular case, PNC_4 carrying the short *n*-butane chains (Figure. 1B), exhibited an anomalous assembling behavior at its isotropic state. At 175 °C, the PNC_4 melt permeated into the glass cell with a thickness of 5 μm through capillary action and then was kept at 160 °C for overnight (see Supporting Method). Interestingly, many green crystalline fibers were formed as radial pattern and crossly distributed in whole cell observed by optical microscope (OM) (Figure. 2A). These crystalline fibers have a large aspect ratio that their length is generally hundreds of micrometers while the width is less than 10 μm . In polarized optical microscope (POM) image (Figure. 2B), these fibers showed a characteristic birefringence of crystals, suggesting the present of ordered structure.

In order to figure out the compositions of these crystalline fibers, I peeled off the cell and washed them by methanol three times. Then, the green fibers were left, since methanol is a poor solvent for the fibrous structures (Figure. S2). Matrix-assisted laser desorption ionization time-of-flight (MALDI-TOF) mass spectrometry is one of most immediate methods to confirm the components in mixtures by analyzing the molecular weight. Figure. 2C presents the mass spectra of crystalline fibers before and after washing with methanol. In the mass spectrum before washing, several molecule-ionic peaks were detected, the strongest of which at 3678.88 is precisely agreed with the molecular weight of Pc_4 (Calcd. for $\text{C}_{200}\text{H}_{285}\text{N}_{16}\text{O}_{32}\text{S}_8$ $[\text{M}+\text{H}]^+$: $m/z = 3678.90$). Through a simple purification by washing, only target peak of Pc_4 was observed, clearly indicating that the fibers are mono-composed of highly pure Pc_4 . Infrared (IR) spectroscopy of the washed crystalline fibers also confirmed that no PNC_4 or the intermediates during its cyclotramerization remained in the fibers (Figure. S3). Figure. 2D gives the UV-visible absorption spectrum of washed crystalline fibers in dilute solution of chloroform. We successfully recognized a splitted absorption band appearing at 700 and 730 nm as the *Q*-band of Pc_4 , which is one of the characteristic absorption bands of melt-free phthalocyanine attributed to the $\text{S}_0 \rightarrow \text{S}_1$ transitions of the 14-electron aromatic ring (22). On the basis of the above results, I believe that PNC_4 spontaneously cyclized and formed the crystalline fibers consisting of highly pure Pc_4 in one step just by

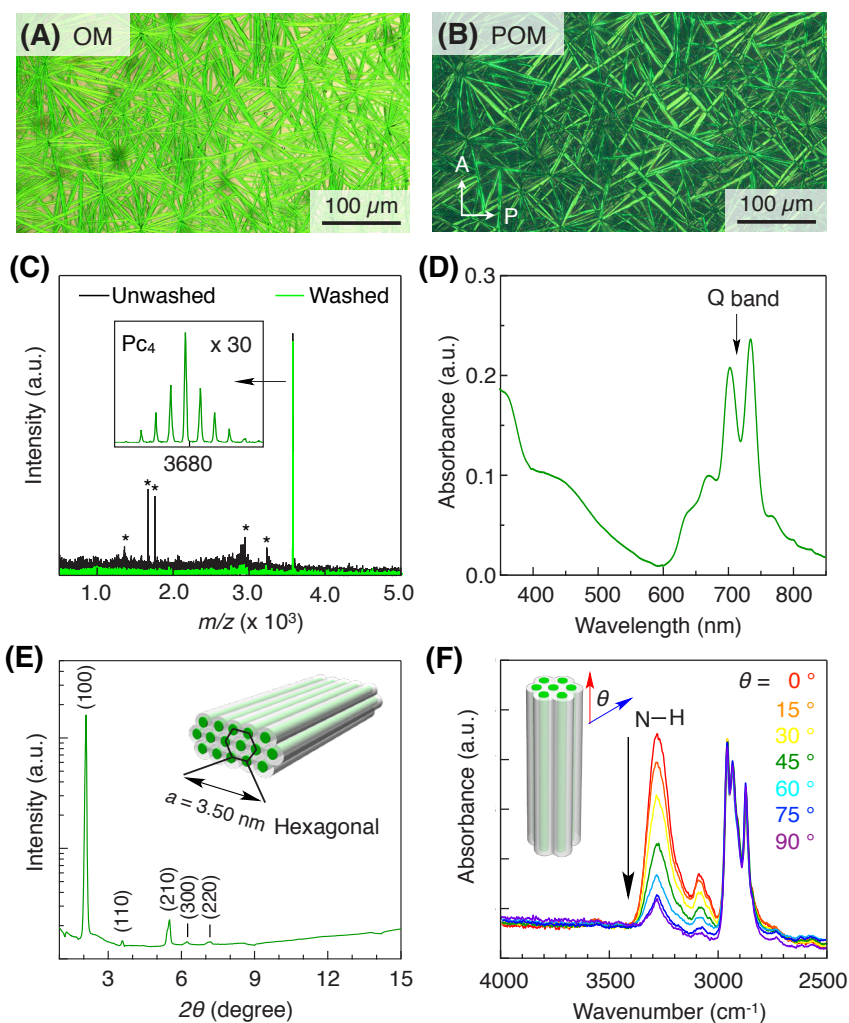


Figure 2 | Characterization of the crystalline fibers formed by heating PNC₄.

(A) OM and (B) POM images of PNC₄ after heating at 160 °C in cells for overnight. White arrows represent the transmission directions of the polarizer (P) and analyzer (A). (C) MALDI-TOF mass spectra of the crystalline fibers prepared at 190 °C before (black line) and after (green line) washing by methanol. The inset is zoomed-in spectrum of the ionic peak. (D) UV-visible absorption spectrum of the washed crystalline fibers in dilute solution of chloroform. (E) XRD patterns of the crystalline fiber at 25 °C (Miller indices in parentheses) and schematic illustrations of its 2D hexagonal packing. (F) Polarized IR spectrum (2500–4000 cm⁻¹) of the parallel oriented fibers at azimuthal angles (θ) from 0° to 90°. The azimuthal angle θ is defined as 0 when the polarizing direction of incident light (blue arrow) is parallel to the long axis of fibers (red arrow).

heating.

The crystalline structure of fibers was evaluated by X-ray diffraction (XRD) and polarized infrared (IR) spectroscopy. In the XRD pattern at small angle (Figure. 2E), the sharp diffraction

peaks were clearly observed, the d -spacing of which were exactly agreed with the $d/d^* = 1 : 1/\sqrt{3} : 1/\sqrt{7} : 1/3 : 1/\sqrt{12}$. This result clearly indicated that the parallel oriented supramolecular polymers of **Pc₄** are closely packed into a 2D hexagonal geometry to form crystalline fibers, which was consistent with the self-assembled structure of bulk sample of **Pc₄** prepared by organic synthesis (Figure. S4). Moreover, polarized IR spectra of the parallel oriented fibers showed a high anisotropy in which the stretching vibration bands attributable to the amide groups (N–H and C=O) displayed a maximum absorbance in the direction parallel (0°) to the long axis of crystalline fibers (Figure. 2F and Figure. S5). Therefore, we speculated that **Pc₄** molecules are cofacially stacking along the long axis of crystalline fibers through the H-bonding interactions of amide groups (Figure. 1B).

4.2.2. Temperature Effect

The heating temperature is one of the crucial parameters to control the crystalline morphology and cyclizing yield of **Pc₄**. Comparing with the morphology of crystalline fibers formed at different temperatures (Figures. 3A–F), I found that only crystal nucleus was observed at 145 °C (Figure. 3A), but once heating up to 150 °C, the fibers were formed (Figure. 3B) and became longer and thicker with the temperature increased (Figure. 3B–F). However, if the temperature was higher than the freezing point of **Pc₄**, for example, 210 °C, no fibers were observed (Figure. S6). Therefore, we claimed that the suitable temperature for supramolecular polymerization to form crystalline fibers of **Pc₄** should be in a range to keep **PNC₄** as an isotropic state but **Pc₄** as a crystalline state (Figure. 3G). The cyclized yield of **Pc₄** at different temperatures were analyzed by size-exclusion chromatography (SEC). In SEC curves of the resultant mixture by heating **PNC₄** at different temperatures (Figure. S7), the peaks corresponding to the resultant **Pc₄**, intermediates, and unreacted **PNC₄** were clearly separated based on their molecular size.

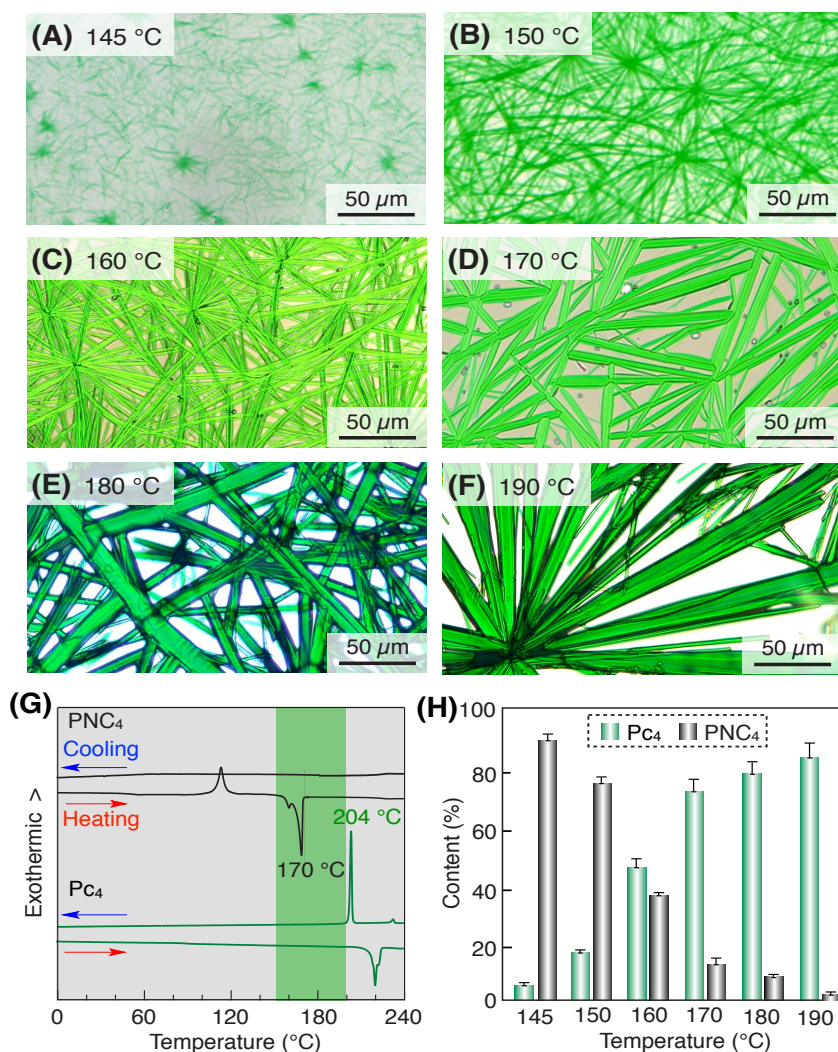


Figure 3 | Temperature effect on the crystalline morphology and cyclized yield of Pc_4 . (A–F) OM images of crystalline morphology of Pc_4 formed at (A) 145, (B) 150, (C) 160, (D) 170, (E) 180, and (F) 190 °C, respectively. (G) DSC traces on second heating/cooling cycles of PNC_4 (black lines) and Pc_4 (green lines). Scan rate is 10 °C /min. Green region represents the temperature range enable to form the crystalline fibers of Pc_4 . (H) %-Contents of Pc_4 and PNC_4 in the resultant mixture by heating PNC_4 at 145, 150, 160, 170, 180, and 190 °C for 24 hours, respectively.

Notably, more PNC_4 were cyclized and converted to Pc_4 with the temperature increased (Figure. 3H). By comparison with the standard SEC curves of PNC_4 and Pc_4 (see Supporting Method and Figure. S8), we quantitatively evaluated the cyclizing yield of Pc_4 , formed by the supramolecular polymerization up to 83% at 190 °C (Figure. 3H), much higher than DBU catalyst strategy (25 %).

4.2.3. Self-replicating Mechanism

Why does **PNC**₄ autocatalytically cyclize to form the crystalline fibers of **Pc**₄ with a high yield? By using a high-definition camera to record heating process of **PNC**₄ at 160 °C (Figures. 4A–D), I clearly observed that only short and thin nucleus were formed in the first few hours, then the nucleus became longer gradually from two ends to assemble a highly anisotropic fiber along with time. Such anisotropic crystalline growth reminds me of the supramolecular polymerization, which has been demonstrated as two steps including nucleation and one-dimensional growth (23–25). In here, I utilized the concept of supramolecular polymerization to demonstrate the self-replicating mechanism of **Pc**₄ (Figure. 1B). Due to molecular collision, it is possible that the isotropic **PNC**₄ were cyclized to form **Pc**₄ at high temperature although the yield was low (Figure. 1B, i). Because the heating temperature was lower than the crystalline temperature of **Pc**₄, the original **Pc**₄ molecules have to self-assemble into a columnar crystal nucleus with the hexagonal geometry (Figure. 1B, ii). Simultaneously, due to the H-bonding interaction with the amide groups of **Pc**₄, four **PNC**₄ preferred to paste onto the template **Pc**₄ at cross-section surface of columnar crystal nucleus, which is extremely promote the occurrence of their cyclotetramerization reaction (Figure. 1B, iii and iv). Although the synthetic mechanism of phthalocyanine is unclear until now, the purpose to add metal catalyst such as CuCl₂ previously may shorten the molecular distance by metal complexation, which is facilitated for the cyclotetramerization reaction of phthalonitrile (26). From this point, H-bonding may play a similar role with metal catalyst. When “template pasting and then cyclotetramerization” process in my system kept rolling repeatedly, **Pc**₄ molecules are efficiently self-replicated to form the crystalline fibers finally (Figure. 1B, v).

[23] T. Aida, E. W. Meijer, S. I. Stupp. *Science* **335**, 813 (2012).

[24] P. A. Korevaar *et al.* *Nature* **481**, 492 (2012).

[25] D. Zhao, J. S. Moore. *Org. Biomol. Chem.* **1**, 3471 (2003).

[26] F. Baumann *et al.* *Angew. Chem.* **68**, 133 (1956).

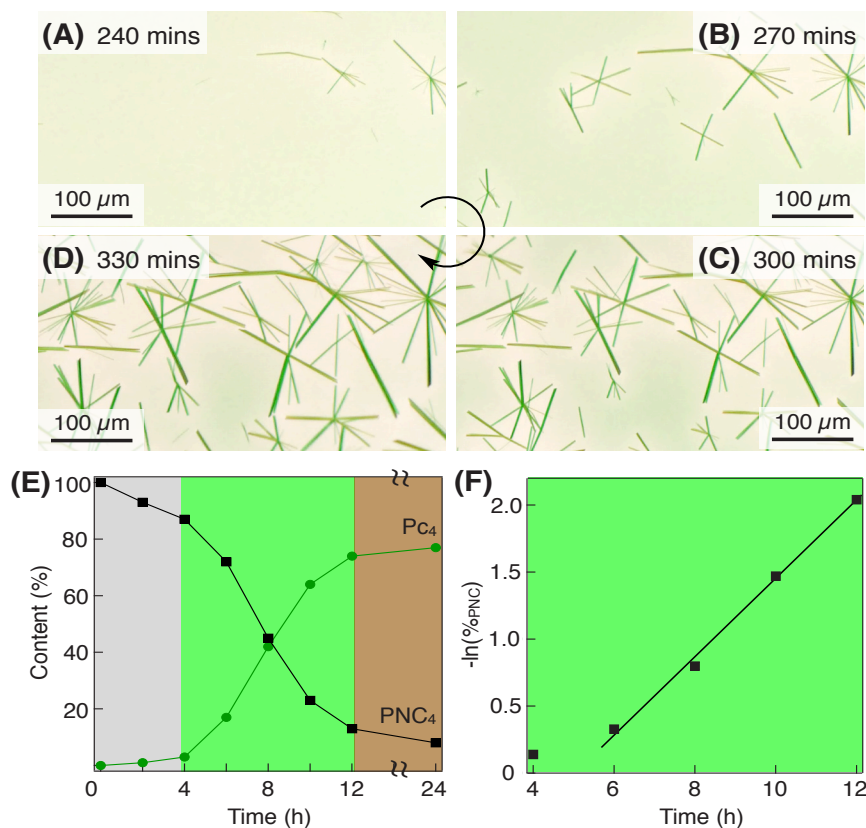


Figure 4 | Kinetic process of self-replicating supramolecular polymerization

(A–D) OM images of crystalline morphology of Pc_4 formed at 180 °C for (A) 240, (B) 270, (C) 300, and (D) 330 mins, respectively. (E) %-Contents of Pc_4 and PNC_4 in the resultant mixture by heating PNC_4 at 180 °C for 0, 2, 4, 6, 8, 10, 12, 16 hours, respectively. (F) Kinetic curve of the cyclization reaction of PNC_4 heating at 180 °C at growing stage (from 6 to 12 hours). The gray, green and brown regions represent the nucleating, growing and terminating stages, respectively.

The kinetic study on self-replicating supramolecular polymerization of Pc_4 further verified my hypothesis. The output growth of resultant Pc_4 displayed a typical S-type curve featuring a slow nucleating but fast growing process (Figure. 4E). Moreover, the cyclotetramerization of PNC_4 in the growing process was well identified as the first-order reaction, strongly supporting the self-replicating mechanism (Figure. 4F).

4.2.4. Structural Requisites for PNC

What are the structural requisites for **PNC** molecules enabled to undergo a self-replicating supramolecular polymerization? Based on the proposed mechanism, I believed that H-bonding interaction is essential. Therefore, a control sample, $\text{PN}_{\text{Me}}\text{C}_4$ was synthesized by methylation of amide groups of PNC_4 to remove the possible H-bonding interactions (Figure. 5A). As I expected, the color of cell full of $\text{PN}_{\text{Me}}\text{C}_4$ changed to green but no crystalline fibers were formed after standing at 160 °C (or even high temperature) for overnight, although the mass spectrum of the resultant mixture confirmed the present of its corresponding **Pc** (Figure. S9). This finding well supports the significant controlling of H-bonding on self-replicating supramolecular polymerization. I also noticed that when the sulfur atoms in 4,5-dithiophthalonitriles were replaced by the oxygen atoms, the color of $\text{PN}^{\text{O}}\text{C}_4$ (Figure. 5A) changed to brown rather than green after heating at 180 °C for overnight, suggesting the absent of its corresponding **Pc** (Figure. S10). This control experiment demonstrated that the dithio groups in **PNC** molecules are one of structural prerequisites for its cyclotetramerization induced by heating. Finally, I compared the assembling behavior of PNC_n having the different side chains from ethyl to hexyl (Figure. 5A and Figure. S12), and found that the length of side chains also plays a key role on self-replicating supramolecular polymerization. In OM images of PNC_2 (Figure. 5B) and PNC_3 (Figure. 5C), long crystalline fibers were observed when heating above 180 °C and 170 °C, respectively (Figures. S11A,B), while short fibers or even no fiber were observed in OM images of PNC_5 (Figure. 5D) and PNC_6 (Figure. 5E) heating at 150 °C (Figures. S11C,D). I have known that the heating temperature for self-replication of **Pc** should be in a suitable range to keep **PNC** as an isotropic state but **Pc** as a crystalline state. The crystalline temperature of Pc_6 was lower than the melt point of PNC_6 (Figure. S11D). Therefore, **PNC** molecules with hexyl

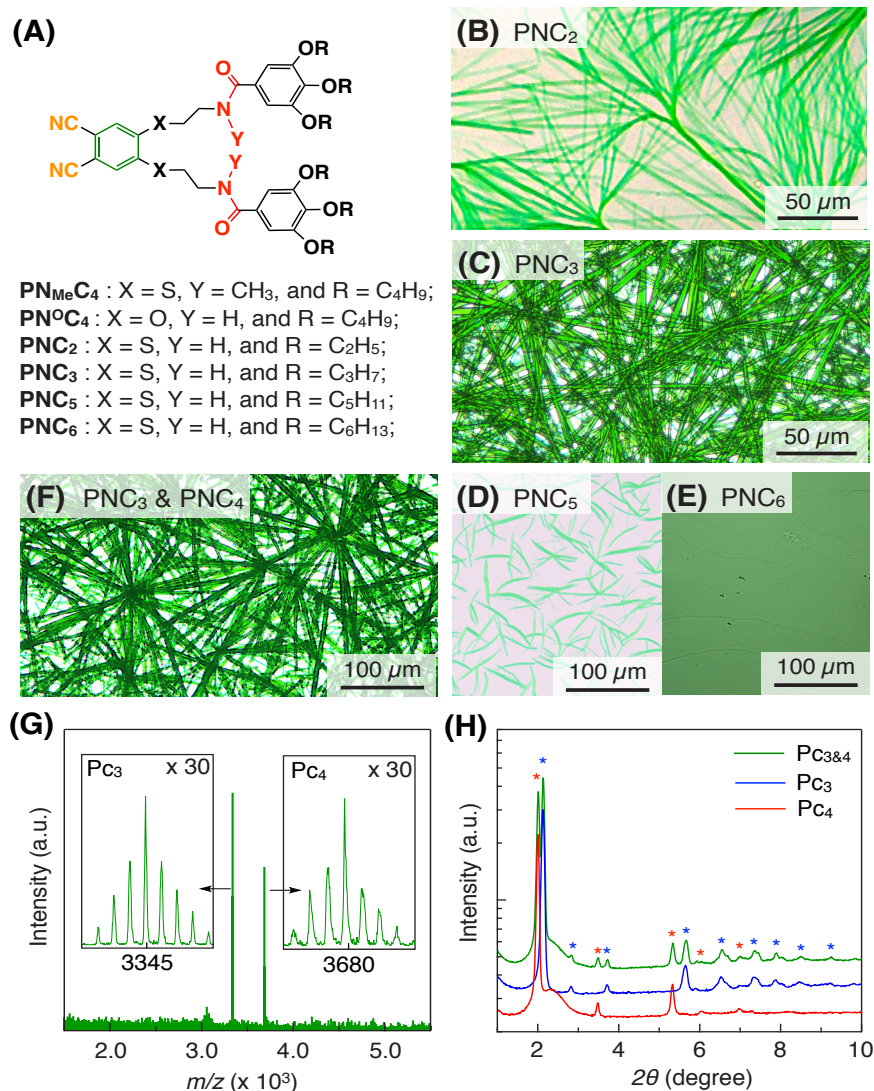


Figure 5 | PNC molecules enabled to undergo a self-replicating supramolecular polymerization. (A) General molecular structures of PNC molecules. (B–F) OM images of (B) PNC₂, (C) PNC₃, (D) PNC₅, (E) PNC₆, and (F) PNC₄ & PNC₃ mixture (mole ratio = 1:1) after heating at 190, 180, 150, 170, and 180 °C for overnight, respectively. (G) MALDI-TOF mass spectrum of the washed crystalline fibers in f. The insets are zoomed-in spectra of the target peaks. (H) XRD patterns of the washed crystalline fibers of f (green line), Pc₃ (blue line) and Pc₄ (red line), respectively. The peaks donated by red and blue star attributes to the crystal patterns of Pc₄ and Pc₃, respectively.

side chains (PNC₆) or longer ones, for example PNC₁₂, cannot do supramolecular polymerization to replicate their corresponding Pc.

Since two PNC molecules, PNC₃ and PNC₄ are excellent precursors for self-replication of Pc, I tried to heat the mixture of PNC₃ and PNC₄ (mole ratio = 1/1) at 180 °C, then observed a clear

fibrous pattern in the OM image (Figure. 5F). Of a big surprise, two distinct ionic peaks appeared at 3345.54 and 3678.72, corresponding to **Pc**₃ (Calcd. for C₁₇₆H₂₃₇N₁₆O₃₂S₈ [M+H]⁺: $m/z = 3345.37$) and **Pc**₄ respectively, were observed in the mass spectrum of washed fibers (Figure. 5G). This result implied that the self-replicating polymerization exhibits a high selectivity for **Pc** synthesis, which is unfulfillable by the mixed system composed of **PNC**₃ and **PNC**₄, together with polyethylene glycol (10%wt) as a H-bonding quencher (Figure. S13). We speculated that such high selectivity stems from the crystalline structural differences of **Pc**₃ and **Pc**₄. Figure 5H gives the XRD pattern of crystalline fibers formed by the mixture of **PNC**₃ and **PNC**₄. Comparing it with the standard patterns of crystalline fibers formed by **Pc**₃ and **Pc**₄, we confirmed that **PNC**₃ and **PNC**₄ are self-sorted to form the individual crystalline fibers of **Pc**₃ (hexagonal, $a = 3.30$ nm, Table S1) and **Pc**₄ (hexagonal, $a = 3.50$ nm, Table S2) in mixtures. As a result, two different crystalline structures provide two different templates to control self-replicating supramolecular polymerization, affording a high selectivity for resultant **Pc**.

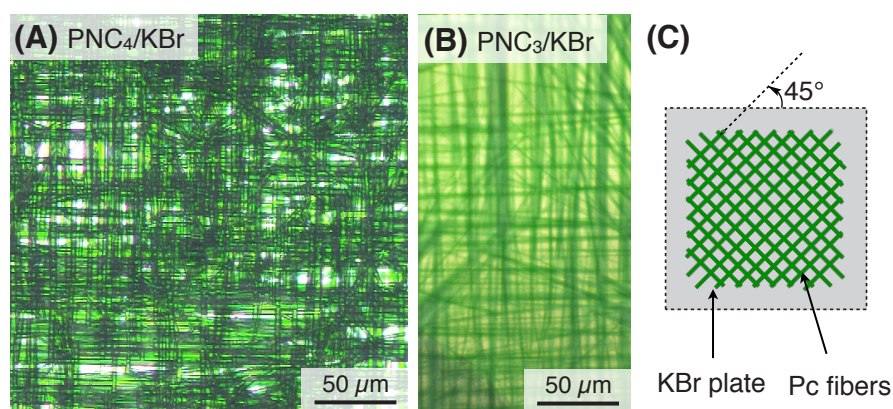


Figure 6 | 2D orthogonal orientation of Pc crystalline fibers on KBr plates. (A, B) OM images of **Pc** crystalline fibers after heating (A) **PNC**₄ and (B) **PNC**₃ sandwiched with two KBr plates at 180 °C for overnight, respectively. (C) Schematic illustration of 2D orthogonal orientation of crystalline fibers on KBr plates.

4.3. Conclusion

In this chapter, I present a self-replicating supramolecular polymerization enabled to accurately control the autocatalyzed cyclizing of 4,5-dithiophthalonitrile derivatives (**PNC**) to assemble the crystalline fibers of metal-free phthalocyanines (**Pc**) featuring a high yield and selectivity in one step. The key process is that the isotropic **PNC** pasted on the template columnar nucleus consisting of **Pc** molecules through a hydrogen-bonding interaction of the amide groups, and spontaneously cyclized to form a new **Pc** in a molecular distance. In one step, **PNC** polymerize to afford a crystalline fiber assembled by highly pure **Pc**.

Driven by the dynamic noncovalent interactions together with the formation of covalent bonds, self-replicating supramolecular polymerization not only inspires a new idea for synthetic methodologies towards a high yield and selectivity, but also provides a one-pot strategy to design self-synthesizing materials. For example, the crystalline fibers of **Pc** obtained in our work may be used as the organic semiconductor materials (27–30). More importantly, considering that a fibrous seed of **Pc** could initiate new **PNC** molecules to form a block crystal on the premise of structural uniformity (Figure. S14), the next generation supramolecular heterojunction will be achievable through molecularly engineered donor/acceptor couples (31).

Finally, I found an interesting orientation of crystalline fibers formed by **Pc** on KBr plates, as shown in Figure 6. These fibers are orthogonally aligned along the diagonal lines of KBr plate. Compared with other substrates, such as NaCl and KCl, only KBr works well (Figure. S15), possibly indicating that the packing of Br atoms in crystal lattice may play a key role to control the 2D orthogonal orientation of crystalline fibers.

[27] O. A. Melville, B. H. Lessard, T. P. Bender. *ACS Appl. Mater. Interfaces* **7**, 13105 (2015).

[28] Z. Bao, A. L. Lovinger, A. Dodabalapur. *Appl. Phys. Lett.* **69**, 3066 (1996).

[29] Z. Bao, A. L. Lovinger, A. Dodabalapur. *Adv. Mater.* **9**, 42 (1997).

[30] A. Varotto *et al.* *J. Am. Chem. Soc.* **132**, 2552 (2010).

[31] W. Zhang *et al.* *Science* **334**, 340 (2011).

- [32] E. Terazzi *et al.* *J. Am. Chem. Soc.* **127**, 888 (2005).
[33] A. S. Achalkumar *et al.* *J. Org. Chem.* **78**, 527 (2013).
[34] A. V. Ivanov *et al.* *Russ. Chem. Bull.* **50**, 919 (2001).

4.4. Supporting Information

4.4.1. Materials and Methods

Materials Unless otherwise noted, reagents were used as received from Tokyo Chemical Industry [*N*-hydroxysuccinimide (NHS), sodium hydride (NaH), iodomethane (MeI), 1,8-diazabicyclo[5.4.0]undec-7-ene (DBU), and 1-pentanol], Wako Pure Chemical Industries [*N,N'*-dicyclohexylcarbodiimide (DCC), trifluoroacetic acid (TFA), triethylamine and potassium carbonate (K₂CO₃)] and Sigma-Aldrich [3,4,5-triethoxybenzoic acid and polyethylene glycol (PEG₅₀₀, molecular weight is 500)]. Compounds **2a** (32), **1** (20), **4a** (32), **5a** (33), **6a** (33), 4,5-dihydroxyphthalonitrile (34) and *t*-butyl 2-bromoethylcarbamate (20) were prepared according to reported procedures. CH₂Cl₂ was dried over CaH₂ and freshly distilled prior to use. THF was refluxed over a mixture of Na and benzophenone and freshly distilled before use. Other dehydrated solvents were purchased from Wako Pure Chemical Industries or Kanto Chemicals.

General Column chromatography was carried out with Wakogel silica C-300 (particle size: 45–75 μm). ¹H and ¹³C NMR spectra were recorded on a JEOL model JNM-ECA500 spectrometer, operating at 500 and 125 MHz, respectively, where chemical shifts (in ppm) were determined with respect to tetramethylsilane as an internal reference. Matrix-assisted laser desorption ionization time-of-flight (MALDI-TOF) mass spectrometry was performed on an Applied Biosystems model MDS SCIEX 4800 Plus MALDI TOF/TOF™ Analyzer using dithranol as a matrix. Differential scanning calorimetry (DSC) was performed on a Mettler–Toledo model DSC 1 differential scanning calorimeter, where temperature and enthalpy were calibrated with In (430 K, 3.3 J mol⁻¹) and Zn (692.7 K, 12 J mol⁻¹) standard samples using sealed Al pans. Cooling and heating profiles were recorded and analyzed using the Mettler–Toledo STARe software system. Optical microscopy (OM) was performed on a Nikon model Eclipse LV100POL optical polarizing microscope equipped with a Mettler–Toledo model FP90 controller attached to a FP82HT hot stage and a high-definition camera. Analytical size-exclusion chromatography (SEC) was performed at 40 °C on a TOSOH model HLC-8220 GPC system equipped with a refractive index (RI) detector, using CHCl₃ as an eluent at a flow rate of 0.35 mL min⁻¹ on linearly connected three polystyrene gel columns (TSKgel SuperHM-M, TOSOH). X-ray diffraction

(XRD) experiments were carried out at BL45XU in Spring-8 (Hyogo, Japan) with an imaging plate area detector, a R-Axis IV++ (Rigaku). Scattering vector, $q = 4\pi\sin\theta/\lambda$, and position of incident X-ray on the detector were calibrated using several orders of layer reflections from silver behenate ($d = 58.380 \text{ \AA}$), where 2θ and λ are scattering angle and wavelength of X-ray (1.08 \AA), respectively. The scattering/diffraction images recorded were integrated along the Debye-Scherrer ring, affording one-dimensional intensity data using the FIT2D software (35). The cell parameters were refined using the CellCalc ver. 2.10 software (36). Infrared (IR) spectra were recorded at $25 \text{ }^\circ\text{C}$ on a JASCO model FT/IR-4100 Fourier transform infrared spectrometer. Polarized IR spectra were recorded at $25 \text{ }^\circ\text{C}$ on a JASCO model FT/IR-4100 Fourier transform infrared spectrometer connected to an Irtron IRT-5000 microscope unit. UV-vis absorption spectra were recorded on a JASCO model V-670 UV/VIS/NIR spectrophotometer.

[35] <http://www.esrf.eu/computing/scientific/FIT2D/>

[36] http://homepage2.nifty.com/~hsc/soft/cellcalc_e.html.

Methods Heating in glass cells. In order to fabricate a cell, two clear glass plates were stick at four corners by using glue. Upon heating to their isotropic state, the powder samples of PNC_n melt spontaneously permeated into the cell through capillary action and stand at certain temperature for overnight. After cooling to room temperature, the cell filled with samples was deposited under the optical microscope to observe the morphology. In order to purification, the cell was peeled off and the resultant glass plates were washed by methanol several times.

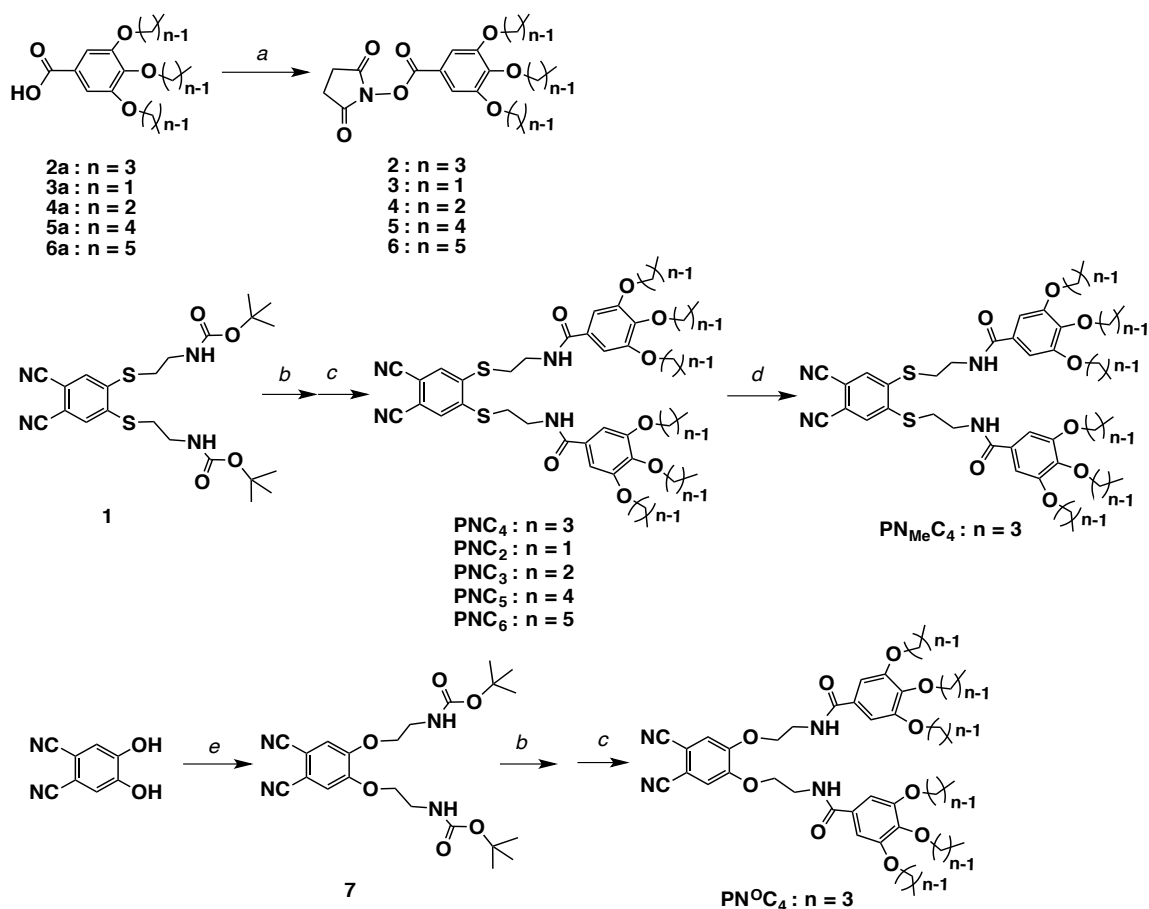
Evaluating the cyclized yield of Pc_4 . A few milligrams ($M \text{ mg}$) of the powder samples of PNC_4 was deposited on a clear glass plate and heated up to its isotropic state, then sandwiched by a second glass plate to keep heating at certain temperature. After heating for certain hours, the resultant sample was dissolved in CHCl_3 by sonication or heating at $50 \text{ }^\circ\text{C}$ and then its clear solution was concentrated to 1 mL . After analyzing the resultant solution by size-exclusion chromatography (Figure. S7), the intensity of refractive index corresponding to the peaks of unreacted PNC_4 and Pc_4 in the resultant mixtures was obtained. Compared with their standard lines in Figure. S8, the concentration of unreacted PNC_4 and Pc_4 was obtained as C_{PNC} and C_{Pc} , respectively (Tables S3 and S4). The %-content of PNC_4 , intermediates, and Pc_4 in the resultant mixtures could be evaluated by the following equations.

$$\%_{\text{PNC}} = 100C_{\text{PNC}}/M;$$

$$\%_{\text{Pc}} = 100C_{\text{Pc}}/M;$$

$$\%_{\text{inter.}} = 100 - \%_{\text{PNC}} - \%_{\text{Pc}}$$

4.4.2. Synthesis



Scheme S1 I Synthesis of **PNC_n** ($n = 2 \sim 6$), **PN_{Me}C₄** and **PN^OC₄**. Reagents and conditions: (a) NHS, DCC, 1,4-dioxane, 25 °C; (b) TFA, CH₂Cl₂, 25 °C; (c) **2** ~ **6**, Et₃N, CH₂Cl₂, 25 °C; (d) NaH, MeI, THF, 25 °C; (e) *t*-butyl 2-bromoethylcarbamate, K₂CO₃, DMF, 70 °C.

Compound 2. To a 1,4-dioxane solution (20 mL) of a mixture of **2a** (3.38 g, 10.0 mmol) and *N,N'*-dicyclohexylcarbodiimide (2.27 g, 11.0 mmol) was added *N*-hydroxysuccinimide (1.27 g, 11.0 mmol), and the mixture was stirred for 4 h at 25 °C. After filtration, the water (50 mL) was added to the collected filtrate, and then the mixture was extracted with CH₂Cl₂ (50 mL) for 2 times. The organic extract was washed with brine (30 mL) for 2 times, dried over MgSO₄, and evaporated to dryness. The residue was subjected to column chromatography (SiO₂, CHCl₃) to allow isolation of **2** as transparent oil (4.00 g, 9.20 mmol) in 92% yield. ¹H NMR (500 MHz, CDCl₃): δ (ppm) 7.34 (s, 2H), 4.07 (t, $J = 6.3$ Hz, 2H), 4.02 (t, $J = 6.3$ Hz, 4H), 2.90 (br, 4H), 1.83-1.78 (m, 4H), 1.74-1.70 (m, 2H), 1.54-1.47 (m, 6H), 0.97 (m, 9H). ¹³C NMR (125 MHz, CDCl₃): δ (ppm) 169.35, 161.66, 153.02, 144.11, 119.08, 108.92, 74.25, 69.82, 33.95, 32.32, 32.11, 31.34, 25.66, 19.22, 19.06, 13.81, 13.76. MALDI-TOF mass: calcd. for C₂₃H₃₄NO₇ [M + H]⁺: $m/z = 436.23$; found: 436.30.

PNC₄. To a CH₂Cl₂ solution (5 mL) of **1** (0.50 g, 1.05 mmol), chilled with an ice bath, was dropwise added TFA (5 mL) over a period of 10 min, and the resulting solution was stirred for 2 h at 25 °C. The reaction mixture was evaporated to dryness under reduced pressure. To the residue was added a CH₂Cl₂ solution

(10 mL) of a mixture of **2** (1.00 g, 2.30 mmol), and Et₃N (0.51 g, 5.00 mmol). Then, to the resulting solution, after being stirred overnight at 25 °C, was added HCl (aq, 1M, 10 mL), and the mixture was extracted with CH₂Cl₂ (30 mL). The organic extract was washed with brine (30 mL) for 2 times, dried over MgSO₄, and evaporated to dryness. The residue was subjected to column chromatography (SiO₂, CHCl₃) to allow isolation of **PNC**₄ as white solid (0.57 g, 0.62 mmol) in 59% yield. ¹H NMR (500 MHz, CDCl₃): δ (ppm) 7.69 (s, 2H), 6.98 (s, 4H), 6.83 (br, 2H), 4.00 (t, *J* = 6.5 Hz, 12H), 3.65 (q, *J* = 6.2 Hz, 4H), 3.31 (t, *J* = 6.2 Hz, 4H), 1.80-1.67 (m, 12H), 1.53-1.45 (m, 12H), 0.96 (m, 18H). ¹³C NMR (125 MHz, CDCl₃): δ (ppm) 167.65, 153.14, 143.42, 141.62, 130.86, 128.21, 115.01, 112.31, 105.78, 73.16, 69.08, 39.28, 33.93, 32.29, 32.07, 31.36, 25.60, 19.23, 19.12, 13.86, 13.82. MALDI-TOF mass: calcd. for C₅₀H₇₀N₄O₈S₂Na [M + Na]⁺: *m/z* = 941.46; found: 941.51.

PN_{Me}C₄. To a THF solution (20 mL) of a mixture of **PNC**₄ (0.30 g, 0.33 mmol) and sodium hydride (24.0 mg, 1.00 mmol), chilled with an ice bath, was dropwise added iodomethane (0.20 g, 1.42 mmol), and the mixture was stirred for 6 h at 25 °C. The water (50 mL) was poured to the resulting solution, and then the mixture was extracted with CH₂Cl₂ (50 mL) for 2 times. The organic extract was washed with brine (30 mL) for 2 times, dried over MgSO₄, and evaporated to dryness. The residue was subjected to column chromatography (SiO₂, CHCl₃) to allow isolation of **PN_{Me}C₄** as amorphous solid (0.30 g, 0.32 mmol) in 97% yield. ¹H NMR (500 MHz, CDCl₃): δ (ppm) 7.69 (s, 2H), 6.58 (s, 4H), 4.00 (t, *J* = 6.5 Hz, 12H), 3.70 (q, *J* = 6.2 Hz, 4H), 3.27 (t, *J* = 6.2 Hz, 4H), 3.05 (s, 6H), 1.80-1.68 (m, 12H), 1.54-1.45 (m, 12H), 0.96 (m, 18H). ¹³C NMR (125 MHz, CDCl₃): δ (ppm) 171.86, 153.14, 153.10, 153.05, 130.20, 115.26, 105.99, 73.14, 69.04, 49.20, 33.95, 32.33, 32.30, 31.42, 31.39, 31.36, 25.62, 24.95, 19.29, 19.27, 19.17, 13.91, 13.85. MALDI-TOF mass: calcd. for C₅₂H₇₄N₄O₈S₂Na [M + Na]⁺: *m/z* = 969.49; found: 969.50.

Compound 7. To a DMF solution (25 mL) of a mixture of 4,5-dihydroxyphthalonitrile (0.80 g, 5.0 mmol) and t-butyl 2-bromoethylcarbamate (2.45 g, 11.0 mmol) was added K₂CO₃ (1.52 g, 11.0 mmol), and the mixture was stirred for 8 h at 70 °C. After filtration, the water (50 mL) was added to the collected filtrate, and then the mixture was extracted with CH₂Cl₂ (50 mL) for 2 times. The organic extract was washed with brine (30 mL) for 2 times, dried over MgSO₄, and evaporated to dryness. The residue was subjected to column chromatography (SiO₂, AcOEt : Hex = 1:1) to allow isolation of **7** as white solid (1.50 g, 3.40 mmol) in 67% yield. ¹H NMR (500 MHz, CDCl₃): δ (ppm) 7.18 (s, 2H), 4.12 (q, *J* = 6.8 Hz, 4H), 3.60 (q, *J* = 6.8 Hz, 4H), 1.45 (s, 18H). ¹³C NMR (125 MHz, CDCl₃): δ (ppm) 155.82, 152.07, 149.52, 116.95, 115.49, 109.23, 83.86, 79.93, 69.18, 61.25, 43.42, 39.71, 28.34, 27.93. MALDI-TOF mass: calcd. for C₂₂H₃₁N₄O₆ [M + H]⁺: *m/z* = 447.22; found: 447.10.

PN^OC₄. By a procedure similar to that for **PNC**₄, **PN^OC₄** was obtained in 70% yield (0.42 g, 0.47 mmol) from **7** (0.30 g, 0.67 mmol), **2** (0.60 g, 1.38 mmol), and Et₃N (0.51 g, 5.00 mmol). ¹H NMR (500 MHz, CDCl₃): δ (ppm) 7.35 (br, 2H), 7.19 (s, 4H), 7.10 (s, 2H), 4.16 (t, *J* = 4.8 Hz, 4H), 3.98 (q, *J* = 6.3 Hz, 12H), 3.77 (t, *J* = 5.3 Hz, 4H), 1.79-1.68 (m, 12H), 1.54-1.42 (m, 12H), 0.95 (m, 18H). ¹³C NMR (125 MHz, CDCl₃): δ (ppm) 167.76, 153.12, 152.16, 141.40, 128.42, 116.74, 115.50, 109.24, 105.89, 73.14, 68.99, 68.62, 32.28, 31.34, 19.21, 19.12, 13.86, 13.79. MALDI-TOF mass: calcd. for C₅₀H₇₀N₄O₁₀Na [M + Na]⁺: *m/z* = 909.51; found: 909.43.

Compound 3. By a procedure similar to that for **2**, **3** was obtained in 95% yield (3.33 g, 9.5 mmol) from 3,4,5-triethoxybenzoic acid (2.50 g, 10.0 mmol), *N,N'*-dicyclohexylcarbodiimide (1.27 g, 11.0 mmol) and *N,N'*-dicyclohexylcarbodiimide

(2.27 g, 11.0 mmol). ^1H NMR (500 MHz, CDCl_3): δ (ppm) 7.34 (s, 2H), 4.17 (q, $J = 6.8$ Hz, 2H), 4.12 (q, $J = 6.8$ Hz, 4H), 2.90 (br, 4H), 1.45 (t, $J = 6.8$ Hz, 6H), 1.37 (t, $J = 6.8$ Hz, 3H). ^{13}C NMR (125 MHz, CDCl_3): δ (ppm) 169.34, 161.64, 153.08, 144.12, 119.06, 108.93, 75.25, 70.82, 39.26, 32.11, 15.62, 14.94. MALDI-TOF mass: calcd. for $\text{C}_{17}\text{H}_{22}\text{NO}_7$ [$\text{M} + \text{H}$] $^+$: $m/z = 352.13$; found: 352.10.

PNC₂. By a procedure similar to that for **PNC₄**, **PNC₂** was obtained in 62% yield (0.49 g, 0.65 mmol) from **1** (0.50 g, 1.05 mmol), **3** (0.77 g, 2.20 mmol), and Et_3N (0.51 g, 5.00 mmol). ^1H NMR (500 MHz, DMSO): δ (ppm) 8.56 (br, 2H), 8.00 (s, 2H), 7.07 (s, 4H), 4.03 (t, $J = 6.5$ Hz, 8H), 3.97 (t, $J = 6.5$ Hz, 4H), 3.50 (t, $J = 6.2$ Hz, 4H), 3.35 (t, $J = 6.2$ Hz, 4H), 1.31 (t, $J = 6.8$ Hz, 12H), 1.22 (t, $J = 6.8$ Hz, 6H). ^{13}C NMR (125 MHz, DMSO): δ (ppm) 167.61, 152.94, 143.43, 141.42, 130.89, 128.33, 115.02, 112.24, 106.02, 69.05, 65.00, 39.28, 32.10, 15.60, 14.92. MALDI-TOF mass: calcd. for $\text{C}_{36}\text{H}_{46}\text{N}_4\text{O}_8\text{S}_2\text{Na}$ [$\text{M} + \text{Na}$] $^+$: $m/z = 773.28$; found: 773.26.

Compound 4. By a procedure similar to that for **1**, **4** was obtained in 90% yield (3.58 g, 9.1 mmol) from **4a** (3.00 g, 10.1 mmol), *N*-hydroxysuccinimide (1.27 g, 11.0 mmol) and *N,N'*-dicyclohexylcarbodiimide (2.27 g, 11.0 mmol). ^1H NMR (500 MHz, CDCl_3): δ (ppm) 7.34 (s, 2H), 4.04 (t, $J = 6.3$ Hz, 2H), 3.98 (t, $J = 6.3$ Hz, 4H), 2.90 (br, 4H), 1.89-1.80 (m, 4H), 1.79-1.73 (m, 2H), 1.05 (m, 9H). ^{13}C NMR (125 MHz, CDCl_3): δ (ppm) 169.32, 161.67, 153.05, 144.09, 119.07, 108.97, 75.23, 70.80, 25.67, 23.50, 22.56, 10.53, 10.46. MALDI-TOF mass: calcd. for $\text{C}_{20}\text{H}_{28}\text{NO}_7$ [$\text{M} + \text{H}$] $^+$: $m/z = 394.43$; found: 394.48.

PNC₃. By a procedure similar to that for **PNC₄**, **PNC₃** was obtained in 55% yield (0.48 g, 0.58 mmol) from **1** (0.50 g, 1.05 mmol), **4** (0.87 g, 2.20 mmol), and Et_3N (0.51 g, 5.00 mmol). ^1H NMR (500 MHz, CDCl_3): δ (ppm) 7.69 (s, 2H), 6.97 (s, 4H), 6.81 (br, 2H), 4.00 (t, $J = 6.5$ Hz, 12H), 3.65 (q, $J = 6.3$ Hz, 4H), 3.32 (t, $J = 6.3$ Hz, 4H), 1.80-1.73 (m, 12H), 1.03 (m, 18H). ^{13}C NMR (125 MHz, CDCl_3): δ (ppm) 167.66, 153.09, 143.42, 141.60, 130.80, 128.22, 115.06, 112.23, 105.84, 75.11, 70.91, 39.27, 32.06, 23.49, 22.66, 10.56, 10.49. MALDI-TOF mass: calcd. for $\text{C}_{44}\text{H}_{58}\text{N}_4\text{O}_8\text{S}_2\text{Na}$ [$\text{M} + \text{Na}$] $^+$: $m/z = 858.08$; found: 858.15.

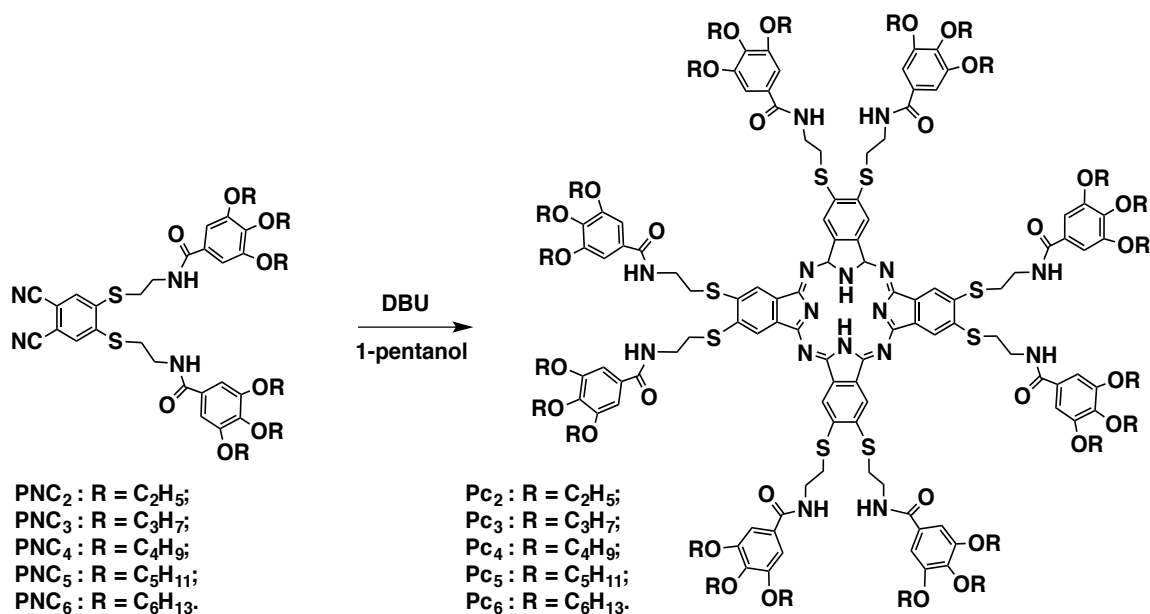
Compound 5. By a procedure similar to that for **2**, **5** was obtained in 92% yield (4.40 g, 9.2 mmol) from **5a** (3.80 g, 10.0 mmol), *N*-hydroxysuccinimide (1.27 g, 11.0 mmol) and *N,N'*-dicyclohexylcarbodiimide (2.27 g, 11.0 mmol). ^1H NMR (500 MHz, CDCl_3): δ (ppm) 7.33 (s, 2H), 4.07 (t, $J = 6.3$ Hz, 2H), 4.00 (t, $J = 6.3$ Hz, 4H), 2.90 (br, 4H), 1.82-1.66 (m, 6H), 1.48-1.34 (m, 12H), 0.92 (m, 9H). ^{13}C NMR (125 MHz, CDCl_3): δ (ppm) 169.33, 161.68, 153.07, 144.12, 119.06, 108.90, 73.60, 69.25, 34.91, 33.94, 29.92, 28.87, 28.16, 28.10, 25.66, 25.43, 24.68, 22.48, 22.37, 14.05, 14.00. MALDI-TOF mass: calcd. for $\text{C}_{26}\text{H}_{40}\text{NO}_7$ [$\text{M} + \text{H}$] $^+$: $m/z = 478.59$; found: 478.62.

PNC₅. By a procedure similar to that for **PNC₄**, **PNC₅** was obtained in 50% yield (0.52 g, 0.52 mmol) from **1** (0.50 g, 1.05 mmol), **5** (1.10 g, 2.30 mmol), and Et_3N (0.51 g, 5.00 mmol). ^1H NMR (500 MHz, CDCl_3): 7.69 (s, 2H), 6.98 (s, 4H), 6.83 (br, 2H), 3.99 (t, $J = 6.5$ Hz, 12H), 3.64 (q, $J = 6.2$ Hz, 4H), 3.31 (t, $J = 6.2$ Hz, 4H), 1.82-1.67 (m, 12H), 1.48-1.33 (m, 24H), 0.93 (m, 18H). ^{13}C NMR (125 MHz, CDCl_3): δ (ppm) 167.66, 153.13, 143.38, 141.62, 130.82, 128.21, 115.10, 112.30, 105.77, 73.49, 69.38, 39.27, 32.07, 29.96, 29.02, 28.19, 28.16, 22.52, 22.41, 14.06, 14.01. MALDI-TOF mass: calcd. for $\text{C}_{56}\text{H}_{82}\text{N}_4\text{O}_8\text{S}_2\text{Na}$ [$\text{M} + \text{Na}$] $^+$: $m/z = 1026.40$; found: 1026.45.

Compound 6. By a procedure similar to that for **2**, **6** was obtained in 90% yield (4.70 g, 9.0 mmol) from **6a** (4.20 g, 10.0 mmol), *N*-hydroxysuccinimide (1.27 g,

11.0 mmol) and *N,N'*-dicyclohexylcarbodiimide (2.27 g, 11.0 mmol). ^1H NMR (500 MHz, CDCl_3): δ (ppm) 7.33 (s, 2H), 4.06 (t, $J = 6.3$ Hz, 2H), 4.01 (t, $J = 6.3$ Hz, 4H), 2.90 (br, 4H), 1.81-1.70(m, 6H), 1.53-1.44 (m, 6H), 1.35-1.29 (m, 12H), 0.92 (m, 9H). ^{13}C NMR (125 MHz, CDCl_3): δ (ppm) 169.36, 161.62, 153.02, 144.08, 119.01, 108.94, 73.62, 70.28, 39.33, 32.23, 31.74, 31.50, 30.23, 29.21, 25.64, 25.55, 22.60, 22.52, 14.05, 14.01. MALDI-TOF mass: calcd. for $\text{C}_{29}\text{H}_{46}\text{NO}_7$ [$\text{M} + \text{H}$] $^+$: $m/z = 520.67$; found: 520.60.

PNC₆. By a procedure similar to that for **PNC₄**, **PNC₆** was obtained in 55% yield (0.63 g, 0.58 mmol) from **1** (0.50 g, 1.05 mmol), **6** (1.20 g, 2.30 mmol), and Et_3N (0.51 g, 5.00 mmol). ^1H NMR (500 MHz, CDCl_3): 7.69 (s, 2H), 6.97 (s, 4H), 6.79 (br, 2H), 3.99 (t, $J = 6.5$ Hz, 12H), 3.64 (q, $J = 6.2$ Hz, 4H), 3.31 (t, $J = 6.2$ Hz, 4H), 1.82-1.71(m, 12H), 1.51-1.43 (m, 12H), 1.34-1.29 (m, 24H), 0.90 (m, 18H). ^{13}C NMR (125 MHz, CDCl_3): δ (ppm) 167.66, 153.13, 143.38, 141.64, 130.89, 128.21, 115.05, 112.35, 105.78, 73.55, 69.42, 39.30, 32.09, 31.72, 31.55, 30.26, 29.32, 25.73, 25.70, 22.66, 22.60, 14.08, 14.02. MALDI-TOF mass: calcd. for $\text{C}_{62}\text{H}_{94}\text{N}_4\text{O}_8\text{S}_2\text{Na}$ [$\text{M} + \text{Na}$] $^+$: $m/z = 1110.56$; found: 1110.60.



Scheme S2 I Synthesis of **P_n** ($n = 2 \sim 6$). Reagents and conditions: DBU, 1-pentanol, 140 °C.

Pc₄. To a 1-pentanol solution (20 mL) of **PNC₄** (0.20 g, 0.22 mmol) was dropwise added DBU (0.50 g, 3.3 mmol), and the mixture was stirred for 48 h at 140 °C. The water (50 mL) was poured to the resulting solution, and then the mixture was extracted with CH₂Cl₂ (50 mL) for 2 times. The green organic extract was washed with brine (30 mL) for 2 times, dried over MgSO₄, and evaporated to dryness. The residue was subjected to column chromatography (SiO₂, CHCl₃) to allow isolation of **Pc₄** as dark-green powder (51.0 mg, 14 μmol) in 25% yield. FT-IR: ν (cm⁻¹) 3280, 3089, 2958, 2932, 2874, 1631, 1579, 1540, 1496, 1463, 1425, 1381, 1362, 1329, 1290, 1234, 1108, 1072, 1023. MALDI-TOF mass: calcd. for C₂₀₀H₂₈₅N₁₆O₃₂S₈ [M + H]⁺: m/z = 3678.90; found: 3678.81.

Pc₂. By a procedure similar to that for **Pc₄**, **Pc₂** was obtained in 15% yield (30.0 mg, 10 μmol) from **PNC₂** (0.20 g, 0.27 mmol) in mixture of DBU (0.50 g, 3.3 mmol) and 1-pentanol solution (20 mL). FT-IR: ν (cm⁻¹) 3280, 3089, 2959, 2932, 2875, 1631, 1578, 1541, 1496, 1463, 1426, 1381, 1362, 1328, 1291, 1234, 1106, 1074, 1023. MALDI-TOF mass: calcd. for C₁₅₂H₁₈₉N₁₆O₃₂S₈ [M + H]⁺: m/z = 3008.73; found: 3008.78.

Pc₃. By a procedure similar to that for **Pc₄**, **Pc₃** was obtained in 25% yield (50.0 mg, 15 μmol) from **PNC₃** (0.20 g, 0.24 mmol) in mixture of DBU (0.50 g, 3.3 mmol) and 1-pentanol solution (20 mL). FT-IR: ν (cm⁻¹) 3281, 3089, 2958, 2932, 2875, 1631, 1579, 1541, 1496, 1464, 1425, 1381, 1363, 1329, 1290, 1235, 1109, 1072, 1024. MALDI-TOF mass: calcd. for C₁₇₆H₂₃₇N₁₆O₃₂S₈ [M + H]⁺: m/z = 3345.37; found: 3345.45.

Pc₅. By a procedure similar to that for **Pc₄**, **Pc₅** was obtained in 20% yield (40.0 mg, 10 μmol) from **PNC₅** (0.20 g, 0.20 mmol) in mixture of DBU (0.50 g, 3.3 mmol) and 1-pentanol solution (20 mL). FT-IR: ν (cm⁻¹) 3281, 3089, 2958, 2932, 2873, 1631, 1580, 1540, 1496, 1464, 1425, 1382, 1362, 1327, 1291, 1234, 1109, 1072, 1024. MALDI-TOF mass: calcd. for C₂₂₄H₃₃₃N₁₆O₃₂S₈ [M + H]⁺: m/z = 4018.64; found: 4018.58.

Pc₆. By a procedure similar to that for **Pc₄**, **Pc₆** was obtained in 18% yield (36.0 mg, 6 μmol) from **PNC₆** (0.20 g, 0.13 mmol) in mixture of DBU (0.50 g, 3.3 mmol) and 1-pentanol solution (20 mL). FT-IR: ν (cm⁻¹) 3280, 3089, 2958, 2934, 2874, 1631, 1580, 1541, 1496, 1463, 1425, 1382, 1362, 1330, 1291, 1234, 1109, 1073, 1024. MALDI-TOF mass: calcd. for C₂₄₈H₃₈₁N₁₆O₃₂S₈ [M + H]⁺: m/z = 4351.64; found: 4351.32.

4.4.3. Supporting Figures

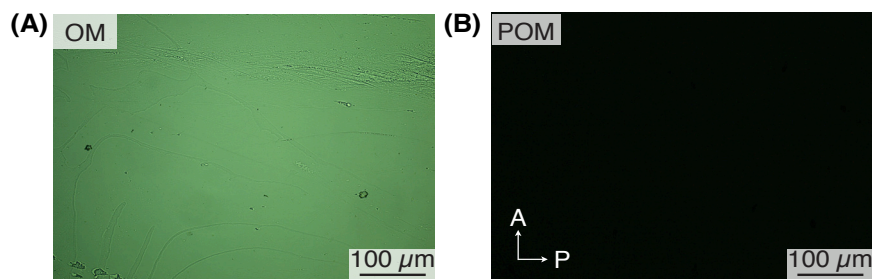


Figure S1 I (A) OM and (B) POM images of PNC_{12} after heating in cells at 160 °C for overnight. White arrows represent the transmission directions of the polarizer (P) and analyzer (A).

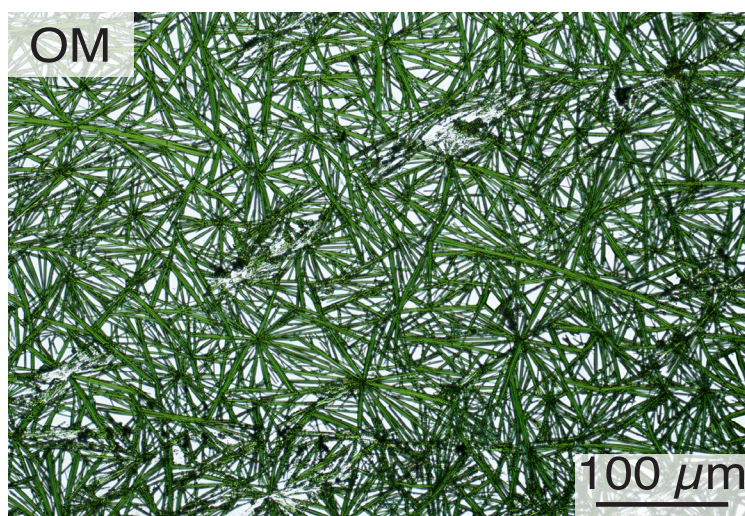


Figure S2 I OM images of the crystalline fibers of Pc_4 washed by methanol at 25 °C.

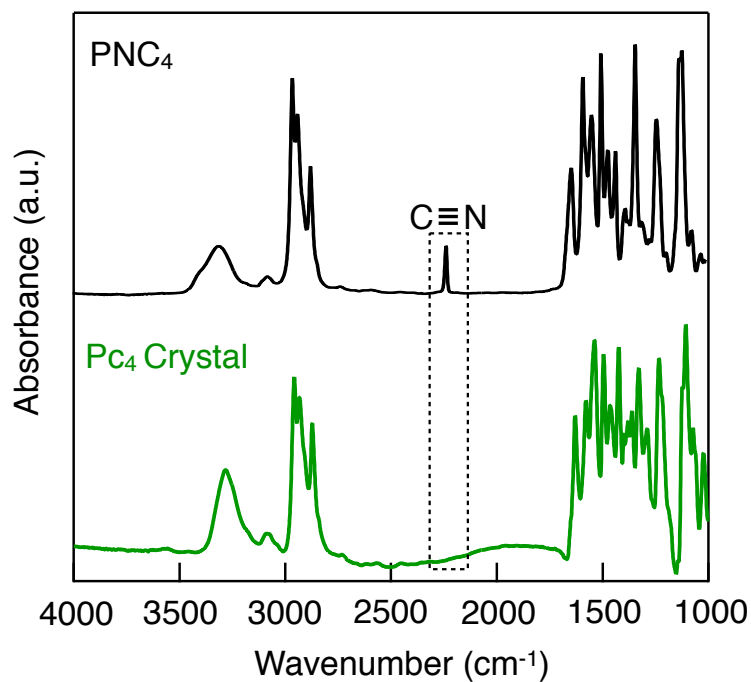


Figure S3 | IR spectra of PNC_4 (black line) and crystalline fibers of Pc_4 (green line) on KBr substrates.

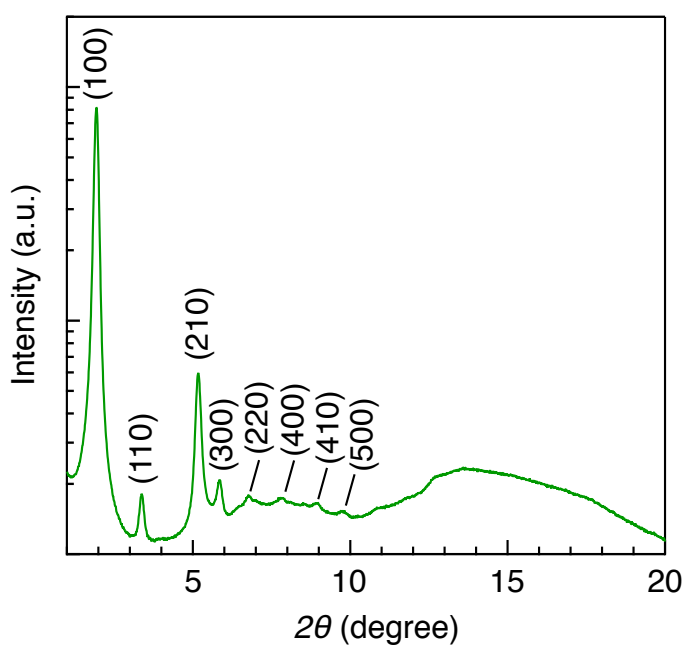


Figure S4 | XRD pattern of powder sample of Pc_4 in a glass capillary at 180 °C. Miller indices in parentheses.

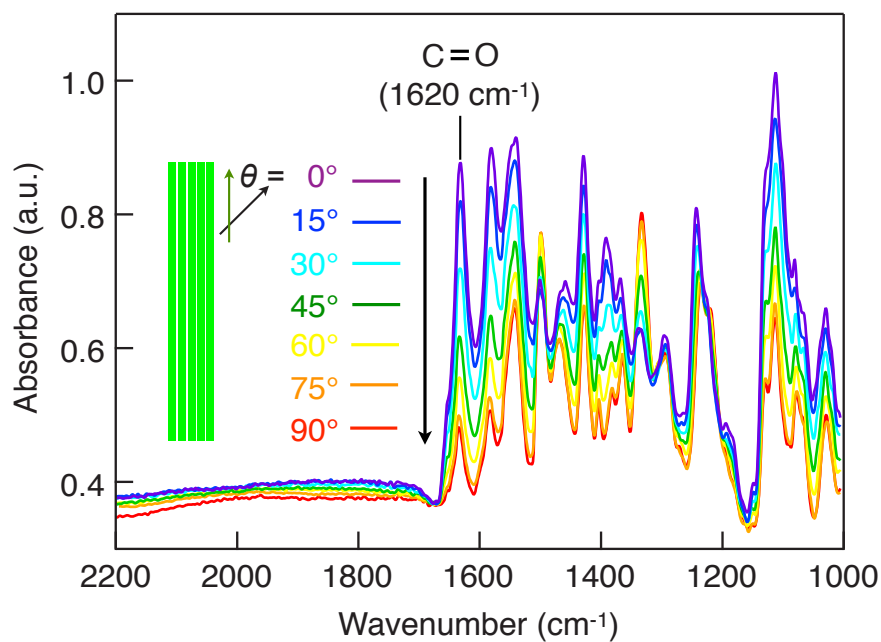


Figure S5 | Polarized IR spectra of the oriented crystalline fibers of Pc4 at azimuthal angle $\theta = 0^\circ, 15^\circ, 30^\circ, 45^\circ, 60^\circ, 75^\circ,$ and 90° . The azimuthal angle θ is defined as zero when the polarizing direction of incident light (blue arrow) is parallel to the long axis of fibrous crystals (green arrow).

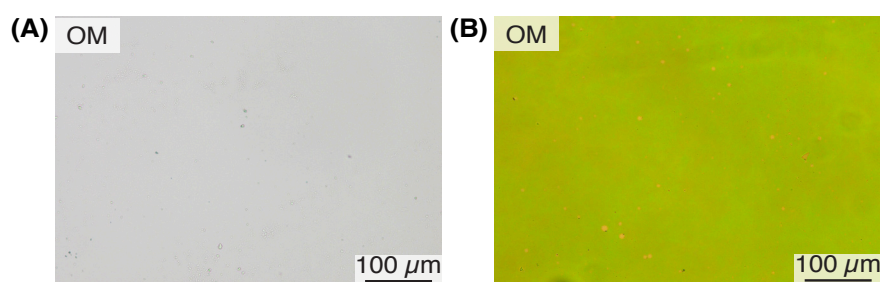


Figure S6 | OM images of PNC₄ after heating at (A) 140 °C and (B) 210 °C, respectively, in cells for overnight.

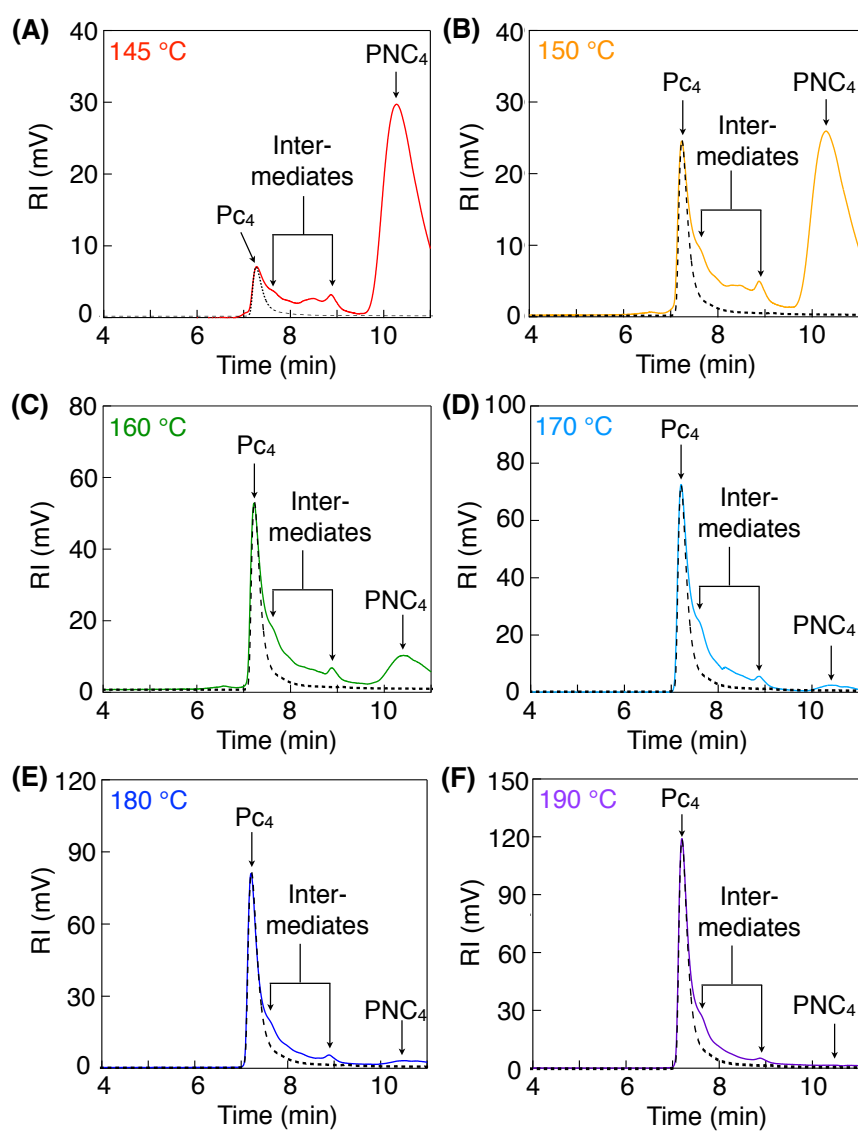


Figure S7 I Analytical SEC curves of the unwashed sample of PNC₄ heating at (a) 145 °C, (b) 150 °C, (c) 160 °C, (d) 170 °C, (e) 180 °C, and (f) 190 °C for 24 hours. Dash line represents the standard curve of the washed fibers of Pc₄.

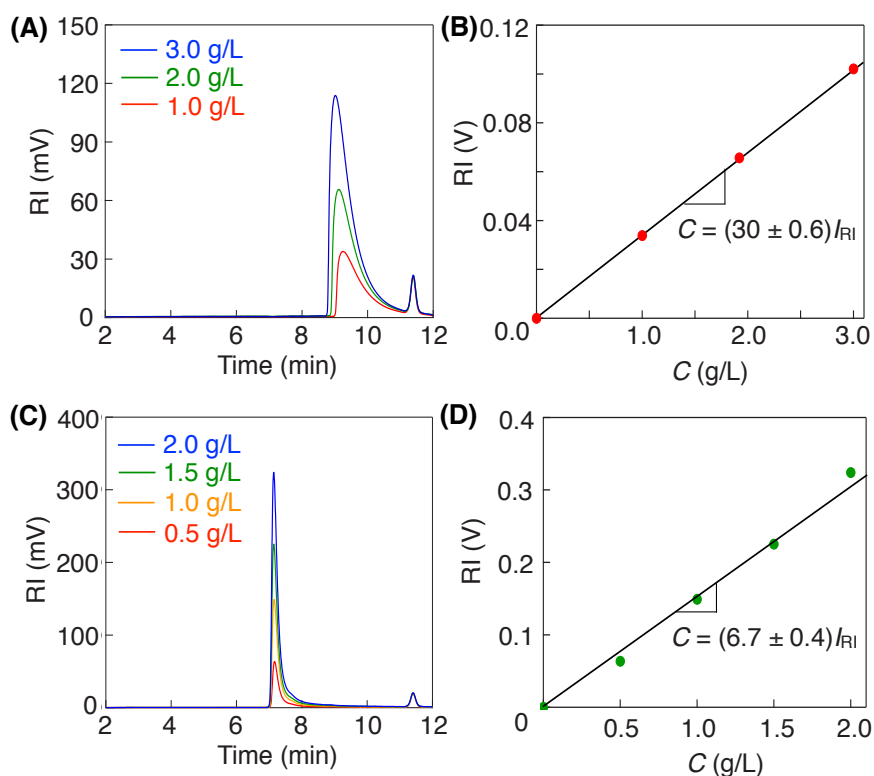


Figure S8 I (A and C) Analytical SEC curves of (A) PNC₄ and (C) Pc₄ in CHCl₃ with different concentrations. (B and D) Standard curves of the intensity of peaks in SEC curves of (B) PNC₄ and (D) Pc₄ versus their concentrations.

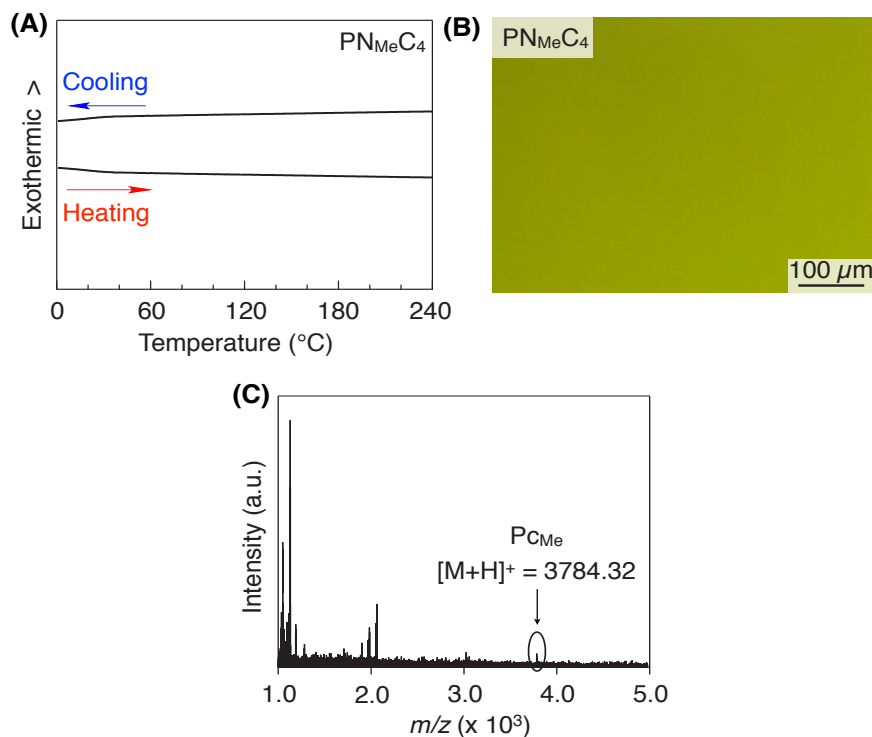


Figure S9 I (A) DSC traces on second heating/cooling cycles (10 °C /min) of PN_{Me}C₄. (B) OM image and (C) MALDI-TOF mass spectra of PN_{Me}C₄ after heating at 180 °C in cells for overnight.

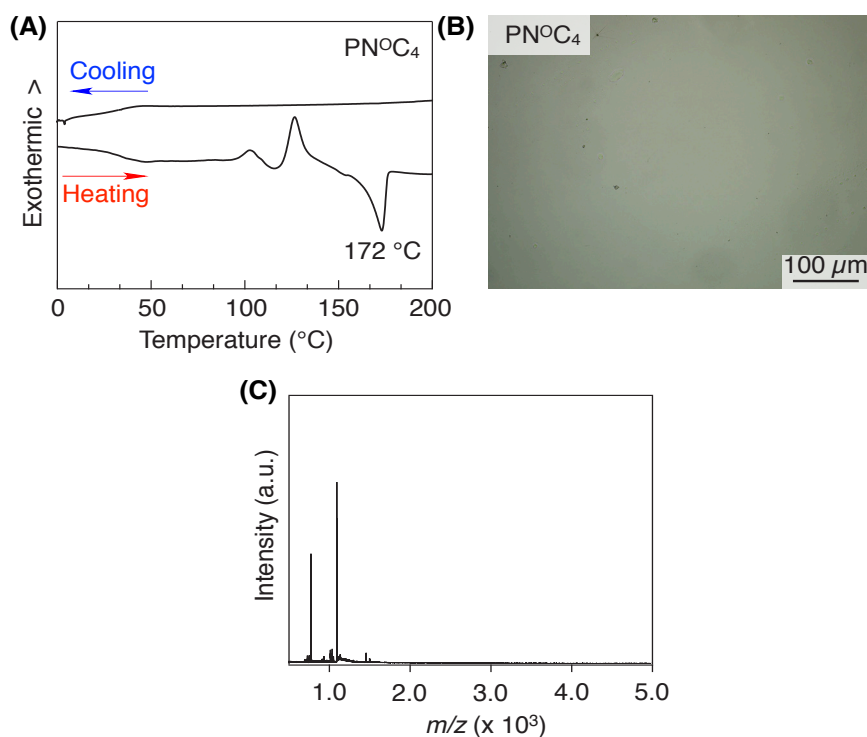


Figure S10 I (A) DSC traces on second heating/cooling cycles ($10\text{ }^\circ\text{C}/\text{min}$) of PNOC_4 . (B) OM image and (C) MALDI-TOF mass spectra of PNOC_4 after heating at $180\text{ }^\circ\text{C}$ in cells for overnight.

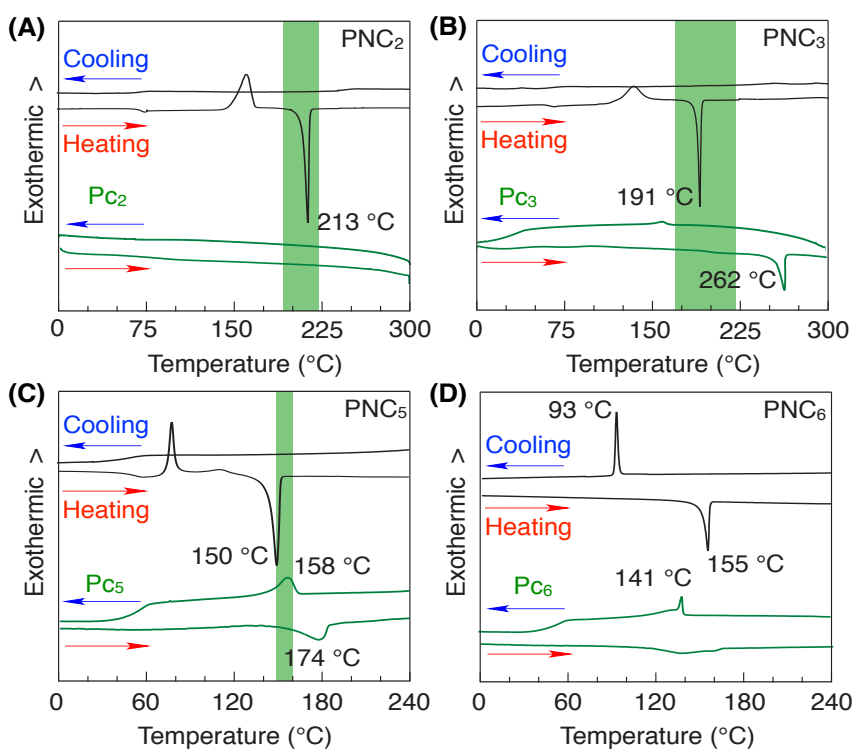


Figure S11 | DSC traces on second heating/cooling cycles ($10\text{ }^{\circ}\text{C}/\text{min}$) of (A) PNC_2 (black lines) and Pc_2 (green lines), (B) PNC_3 (black lines) and Pc_3 (green lines), (C) PNC_5 (black lines) and Pc_5 (green lines), and (D) PNC_6 (black lines) and Pc_6 (green lines). Green regions represent the temperature range enable to form the crystalline fibers of Pc.

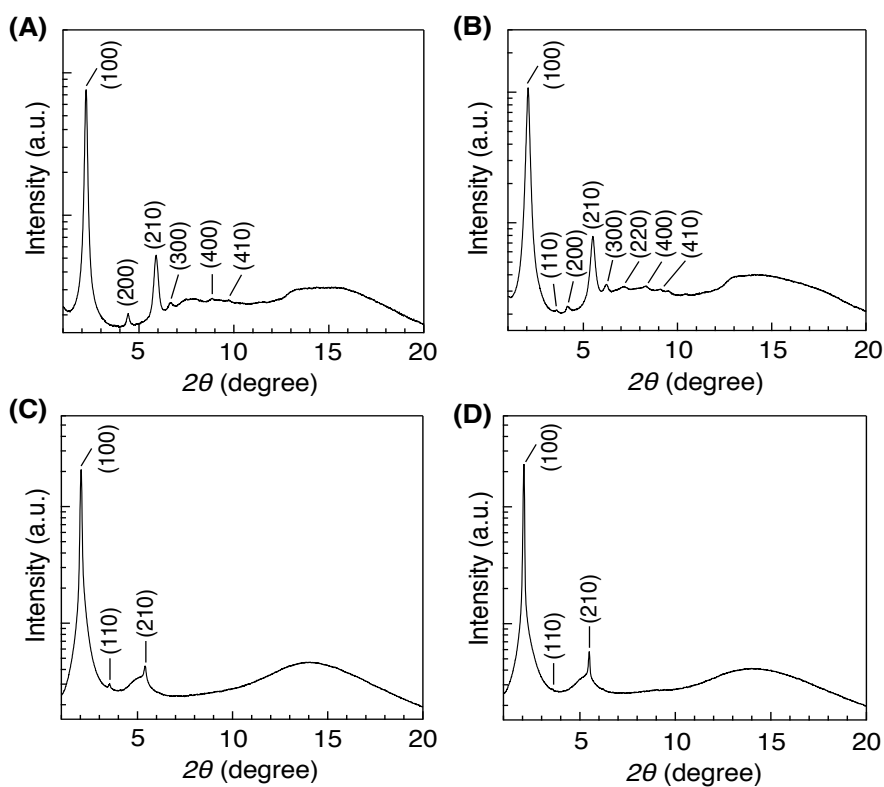


Figure S12 | XRD pattern of powder sample of Pc_2 , Pc_3 , Pc_5 and Pc_6 in a glass capillary at $200\text{ }^{\circ}\text{C}$, $200\text{ }^{\circ}\text{C}$, $150\text{ }^{\circ}\text{C}$ and $140\text{ }^{\circ}\text{C}$, respectively. Miller indices in parentheses.

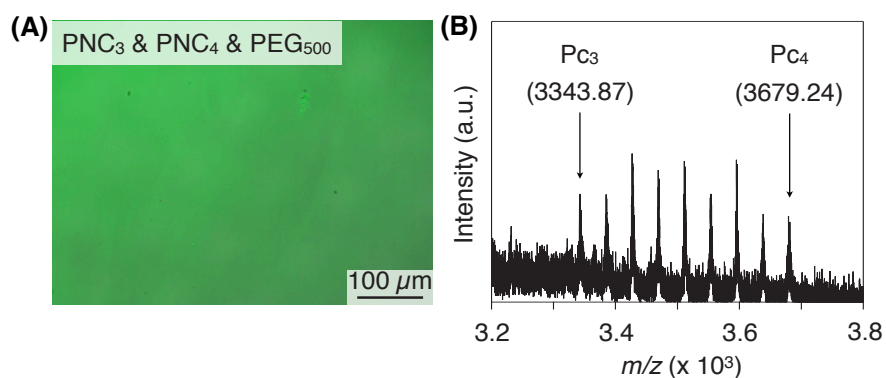


Figure S13 I (A) OM image and (B) MALDI-TOF mass spectra of a mixture of PNC₃, PNC₄ (mole ratio = 1/1) and PEG₅₀₀ (10%wt) heating at 180 °C for overnight.

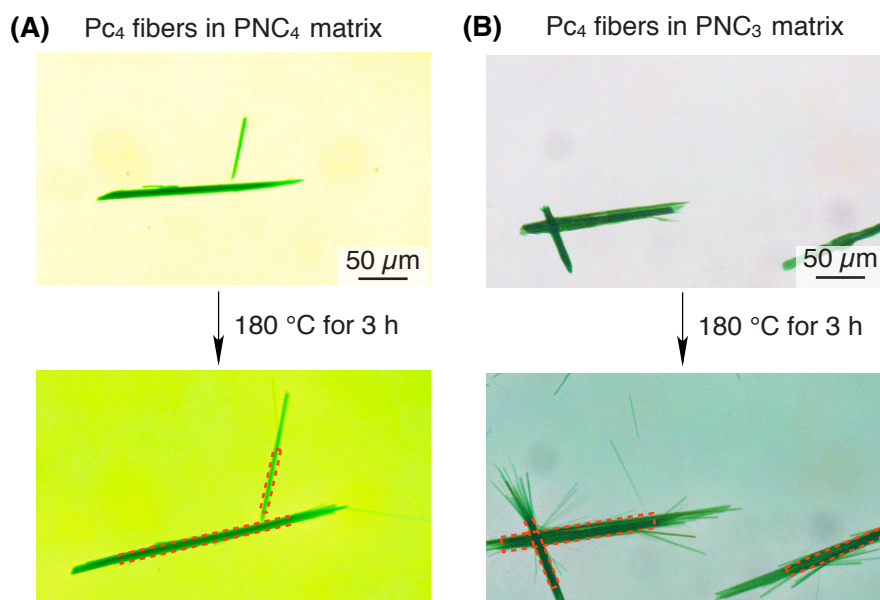


Figure S14 I OM images of the P_c₄ fibrous seeds in (A) PNC₄ and (B) PNC₃ matrix heating at 180 °C for 3 hours. The red frames represent the initial shape of P_c₄ fibrous seeds.

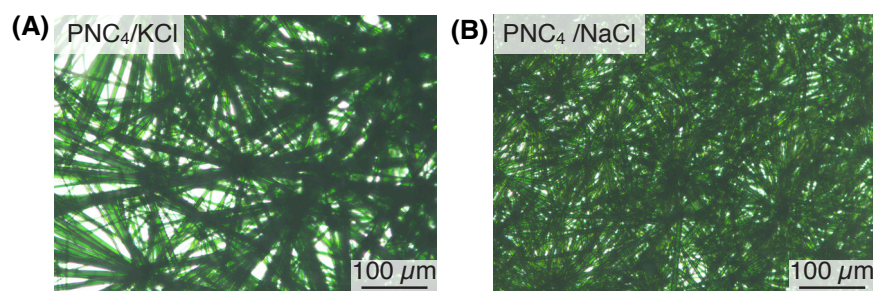


Figure S15 I OM images of PNC₄ sandwiched with two (A) KCl and (B) NaCl plates heating at 180 °C for overnight, respectively.

4.4.4. Supporting Tables

Table S1 | XRD Data of the Crystalline Fibers (left) and Bulk Sample (right) of Pc₃.

Sample	2 θ (degree)	$d_{\text{obs.}}$ (nm)	$d_{\text{calc.}}$ (nm)	hkl	Sample	2 θ (degree)	$d_{\text{obs.}}$ (nm)	$d_{\text{calc.}}$ (nm)	hkl
Crystal	2.13	2.91	2.90	100	Bulk	2.07	2.99	2.99	100
(25 °C)	2.83	2.19	1.76	--	(180 °C)	3.58	1.73	1.73	110
<i>P6mm</i> ^a	3.72	1.66	1.67	110	<i>P6mm</i> ^b	4.15	1.49	1.50	200
	5.67	1.09	1.10	210		5.51	1.12	1.13	210
	6.55	0.95	0.96	300		6.21	1.00	1.00	300
	7.39	0.84	0.84	220		7.14	0.87	0.86	220
	7.88	0.79	0.80	310		8.30	0.75	0.75	400
	8.50	0.73	0.73	400		9.12	0.68	0.66	410

^a*P6mm* hexagonal lattice parameters: $a = 3.30$ nm. ^b*P6mm* hexagonal lattice parameters: $a = 3.45$ nm.

Table S2 | XRD Data of the Crystalline Fibers (left) and Bulk Sample (right) of Pc₄.

Sample	2 θ (degree)	$d_{\text{obs.}}$ (nm)	$d_{\text{calc.}}$ (nm)	hkl	Sample	2 θ (degree)	$d_{\text{obs.}}$ (nm)	$d_{\text{calc.}}$ (nm)	hkl
Crystal	2.04	3.04	3.05	100	Bulk	1.94	3.19	3.18	100
(25 °C)	3.52	1.76	1.76	110	(180 °C)	3.37	1.84	1.84	110
<i>P6mm</i> ^a	5.40	1.15	1.15	210	<i>P6mm</i> ^b	5.17	1.20	1.20	210
	6.14	1.00	1.00	300		5.85	1.06	1.06	300
	7.05	0.88	0.88	220		6.76	0.92	0.92	220
						7.81	0.79	0.79	400
						8.94	0.69	0.69	410
						9.72	0.64	0.64	500

^a*P6mm* hexagonal lattice parameters: $a = 3.50$ nm. ^b*P6mm* hexagonal lattice parameters: $a = 3.67$ nm.

Table S3 | Evaluating the cyclized yield of Pc_4 heating at different temperatures.

Temp. (°C)	M ^a (mg)	C _{Pc} ^b (mg/mL)	C _{PNC} ^c (mg/mL)	% _{Pc} ^d (%)	% _{PNC} ^e (%)	% _{iner.} ^f (%)
145	1.00	0.05±0.01	0.89±0.02	5±1	89±2	6±2
150	1.08	0.17±0.01	0.80±0.02	16±1	74±2	10±3
160	0.78	0.35±0.02	0.28±0.01	45±3	36±1	19±3
170	0.69	0.49±0.03	0.08±0.01	71±4	12±2	17±4
180	0.71	0.54±0.03	0.06±0.01	77±4	8±1	15±4
190	0.96	0.80±0.05	0.03±0.01	83±5	2±1	15±5

^aM: original weight of the powder samples of PNC_4 ; ^bC_{Pc}: the concentration of Pc_4 in the resultant mixtures is evaluated by the equation, $C_{\text{Pc}} = (6.7 \pm 0.4)I_{\text{RI}}$, in which I_{RI} represents the intensity of refractive index corresponding to the peak of Pc_4 in Figure. S7; ^cC_{PNC}: the concentration of unreacted PNC_4 in the resultant mixtures is evaluated by the equation, $C_{\text{PNC}} = (30 \pm 0.6)I_{\text{RI}}$, in which I_{RI} represents the intensity of refractive index corresponding to the peak of PNC_4 in Figure. S7; ^d%_{Pc}: the %-content of Pc_4 in the resultant mixtures is evaluated by the equation, $\%_{\text{Pc}} = 100C_{\text{Pc}}/M$; ^e%_{PNC}: the %-content of unreacted PNC_4 in the resultant mixtures is evaluated by the equation, $\%_{\text{PNC}} = 100C_{\text{PNC}}/M$; ^f%_{iner.}: the %-content of intermediates in the resultant mixtures is evaluated by the equation, $\%_{\text{iner.}} = 100 - \%_{\text{PNC}} - \%_{\text{Pc}}$.

Table S4 | Evaluating the cyclized yield of Pc_4 heating at different temperatures.

Time (hours)	M ^a (mg)	C _{Pc} ^b (mg/mL)	C _{PNC} ^c (mg/mL)	% _{Pc} ^d (%)	% _{PNC} ^e (%)	% _{iner.} ^f (%)
2	1.10	0.01±0.01	1.02±0.02	1±1	93±2	6±2
4	0.90	0.03±0.01	0.78±0.02	3±3	87±2	10±3
6	0.95	0.16±0.01	0.68±0.01	17±1	72±1	11±1
8	0.85	0.36±0.02	0.38±0.01	42±2	45±1	13±2
10	0.80	0.51±0.03	0.18±0.01	64±4	23±1	13±4
12	0.83	0.61±0.04	0.11±0.01	74±5	13±1	13±5

^aM: original weight of the powder samples of PNC_4 ; ^bC_{Pc}: the concentration of Pc_4 in the resultant mixtures; ^cC_{PNC}: the concentration of unreacted PNC_4 in the resultant mixtures; ^d%_{Pc}: the %-content of Pc_4 in the resultant mixtures; ^e%_{PNC}: the %-content of unreacted PNC_4 in the resultant mixtures; ^f%_{iner.}: the %-content of intermediates in the resultant mixtures. The detail computational method is identical to Table S3.

Acknowledgements

During the five years of my PhD course, a lot of people need to be thanks. First of all, I gratefully express acknowledge with my deepest appreciation to Professor Takuzo Aida, who gave me an opportunity to climb the scientific height and explore an unknown world. His unique opinions on scientific research and life experience will deeply impact me in my whole life. I am also profoundly grateful to the other members of my thesis committee: Professor Kyoko Nozaki, Takanori Fukushima, Associate Professor Masafumi Yoshio, and Team Leader Yasuhiro Ishida.

Inhere, I specially extend my sincere gratitude to Prof. Takanori Fukushima, Lecture Takashi Kajitani at Tokyo Institute of Technology and Dr. Yi-Tsu, Chan at Riken for their guidance, valuable advices and suggestions, and constructive discussions. I am affected by their cautious and insistent attitudes to science and learned essential experimental techniques and skills to carry out a research work. Discussion with them affords me major breakthroughs in my first work and inspired a lot.

I also feel sincerely grateful for the great help from Dr. Daigo Miyajima at Riken to write the manuscript of my first work. Especially, I successfully completed the second interesting project,

cooperated with Dr. Miyajima, who always gives a lot of constructive comments and ideas. Highly appreciated again!!

Grateful acknowledgements are also made to the following collaborators. Assisted synthesis work from Dr. Jose M. Lobe, Dr Ayumi Imayoshi and Ms. Atsuko Kosaka at Riken significantly improved the work efficiency. X-ray scattering analysis by using synchrotron radiation was successfully completed thanks to the considerable contribution from Prof. Masaki Takata in Riken Spring-8 Center.

I also should thank the foreign students exchange program between Tsinghua University (Beijing) and The University of Tokyo in 2011, which provided me a chance to study abroad in Japan. And I thank the financial support of Monbukagakusho (MEXT) scholarship from Japanese government.

Finally, I wish to express my heartfelt gratitude for my parents, and my supervisor in Tsinghua Associate Prof. Yaning He, who have supported my education, and all my friends in China and Japan, who help me a lot.

- [1] **Zhen Chen**, Ayumi Imayoshi, Daigo Miyajima,* and Takuzo Aida.* Solid-state self-replication of phthalocyanine in conjugation with supramolecular polymerization. to be submitted.
- [2] **Zhen Chen**, Yi-Tsu Chan, Daigo Miyajima, Takashi Kajitani,* Atsuko Kosaka, Takanori Fukushima,* Jose M. Lobeze, and Takuzo Aida.* A design principle of polymers processable into 2D homeotropic order. *Nature Commun.* in press (2016).
- [3] Yaning He,* Yan Zhu, **Zhen Chen**, Wei He, and Xiaogong Wang*. Remote-control photocycloreversion of dithienylethene driven by strong push–pull azo chromophores. *Chem. Commun.* **49**, 5556 (2013).
- [4] Yu Zhu, Yuqi Zhou, **Zhen Chen**, Ran Lin, and Xiaogong Wang*. Photoresponsive diblock copolymers bearing strong push–pull azo chromophores and cholesteryl groups. *Polymer.* **53**, 3566 (2012).
- [5] Yaning He,* Wei He, Renbo Wei, **Zhen Chen**, and Xiaogong Wang*. Synthesizing amphiphilic block copolymers through macromolecular azo-coupling reaction. *Chem. Commun.* **48**, 1036 (2012).
- [6] **Zhen Chen**, Yaning He,* Yang Wang, and Xiaogong Wang*. Amphiphilic diblock copolymer with dithienylethene pendants: synthesis and photo-modulated self-assembly. *Macro. Rapid. Commun.* **32**, 977 (2011).